Phase transitions in monitored fermions

Inaugural-Dissertation zur Erlangung des Doktorgrades der
Mathematisch-Naturwissenschaftlichen Fakultät der
Universität zu Köln

Vorgelegt von
Thomas Martin Müller
aus Köln

Köln
2024

Berichterstatter: Prof. Dr. Sebastian Diehl
(Gutachter) Prof. Dr. Matteo Rizzi
Prof. Dr. Reinhold Egger

Dissertation durch die Mathematisch-Naturwissenschaftliche Fakultät der Universität zu Köln 2024 angenommen.

Tag der mündlichen Prüfung: 10.07.2024

Eidesstattliche Versicherung

Hiermit versichere ich an Eides statt, dass ich die vorliegende Dissertation selbstständig und ohne die Benutzung anderer als der angegebenen Hilfsmittel und Literatur angefertigt habe. Alle Stellen, die wörtlich oder sinngemäß aus veröffentlichten und nicht veröffentlichten Werken dem Wortlaut oder dem Sinn nach entnommen wurden, sind als solche kenntlich gemacht. Ich versichere an Eides statt, dass diese Dissertation noch keiner anderen Fakultät oder Universität zur Prüfung vorgelegen hat; dass sie - abgesehen von unten angegebenen Teilpublikationen und eingebundenen Artikeln und Manuskripten - noch nicht veröffentlicht worden ist sowie, dass ich eine Veröffentlichung der Dissertation vor Abschluss der Promotion nicht ohne Genehmigung des Promotionsausschusses vornehmen werde. Die Bestimmungen dieser Ordnung sind mir bekannt. Darüber hinaus erkläre ich hiermit, dass ich die Ordnung zur Sicherung guter wissenschaftlicher Praxis und zum Umgang mit wissenschaftlichem Fehlverhalten der Universität zu Köln gelesen und sie bei der Durchführung der Dissertation zugrundeliegenden Arbeiten und der schriftlich verfassten Dissertation beachtet habe und verpflichte mich hiermit, die dort genannten Vorgaben bei allen wissenschaftlichen Tätigkeiten zu beachten und umzusetzen. Ich versichere, dass die eingereichte elektronische Fassung der eingereichten Druckfassung vollständig entspricht.

Teilpublikationen:

- T. Müller, S. Diehl, and M. Buchhold: "Measurement-induced dark state phase transitions in long-ranged fermion systems", Physical Review Letters **128** (1), 010605 (2022), DOI: 10.1103/PhysRevLett.128.010605.

- M. Buchhold, T. Müller, and S. Diehl: "Revealing measurement-induced phase transitions by pre-selection", ArXiv:2208.10506 (2022),
  DOI: 10.48550/arXiv.2202.01037

Bemerkungen: Abschnitte, die diesen Teilpublikationen sowie weiteren zur Veröffentlichung vorgesehenen Manuskripten entnommen wurden habe ich in der Dissertation gekennzeichnet. Mein eigener Beitrag zu diesen ist ebenfalls für jeden dieser Abschnitte separat beschrieben. Aus beiden Teilpublikationen wurden Abbildungen in dieser Arbeit wiederverwendet beziehungsweise adaptiert.
Ein Teil dieser Arbeit beruht auf den Ergebnissen von zum Teil aufwändigen numerischen Simulationen. Die Rohdaten hierzu sind auf der Plattform Zenodo unter den DOIs 10.5281/zenodo.10455797 und 10.5281/zenodo.10455004 zu finden.

Thomas Müller
Köln, den 04.05.2024

Acknowledgements

I thank Sebastian Diehl and Michael Buchhold for being great advisors and collaborators on the projects presented in this work. The progress I made as a researcher in the past four years would not have been possible without them.

I especially thank Carl Zelle, Johannes Lang and Romain Daviet for discussing my work and giving me valuable input from a more distant perspective.

I want to also thank the members of my research group and those closely connected with whom I discussed contents of my work: Michael Scherer, Alessio Chiocchetta, Steven Mathey, Ori Alberton, Björn Ladewig, Heinrich Fröml, Jiangtian Yao, Sebastian Kalhöfer, Tom Zander, René Wolters, Rohan Mittal and Zemin Huang. I very much appreciate the open scientifically interested community at the institute for theoretical physics in Cologne, especially in the condensed matter group seminar that I enjoyed very much. Very important to shape this culture where Sebastian Diehl, Achim Rosch, Simon Trebst and Matteo Rizzi. Special thanks go also to Guo-Yi Zhu, Karim Chahine and Daniel Alcalde Puente for their expertise especially on the numerical side of theoretical physics that I learned to appreciate in the past four years.

I thank the Cluster of Excellence Matter and Light for Quantum Computing (ML4Q) and the DFG Collaborative Research Center (CRC) 183 for their financial support and the possibility to attend the nice conferences that they offered, and the Jülich supercomputing center for the chance to run large scale simulations on the JUWELS cluster. Special thanks to Matteo Rizzi and Daniel Alcalde Puente for their support on that matter.

Finally, I want to thank Sebastian Diehl, Matteo Rizzi, Reinhold Egger, Markus Grüninger and Johannes Lang for evaluating this work, and Michael Buchhold, Carl Zelle and Johannes Lang for feedback on the manuscript.

Abstract

The recently developed possibility to implement non-destructive mid circuit measurements in synthetic quantum matter provides a new angle to understand quantum many-body dynamics. Measurements can now be seen not only as a way to extract information about a system, but also as a dynamical resource. This sparks a lot of interest in studying the interplay of the three generators of dynamics of quantum states, unitaries, dissipation and measurements, in many-body systems. Historically first, random dynamics of this type in absence of conservation laws have been studied, giving rise to so called measurement-induced phase transitions.

Based on this, we study the effects of symmetries in monitored dynamics, focusing on the paradigmatic model of spinless fermions in one dimension. We develop a systematic field theoretical description of the relevant degrees of freedom of this model. In particular, the entanglement entropy is studied both using this framework and numerical simulations. We find, that this quantity qualitatively changes its behavior at a finite critical measurement strength, from logarithmic growth with system size for small measurement strength, to area law for strong measurement. The transition is confirmed to be of Berezinskii-Kosterlitz-Thouless universality. To explore the scope of applicability of the developed replica field theory method, we also extend this model including long-range interactions, giving rise to a third phase with algebraic sub-volume entanglement scaling.

A even more recent development is the experimental realization of adaptive quantum circuits. While this is required on the path towards efficient quantum error correction and therefore fault tolerant quantum computing, it also provides yet another new type of quantum dynamics. We therefore study measurement-based active feedback in the light of non-equilibrium universality. This gives rise to a type of absorbing state phase transitions with a strong notion of quantum physics. This is seen in the fact that an entanglement- and an absorbing state phase transition happen at the same critical measurement rate. Besides being interesting for a broader understanding of non-equilibrium criticality, we argue that the correspondence of measurement-induced phase transitions and quantum absorbing state phase transitions provides a way to overcome the post-selection problem.

Contents

1 Introduction

The recent experimental progress in the development of quantum devices [1–4] in the era of noisy intermediate scale quantum computing (NISQ) [5] offers exciting perspectives for future realizations of quantum algorithms [6]. A universal quantum computer would be able to solve certain classically exponentially hard numerical problems algebraically fast [7]. This has potential applications in, for instance, cryptography [8, 9] or optimization tasks [10, 11] with relevance for the existing digital industry. However, in the current noisy devices, quantum supremacy [12] is not yet achieved in the implementation of useful quantum algorithms. The main obstruction is that the error thresholds to perform efficient quantum error correction [13, 14] are not yet reached.

Besides this scope of applications, NISQ devices have a huge potential for the simulation of quantum systems [15]. So called synthetic quantum matter [16] such as Rydberg atoms [17] or ultracold trapped ions [18, 19] allows to implement model Hamiltonians to study them isolated from other effects present in solid state systems. The first instance of that was the realization of the fundamental many-body quantum effect of Bose-Einstein condensation [20] in a lab [21, 22]. Later, more complex problems were studied adding optical lattices [23, 24]. Furthermore, the versatility of quantum simulators allows to study the properties of complex quantum systems such as large molecules which drives developments in quantum chemistry [25]. This type of application does not require quantum error correction.

On a more fundamental level, the fact that NISQ devices behave quantum mechanically but are necessarily coupled to their environment also makes them the ideal platform to study the universal behavior of open quantum systems [26, 27]. The presence of noise opens up a wide range of questions concerning the interplay of quantum mechanics and thermodynamics, such as which universality classes are realized in stationary states out of equilibrium [28, 29]. These considerations take the perspective that the noise in the system is an external ingredient, and the type of coupling to the environment may be engineered to design designated stationary states [30], such as non-trivial dark states [31].

Besides the precise control of engineered unitary and non-unitary dynamics, NISQ devices have another important feature: the experimenter may perform mid-circuit measurements of local operators that do not destroy the coherence of the quantum state of the device [32–35]. Such operations are necessary since in quantum error correction [13, 14], those mid-circuit measurements are required to detect syndromes and perform the appropriate error correction. While this feature is motivated by the practical purpose of achieving noise-resilient quantum computing, it also enables another angle to study noise: since the outcome of a quantum measurement is fundamentally random, mid-circuit measurements induce a stochastic element to the dynamics. In

that sense, a monitored quantum system can be understood as an open quantum system where the coupling to the environment is realized by a measurement. Generically, the stationary state of a system undergoing repeated measurements is a trivial infinite temperature state due to the configurational entropy of the random measurement outcomes [36–39]. At first sight, the story about stationary states and phases of matter ends here.

However, due to the fact that the measurement read-outs for every run of the experiment are recorded, additional information about the evolving state along each so called quantum trajectory is available [40]. Equipping the analysis of these trajectories with tools from disorder physics [41–43] reveals non-trivial behavior beyond the infinite temperature state [44]. In particular, the entanglement entropy [45, 46] is an important witness of the non-trivial phase of matter in the stationary state of a measurement process: frequent local measurements act disentangling while unitary dynamics that couples different Qbits entangles the state. It turns out, that this competition results in a measurement-induced phase transition (MIPT) in a variety of model systems. Originally, this was discussed in systems without conservation laws such as random unitary circuits with local measurements and certain Hamiltonian systems in one dimension [47–58]. For strong (frequent) measurements, the system is in an area-law phase while weak (rare) measurements do not affect the volume law that is also obtained in absence of measurements [59]. The phase transition at a critical measurement strength (rate) rate has been shown to lay in the universality class of percolation [60].

This discovery sparked a lot of of interest in exploring the possible phases and phase transitions in monitored quantum systems. For instance, models in higher dimensions [61–64], have been studied, as well as the interplay of non-commuting measurements [65, 66]. Another direction, on which we want to focus in more detail in this thesis, is to study what happens in the presence of conservation laws [44, 67–69]. In both classical and quantum systems in steady states in and out of equilibrium, the universality class of a phase transition is determined by the dimension and the symmetries of the model [70, 71]. This can be systematically studied on the level of moment generating functionals. In equilibrium, this role is taken by the free energy while in a driven open classical or quantum system, the appropriate object is the Martin-Siggia-Rose-Janssen-de Dominicis (MSRJD) or Keldysh path integral [28, 29]. The conservation laws are related to symmetries of the moment-generating functionals due to Noether's theorem [72]. This means, that conservation laws require an additional symmetry of the generating functional which results in hydrodynamic modes and subsequently in modified universal phenomena. These can be analyzed in the renormalization group (RG) framework [70, 71, 73–77].

In the case of MIPTs, the situation is more challenging: here, the Keldysh path integral describes only the trivial stationary state while non-trivial entanglement sig-

natures require a replica treatment similarly to disorder problems [41–43]: we need to study non-linear averages of the state of a system out of equilibrium and define a moment generating functional capturing this [44, 69]. The triviality of the stationary state is crucial for the analysis, distinguishing MIPTs from Anderson transitions in disordered systems [78]. Therefore, it is an important structural question, how properties of the various discussed microscopic models precisely translate into symmetries of the effective action describing the MIPT. The tool of choice is the replica Keldysh formalism [28, 29, 44, 69], which we discuss in detail in this thesis.

A paradigmatic model for quantum phases of matter in one dimension is the Tomonaga-Luttinger liquid [79–82]. Due to the peculiarities of one-dimensional systems such as the possibility to count particles by a single monotonously increasing function [83, 84], it effectively describes a large class of microscopic models with particle number conservation in and out of equilibrium [85]. While the precise microscopic mapping to a Luttinger liquid is tedious, especially for lattice models [86, 87], one typically constructs effective models based on symmetries which is very successful in describing e.g. transport experiments on quantum wires [88]. On the other hand, fermions have the property that the particle number operator is a projection $\hat{n}^2 = \hat{n}$ which implies that measurements of the particle number leave a many-body quantum state Gaussian. Therefore, a free fermion model with particle number measurement can be efficiently simulated [67–69]. The combination of these two perspectives makes monitored free fermions in one dimension with particle number conservation the ideal system to study criticality in MIPTs with conservation laws: we can write down a generating functional based on symmetry arguments and analyze the phase structure, and we can also benchmark the results with efficient numerical simulations.

For that reason, this system has been studied extensively using different analytical approaches, ranging from generalized hydrodynamics [67] via Abelian bosonization [44] to disorder-inspired non-linear sigma models [69]. However, even though such an effort was made to understand this system, it is still debated, what the structure of the phase diagram of this model is. Abelian bosonization predicts the existence of a Berezhinskii-Kosterlitz-Thouless (BKT) [89–91] phase transition at a finite measurement strength between a phase with logarithmic entanglement scaling and area law [44]. In contrast, the non-linear sigma model approach suggests that the apparent existence of the logarithmic scaling phase is a finite size effect and in the thermodynamic limit, the system is ultimately in an area law phase for any non-zero measurement rate or strength [69]. Both these results capture essential features of the results of numerical simulations while their universality is clearly different. Therefore, we believe that there is need for a better structural understanding of the generating functional for MIPTs in general and specifically for the case of free fermions with measurements. A large part of this thesis is dedicated to making progress here, and we present new analytical and numerical

evidence for the BKT scenario.

On the microscopic side, different measurement protocols have been considered: projective measurements at random positions [69], weak continuous measurements [44, 67, 68] and also interpolations between these two limiting cases [92, 93] and post-selected dynamics [94]. While these differences do not change the symmetries of the microscopic model, it is unclear, if, on a coarse grained level, different symmetries emerge. Therefore, we also systematically compare simulations of the system with projective and continuous measurements. Connected to that, an open research question is to identify whether weak and strong measurements in principle are described by the same effective action at MIPTs or if the critical behavior is altered depending on the precise protocol. To settle this question, a better understanding of field theories for MIPTs is required.

Furthermore, extensions to the model including spatial disorder [95], coupling to an environment [96], or higher dimensions [97, 98] yield a broader understanding of this model. In particular, in this thesis we focus on the effect of long-range hoppings with algebraically decaying strength [99]. This is motivated by the observation that, even without breaking symmetries, ground states of long-ranged Hamiltonians behave qualitatively different from the short-ranged counterparts [100–102]: new phases emerge and the transitions into these phases show typical long-range critical behavior. On the other hand, experimental platforms, especially quantum-optical systems such trapped ions [103–106], cold atoms in cavities [107, 108], Rydberg atoms [109] or polar molecules [110], are by design suitable to study such long-range interactions mediated by light. Therefore, it is natural to study the interplay of long-range hopping and monitoring in a system of free fermions. It turns out, that the long-range hopping indeed lets a new phase emerge, where the entanglement scales algebraically with system size, but slower than volume law. Besides this prediction of a new type of MIPT, this model is a useful benchmark for the validity of the replica Keldysh field theory method with Abelian bosonization: using this method, we can analytically predict the entanglement growth exponent which perfectly matches what is found in numerical simulations. To obtain this result correctly, it is crucial that the infinite temperature state is used to eliminate one degree of freedom from the theory. This is a key element of our understanding of replica Keldysh field theory for MIPTs.

Let us now take a step back and think about the observability of MIPTs: despite the fact that the dynamics is driven by measurements and the read-outs of these measurements are recorded by the experimentalist, it is notoriously hard to observe MIPTs due to the post-selection problem [49]. One fundamental common property of MIPTs is that they are only observable in trajectory-resolved quantities such as entanglement, while there is no order parameter witnessing the transition. Therefore, one is required to measure these trajectory-resolved quantities in an experiment in order to detect

a MIPT. However, this typically requires trajectory-resolved quantum state tomography [34, 111]. In disordered systems, observables can be repeatedly measured for a single disorder configuration which allows to extract averages efficiently. In contrast, in measurement-induced dynamics, every run of the experiment results in a different sequence of measurements, i.e. a different trajectory The number of different trajectories scales exponentially with the number of measurements that are performed [40]. Therefore, the number of required repetitions of the experiment scales exponentially in the system size and trajectory-resolved observables are inaccessible in thermodynamically large systems [34, 111].

One commonly taken route to overcome this problem is to focus on systems that can be efficiently simulated such that informed by the measurement read-outs, the final state of the system can be estimated. Then, the MIPT can be witnessed by either performing a unitary operation at the end of the process that reveals the trajectory-resolved information [112–114], or computing cross-correlations between experimental data and the numerical simulation [111, 115–118]. These approaches all share that they require that the state and the dynamics of the quantum system at hand can be efficiently simulated on a classical computer, for instance because one studies Clifford circuits [119, 120], Gaussian time-evolution [68] or weakly entangled systems [121, 122]. Since the system on which measurement-induced dynamics is realized is always thought of as a quantum computer or quantum simulator, this raises a provocative question: why should we perform the experiment on the quantum computer, if we could equivalently run the same experiment in a more controlled and less noisy way directly on a classical computer, where even the trajectory resolved observables are directly accessible?

This is very different to the typical experimental situation in condensed matter physics: here, self-assembling thermodynamically large systems are studied and observables are extracted at the macroscopic classical scale. Typically, we want to explain emergent phenomena at these large scales by studying effective models while the microscopic reality at the smallest scales is complicated or even unknown [71]. Therefore, classical simulations can only be performed with the input of an effective model on a microscopic scale. The benchmark for accuracy of the simulated model is then a comparison to experiments that are naturally performed at macroscopic scales. However, the behavior at large scales can be experimentally extracted independently of an understanding of the microscopic model or the phenomenon that leads to the emergence of new physics at larger scales.

Of course, an understanding of measurement-induced phenomena is an interesting challenge by itself despite this detection issue. For instance, they provide valuable insights into the role of complexity in many-body systems and quantum measurement as a dynamical resource in the first place. However, with the goal of connecting

measurement-induced dynamics to the physics of open quantum systems [123] in mind, we propose to make use of another feature that is characteristic for synthetic quantum matter: due to the fact that the individual operations in these systems can be engineered in runtime of the experiment [124–126], we study the effects of feedback based on the measurement read-outs.

The idea is the following: after the mid-circuit measurement of an observable, we apply a unitary operation (or potentially another measurement) that depends on the outcome of that measurement [127, 128]. This provides a way to transform MIPTs into another exciting class of phase transitions in open quantum systems, namely quantum absorbing state phase transitions [129–132]. On one hand, frequent or strong measurements steer the system into an area law entangled state which can be understood classically. Based on such a state, feedback efficiently allows to steer a state into a pre-defined target state [133–135]. For weak or rare measurements, on the other hand, typically the unitary dynamics entangles the state strongly such that no efficient steering is possible. The difference is then visible in an order parameter that can be computed without the need of trajectory-resolved averaging. We call this approach pre-selection [127] and discuss it in detail in the end of this thesis, applied to the paradigmatic model of monitored fermions in one dimension.

Outline This thesis is structured as follows: to discuss measurement-induced phenomena, it is necessary to carefully define what a quantum-mechanical measurement is, and how it can be formulated in terms of stochastic Schrödinger equations. We also need to understand, what is observable and what is not. These question can be discussed already on the level of a single degree of freedom that undergoes measurement-induced dynamics. Therefore, Sec. 2 is dedicated to a discussion of the single-particle phenomena mentioned above. After that, in Sec. 3, we turn to the model of free fermions with nearest neighbor hopping and monitoring of the particle number in one dimension. We provide a detailed discussion of the construction of the replica Keldysh field theory and the Abelian bosonization approach. This demonstrates a way to define the moment generating functional for a measurement problem with a conservation law. Based on this, in Sec. 4, we discuss the effects of long-range hopping on this model. Finally, in Sec. 5, we discuss the pre-selection approach to pull the measurement-induced effects in monitored fermions onto the level of order parameters. In that context, we discuss different realizations of quantum absorbing state phase transitions in that system.

2 Measurement-induced dynamics of quantum systems

Before delving into the study of many-body phenomena induced by measurements, in this section we introduce measurement-induced dynamics. We make very few assumptions about the type of system under consideration, besides that it is a quantum system which is repeatedly measured and that it also undergoes (continuous) unitary time-evolution. For this construction, a few-body picture is sufficient as we indeed construct a microscopic model that describes the local properties of a generic mesoscopic or even thermodynamic system. This is the basis for the analysis of many-body effects such as critical phenomena in the subsequent sections.

This introduction is structured as follows: First, in Sec. 2.1 we introduce the quantum state diffusion (QSD) and quantum jump (QJ) protocol both by explicitly introducing quantum measurement as a generator of non-unitary dynamics and as a strategy to unravel a Markovian quantum master equation. After that, in Sec. 2.2, we discuss observables that are non-linear in the state along measurement trajectories. These are necessary to characterize non-trivial measurement-induced physics as linearly averaged observables only show infinite temperature state behavior due to the configurational entropy of the random measurement outcomes [36–39]. Then, we introduce the replica trick that we use in order to compute these non-linear observables analytically. Finally, we comment on the post-selection problem and potential ways to overcome it in Sec. 2.3. In short, we point out the fact that the observation of non-linear observables in a perfect experimental realization requires to run the experiment exponentially often in the number of measurements that are performed. We show, that this is already problematic for studying the stationary state of a two-level system beyond linearly averaged observables.

2.1 Stochastic Schrödinger equations

In this section, we present the quantum jump (QJ) and quantum state diffusion (QSD) protocol, as shown in Fig. 1 from two different perspectives:

(a) If we perform projective measurements at random points in space and time in a system undergoing unitary time-evolution, we obtain the QJ protocol. Instead, coupling the system locally to an auxiliary degree of freedom that is projectively measured introduces a finite time scale on which the system is measured such that the discrete stochastic measurement process is replaced by a continuous stochastic one [136]. Mixing this procedure with a Hamiltonian yields QSD. This construction shows that both resulting stochastic Schrödinger equations describe a physically implementable measurement process.

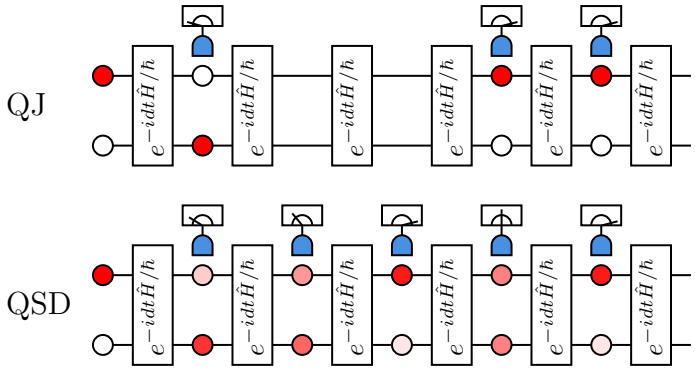

Figure 1: Illustration of the QJ and QSD protocol for the toy model with time running from left to right. The system is initialized with the particle being at the top and then it evolves according to the Hamiltonian. In between time steps, we either projectively measure the position at a fraction of the time steps (QJ) or we weakly measure at every time step (QSD), performing an imperfect projection.

(b) One is interested in an efficient way to simulate a Markovian quantum master equation [123, 137, 138] for the density operator $\hat{\rho}(t)$ by representing it in terms of a stochastic differential equation for pure states $|\psi(t)\rangle$ such that the average over the noise reproduces this quantum master equation. This is in principle not related to any actual physical process but rather a tool to enable efficient numerical simulation of quantum master equations.

While both perspectives are used in the literature to derive stochastic Schrödinger equations [136, 139–143], we stress in the following that not every unraveling necessarily bears physical relevance beyond the linear average over trajectories. Instead, when thinking about measurement-induced entanglement transitions, we need to fix the microscopic protocol leading to the considered stochastic Schrödinger equation (a).

We demonstrate both approaches applied to a toy model: Consider a single fermion $\{\hat{c}_l, \hat{c}_m^\dagger\} = \delta_{lm}$, $\{\hat{c}_l, \hat{c}_m\} = 0$ on a system of two lattice sites with positions $l = 0, 1$. We are now interested in the competition between hopping $\hat{H} = \hat{c}_0^\dagger \hat{c}_1 + \text{h.c.}$ and monitoring of the location of the particle $\hat{x} = \hat{n}_1 = \hat{c}_1^\dagger \hat{c}_1$[1]. See Fig. 1 for an illustration of this toy model undergoing the two different measurement protocols QJ and QSD. In Fig. 2 we show single runs of the simulation for the two measurement protocols[2]. They show that in both protocols, a large measurement strength γ pins the system into an eigenstate of the measurement operator i.e. localizes the particle at one of the sites. The Hamiltonian in contrast makes the system undergo Rabi oscillations. Both protocols can describe the competition between these two processes but the details of the individual trajectories are different. These differences will be discussed in the following.

[1]This model is equivalent to a single spin-1/2 with $\hat{Z}$ measurement. We choose the presented formulation due to its direct relation to the many-body system we study in the subsequent sections.

[2]These simulations where implemented in Julia [144], like all other simulations shown in this thesis.

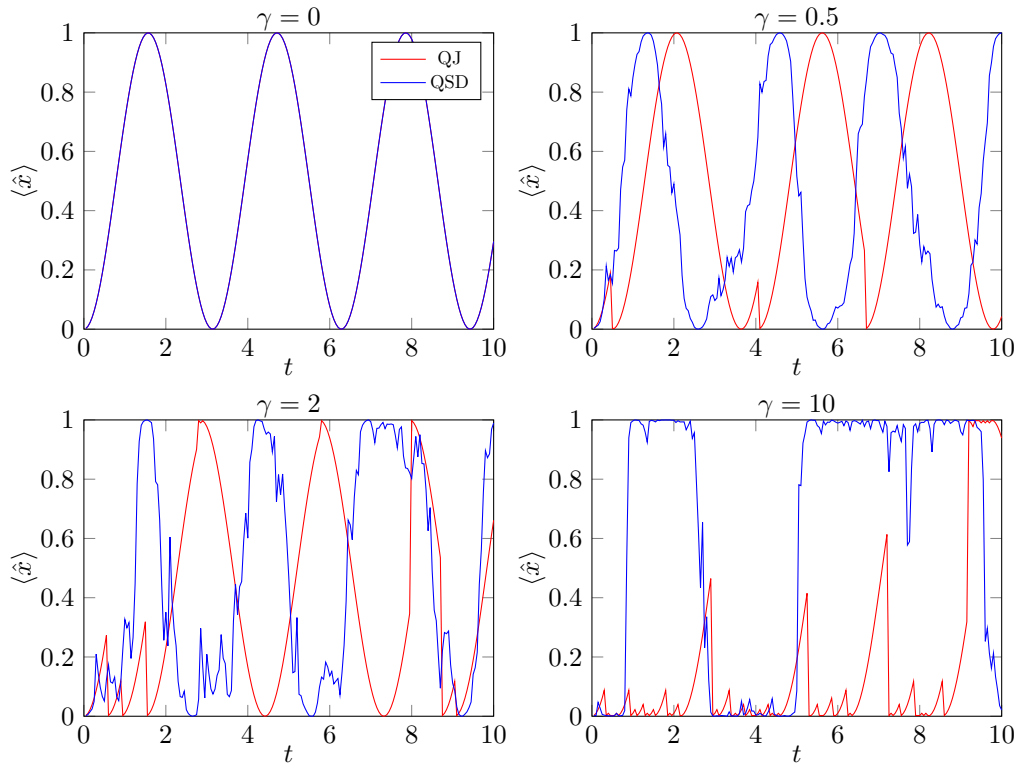

Figure 2: Single trajectories for the QSD and QJ protocol applied to the toy model of a single particle hopping between two sites where the position of the particle is the measured operator. In both cases, the measurement pins the system to a measurement eigenstate while the Hamiltonian lets the particle oscillate between the sites. The scale of the Hamiltonian is set to 1 and we use $dt = 0.05$ in all plots and we always initialize the system in the state $|10\rangle$ i.e. the particle being at position 0.

2.1.1 From projective to continuous measurements

Measurement in absence of unitary dynamics Consider the action of a projective measurement $\hat{O}_\alpha$ on a given pure quantum state $|\psi\rangle$. Any Hermitian operator can be decomposed into a set of projection operators corresponding to the eigenstates of the measurement operator, i.e.

$$\hat{O}_\alpha = \sum_n O_{\alpha,n} \hat{P}_{\alpha,n}, \tag{2.1}$$

where $\hat{P}_{\alpha,n}\hat{P}_{\alpha,m} = \delta_{n,m}\hat{P}_{\alpha,n}, \hat{P}^\dagger_{\alpha,n} = \hat{P}_{\alpha,n}$ and $\sum_n \hat{P}_{\alpha,n} = \hat{1}$. The operators $\hat{P}_{\alpha,n}$ project the system onto an eigenstate of the measurement operator and $O_{\alpha,n} \in \mathbb{R}$ are the corresponding measurement results. For a single realization, according to Born's rule [145], the state evolves in an infinitesimal time step according to

$$|\psi\rangle \to \frac{\hat{P}_{\alpha,n}|\psi\rangle}{\sqrt{\langle\psi|\hat{P}_{\alpha,n}|\psi\rangle}}, \tag{2.2}$$

with a probability

$$\mathcal{P}_\alpha(O_{\alpha,n}) = \langle\psi|\,\hat{P}_{\alpha,n}\,|\psi\rangle, \tag{2.3}$$

and the measurement readout in that case is $O_{\alpha,n}$. This is a very drastic process as can be seen in the toy model, where $\hat{O} = \hat{x}$ i.e. the two projection operators $\hat{P}_\alpha$ are $\hat{n}_1$ and $1 - \hat{n}_1$ and the corresponding measurement readouts O_α are 1 and 0. If the system is initialized in an arbitrary state, in a single infinitesimal time-step it reaches a product state

$$|\psi\rangle = a\,|10\rangle + b\,|01\rangle \to \begin{cases} \frac{a}{|a|}\,|10\rangle\,, & P(0) = |a|^2 \\ \frac{b}{|b|}\,|01\rangle\,, & P(1) = |b|^2 \end{cases}. \tag{2.4}$$

This means, that if we permanently measure, the system is totally pinned to one of the measurement eigenstates. In a many-body setting that corresponds to performing a local measurement at all sites at the same time, which would lead to the same scenario: the system immediately goes into a product state. This is an incarnation of the quantum Zeno effect: measurements freeze the dynamics of a quantum system [146–150]. To study a non-trivial interplay of Hamiltonian and measurement dynamics, there are now two different ways to achieve this, both relying on first discretizing time in steps dt: either we introduce a finite probability of performing a measurement such that we do not measure all $\hat{O}_\alpha$ at the same time, or we perform an incomplete projection everywhere. The first option leads to *strong projective* measurement dynamics while the other one leads to *weak continuous* measurement dynamics. Note that one may also mix the two which allows to study the precise differences emerging [92, 93]. The different limits correspond to different experimental realizations, depending on the time a single measurement takes to be performed compared to the typical time-scale of the Hamiltonian.

Strong measurement time evolution In the QJ protocol, a many-body state $|\psi\rangle$ evolves according to a Hamiltonian $\hat{H}$ and after a time-step dt, we measure a fraction of the measurement operators $\hat{O}_\alpha$ projectively. For any given α, with a probability p_α we measure the observable $\hat{O}_\alpha$ and with a probability $1 - p_\alpha$ we do not. Then we repeat the process. Assuming that all measurement-operators commute $[\hat{O}_\alpha, \hat{O}_\beta] = 0$, the order in which all of the measurements are performed does not matter. The resulting temporal update then reads[3]

$$|\psi_{t+dt}\rangle = e^{-\frac{i}{\hbar}\hat{H}dt} \prod_\alpha \left((1 - m_\alpha) + m_\alpha \sum_n \frac{\delta_{O_\alpha, O_{\alpha,n}} \hat{P}_{\alpha,n}}{\sqrt{\langle\psi_t|\,\hat{P}_{\alpha,n}\,|\psi_t\rangle}} \right) |\psi_t\rangle\,. \tag{2.5}$$

[3]The order of the measurement and Hamiltonian action does not matter because they are applied alternatingly.

We introduced two random variables, $m_\alpha = 1$ with probability p_α and $m_\alpha = 0$ with probability $1 - p_\alpha$ and $O_\alpha = O_{\alpha,n}$ with probability $\langle\psi| \hat{P}_{\alpha,n} |\psi\rangle$. All of these probabilities are uncorrelated: the probability to perform a measurement in the first place is an external ingredient and the different measurement-operators commute. Thus, the outcome of one measurement does not affect the outcome of a different measurement at the same time. Note that p_α should be linear in dt such that the continuous limit $dt \to 0$ is non-trivial. Let us now consider the evolution of the density-operator under this protocol and average over all realizations of the measurement placement, denoted as $\overline{(\dots)}^{\{m_\alpha\}}$. We neglect products $\overline{m_\alpha m_\beta}^{\{m_\alpha\}} \sim dt^2$ for $\alpha \neq \beta$ but we need to keep terms $\overline{m_\alpha^2}^{\{m_\alpha\}} = \overline{m_\alpha}^{\{m_\alpha\}} \sim dt$ which yields

$$\begin{aligned}\overline{d\,|\psi\rangle\langle\psi|}^{\{m_\alpha\}} = \overline{|\psi_{t+dt}\rangle\langle\psi_{t+dt}|}^{\{m_\alpha\}} - |\psi_t\rangle\langle\psi_t| = -\frac{i}{\hbar}[\hat{H}, |\psi\rangle\langle\psi|]dt \\ + \sum_\alpha p_\alpha \left(\sum_{n,m} \frac{\delta_{O_\alpha, O_{\alpha,n}} \hat{P}_{\alpha,n}}{\sqrt{\langle\psi| \hat{P}_{\alpha,n} |\psi\rangle}} |\psi\rangle\langle\psi| \frac{\delta_{O_\alpha, O_{\alpha,m}} \hat{P}_{\alpha,m}}{\sqrt{\langle\psi| \hat{P}_{\alpha,m} |\psi\rangle}} - |\psi\rangle\langle\psi| \right). \quad (2.6)\end{aligned}$$

Next, we take the average over measurement outcomes O_α in that time-step, given a specific input state. Since O_α can only have either read-out $O_{\alpha,n}$ or $O_{\alpha,m}$, assuming that they are different, we only get the diagonal part. The probability to measure a given measurement result is given by the quantum-mechanical expectation value in the given state which yields a cancellation of the normalization and the result simplifies to

$$\frac{1}{dt}\overline{d\,|\psi\rangle\langle\psi|}^{\{m_\alpha\},\{O_\alpha\}} = -\frac{i}{\hbar}[\hat{H}, |\psi\rangle\langle\psi|] + \sum_\alpha \frac{p_\alpha}{dt} \left(\sum_n \hat{P}_{\alpha,n} |\psi\rangle\langle\psi| \hat{P}_{\alpha,n} - |\psi\rangle\langle\psi| \right). \quad (2.7)$$

The crucial result is here that the update is again linear in the state $|\psi\rangle\langle\psi|$ which means that we can now also take an average over all possible trajectories leading to the time-step we are considering, which are defined by the initial state and all previous measurements. This average is *independent* of the state update we just computed. The density operator $\hat{\rho} = \overline{|\psi\rangle\langle\psi|}$ describing the ensemble of all trajectories evolving over time therefore obeys a closed linear equation

$$\partial_t \hat{\rho} = -\frac{i}{\hbar}[\hat{H}, \hat{\rho}] + \sum_\alpha \frac{p_\alpha}{dt} \left(\sum_n \hat{P}_{\alpha,n} \hat{\rho} \hat{P}_{\alpha,n} - \hat{\rho} \right). \quad (2.8)$$

This is in fact a way to represent the Lindblad equation: it is norm-preserving and Markovian. To match it with the usual form, let us assume that the measurement operators are proportional to projectors themselves, $\hat{O}_\alpha = O_\alpha \hat{P}_\alpha$, where $O_\alpha \in \mathbb{R}$. This means that there is a binary measurement outcome which covers a large class of typical local measurements applied to quantum circuits, including particle number operators

and Pauli-operators. This yields

$$\begin{aligned}\partial_t\hat{\rho} &= -\frac{i}{\hbar}[\hat{H},\hat{\rho}] + \sum_\alpha \frac{p_\alpha}{dt}\left(\hat{P}_\alpha\hat{\rho}\hat{P}_\alpha + (1-\hat{P}_\alpha)\hat{\rho}(1-\hat{P}_\alpha) - \hat{\rho}\right)\\ &= -\frac{i}{\hbar}[\hat{H},\hat{\rho}] + \sum_\alpha \frac{p_\alpha}{dt}\left(2\hat{P}_\alpha\hat{\rho}\hat{P}_\alpha - \{\hat{P}_\alpha^2,\hat{\rho}\}\right)\\ &= -\frac{i}{\hbar}[\hat{H},\hat{\rho}] + \sum_\alpha \frac{2p_\alpha}{O_\alpha^2 dt}\left(\hat{O}_\alpha\hat{\rho}\hat{O}_\alpha - \frac{1}{2}\{\hat{O}_\alpha^2,\hat{\rho}\}\right). \end{aligned} \tag{2.9}$$

We can therefore identify $p_\alpha = \frac{O_\alpha^2\gamma_\alpha dt}{2}$ and find the Lindblad equation for measurements

$$\partial_t\hat{\rho} = -\frac{i}{\hbar}[\hat{H},\hat{\rho}] + \sum_\alpha \gamma_\alpha\left(\hat{O}_\alpha\hat{\rho}\hat{O}_\alpha - \frac{1}{2}\{\hat{O}_\alpha^2,\hat{\rho}\}\right). \tag{2.10}$$

The protocol introduced here is realized in measurement-induced dynamics if the time the measurement takes is much shorter than the typical time-scale of the Hamiltonian that evolves the system between measurement events. If the measurement itself takes comparably long or even longer than this typical timescale, we need to resolve the measurement process via an ancilla, as we discuss below. In this case, the random placement of the measurements is not needed and we can measure all operators in parallel because a single time-step does not project the system onto a product state.

Incomplete measurement via ancillas Instead of a direct projective measurement, we here assume that the measurement device takes a finite time to perform the measurement. This is a more realistic description of homodyne detection in relevant experimental settings for MIPTs [40, 151], where the measurement-process happens by a weak coupling of the measured object to a bath which is then read out which takes a finite amount of time. This can be for instance done by coupling the observable to a monitored continuous bath degree of freedom (pointer) or a cavity mode [92, 152, 153]. If the bath is read out before the system is maximally entangled with the measurement device, it undergoes an imperfect projection, as illustrated in Fig. 3.

We here first study a single measurement device and focus on a pointer realization following Ref. [152]. In a single time step, we first add a measurement device $|\psi\rangle \to |\psi\rangle\otimes|\phi\rangle$ where $|\phi\rangle$ is the (normalized) initial state of the measurement device which is not entangled with the system. We treat the measurement device as a single continuous degree of freedom, with 'position' eigenstates $|X\rangle$ of the bath operator $\hat{X} = \hat{X}^\dagger$ and 'momentum' eigenstates $|Q\rangle$ of the conjugate momentum $\hat{Q} = \hat{Q}^\dagger$ with canonical commutation relations $[\hat{X},\hat{Q}] = i\hbar$. We then couple the system and the pointer for a time dt using a Hamiltonian $\hat{H}_{\rm sb} = \omega\hat{O}\otimes\hat{Q}$, where ω sets the scale and

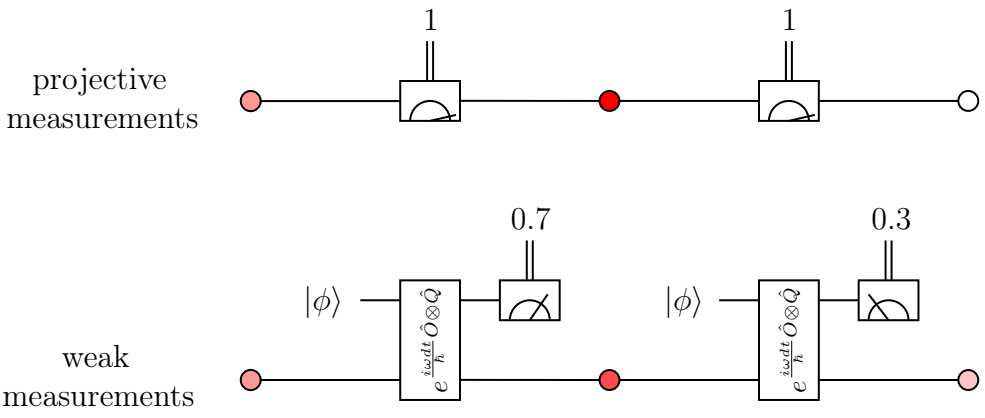

Figure 3: If a projective measurement is performed on an arbitrary state, after that measurement, the state is in an eigenstate of the measurement operator. Therefore, a repeated measurement of the same observable will always yield the same readout. For weak measurements, we first couple the system to an auxiliary degree of freedom which is then read out. This extracts information about the system when the measurement on the auxiliary system is performed but it does not fully project the system onto an eigenstate. Therefore, a second measurement of the same observables might result in a different measurement outcome as well as a different post measurement state.

dimension of the coupling[4] and $\hat{O}$ is an arbitrary Hermitian operator acting on the system. This is chosen because the application of the Hamiltonian for a time dt,

$$|\psi\rangle \to e^{-\frac{i\omega dt}{\hbar}\hat{O}\otimes\hat{Q}} |\psi\rangle \otimes |\phi\rangle \,, \tag{2.11}$$

essentially shifts the initial state of the pointer depending on the state of the system $|\psi\rangle$. $\hat{O}$ has to be Hermitian to ensure that the Hamiltonian is Hermitian. We can always choose a proper basis of the pointer to bring the coupling Hamiltonian into such a form. After that shift, we measure the state of the pointer in the 'position' basis, i.e. the operator $\hat{X}$. For a measurement-outcome X, the resulting state is then given by the normalized projection $\hat{1}\otimes|X\rangle\langle X|$ of the state. Without the normalization, we obtain for the system state after the measurement

$$|\psi\rangle \to \underbrace{\langle X| e^{-\frac{i\omega dt}{\hbar}\hat{O}\otimes\hat{Q}} |\phi\rangle}_{\hat{P}(X)} |\psi\rangle \,. \tag{2.12}$$

Note that due to the measurement of the pointer, it is in an eigenstate of $\hat{X}$ which means that we recover a product state of system and pointer such that we can consider system and bath to be decoupled again and restart the same procedure with a re-initialized pointer. Therefore, $\hat{P}(X)$ is again an operator acting only on the system without entangling it with the pointer. The probability of finding the readout X and

[4]We could of course equivalently exchange the roles of position and momentum. The important point is, that the observable couples to either of them and after the coupling, the other one is measured.

therefore finding the measurement process

$$|\psi\rangle \to \frac{\hat{P}(X)\,|\psi\rangle}{||\hat{P}(X)\,|\psi\rangle\,||}, \tag{2.13}$$

is given by its norm as

$$\mathcal{P}(X) = ||\hat{P}(X)\,|\psi\rangle\,||^2 = \langle\psi|\,\hat{P}^\dagger(X)\hat{P}(X)\,|\psi\rangle\,. \tag{2.14}$$

Next, we may fix proper choices of the measurement basis and initial states to make the process useful in the sense that it extracts information about the system. If we would measure in the same basis as the coupling $\hat{Q}$ to the system, the result would be trivial,

$$\langle Q|\,e^{-\frac{i\omega dt}{\hbar}\hat{L}\otimes\hat{Q}}\,|\phi\rangle = \langle Q|0\rangle\,e^{-\frac{i\omega Q dt}{\hbar}.\hat{O}} \tag{2.15}$$

The overlap $\langle Q|0\rangle$ is independent of the state $|\psi\rangle$ on which the operation acts and the exponential does not affect the norm of the state. Hence, the measurement-outcome (Q in this case) does not depend on the state and we therefore do not extract any information about the state. Therefore, we need to measure an operator that does not commute with $\hat{Q}$, for which we choose $\hat{X}$ for simplicity. Furthermore, we can use that $\hat{O}$, as a Hermitian operator, can be decomposed into a complete set of projectors $\{\hat{P}_n\}_n$ onto its eigenstates, $\hat{O} = \sum_n O_n\hat{P}_n$. O_n are the eigenvalues of $\hat{O}$. This allows to simplify

$$\hat{P}(X) = \sum_n \hat{P}_n\,\langle X|\,e^{-\frac{i\omega O_n dt}{\hbar}\hat{Q}}\,|\phi\rangle\,. \tag{2.16}$$

Now, we can employ the action of the projection onto a state of the pointer: it shifts a given state $|X'\rangle \to |X' - \omega O_n dt\rangle$ and then we need to take the overlap with the output state. If we initialized the pointer in a position eigenstate, for instance $|\phi\rangle = |X = 0\rangle$, the overlap would only be non-zero for exactly $X = -\omega O_n dt$. This means, that the system is projected onto an eigenstate of $\hat{O}$ by $\hat{P}_n$ and we can infer the corresponding eigenvalue O_n from the measurement-result of the pointer as $O_n = -X/\omega dt$. Therefore we find that a single time-step realizes a projective measurement of the system operator $\hat{O}$. However, this distribution is delta-peaked since the measurement apparatus has continuous read-outs while the typical system observables have discrete measurement results. However, we now have a simple way of generalizing this problem to a continuous measurement by introducing a finite width for the initial state of the pointer, using a normalized Gaussian state with width σ,

$$|\phi\rangle = \frac{1}{(2\pi\sigma^2)^{1/4}}\int dX e^{-\frac{X^2}{4\sigma^2}}\,|X\rangle\,. \tag{2.17}$$

Hence, the generalized projector becomes

$$\hat{P}(X) = \frac{1}{(2\pi\sigma^2)^{1/4}} \sum_n \hat{P}_n e^{-\frac{(X-\omega O_n dt)^2}{4\sigma^2}} = \frac{1}{(2\pi\sigma^2)^{1/4}} e^{-\frac{(X-\omega\hat{O}dt)^2}{4\sigma^2}}. \tag{2.18}$$

The result is now peaked around all eigenvalues of the operator $\hat{O}$ i.e. the possible measurement results. While X is read off from the pointer, we can identify $J = \frac{X}{\omega dt}$ to be the proper random variable that takes the eigenvalues in the limit of a projective measurement. Hence, we rewrite the generalized measurement operator as

$$\hat{P}(J) = \mathcal{N} e^{-\gamma dt(J-\hat{O})^2} \tag{2.19}$$

where $\gamma = \frac{\omega^2}{4\sigma^2} > 0$ describes the strength of the measurement. The normalization condition is fixed by assuming a dimensionless measurement-result and using an adapted integration measure for the probability distribution. This yields the quantum state diffusion protocol

$$|\psi\rangle \to \frac{\hat{P}(J)\,|\psi\rangle}{||\hat{P}(J)\,|\psi\rangle\,||}, \qquad \hat{P}(J) = \left[\frac{2\gamma dt}{\pi}\right]^{1/4} e^{-\gamma dt(J-\hat{O})^2}. \tag{2.20}$$

To get a better intuition about this result, let us decompose $\hat{O}$ again in terms of its eigenvalues and projections onto the eigenstates,

$$\hat{P}(J) = \left[\frac{2\gamma dt}{\pi}\right]^{1/4} \sum_n e^{-\gamma dt(J-O_n)^2} \hat{P}_n. \tag{2.21}$$

The imperfect projection maps a state onto a superposition of eigenstates of $\hat{O}$, with larger weight for states with an eigenvalue close to J and smaller weight if the eigenvalue is far away from J. For $\gamma dt \to \infty$, this becomes more and more peaked around the eigenvalues. The probability-distribution after the measurement is

$$\mathcal{P}(J) = \langle\psi|\,\hat{P}^\dagger(J)\hat{P}(J)\,|\psi\rangle = \sqrt{\frac{2\gamma dt}{\pi}} \sum_n e^{-2\gamma dt(J-O_n)^2}\,\langle\psi|\,\hat{P}_n\,|\psi\rangle\,. \tag{2.22}$$

In the limit $\gamma dt \to \infty$, this distribution is δ-peaked around the eigenvalues of $\hat{O}$ such that we recover the projective measurement of this operator. For $\gamma dt \to 0$, the measurement process becomes deterministic and just acts as unity on the state. Finite γdt interpolate smoothly between the two cases and successive application of the generalized projection continuously collapses the state into a measurement eigenstate (see Fig. 2). J is the measurement readout during the process of measuring. This is what we understand by weak continuous measurements.

Combining weak measurements and Hamiltonian evolution yields the evolution

$$|\psi_{t+dt}\rangle = \frac{e^{-\frac{i}{\hbar}\hat{H}dt}\hat{P}(\{J_{\alpha,t}\}_\alpha)\,|\psi_t\rangle}{\left|\left|\hat{P}(\{J_{\alpha,t}\}_\alpha)\,|\psi_t\rangle\right|\right|} \tag{2.23}$$

Where $\hat{H}$ is the Hamiltonian operator and we allow for multiple measured observables $\hat{O} \to \hat{O}_\alpha$ with measurement rates $\gamma \to \gamma_\alpha$ in a many-body setting that however shall be commuting $[\hat{O}_\alpha, \hat{O}_\beta] = 0$ as before, such that $\hat{P}(\{J_{\alpha,t}\}_\alpha) = \prod_\alpha \hat{P}_\alpha(J_{\alpha,t})$ is unambiguous. In the limit $dt \to 0$, this can be written as a stochastic Schrödinger equation. To see this, let us again focus on a single measured operator, as simultaneous measurement of commuting operators does not interfere. Using the decomposition in terms of projections allows to evaluate the probability distribution for the measurement readout. It can be characterized in terms of its moments,

$$\overline{J} = \sum_n \langle \hat{P}_n \rangle \sqrt{\frac{2\gamma dt}{\pi}} \int dJ J e^{-2\gamma dt(J-O_n)^2} = \langle \hat{O} \rangle, \tag{2.24}$$

$$\overline{J^2} = \sum_n \langle \hat{P}_n \rangle \sqrt{\frac{2\gamma dt}{\pi}} \int dJ J^2 e^{-2\gamma dt(J-O_n)^2} = \langle \hat{O}^2 \rangle + \frac{1}{4\gamma dt}. \tag{2.25}$$

The overbar here denotes the average over weak measurements of a given pure state $|\psi\rangle$. This means that while the first moment of the current just yields the quantum-mechanical expectation value of the monitored system operator, the higher moments capture additional fluctuations since we cannot extract the full information about all moments in finite time[5]. This motivates to represent the random variables J_α as

$$J_\alpha = \langle \hat{O}_\alpha \rangle + \frac{dW_\alpha}{\sqrt{4\gamma_\alpha dt}}, \tag{2.26}$$

where $\overline{dW_\alpha} = 0$ and $\overline{dW_\alpha dW_\beta} = \delta_{\alpha,\beta} dt$ is Gaussian white noise. Since the distribution of weak measurement read-outs $\mathcal{P}(\{J_\alpha\})$ is Gaussian, both formulations are equivalent. However, we may now expand the state update in powers of dW_α and use the Itō-calculus to derive a stochastic Schrödinger equation. To do so, it is convenient to again introduce $\hat{M}_\alpha = \hat{O}_\alpha - \langle \hat{O}_\alpha \rangle$. We find

$$\begin{aligned}
\hat{P}_\alpha\,|\psi\rangle &= \sqrt{\frac{2\gamma_\alpha dt}{\pi}} e^{-\gamma_\alpha dt(\hat{M}_\alpha - dW_\alpha/\sqrt{4\gamma_\alpha dt})^2}\,|\psi\rangle \\
&= \sqrt{\frac{2\gamma_\alpha dt}{\pi}} e^{-\frac{1}{4}} e^{\sqrt{\gamma_\alpha}\hat{M}_\alpha dW_\alpha - \gamma_\alpha dt \hat{M}_\alpha^2}\,|\psi\rangle \\
&= \sqrt{\frac{2\gamma_\alpha dt}{\pi}} e^{-\frac{1}{4}} \left(1 + \sqrt{\gamma_\alpha}\hat{M}_\alpha dW_\alpha - \frac{\gamma_\alpha}{2}\hat{M}_\alpha^2 dt + \mathcal{O}(dt^{3/2})\right)|\psi\rangle\,.
\end{aligned} \tag{2.27}$$

[5]For $\gamma dt \to \infty$, projective and weak measurements coincide which is signalled by $\overline{J^m} = \langle \hat{O}^m \rangle \forall m$

We used that in the Itō-calculus for $dt \to 0$, $dW_\alpha dW_\beta = \delta_{\alpha\beta} dt$[6]. The global prefactor drops out of the stochastic time-evolution as it appears both in the denominator and the numerator. When taking the product over all projections, we always pair different α such that $dW_\alpha dW_\beta = 0$ and all other product terms are higher than linear order in dt, such that

$$\prod_\alpha \hat{P}_\alpha |\psi\rangle \propto \left(1 + \sum_\alpha \sqrt{\gamma_\alpha} \hat{M}_\alpha dW_\alpha - \frac{1}{2} \sum_\alpha \gamma_\alpha \hat{M}_\alpha^2 dt + \mathcal{O}(dt^{3/2})\right) |\psi\rangle . \tag{2.28}$$

When taking the norm of this state, we find that $\langle \hat{M}_\alpha \rangle = 0$ by definition and the $dW_\alpha dW_\beta$ term from taking the square of the bracket exactly cancels out the other term in $\mathcal{O}(dt)$ such that the norm of the state is just the global prefactor up to $\mathcal{O}(dt^{3/2})$. Hence, we obtain

$$|\psi_{t+dt}\rangle = e^{-\frac{i}{\hbar}\hat{H}dt} \left(1 + \sum_\alpha \sqrt{\gamma_\alpha} \hat{M}_\alpha dW_\alpha - \frac{1}{2} \sum_\alpha \gamma_\alpha \hat{M}_\alpha^2 dt + \mathcal{O}(dt^{3/2})\right) |\psi_t\rangle , \tag{2.29}$$

which yields the stochastic Schrödinger equation

$$d|\psi\rangle = \left(\left(-\frac{i}{\hbar}\hat{H} - \frac{1}{2} \sum_\alpha \gamma_\alpha \hat{M}_\alpha^\dagger \hat{M}_\alpha\right) dt + \sum_\alpha \sqrt{\gamma_\alpha} \hat{M}_\alpha dW_\alpha\right) |\psi\rangle . \tag{2.30}$$

The corresponding time-evolution of the linearly averaged density operator $\hat{\rho}_t = \overline{|\psi_t\rangle \langle\psi_t|}$, where $\overline{(...)}$ denotes the average over realizations of the measurement outcomes along the evolution of the system, $J_{\alpha,\tau}$ for $\tau < t$, is

$$\partial_t \hat{\rho}_t = -\frac{i}{\hbar}[\hat{H}, \hat{\rho}_t] - \frac{1}{2} \sum_\alpha \gamma_\alpha [\hat{O}_\alpha, [\hat{O}_\alpha, \hat{\rho}_t]]. \tag{2.31}$$

This means that the average over measurement outcomes yields a quantum master equation with Hermitian jump operators, which coincides with the QJ protocol. Hence, on the level of the trajectory-averaged density operator, the QSD and the QJ protocol cannot be distinguished, and are described by a master equation, which allows in the Toy model to solve the evolution analytically, see Fig. 4 Generically, if all degrees of freedom of the system are monitored at a finite rate, the only stable stationary solution of the quantum master equation for Hermitian Lindblad operators is $\hat{\rho} \sim \hat{1}$ [36–39], e.g. a featureless infinite temperature state. That means that all information on quantum entanglement and correlations within single states during the dynamics is erased by the linear averaging. The microscopic model of fermions under monitoring of the local occupation number on all sites falls into this class of systems and therefore we need

[6]Note that the term linear in dt vanishes due to cancellation of the first and second order contribution in the expansion of the exponential.

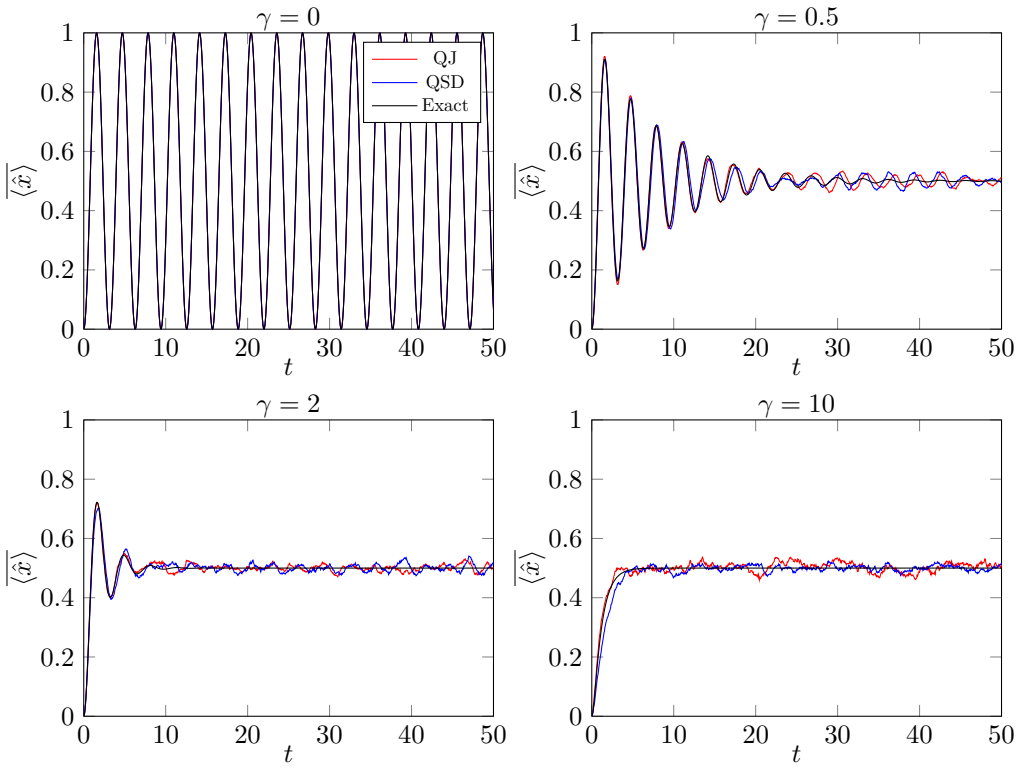

Figure 4: Taking the average over 1000 runs shows that indeed both QSD and QJ describe the relaxation towards a trivial state, where we have no information about the position of the particle. While the stationary state after long times does not depend on γ as long as $\gamma > 0$, the time-scale on which the oscillations due to the hopping are washed out does depends on it. The deviations of the two curves show, that the quality of the approximation of the density operator depends on the choice of the unraveling, the number of trajectories and the time until which we simulate. For comparison, we also show the exact solution.

to go beyond this to be able to compute non-trivial observables such as entanglement. We therefore need to consider higher orders in $|\psi_t\rangle \langle\psi_t|$ before averaging, i.e. a replica construction. This insight is the backbone of any analytical approach to understand measurement-induced phases and phase transitions both in generic circuit models and the specific continuous models that we consider here in this thesis. Therefore, we begin our comparison of the complementary approaches to the problem of free monitored fermions by constructing a replica field theory for the weak measurement protocol without relying on the properties of the specific microscopic model. Before doing so, we first discuss an alternative way to obtain the QSD protocol by unraveling a generic Lindblad equation.

2.1.2 Unraveling of a quantum master equation

General idea Here we follow the references [139–143]. The idea of unravelings is to take a top down approach, starting from a given quantum master equation. We

construct a Markovian, stochastic, norm-preserving evolution equation for pure states $|\psi(t)\rangle$, that results in the desired master equation for the associated trajectory-averaged density operator $\hat{\rho}(t) = \overline{|\psi(t)\rangle \langle\psi(t)|}$. For the precise formulation, there is a freedom to choose a particular unraveling procedure but the benchmark is that the density operator evolves according to the Lindblad equation that is supposed to be solved [71, 123, 137, 138, 154–156],

$$\partial_t \hat{\rho} = -\frac{i}{\hbar}[\hat{H}, \hat{\rho}] + \sum_\alpha \gamma_\alpha \left(\hat{L}_\alpha \hat{\rho} \hat{L}_\alpha^\dagger - \frac{1}{2} \left\{ \hat{L}_\alpha^\dagger \hat{L}_\alpha, \hat{\rho} \right\} \right), \tag{2.32}$$

where $\hat{H} = \hat{H}^\dagger$ is the Hamiltonian, $\gamma_\alpha \geq 0$ are parameters describing the strength and $\hat{L}_\alpha$ with $\operatorname{tr} \hat{L}_\alpha^\dagger \hat{L}_\beta = \delta_{\alpha\beta}$ are operators that describe the type of the coupling to the environment.

In our toy model, where the particle's position $\hat{x}$ is measured, it is natural to consider a single Lindblad operator $\hat{L} = \hat{x}$. However, since $\hat{x} = \hat{x}^\dagger$ is Hermitian, the state $\hat{\rho} = \frac{1}{\sqrt{2}}(|01\rangle \langle 01| + |10\rangle \langle 10|) \simeq \hat{1}$ is the only stationary solution to eq. (2.32). Thus, after a quench the system evolves into a featureless infinite temperature state that does not depend on γ.

This scenario should now be reproduced by a time-evolution for pure states, which have a lower computational complexity as compared to density matrices of mixed states. The starting point should be here the Schrödinger equation [157] describing closed systems. For $dt \to 0$ it reads

$$d|\psi\rangle = -\frac{i}{\hbar} dt \hat{H} |\psi\rangle, \tag{2.33}$$

which reproduces the Hamiltonian part[7] of the quantum master equation (2.32) for $\hat{\rho}(t)$, but does not explain the dissipative term. The Schrödinger equation can be derived as the general form of a time-evolution that fulfills the following properties

(i) It is norm-preserving $\langle\psi|\psi\rangle = 1$.

(ii) It is local in time and has no memory of the past evolution of $|\psi\rangle$.

(iii) It is continuous in the sense that $\lim_{dt\to 0} \langle\psi(t+dt)|\psi(t)\rangle = 1$.

(iv) It is linear in $|\psi\rangle$.

(v) It is deterministic.

All of these conditions are fundamental to describe closed quantum systems. However, as we just intend to reproduce the correct open system dynamics in an averaged sense,

[7] Note that the average over trajectories only affects the initial conditions as the evolution itself is deterministic.

we may explicitly break some of these constraints. Condition (i) is necessary to have an interpretation of $|\psi\rangle$ as an actual quantum state describing a single realization of the system coupled to the bath. Therefore we should not violate it. Condition (ii) shall also be kept as the quantum master equation is Markovian which is a property that should be shared by the underlying dynamics of pure states in the chosen unraveling. Additionally, simulating a time-evolution with explicit memory is computationally hard and should be avoided. Condition (iii) may be lifted depending on the specific case but in order to treat measurements and unitary dynamics on an equal footing it is useful to insist on it. Therefore, we will in the following explicitly deviate from conditions (iv) and (v).

Let us first explicitly break condition (v) by making the following ansatz for a stochastic Schrödinger equation,

$$d\,|\psi\rangle = \left(\hat{A}dt + \sum_\alpha \hat{B}_\alpha dW_\alpha\right)|\psi\rangle\,. \tag{2.34}$$

$\hat{A}$ describes the deterministic part of the dynamics and $\hat{B}_\alpha$ occur coupled to a stochastic variable dW_α. We anticipate a single random variable for every operator coupling to an environment. To preserve condition (iii), $dW_\alpha \sim dt^p$ should vanish[8] in the limit $dt \to 0$ such that we take independent real[9] Gaussian random variable, characterized by $\overline{dW_\alpha} = 0$ and $\overline{dW_\alpha dW_\beta} = dt^{2p}\delta_{\alpha\beta}$. Next, we need to constrain $\hat{A}$ and $\hat{B}_\alpha$ such that condition (i) is valid. Consider the variation

$$d\,\langle\psi|\psi\rangle = \langle\psi|\,dt(\hat{A}+\hat{A}^\dagger) + \sum_\alpha dW_\alpha(\hat{B}_\alpha+\hat{B}_\alpha^\dagger) + \sum_{\alpha,\beta} dW_\alpha dW_\beta \hat{B}_\alpha^\dagger\hat{B}_\beta\,|\psi\rangle\,, \tag{2.35}$$

which needs to vanish up to $\mathcal{O}(dt)$. In the limit $dt \to 0$, $dW_\alpha dW_\beta \to \overline{dW_\alpha dW_\beta}$. We choose $p = 1/2$, i.e. a Wiener process, such that the two deterministic terms survive in the limit $dt \to 0$ and find

$$d\,\langle\psi|\psi\rangle = \langle\psi|\,dt\left(\hat{A}+\hat{A}^\dagger+\sum_\alpha \hat{B}_\alpha^\dagger\hat{B}_\alpha\right) + \sum_\alpha dW_\alpha(\hat{B}_\alpha+\hat{B}_\alpha^\dagger)\,|\psi\rangle\,. \tag{2.36}$$

Both the deterministic term $\sim dt$ and all the fluctuating terms need to vanish independently to preserve the norm of the state. While this can be fulfilled in choosing $\hat{A}$ and $\hat{B}_\alpha$ independently of the state, which also trivially fulfills condition (ii), let us here allow for *state-dependent* operators. It turns out that this is necessary to obtain the

[8] for some parameter $p > 0$

[9] Alternatively, one may use complex noise to reproduce the same Lindblad equation but the resulting SSE does not describe measurements.

Lindblad equation including the jump operators. We find the constraints

$$0 = \langle\psi| \hat{A} + \hat{A}^\dagger + \sum_\alpha \hat{B}_\alpha^\dagger \hat{B}_\alpha |\psi\rangle , \tag{2.37}$$

$$0 = \langle\psi| \hat{B}_\alpha + \hat{B}_\alpha^\dagger |\psi\rangle \qquad \forall\alpha. \tag{2.38}$$

On the other hand, we may compute the time-evolution of the density operator, averaged over noise realizations,

$$\partial_t \hat{\rho} = \hat{A}\hat{\rho} + \hat{\rho}\hat{A}^\dagger + \sum_\alpha \hat{B}_\alpha \hat{\rho} \hat{B}_\alpha^\dagger. \tag{2.39}$$

Any operator can be written in terms of a Hermitian and an anti-Hermitian operator. We use this to rewrite $\hat{A} = -\frac{i}{\hbar}\hat{H} - \frac{1}{2}\hat{C}$ where both $\hat{H}$ and $\hat{C}$ are Hermitian operators. This yields

$$\partial_t \hat{\rho} = -\frac{i}{\hbar}[\hat{H}, \hat{\rho}] + \sum_\alpha \hat{B}_\alpha \hat{\rho} \hat{B}_\alpha^\dagger - \frac{1}{2}\{\hat{C}, \hat{\rho}\}. \tag{2.40}$$

To match this with the Lindblad equation, the only choice of the operators assuming that they do not depend on the state can be read off as $\hat{H}$ being the Hamiltonian, $\hat{B}_\alpha = \sqrt{\gamma_\alpha}\hat{L}_\alpha$ and $\hat{C} = \sum_\alpha \hat{B}_\alpha^\dagger \hat{B}_\alpha$. However, this violates the normalization constraint. While eq. (2.37) is still fulfilled, $\hat{L}_\alpha$ is in general not anti-Hermitian and therefore eq. (2.38) is violated. Therefore, the operators $\hat{A}$ and $\hat{B}_\alpha$ need to depend on the state itself, which makes the equation non-linear. This also matches the intuition that a quantum measurement is a statistical operation that depends on the state before the measurement is performed in a nonlinear way. The precise way of choosing the operators is however not unique and for the sake of a simple numerical tool to simulate quantum master equations, it is reasonable to assume a simple representation. To solve eq. (2.38), we therefore apply a shift

$$\hat{B}_\alpha = \sqrt{\gamma_\alpha} \underbrace{\left(\hat{L}_\alpha - \frac{1}{2}\langle \hat{L}_\alpha + \hat{L}_\alpha^\dagger \rangle\right)}_{\hat{M}_\alpha}. \tag{2.41}$$

This choice was used because it does not introduce any additional operator and, if applied to $\hat{C}$ accordingly, leaves both the form of the Lindblad equation for the trajectory-averaged state and the other normalization condition unaffected for an arbitrary choice of $\hat{L}_\alpha$. Therefore, we conclude that we may use the stochastic and non-linear equation,

$$d|\psi\rangle = \left(\left(-\frac{i}{\hbar}\hat{H} - \frac{1}{2}\sum_\alpha \gamma_\alpha \hat{M}_\alpha^\dagger \hat{M}_\alpha\right) dt + \sum_\alpha \sqrt{\gamma_\alpha}\hat{M}_\alpha dW_\alpha\right)|\psi\rangle . \tag{2.42}$$

In the case of Hermitian Lindblad operators $\hat{L}_\alpha = \hat{L}_\alpha^\dagger = \hat{O}_\alpha$, we find

$$\hat{M}_\alpha = \hat{M}_\alpha^\dagger = \hat{O}_\alpha - \langle \hat{O}_\alpha \rangle. \tag{2.43}$$

Averaging this stochastic evolution over trajectories yields the Lindblad time-evolution as we demonstrated for the toy model in Fig. 4. Note in particular, that the unraveling that was purely based on minimizing the computational complexity of the time evolution and the assumption that Gaussian white noise implements the coupling to a bath exactly coincides with the explicit construction of a time evolution due to weak measurements that describes an actual physical scenario.

Interpretation of the result as a measurement process In this derivation, we never used that the open system dynamics resembles measurements and the unraveling was entirely based on assumptions (i)-(v) and simplicity of the result as guiding principle. Nevertheless, we saw that the resulting SSE matches explicit derivations with the interpretation of the Lindblad operators as monitored quantities and therefore describes measurement. This is however only well defined for Hermitian operators and it does not mean that unravelings by themselves in general describe physical reality beyond the average density operator, as illustrated in Fig. 5. We can still recognize

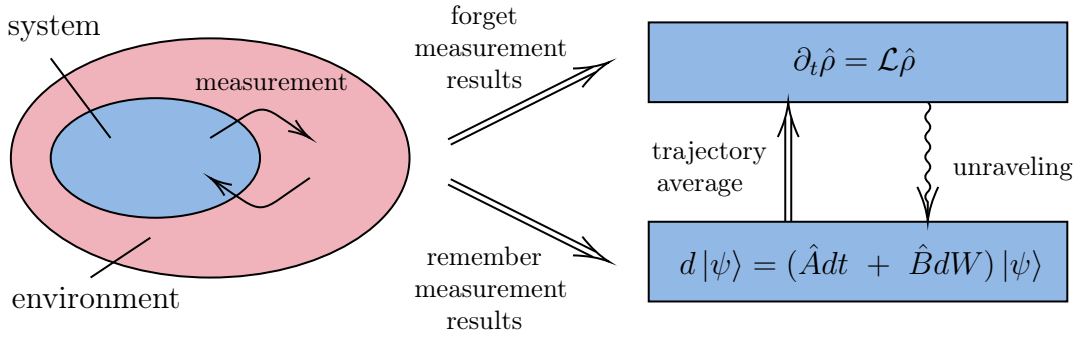

Figure 5: Construction of the QSD protocol via different paths. The system that we want to describe couples to its environment via measurements. If the measurement read-outs are not recorded, this is equivalent to a Lindblad quantum master equation for the reduced density operator of the system $\hat{\rho}$. If they are recorded, we know the pure state of the system $|\psi\rangle$ at all times. The randomness of the measurement read-outs results in a stochastic Schrödinger time evolution. Taking the trajectory average uniquely yields the Lindblad equation. The opposite direction is however not unique (symbolized by the wiggled arrow) as there exist different unravelings for the same master equation.

that qualitatively, this unraveling describes the interplay of measurements and unitary dynamics which we can specifically see in the different limiting cases. Consider first all $\gamma_\alpha = 0$. In this case, the state just undergoes deterministic unitary dynamics. In the opposite case of $\hat{H} = 0$, the state evolves stochastically. This evolution stops as soon

as $\hat{O}_\alpha |\psi\rangle = \langle\psi| \hat{O}_\alpha |\psi\rangle |\psi\rangle$ which means that $|\psi\rangle$ is an eigenstate of $\hat{O}_\alpha$. This is typical for a measurement of an operator $\hat{O}_\alpha$. Besides that, these states are also attractive fixed points of the average dynamics of the state. This can be seen by studying the second cumulant of $\hat{O}_\alpha$ in a given state:

$$C_{\alpha,\beta} \equiv \langle \hat{M}_\alpha \hat{M}_\beta \rangle = \langle \hat{O}_\alpha \hat{O}_\beta \rangle - \langle \hat{O}_\alpha \rangle \langle \hat{O}_\beta \rangle. \tag{2.44}$$

This vanishes for any eigenstate of all $\hat{O}_\alpha$ and it is positive for any state that is not an eigenstate. Therefore it is a good measure for the proximity to an eigenstate of $\hat{O}_\alpha$. When setting $\hat{H} = 0$, we find

$$\begin{aligned} dC_{\alpha,\beta} = -4 \sum_\delta \gamma_\delta dt C_{\alpha,\delta} C_{\beta,\delta} + 2 \sum_\delta dW_\delta \sqrt{\gamma_\delta} (\langle \hat{O}_\alpha \hat{O}_\beta \hat{O}_\delta \rangle + 2 \langle \hat{O}_\alpha \rangle \langle \hat{O}_\beta \rangle \langle \hat{O}_\delta \rangle \\ - \langle \hat{O}_\alpha \rangle \langle \hat{O}_\beta \hat{O}_\delta \rangle - \langle \hat{O}_\alpha \hat{O}_\beta \rangle \langle \hat{O}_\delta \rangle - \langle \hat{O}_\alpha \hat{O}_\delta \rangle \langle \hat{O}_\beta \rangle). \end{aligned} \tag{2.45}$$

This generates a hierarchy of coupled equations for higher order cumulants of the observables which makes it impossible to solve the average evolution exactly. The toy model is a special one for that matter: Since the evolution is Gaussian even in the presence of the measurement, if initialized in a Gaussian state, the third cumulant vanishes and therefore the stochastic part of the time evolution of the second cumulant vanishes. In this case, we only measure a single operator $\hat{x} = \hat{n}_1$ such that there is just a single cumulant which obeys the closed equation $\partial_t C = -4\gamma C^2$ which asymptotically behaves as $C \simeq \frac{1}{4\gamma t}$. Hence, the QSD unraveling predicts that the second cumulant algebraically vanishes, localizing the particle at either 0 or 1. This phenomenologically describes a continuous measurement. This becomes apparent, when this is compared to a projective measurement. In this case, in a single time-step the state is projected onto an eigenstate of the measurement operator, such that the particle localizes immediately. This operation is here stretched over a time-scale $\sim 1/\gamma$. In Fig. 6, we demonstrate the relaxation of the covariance to its stationary state in the presence of the Hamiltonian. Let us now return to the general case. As long as the state is close to a Gaussian one, we can neglect the higher cumulants and find

$$\partial_t C_{\alpha,\beta} \approx -4 \sum_\delta \gamma_\delta C_{\alpha,\delta} C_{\beta,\delta}. \tag{2.46}$$

Assuming no initial covariance between different operators, this can be trivially solved and we find

$$C_{\alpha,\alpha} = \frac{1}{\frac{1}{C_{\alpha,\alpha,0}} + 4\gamma_\alpha t} \simeq \frac{1}{4\gamma_\alpha t}. \tag{2.47}$$

$C_{\alpha,\beta,0}$ is here the covariance at an initial time $t = 0$. We therefore find that the action of the Hermitian Lindblad operators $\hat{O}_\alpha$ indeed corresponds to a measurement that is

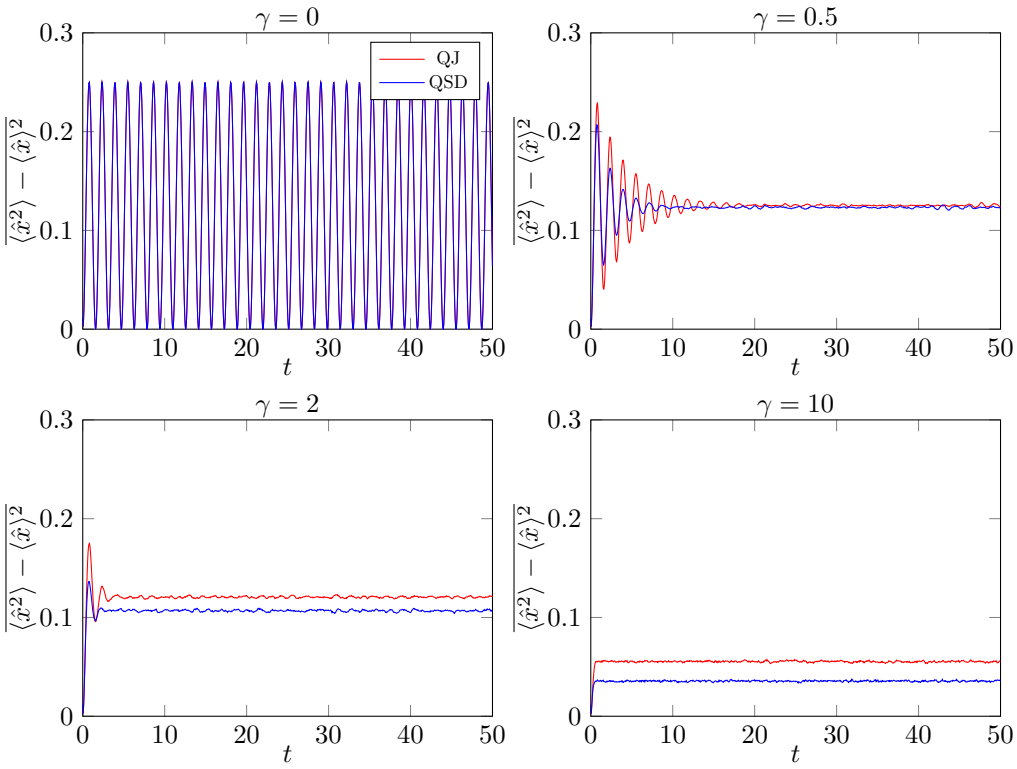

Figure 6: The covariance of the position of the particle in the toy model is an example for which the stationary result depends on the measurement strength. This happens because the observable is non-linear in the density-operator and therefore contains information about trajectories beyond the regular average. Indeed, we find that especially for strong measurement there is also a clear difference between the QSD and QJ result even though they describe the same evolution on the level of the linear average, see Fig. 4. In this plot, we show the average over 10000 trajectories.

spread out over a time $\sim 1/\gamma_\alpha$. If this is combined with the Hamiltonian evolution, QSD therefore describes a continuous protocol which involves measurement and unitary dynamics on equal footing.

In this section, we reviewed the origin of the QSD and QJ stochastic Schrödinger equations and argued that both unravelings of generic quantum master equations with Hermitian Lindblad operators describe measurements. While in the case of QSD, the measurement takes a finite time to collapse the system into an eigenstate, which enables a competition between the Hamiltonian and the measurement, this is achieved by a random placement of instantaneous projective measurements in the QJ protocol. It is also possible to interpolate between the two limits by introducing a random placement of measurement-operators and a finite measurement time [92, 93]. Throughout this work, we want to focus on the two limiting cases for simplicity. We also demonstrated the effect on the two-site toy model where the essential features of the different unravelings already appear and we showed the differences and similarities numerically (see Figs. 2,4,6). In particular, we realized that in generic systems that evolve due to mea-

surements, the linearly averaged density operator behaves trivially in the stationary state. Therefore, we need to introduce a framework in which effects that can only be seen in the unravelings are captured. Therefore, in the following chapter, we introduce the replica formalism for measurement-induced dynamics.

2.2 Replica-approach to the QSD protocol

2.2.1 Structure of non-trivial observables

To motivate the replica construction, let us first discuss observables in the setting described above. Usually the state of a quantum system is characterized by the expectation value of some observable $\hat{Q} = \hat{Q}^\dagger$ in the given state at some time t,

$$\langle \hat{Q} \rangle_t = \langle \psi_t | \, \hat{Q} \, | \psi_t \rangle \, . \tag{2.48}$$

Since $|\psi_t\rangle$ is a fluctuating object, the corresponding experimentally accessible quantity is the average of this object with respect to all possible realizations of the protocol,

$$Q_t = \overline{\langle \hat{Q} \rangle_t} = \overline{\mathrm{Tr}\, \hat{Q} \, |\psi_t\rangle \, \langle \psi_t|} = \mathrm{Tr}\, \hat{Q} \hat{\rho}_t \to \mathrm{Tr}\, \hat{Q} / \mathrm{Tr}\, \hat{1}. \tag{2.49}$$

In the last step, we used that in monitored systems, generically the density operator approaches an infinite temperature state.

In contrast to that, higher moments of $|\psi_t\rangle \, \langle \psi_t|$ are not necessarily trivial (see Fig. 6) and indeed contain information about correlations within individual realizations of the measurement-induced dynamics. This may be accessed by repeatedly running the protocol such that a quantum-mechanical expectation value in the state obtained after a specific series of measurement outcomes can be evaluated. Correlations between these expectation values then contain information beyond what is captured in $\hat{\rho}_t$. The simple-most non-trivial object that we can construct out of a regular observable $Q(t)$ is

$$Q_N(t) = \overline{\langle \hat{Q} \rangle_t^N} = \overline{\left(\mathrm{Tr}\, \hat{Q} \, |\psi_t\rangle \, \langle \psi_t| \right)^N}, \tag{2.50}$$

where $N > 1$, depending on the N-th moment of the state $|\psi_t\rangle \, \langle \psi_t|$. This can be conveniently rewritten as

$$Q_N(t) = \overline{\mathrm{Tr} \otimes_{r=1}^N \hat{Q} \, |\psi_t\rangle \, \langle \psi_t|} = \mathrm{Tr} \left(\otimes_{r=1}^N \hat{Q}^{(r)} \right) \overline{(\otimes_{r=1}^M \, |\psi_t\rangle \, \langle \psi_t|)}, \tag{2.51}$$

if $M \geq N$. The index $(\dots)^{(r)}$ indicates that the operator acts only on the r-th copy of the state[10]. The trace now runs over the whole M times copied Hilbert space. The

[10]Note that we implicitly add $M - N$ copies of the unit matrix in Hilbert space $\otimes_{r=N+1}^M$ in order to get an operator of the same dimension as the replicated density-operator over which its expectation value is computed.

experimental protocol needed to extract observables of this type is exponentially costly due to the large number of repetitions needed to extract expectation values after any given sequence of measurement outcomes, which is known as post-selection problem [34, 115]. However, this perspective allows to construct observables that characterize non-trivial features of the quantum state in terms of the M times replicated density operator

$$\hat{\rho}_{M,t} = \overline{\otimes_{r=1}^{M} |\psi_t\rangle \langle\psi_t|} \not\to \hat{1}, \tag{2.52}$$

for $M \in \mathbb{N}_+$.

To make the kind of observables accessible through this replicated density operator more explicit, let us consider the case of Gaussian spinless fermions $\{\hat{c}_l, \hat{c}_m^\dagger\} = \delta_{nm}$, $\{\hat{c}_l, \hat{c}_m\} = 0$. In the particle-number conserving setting, all non-zero linear equal time correlators are linear combinations of

$$\langle \hat{c}_{l_1}^\dagger \dots \hat{c}_{l_n}^\dagger \hat{c}_{m_1} \dots \hat{c}_{m_n} \rangle_t = \langle\psi_t| \hat{c}_{l_1}^\dagger \dots \hat{c}_{l_n}^\dagger \hat{c}_{l_1} \dots \hat{c}_{l_n} |\psi_t\rangle , \tag{2.53}$$

for $n = 1, \dots, L$ and $l_a \neq l_b$ and $m_a \neq m_b$ if $a \neq b$. Since the state $|\psi_t\rangle$ is Gaussian along all measurement trajectories, we may use Wick's theorem to decompose this object into a sum of products of elementary pair correlations

$$D_{lm}(t) = \langle \hat{c}_l^\dagger \hat{c}_m \rangle_t, \tag{2.54}$$

entirely characterizing the state $|\psi_t\rangle$. As discussed above, any observable is trivial in the infinite temperature state when we just average over trajectories. Hence $\overline{D_{l,m}(t)}$ does not contain any non-trivial information on the stationary state, just like all higher order correlators that can be written in this form. Therefore, all observables, including measures for the correlations within the ensemble of measurement trajectories, can be understood as linear combinations of

$$C^{(N)}_{l_1,\dots,l_{2N}}(t) = \overline{D_{l_1,l_2}(t) \dots D_{l_{2N-1},l_{2N}}(t)}. \tag{2.55}$$

In terms of the $M \geq N$ times replicated density operator, this reads

$$C^{(N)}_{l_1,\dots,l_{2N}}(t) = \mathrm{Tr}\left[\hat{c}_{l_1}^{(1)\dagger} \hat{c}_{l_2}^{(1)} \dots \hat{c}_{l_{2N-1}}^{(N)\dagger} \hat{c}_{l_{2N}}^{(N)} \hat{\rho}_{M,t} \right]. \tag{2.56}$$

Let us briefly discuss typical observables that are accessible both analytically and numerically and discussed in Sec. 3. A very commonly considered [44, 47–52, 68, 69, 98] example is the von Neumann entanglement entropy of a subsystem A with its complement $\overline{A}$,

$$S(A) = \overline{-\mathrm{Tr}(\hat{\rho}_A \ln \hat{\rho}_A)}, \tag{2.57}$$

where $\hat{\rho}_A = \mathrm{tr}_{\overline{A}} |\psi\rangle\langle\psi|$. Since the states are Gaussian, we may use the exact Klich-Levitov formula [158] to reconstruct the entanglement entropy as

$$S(A) = \sum_{q=1}^{\infty} 2\zeta(2q) C_A^{(2q)} = \frac{\pi^2}{3} C_A^{(2)} + \mathcal{O}(C_A^{2q>4}), \tag{2.58}$$

where $C_A^{(N)}$ is the N-th cumulant of the number of particles in subsystem A, averaged over all measurement trajectories. Hence, we in principle need to solve the problem for all $M \in \mathbb{N}_+$ to exactly resolve the entanglement entropy. However, the dominant scaling of the entanglement entropy occurs due to the lowest cumulants as we see later by comparing numerical data for both quantities in Sec. 3. This makes $C_A^{(N)}$ for small N an interesting observable itself. Since the expectation value $C_A^{(1)} = \overline{\langle \sum_{l\in A} \hat{n}_l \rangle}$ is trivial in the infinite temperature state, the second cumulant is the first one capturing the essential physics of the measurement problem. It reads

$$C_A^{(2)} = \overline{\left\langle \left(\sum_{l\in A} \hat{n}_l - \left\langle \sum_{l'\in A} \hat{n}_{l'} \right\rangle \right)^2 \right\rangle} = \sum_{l,l'\in A} \left(\overline{\langle \hat{n}_l \hat{n}_{l'} \rangle} - \overline{\langle \hat{n}_l \rangle \langle \hat{n}_{l'} \rangle} \right). \tag{2.59}$$

In this way, we may directly connect the leading contribution to the entanglement entropy to the connected density-density correlation function, that is an additional observable by itself. We label it as

$$C_{l,l'} = \overline{\langle \hat{n}_l \hat{n}_{l'} \rangle - \langle \hat{n}_l \rangle \langle \hat{n}_{l'} \rangle} = \overline{|\langle \hat{c}_l^\dagger \hat{c}_{l'} \rangle|^2} = C^{(2)}_{l,l',l',l}. \tag{2.60}$$

The entanglement entropy is a basis-independent quantity characterizing generic quantum correlations in the system, while $C_A^{(N)}$ and $C_{l,l'}$ quantify the local particle number fluctuations. Therefore they enable the viewpoint of localization vs. delocalization in addition to the more information theoretic perspective of entanglement. From this discussion, we conclude that the relevant observable that we intend to compute is the correlation function $C_{l,l'}$, especially for large $l - l'$ to characterize the long-distance physics and potential critical behavior of the system. The replica structure of these observables is sketched in Fig. 7.

2.2.2 Construction of the replica master equation

As argued above, we ultimately intend to compute the replica density operator $\hat{\rho}_M$ for $M \geq 2$. In order to construct a convenient representation of the time-evolution of this object [44, 69, 98], let us reconsider the definition of the QSD measurement protocol (c.f. Sec. 2.1). Suppose we drop the normalization condition for quantum states $\left|\tilde{\psi}_t\right\rangle$, just initializing it at a time t_0 to be normalized $\left|\tilde{\psi}_{t_0}\right\rangle = |\psi_{t_0}\rangle = |\psi_0\rangle$ and non-random.

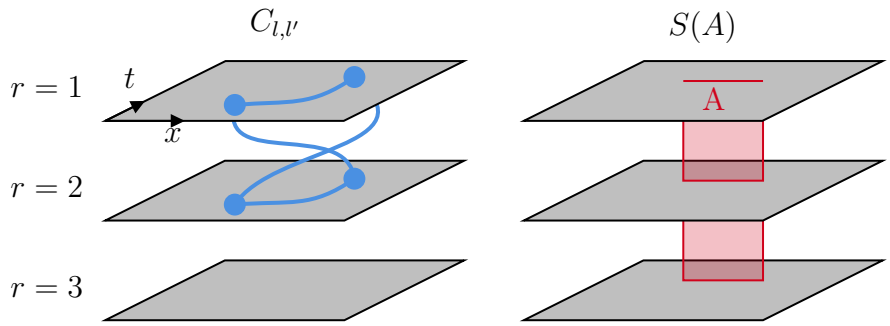

Figure 7: Visualization of the non-linear observables in replica space. The planes symbolize spacetime on the different replicas. Observables like the density-density correlation function between positions and (potentially) different times involves correlations within one replica with another one, symbolized by blue lines. Only two replicas are needed here for the computation. The von-Neumann entanglement entropy of a subsystem A involves all orders in the state and therefore we need correlations between all points in space within A and all infinitely many replicas (here we only show 3), at equal times. This is shown in red.

The state update for the non-normalized states is

$$\left|\tilde{\psi}_{t+dt}\right\rangle = e^{-\frac{i}{\hbar}\hat{H}dt}\hat{P}(\{J_{\alpha,t}\}_\alpha)\left|\tilde{\psi}_t\right\rangle . \tag{2.61}$$

Hence, for any finite measurement strengths γ_α, $\left|\tilde{\psi}_t\right\rangle$ depends on the sequence of measurement outcomes $\{J_{\alpha,\tau}\}_{\alpha,t_0\leq\tau<t}$. We do not write out this dependence for simplicity, but we note that the probability of finding a measurement sequence leading to that specific state is given by the norm of the state $\mathrm{Tr}\left|\tilde{\psi}_t\right\rangle\left\langle\tilde{\psi}_t\right|$. Therefore, the probability of finding the system in a state $|\psi_t\rangle = \left|\tilde{\psi}_t\right\rangle / \left|\left|\left|\tilde{\psi}_t\right\rangle\right|\right|$ at time t, or equivalently finding the non-normalized state $\left|\tilde{\psi}_t\right\rangle$ is equal to the probability of measuring the corresponding sequence of measurement outcomes $\{J_{l,\tau}\}_{l,t_0\leq\tau<t}$.

$$p(\{J_{\alpha,\tau}\}_{\alpha,t_0\leq\tau<t}) = \left|\left|\left|\tilde{\psi}_t\right\rangle\right|\right|^2 = \mathrm{Tr}\left|\tilde{\psi}_t\right\rangle\left\langle\tilde{\psi}_t\right| . \tag{2.62}$$

We realize that at a given time t, the statistical average over realizations amounts to an average over all possible trajectories of measurement outcomes $\{J_{\alpha,\tau}\}_{\alpha,t_0\leq\tau<t}$. Therefore, we make the average over trajectories more explicit, obtaining

$$\overline{(\dots)} = \int \mathcal{D}J p(\{J_{\alpha,\tau}\}_{\alpha,t_0\leq\tau<t})(\dots), \tag{2.63}$$

where $\int \mathcal{D}J$ denotes the integral over all $J_{\alpha,t_0\leq\tau<t} \in \mathbb{R}$. This allows to rewrite the replica density operator as

$$\begin{aligned}\hat{\rho}_{M,t} &= \overline{\otimes_{r=1}^{M} |\psi_t\rangle \langle\psi_t|} \\ &= \int \mathcal{D}J p(\{J_{\alpha,\tau}\}_{\alpha,t_0\leq\tau<t}) \otimes_{r=1}^{M} |\psi_t\rangle \langle\psi_t| \\ &= \int \mathcal{D}J \left(\mathrm{Tr}\left|\tilde{\psi}_t\right\rangle \left\langle\tilde{\psi}_t\right|\right)^{1-M} \otimes_{r=1}^{M} \left|\tilde{\psi}_t\right\rangle \left\langle\tilde{\psi}_t\right|. \end{aligned} \tag{2.64}$$

Note the dependence of the states $|\psi_t\rangle$ and $\left|\tilde{\psi}_t\right\rangle$ on the measurement record $\{J_{\alpha,\tau}\}_{\alpha,t_0\leq\tau<t}$. The division by the trace for each replica causes problems in obtaining a closed expression for the time-evolution expression of the replica density operator. Therefore, we employ the following replica trick[11] introducing

$$\hat{\rho}_{R,M,t} = \overline{\left(\mathrm{Tr}\left|\tilde{\psi}_t\right\rangle \left\langle\tilde{\psi}_t\right|\right)^{R-M} \otimes_{r=1}^{M} \left|\tilde{\psi}_t\right\rangle \left\langle\tilde{\psi}_t\right|}. \tag{2.65}$$

For $M \leq R$, this may be written as

$$\hat{\rho}_{R,M,t} = \mathrm{Tr}_{r>M}\, \tilde{\rho}_{R,t}, \qquad \tilde{\rho}_{R,t} = \int \mathcal{D}J \otimes_{r=1}^{R} \left|\tilde{\psi}_t\right\rangle \left\langle\tilde{\psi}_t\right|. \tag{2.66}$$

This expression allows us to formulate a linear generalized Lindblad quantum master equation describing the time-evolution of for a general replica number R in absence of normalization in every time-step which makes $\tilde{\rho}_{R,t}$ a convenient object to study analytically. On the other hand, we only recover the properly normalized state for $R = 1$. When interested in $M > 1$ replica observables, we therefore solve the problem for general $R \geq M$ and, after computing these observables, we take the replica limit $R \to 1$ using analytic continuation in replica space. Hence, the following derivation is to be understood in this limit. The typical correlation function, discussed above, may therefore be written as ($r \neq r', M \geq 2$)

$$\begin{aligned} C_{l,l'} &= \overline{\langle\hat{n}_l\hat{n}_{l'}\rangle - \langle\hat{n}_l\rangle\langle\hat{n}_{l'}\rangle} = \mathrm{Tr}\left(\hat{n}_l^{(r)}(\hat{n}_{l'}^{(r)} - \hat{n}_{l'}^{(r')})\hat{\rho}_{M,t}\right) \\ &= \lim_{R\to 1} \mathrm{Tr}\left(\hat{n}_l^{(r)}(\hat{n}_{l'}^{(r)} - \hat{n}_{l'}^{(r')})\hat{\rho}_{R,M,t}\right) = \lim_{R\to 1} \mathrm{Tr}\left(\hat{n}_l^{(r)}(\hat{n}_{l'}^{(r)} - \hat{n}_{l'}^{(r')})\tilde{\rho}_{R,t}\right). \end{aligned} \tag{2.67}$$

For that reason, solving for the stationary state of $\tilde{\rho}_{R,t}$ yields the solution for the connected correlation function. Applying Eq. (2.61), the exact time-evolution of the replicated density operator is

$$\tilde{\rho}_{R,t+dt} = \left(e^{-\frac{i}{\hbar}\hat{H}dt}\right)^{\otimes R} \overline{\hat{P}^{\otimes 2R}}(t, \tilde{\rho}_{R,t}) \left(e^{\frac{i}{\hbar}\hat{H}dt}\right)^{\otimes R}. \tag{2.68}$$

[11] Even though well accepted in the literature on disordered systems, the replica trick is not mathematically rigorous. An alternative approach involves the introduction of auxiliary supersymmetric degrees of freedom to account for the normalization [159–162], which is subject of current research.

Here,

$$\overline{\hat{P}^{\otimes 2R}}(t,\tilde{\rho}_{R,t}) = \int \mathcal{D}J_t \left(\otimes_{r=1}^{R}\hat{P}(\{J_{\alpha,t}\}_\alpha)\right)\tilde{\rho}_{R,t}\left(\otimes_{r=1}^{R}\hat{P}(\{J_{\alpha,t}\}_\alpha)\right), \tag{2.69}$$

is acting on the density-operator from both sides and the integral runs over all $\{J_{\alpha,t}\}_\alpha$ at a fixed time t describing the update from time $t \to t+dt$ due to the measurements at that time step. Since the generalized projectors are Gaussian in the measurement results $J_{l,t}$, the integral may be evaluated exactly, which allows to derive a closed differential equation for the time-evolution of the un-normalized replica density operator (see App. A.1)

$$\partial_t\tilde{\rho}_{R,t} = \mathcal{L}_R\tilde{\rho}_{R,t} = \sum_{r=1}^{R}\mathcal{L}^{(r)}\tilde{\rho}_{R,t} + \sum_{r,r',r\neq r'}\mathcal{M}^{(r,r')}\tilde{\rho}_{R,t}, \tag{2.70}$$

$$\mathcal{L}^{(r)}(.) = -\frac{i}{\hbar}[\hat{H}^{(r)},(.)] - \frac{1}{2}\sum_\alpha \gamma_\alpha\left[\hat{O}_\alpha^{(r)},\left[\hat{O}_\alpha^{(r)},(.)\right]\right], \tag{2.71}$$

$$\mathcal{M}^{(r,r')}(.) = \frac{1}{2}\sum_\alpha \gamma_\alpha\left\{\hat{O}_\alpha^{(r)},\left\{\hat{O}_\alpha^{(r')},(.)\right\}\right\}. \tag{2.72}$$

Note that if we take $R = 1$ everywhere, this yields the Lindblad quantum master equation (2.32). Otherwise, besides just copying the dynamics, we obtain a term $\mathcal{M}^{(r,r')}$ pairwise coupling the replicas. On every individual replica, we obtain the same dynamics as we would get for the linear average, i.e. heating to an infinite temperature state $\tilde{\rho} \sim 1$ while this is not a solution for the inter-replica coupling terms due to the replacement of commutators $[,]$ by anti-commutators $\{,\}$. Note as well that R does not appear as a prefactor at all but we had to set $R \to 1$ in order to obtain a proper differential equation in the first place.

The replica construction introduced in this section does not require any approximations or assumptions about the specific system. For that reason, any reasonable approach to a theoretical understanding of the specific microscopic model of monitored fermions will follow the given arguments[12]. To solve (2.70), we however need to use approximations as the replica model is interacting and cannot be solved exactly. This is the reason why there previously have been two complementary approximation schemes for monitored free fermions, bosonization and a non-linear sigma model construction, predicting qualitatively different behavior in the thermodynamic limit [44, 68, 69].

[12] besides technical differences in the definition of the replicas that do not qualitatively change the result

2.2.3 Toy model

Let us now study the replica quantum master equation using the toy model of a single particle hopping between two sites. The replica density matrix of the system can be represented as a $2^R \times 2^R$ matrix, corresponding to the 2 basis states of the original Hilbert space which is copied R times. Copying corresponds here to taking the tensor product of the state matrices (see Eq. (2.66)). The generator of the dynamics described by the replica master equation (2.70) acts as a superoperator from both sides onto this replica density matrix. To solve the full replicated evolution numerically for this case, we may employ the third quantization approach [163] and reshape the state matrix into a 4^R component vector, which allows to write the generator of the dynamics as a $4^R \times 4^R$ dimensional matrix acting only from the left onto the state vector. As we can see, the computational complexity to solve this for a given number of replicas R amounts to diagonalizing a matrix of exponential dimension $(4^R \times 4^R)$ such that the analytical continuation discussed above turns out to be very computationally demanding even for the toy model. Therefore, we treat the toy model as a proof of principle for the replica construction while the actual numerical simulation of non-linear measurement operators is done using individual trajectories as shown in Figs. 2,4,6.

The construction of the explicit matrix can be done in three steps: First, we write all appearing operators as matrices in the original Hilbert space,

$$\hat{H} = \begin{pmatrix} 0 & 1 \\ 1 & 0 \end{pmatrix}, \qquad \hat{x} = \begin{pmatrix} 0 & 0 \\ 0 & 1 \end{pmatrix}. \tag{2.73}$$

Then, we copy the Hilbert space once, going from pure states to density-operators. The 'ket' states correspond to the first copy and the 'bra' states to the second copy. Therefore, we can write an operator $\hat{O}$ acting from the left on the density operator as $\hat{O} \otimes \hat{1}$ and an operator acting from the right as $\hat{1} \otimes \hat{O}$. Using this construction yields

$$\begin{aligned} \mathcal{L} &= -\frac{i}{\hbar}\left[\hat{H}, (.)\right] - \frac{1}{2}\gamma\left[\hat{x}, [\hat{x}, (.)]\right] \\ &= -\frac{i}{\hbar}\left(\hat{H} \otimes \hat{1} - \hat{1} \otimes \hat{H}\right) - \frac{1}{2}\hat{x}^2 \otimes \hat{1} - \frac{1}{2}\hat{1} \otimes \hat{x}^2 + \hat{x} \otimes \hat{x} \\ &= \frac{1}{\hbar}\begin{pmatrix} 0 & i & -i & 0 \\ i & -\frac{\hbar\gamma}{2} & 0 & -i \\ -i & 0 & -\frac{\hbar\gamma}{2} & i \\ 0 & -i & i & 0 \end{pmatrix}. \end{aligned} \tag{2.74}$$

This matrix has the eigenvalues $0, -\frac{\gamma}{2}, -\frac{\gamma}{4}(1 \pm \alpha)$ where $\alpha = \sqrt{\gamma^2 - (8/\hbar)^2}$. The eigenvalue 0 corresponds to the stationary density operator since all other terms decay over time. The normalized result reads $\tilde{\rho}_1 = \frac{1}{2}|01\rangle\langle 01| + \frac{1}{2}|10\rangle\langle 10|$ i.e. an equal

superposition of the eigenstates of the measurement-operator. This is the featureless infinite-temperature state. We also observe that for $\gamma < 8/\hbar$, the approach towards this state is oscillatory since the eigenvalues become complex, matching the result of a simulation of the linear averaged observable $\hat{x} = |01\rangle\langle 01|$ (see Fig. 4). We therefore find that the linearly averaged observables can be analytically predicted, including the time-evolution towards the stationary state. If we, for instance, initialize the system in the pure state $|10\rangle\langle 10|$, the solution for the density matrix reads

$$\hat{\rho}_t = \begin{pmatrix} \frac{1}{2}\left(1 + e^{-\frac{\gamma t}{4}}\left(\cosh\frac{\alpha t}{4} + \frac{\gamma}{\alpha}\sinh\frac{\alpha t}{4}\right)\right) & \frac{-4i}{\alpha}e^{-\frac{\gamma t}{4}}\sinh\frac{\alpha t}{4} \\ \frac{4i}{\alpha}e^{-\frac{\gamma t}{4}}\sinh\frac{\alpha t}{4} & \frac{1}{2}\left(1 - e^{-\frac{\gamma t}{4}}\left(\cosh\frac{\alpha t}{4} + \frac{\gamma}{\alpha}\sinh\frac{\alpha t}{4}\right)\right) \end{pmatrix}. \tag{2.75}$$

This means, that we can compute the evolution of the observable

$$\overline{\langle\hat{x}\rangle} = \mathrm{Tr}\,\hat{x}\hat{\rho}_t = \frac{1}{2}\left(1 - e^{-\frac{\gamma t}{4}}\left(\cosh\frac{\alpha t}{4} + \frac{\gamma}{\alpha}\sinh\frac{\alpha t}{4}\right)\right). \tag{2.76}$$

This result matches with the simulation result for both QSD and QJ unravelings as shown in Fig. 4, as it should be since the unravelings are constructed such that they are equivalent to the quantum master equation on average over trajectories.

We are now interested in observables beyond the linear average as discussed above, as only those reveal non-trivial measurement-induced effects. To demonstrate, how these are described by the replica quantum master equations, let us compute the matrix that generates the time-evolution of the R times replicated, un-normalized density operator. First, we need to sum over the terms diagonal in replica space $\mathcal{L}^{(r)}$, which do not act on the other replicas such that

$$\mathcal{L}^{(r)} = \left(\bigotimes_{r'=1}^{r-1}\mathbf{1}\right) \otimes \mathcal{L} \otimes \left(\bigotimes_{r'=r+1}^{R}\mathbf{1}\right), \tag{2.77}$$

where $\mathbf{1}$ is a unit-matrix in the 4×4 vector space of density matrices on a single replica. Similarly, we construct the term that couples different replicas. This is readily seen considering two replicas,

$$\mathcal{M}^{(1,2)} = \frac{\gamma}{2}(\hat{x}\otimes\hat{1} + \hat{1}\otimes\hat{x}) \otimes (\hat{x}\otimes\hat{1} + \hat{1}\otimes\hat{x}). \tag{2.78}$$

The tensor-product within the bracket is between the 'ket' and 'bra' states on a single replica and in between there is a tensor product between different replicas. The corresponding terms for larger number of replicas are found by adding tensor products with $\mathbf{1}$ for all replicas on which $\mathcal{M}^{(r,r')}$ does not act.

Since the size of the matrix quickly becomes large and we can only rely on the extrapolation to $R = 1$ due to the lack of normalization for larger R, we focus on the

stationary state only. It can be found as the eigenstate of the superoperator with the largest real part of its eigenvalue since this term dominates at large times. While for $R = 1$, we generically find that the stationary state has eigenvalue 0, we now obtain eigenvalues with real parts larger than 0 indicating that the normalization is explicitly broken (see Fig. 8). Still, we identify the density-operator $\tilde{\rho}_R$ with the largest eigenvalue

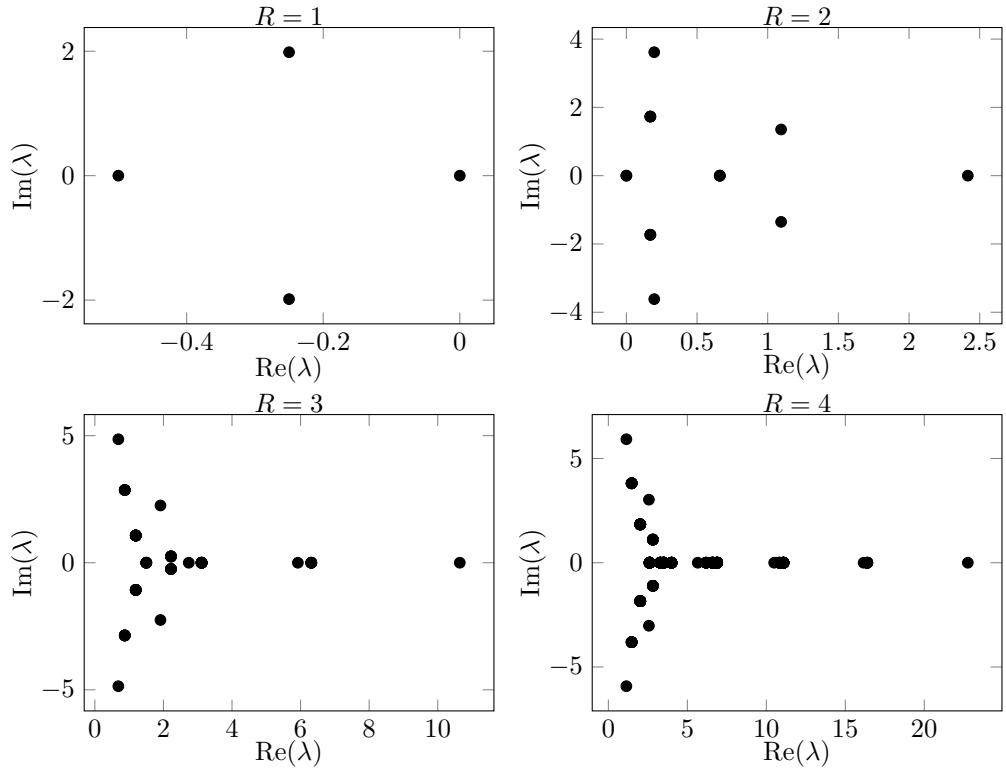

Figure 8: Eigenvalues of the R replica superoperator for $\gamma = \hbar = 1$. The stationary state is determined by the eigenvalue with the largest real part as this determines the exponential growth with time.

as the (up to a growing global prefactor) stationary state that is approached for late times. Therefore, we have numerical access to the stationary state of

$$C_R = \frac{1}{\operatorname{Tr} \tilde{\rho}_R} \operatorname{Tr} \left(\hat{x}^{(r)} \left(\hat{x}^{(r)} - \hat{x}^{(r')} \right) \tilde{\rho}_R \right), \tag{2.79}$$

for $R > 1$ and $r \neq r'$. Since the computation of the stationary state is not noisy, we may fix $r = 1, r' = 2$. In the construction of the replica quantum master equation, we identified (see Eq. (2.67)) that[13]

$$C = \overline{\langle \hat{x}^2 \rangle - \langle \hat{x} \rangle^2} = \lim_{R \to 1} C_R. \tag{2.80}$$

To solve this limit, we now need to compute C_R where accessible and perform the

[13]Note that we normalized the result for a given R since otherwise the growing prefactor would affect the result which is then time-dependent. This modification drops out in the limit $R \to 1$ as $\tilde{\rho}_1$ is normalized.

analytic continuation by computing an analytic function that interpolates between the points. Would we exactly know all C_R for $R > 1$, this yields a unique function that we can extrapolate to $R = 1$. However, if only a discrete number of C_R is known, the analytic function that interpolate between all points is ambiguous and it is impossible to uniquely identify the extrapolation to $R = 1$. Trying this for the first few values of R even shows that the scattered points behave non-trivially as we demonstrate in Fig. 9. Therefore, this approach is not suitable to numerically study any

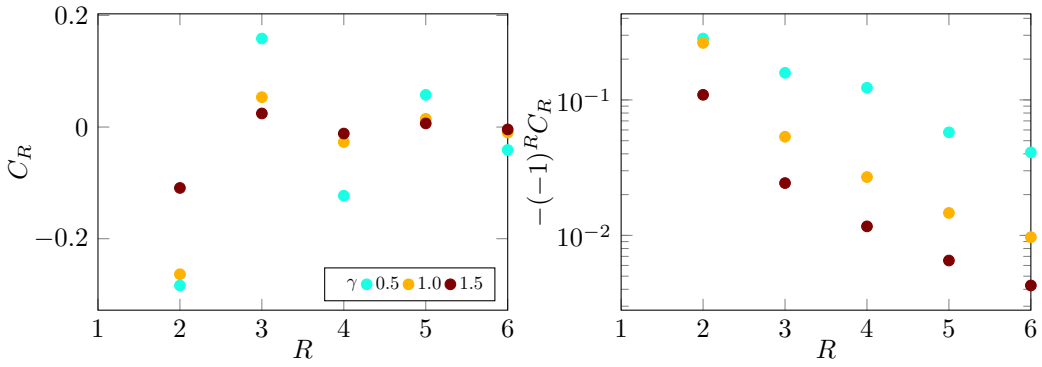

Figure 9: The auto-correlation $C = \overline{\langle \hat{x}^2 \rangle - \langle \hat{x} \rangle^2}$ is given by the extrapolation of C_R to $R = 1$ obtained from knowledge of all C_R for $R > 1$. Numerically, we can only determine a finite number of R up to $\mathcal{O}(6)$ due to the exponential growth of the generator of the replica dynamics. There is no obvious functional dependence of the results C_R on R such that the extrapolation from such a small number of data points is impossible, even for the toy model.

system, even a toy model, while an analytical treatment in principle allows to compute C_R for any R such that we continue to use the replica construction for analytical treatment of measurement-induced phenomena. Numerical simulations, in contrast are performed using the stochastic Schrödinger equation directly, sampling the probability distribution which is much more efficient as we demonstrated in Fig. 6.

2.3 Post-selection problem and pre-selection strategy

In the previous section, we discussed a way to compute objects that are non-linear in the state, like the observables introduced in Sec. 2.2.1 analytically. While this is certainly a useful approach to identify phases and phase transition in monitored systems analytically and numerically, it does not provide an efficient way to extract this information in an experimental setting. This is due to the so-called *post-selection problem* [49]. It can be illustrated in the toy model of a single particle hopping between two sites (see Fig. 10), where the correlation function $C = \overline{\langle \hat{x}^2 \rangle - \langle \hat{x} \rangle^2}$ is assumed to be the non-linear observable. Consider what is now necessary to reconstruct this object from an ensemble of QJ trajectories at a given time t: The symbol $\overline{(\dots)}$ in this case actually denotes an average over both all series of placing measurements at

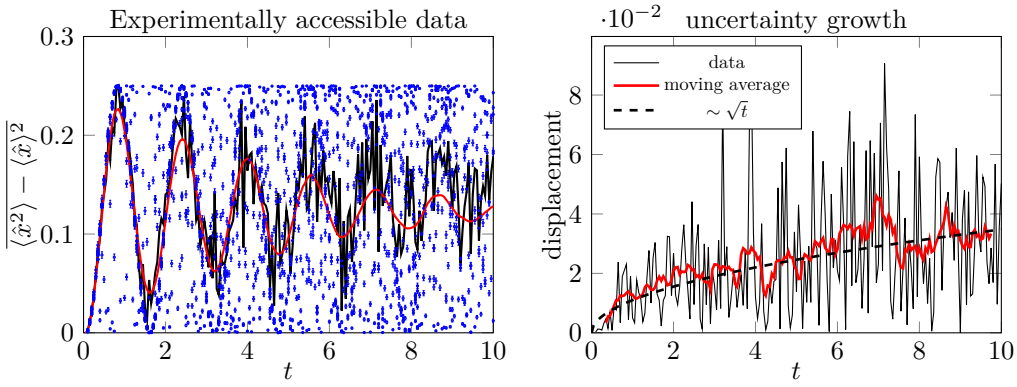

Figure 10: Simulation of the experimentally accessible data in the toy model using only the measurement readouts. For $\gamma = 0.5$ we generate 1000 different samples for the sequence in which the system is measured. For each sequence we run 5000 different trajectories to determine the conditioned expectation values at the points where the measurement is performed anyways. This ensures that we sample every trajectory sufficiently often. We then calculate the auto-correlation C and (arithmetically) average over measurement read-out trajectories. For each measurement sequence sample we obtain ~ 5 in principle experimentally accessible data-points shown in blue with error-bars. The black curve shows the average over these points for every time-step which we compare to the only numerically accessible data obtained from direct calculation of the quantum mechanical expectation values (red) as shown in Fig. 6. Due to the 5000000 simulated trajectories, noise is strongly suppressed here such that we take this as reference to determine the error of the simulated experimentally accessible data, as shown in the right panel. Taking a moving average shows that the uncertainty of C grows over time. This is in contrast to linear observables approaching a stationary state, where the uncertainty saturates at a finite value. This occurs as the number of different trajectories exponentially diverges with the number of performed measurements such that the conditioned average is taken over a shrinking sample size.

the (discrete) times t according to the Poisson distribution, $\{m_\tau\}_{t<\tau}$, where $m_\tau = 1$ if a measurement is performed at time τ and $m_\tau = 0$ if not. On top of that, we need to average over the different measurement outcomes $\{x_\tau\}_{\tau<t}$ at these times, whose probability distribution depends on the state on which the measurement is performed i.e. on the entire history of the state. Let us here assume that the system is initialized in the same state at $t = 0$ for all trajectories. Then, the trajectory-average reads

$$\overline{(\dots)}_t = \overline{(\dots)}^{\{m_\tau\}_{\tau<t},\{x_\tau\}_{\tau<t}} \tag{2.81}$$

The number of possible trajectories over which this average is taken for a given sequence of measurements now scales exponentially with the number of measurements performed until the time t. On top of this averaging, we also need to compute the averaged object in the given state that is obtained at time t. To determine $\langle \hat{x} \rangle_t$, this amounts to additionally performing a projective measurement of $\hat{x}$ at time t repeatedly to extract

the *conditional* expectation value for the given trajectory.

$$\langle\hat{x}\rangle_t = \langle\hat{x}\rangle_{t,\{m_\tau\}_{\tau<t},\{x_\tau\}_{\tau<t}} = {}^{\{m_\tau\}_{\tau<t},\{x_\tau\}_{\tau<t}}\overline{x_t}^{x_t}. \tag{2.82}$$

The left superscript denotes that the average is taken conditioned on the trajectory leading to this point. This allows to rewrite

$$\overline{\langle\hat{x}\rangle_t} = \overline{x_t}^{\{m_\tau\}_{\tau<t},\{x_\tau\}_{\tau\leq t}}. \tag{2.83}$$

Note that the quantum-mechanical expectation value can here be replaced by a stochastic variable, which is the measurement read-out at time t (see Fig. 10). Hence, it is sufficient to generate trajectories and average the final measurement read-out over both series of measurement placements and read-outs of the measurements that lead to the conditioned state at time t. The standard estimate for the error in determining the average in this way in this case scales with the number of performed trajectories

$$\Delta\overline{\langle\hat{x}\rangle_t} \sim (\text{number of trajectories})^{-1/2}. \tag{2.84}$$

In particular, this does not depend on the number of performed measurements along a single trajectory. Therefore, such standard observables are efficiently computed and are even resilient to additional noise not captured in the model, or an imperfect measurement record. In contrast, such a simplification cannot be done for non-linear observables. In the present example, we obtain

$$\overline{\langle\hat{x}\rangle_t^2} = \overline{\left(^{\{m_\tau\}_{\tau<t},\{x_\tau\}_{\tau<t}}\overline{x_t}^{x_t}\right)^2}^{\{m_\tau\}_{\tau<t},\{x_\tau\}_{\tau<t}} \tag{2.85}$$

Therefore, the individual terms over which the trajectory-average needs to be computed are conditioned on a given trajectory of measurement read-outs. A given trajectory needs to be reproduced several times in order to obtain an estimate for the average. The number of possible trajectories scales exponentially with the number of measurements performed for a single realization of the placement of measurements such that the number of trajectories that need to be simulated to reach a given error threshold also scales exponentially in the number of performed measurements. This is generic for measurement-induced dynamics and non-linear observables.

While in a simple system such as the toy-model, the short-time dynamics for moderate measurement rates can be resolved by direct generation of these exponentially many trajectories (see Fig. 10), a generic many-body system heavily suffers from this problem since the number of measurements performed in a given time scales typically linearly in the system size. Therefore, the experimental determination of non-linear observables such as $\overline{\langle\hat{x}^2\rangle - \langle\hat{x}\rangle^2}$ but also for instance the entanglement entropy, has an

exponential overhead compared to linear observables. At first sight, this leads to the conclusion that non-linear observables are in principle not experimentally accessible in thermodynamically large systems with measurement.

To investigate if this problem makes questions about measurement-induced phases and phase transitions in principle purely academic, there are broadly three different ideas that are put forward:

(1) Choosing a specifically tailored model and sufficiently small system sizes allows to run of a huge amount of trajectories on a state of the art quantum simulator [34]. However, this approach is not scalable due to the exponential overhead and therefore not appropriate to resolve emergent large distance physics. For instance, the question if the model of one-dimensional free fermions with measurements undergoes an entanglement transition for weak measurement rates can only be answered if system sizes up to at least $\mathcal{O}(1000)$ sites can be resolved [68, 69], as discussed in sec. 3.3.

(2) Explicit and precise knowledge about the microscopic details of the problem allow, at least for systems that can be efficiently simulated, to run a classical simulation of the system. This can be used to decode the information obtained from the measurements and compute observables based on a combination of the classical simulation and the experimental measurement read-outs. This can either be done by revealing the quantum information performing a unitary operation based on the classical simulation and measurement read-outs [112–114], or studying cross-correlations between experimental data and classical simulations [111, 115–118]. While for an appropriately chosen model, one may study rather large systems and the protocols are reasonably resilient to noise, this approach fundamentally relies on knowledge about microscopic details and does not provide model-independent signatures of measurement-induced phase transitions. Besides that, this approach can only be applied if the model is simple enough to be efficiently simulated, for instance because it is a Clifford-circuit [119, 120], non-interacting and therefore described by Gaussian states [68], or weakly entangled such that tensor-network approaches are suitable [121].

(3) Finally, we may alter one defining feature of the model, namely that the linearly averaged density-operator goes into an infinite temperature state, by adding the additional ingredient of feed forward [127, 164]. In this thesis we focus on this approach which we call 'pre-selection', and discuss the model of monitored fermions in one dimension in Sec. 5. The idea is here to perform a unitary gate after each (projective) measurement that is performed, which depends on the measurement read-out obtained in that measurement. This means, that the state update, here fore the QJ protocol (2.5), is modified to

$$|\psi_{t+dt}\rangle = e^{-\frac{i}{\hbar}\hat{H}dt} \prod_{\alpha} \left((1-m_\alpha) + m_\alpha \sum_n \frac{\delta_{O_\alpha, O_{\alpha,n}} \hat{C}_{\alpha,n} \hat{P}_{\alpha,n}}{\sqrt{\langle\psi_t| \hat{P}_{\alpha,n} |\psi_t\rangle}} \right) |\psi_t\rangle \,. \tag{2.86}$$

Here, $\hat{C}_{\alpha,n}$ with $\hat{C}_{\alpha,n}^{\dagger}\hat{C}_{\alpha,n} = \hat{1}$ are in principle arbitrary unitary operations. It turns out that they can be chosen for appropriate model systems such that they do not change the universal properties of the entanglement transition that the system undergoes, while they do affect the linearly averaged density operator as they render the Lindblad operators non-Hermitian. This means that the stationary state becomes non-trivial as the feedback operation induces a directed motion in the Hilbert space. Hence, instead of studying non-linear observables, we may characterize the stationary state of the trajectory ensemble in terms of the usual linearly averaged density operator. The associated observables do not suffer from the post-selection problem as they are of the form of Eq. (2.83).

While it is not a priori ensured that such a protocol exists such that the universal properties of the entanglement transition remain unchanged, it is in principle applicable independently of the possibility to perform a classical simulation and even without explicit knowledge of the microscopic details of, for instance, the Hamiltonian. Therefore, once further developed, it provides a universal protocol for the experimental detection of measurement-induced phase transitions. Besides that, the resulting dynamics turns out to realize quantum absorbing state phase transitions [129–131], which is of interest by itself, independently of the connection to measurement-induced phase transitions.

3 Free fermions with nearest neighbor hopping

The contents of this section are equal to those of a manuscript in preparation for publication. The other co-authors will be M. Buchhold and S. Diehl. The author of this thesis extended the existing theory of bosonizing the measurement problem in free monitored fermions by using the replica trick $R \to 1$ and re-deriving all subsequent steps in this new framework. He also performed the study of the fermionic path integral in perturbation theory and performed all numerical simulations. All analytical and numerical results where interpreted in discussions with M. Buchhold and S. Diehl. The entire manuscript presented in this section was written by the author of this thesis.

After the introduction of measurement-induced dynamics, in this section, we focus on a specific many-body system under monitoring. We discuss the question, whether measurements of the local occupation number of spinless fermions in a one-dimensional chain induce a phase transition and if so, what the universality class of this phase transition is. This question has been addressed extensively in the literature [44, 67–69, 165]. However, this issue is still debated as there is evidence both for the existence of a phase transition at a finite measurement strength γ_c of the Berezinskii–Kosterlitz–Thouless (BKT) type [44, 68, 89–91], and for the absence of a phase transition where the numerical results are understood within the picture of weak localization [69, 165, 166]. To make progress in identifying the nature of the thermodynamic limit of this model, we introduce an advanced formal description in terms of a replica field theory and also present new numerical evidence supporting the BKT scenario.

We proceed as follows: First, in Sec. 3.1 we introduce the lattice model of free fermions undergoing unitary nearest neighbor hopping dynamics and and either projective or weak measurement of the particle number, and discuss how single trajectories can be simulated using Gaussian states. This is used to gain intuition about the trajectory resolved many-body system. After that, in Sec. 3.2 we apply the replica construction presented in Sec. 2.2 to the weak measurement problem and derive the field theory representation describing the dynamics of the trajectory ensemble. This is done in 4 Steps: (i) We map the model directly to a fermionic Keldysh replica path integral and treat the measurements perturbatively. This allows to identify a single mode in replica space that heats up to an infinite temperature state while all other modes cool to a ground state. (ii) This justifies to apply Abelian bosonization on the operator level and then map it to a bosonic Keldysh replica path integral. (iii) In the bosonic path integral, we can identify again a single mode heating up to an infinite temperature state which is used to integrate out this mode and identify a model where the remaining degrees of freedom are cooled into a ground state. (iv) Finally, we analyze the resulting non-Hermitian Sine-Gordon model using Wilsonian renormalization group (RG) [73] to identify the universality class of the phase transition which

turns out to be BKT. The steps (ii-iv) follow previous work [44], lifting them to an advanced treatment of the replica limit by keeping the replica number arbitrary, which is a new development. Along this calculation, we demonstrate how the the observables are represented in terms of the effective degrees of freedom and derive that in the weak measurement phase, the entanglement is scaling logarithmically with the partition size and in the strong measurement phase, it saturates to a constant. These findings are then compared in Sec. 3.3 to numerical simulations of individual trajectories. After the average over trajectories, we find good agreement with the analytical prediction, both for weak and projective measurements. In particular, the finite size scaling collapse of the entanglement entropy indicates a divergence of the correlation length at the critical point that is compatible with the BKT scenario but deviates from what is expected in weak localization. These results come with the caveat that the predicted critical measurement strength is very small (≈ 0.1) in units of the timescale of the Hamiltonian such that the apparent volume law scaling at short distances and weak measurements requires exponentially large system sizes that are not numerically accessible even using the Gaussian property of the states. Therefore, we can not confidently rule out the possibility that the critical measurement strength is zero, which would mean that the logarithmic scaling phase does not exist. Instead, we provide evidence for the BKT scaling behavior and show, that the results are compatible with the field theory approach.

3.1 Model and single trajectories

Let us consider free fermions on a 1D lattice with nearest neighbor hopping, i.e. a Hamiltonian

$$\hat{H} = -\sum_{l=1}^{L} \left(\hat{c}_l^\dagger \hat{c}_{l+1} + \hat{c}_{l+1}^\dagger \hat{c}_l \right), \tag{3.1}$$

where L is the number of sites and $\hat{c}_l, \hat{c}_l^\dagger$ obey fermionic anti-commutation relations, $\{\hat{c}_l, \hat{c}_m^\dagger\} = \delta_{lm}$ and $\{\hat{c}_l, \hat{c}_m\} = 0$. We always implement periodic boundary conditions and are interested ultimately in the thermodynamic limit $L \to \infty$ and half filling. On top of that, we monitor the particle number on each site weakly with a rate γ, i.e. we perform QSD dynamics, as visualized in Fig. 11. The pure state of the system $|\psi\rangle$ is therefore evolving according to Eq. (2.42), which reads in this case

$$d|\psi\rangle = \left(\left(-\frac{i}{\hbar}\hat{H} - \frac{1}{2}\sum_l \gamma \hat{M}_l^\dagger \hat{M}_l \right) dt + \sum_l \sqrt{\gamma} \hat{M}_l dW_l \right) |\psi\rangle \tag{3.2}$$

where l is again the lattice site and $\hat{M}_l = \hat{O}_l - \langle \hat{O}_l \rangle$ where $\hat{O}_l = \hat{n}_l$ is the monitored operator, the particle number $\hat{n}_l = \hat{c}_l^\dagger \hat{c}_l$ on lattice site l and dW_l is Gaussian white noise with $\overline{dW_l dW_m} = \delta_{lm} dt$. This generalizes the toy model discussed in Sec. 2.1

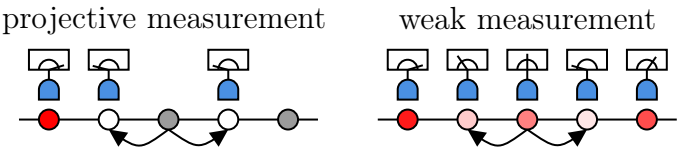

Figure 11: Setup in a single time-step of the QJ (left) and the QSD (right) protocol. Besides applying the Hamiltonian, we perform projective measurements on a subset of the lattice sites for the QJ protocol, such that the occupation number of these lattice sites is known. For QSD on the other hand, all lattice sites are monitored, while the measurement outcome is continuous and yield imperfect information about the system due to noise.

and Sec. 2.2 to a many-body system. To understand the dynamics of this system, we numerically simulate it by parametrising the state $|\psi\rangle$ in the form [67, 167][14],

$$|\psi\rangle = \prod_{j=1}^{L/2} \left(\sum_{l=1}^{L} U_{lj} \hat{c}_l^\dagger \right) |0\rangle \,. \tag{3.3}$$

The columns of the matrix $U = \{U_{lj}\}_{lj}$ are single-particle wave functions which means that we demand $U^\dagger U = 1$ due to the Pauli principle (see App. B.1). Given such a state, we may compute expectation values of fermion bilinears using (see App. B.1)

$$D_{mn} = \langle \hat{c}_m^\dagger \hat{c}_n \rangle = (UU^\dagger)_{mn} \tag{3.4}$$

In particular, the particle density reads $\langle \hat{n}_l \rangle = (UU^\dagger)_{ll}$. We call the state $|\psi\rangle$ Gaussian, because it obeys Wicks theorem (see App. B.1) such that also all higher order contractions are accessible, which is also discussed in sec. 2.2.1. For instance,

$$\langle \hat{c}_a^\dagger \hat{c}_b^\dagger \hat{c}_c \hat{c}_d \rangle = D_{ad} D_{bc} - D_{ac} D_{bd}. \tag{3.5}$$

Given such a state, we may apply the generator of the time-evolution 3.2 for a finite time-step dt and obtain up to normalization and to leading order in dt that this corresponds to an evolution of the matrix U which reads (see App. B.1)

$$U \to e^{-\frac{i}{\hbar} h} \mathrm{diag}(\{e^{-\gamma dt (2\langle \hat{n}_l \rangle - 1) + \sqrt{\gamma dt}\xi_l}\}_l) U. \tag{3.6}$$

h is here the hopping matrix of the particle-number conserving Hamiltonian, $\hat{H} = \sum_{mn} h_{mn} \hat{c}_n^\dagger \hat{c}_m$, i.e. for the case of nearest neighbor hopping it reads $h_{nm} = \delta_{n,m+1} + \delta_{n,m-1}$ imposing periodic boundary conditions. The randomness of measurement-outcomes is implemented by independent Gaussian white noise $\overline{\xi_l} = 0$, $\overline{\xi_l \xi_m} = \delta_{lm}$.

While the normalization of the state can be easily restored dividing by the norm,

[14] For the implemented half filling we need to assume an even number of sites. This is not expected to be important at large system sizes.

we realize that the higher order terms in dt also slightly break the orthogonality of the single particle states. However, for any matrix U there exists a decomposition into $U = QR$ where $Q^\dagger Q$ is unitary and R is an upper triangular matrix $L/ \times L/2$ matrix. R contains the normalization of the single particle states while the off-diagonal terms capture the broken orthogonality due to higher orders in dt. Therefore, we identify $U \to Q$ as the update rule after a time step dt, ensuring preservation of the Gaussian nature of the state and the particle number. Note that we thereby found a closed expression for the time-evolution in terms of the matrix U since $\langle \hat{n}_l \rangle = (UU^\dagger)_{ll}$ is accessible in every time step. Note that this construction only works because all operators in Eq. (3.2) are quadratic in fermionic creation and annihilation operators[15], and the QSD protocol preserves Gaussianity in every single time-step. This vastly reduces the computational complexity compared to the 2^L-component state vector of a generic spinless fermion model on L lattice sites and allows for very efficient numerical simulation as we demonstrate in Sec. 3.3.

From the correlation matrix D_{mn}, we can compute for instance the local density $n_l = \langle \hat{n}_l \rangle = D_{ll}$, as shown for single trajectories in Fig. 12, but also objects that are non-linear in the state, such as the density-density correlation function

$$C_{l,m} = \langle \hat{n}_l \hat{n}_m \rangle - \langle \hat{n}_l \rangle \langle \hat{n}_m \rangle = |\langle \hat{c}_l^\dagger \hat{c}_m \rangle|^2 = |D_{lm}|^2. \tag{3.7}$$

Besides that, we may also compute the von-Neumann entanglement entropy of a subsystem A along a given trajectory [68, 168, 169] as

$$S_{\mathrm{vN}}(A) = \mathrm{Tr}\, \hat{\rho}_A \log \hat{\rho}_A = -\sum_j \left(\lambda_j^{(A)} \log\left(\lambda_j^{(A)}\right) + (1 - \lambda_j^{(A)}) \log\left(1 - \lambda_j^{(A)}\right) \right), \tag{3.8}$$

where $\hat{\rho}_A$ is the reduced density operator of found as the trace of $|\psi\rangle \langle\psi|$ over the adjoint of A and $\lambda_j^{(A)}$ are the eigenvalues of $\{D_{lm}\}_{l,m \in A}$, restricting l and m to be in the subset of lattice sites within the subsystem A.

In precisely this form, this model has been first discussed, mainly numerically, in Ref. [67]. The authors found that the system does not undergo a phase transition at finite measurement strength and is always dominated by the measurements as long as $\gamma > 0$. Later, in Refs. [44, 68] the same system was analyzed with more extensive numerical treatment and replica field theory based on bosonization where indications for the existence of an additional phase where the Hamiltonian dominates and entanglement properties are changed from an area law $S_{\mathrm{vN}} \sim L^0$ to logarithmic scaling $S_{\mathrm{vN}} \sim \log L$, where found.

Later, the corresponding model with projective measurement was also discussed using both numerical simulations and replica field theory based on non-linear sigma

[15] $\hat{n}_l^2 = \hat{n}_l$

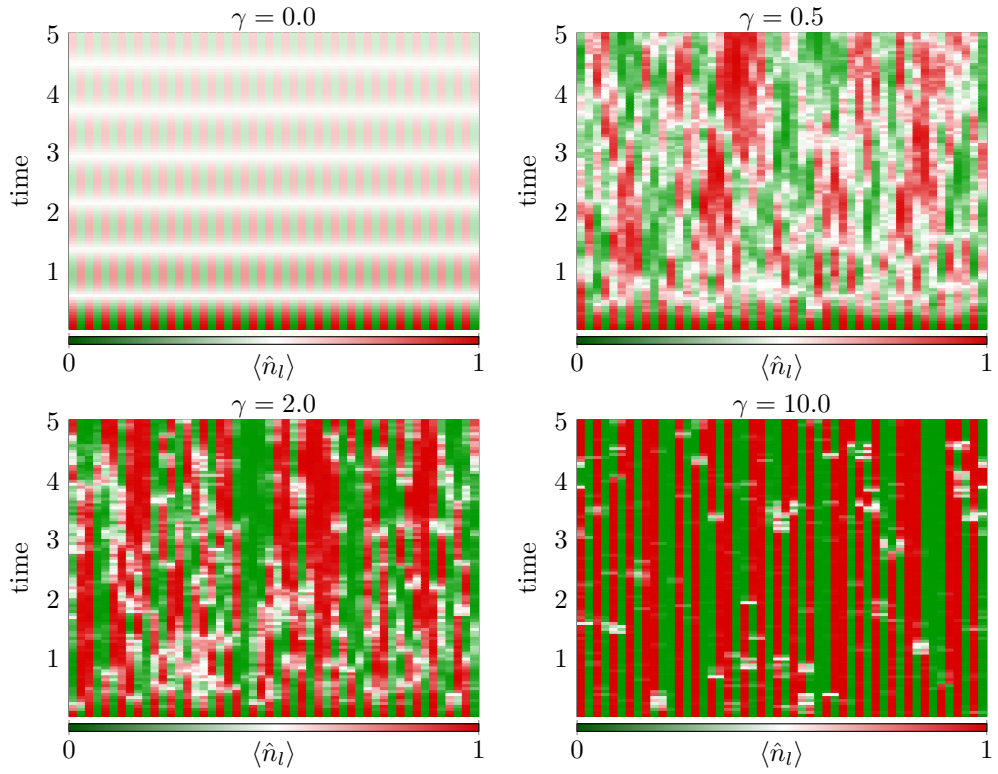

Figure 12: Single trajectory for the QSD protocol with $dt = 0.05$ and $\hbar = 1$ for a state initialized in a Néel state. Strong measurement act as projections onto eigenstates of the measurement operator while weak measurements merely add noise to the quantum state.

models [69, 165]. Their results indicate that this model does not feature a phase transition but instead undergoes weak localization where the correlation length diverges exponentially as a function of $1/\gamma$ which is easy to confuse with a phase transition at finite critical γ from finite size numerical simulations. The model with projective measurements can be implemented by the quantum jump protocol (2.5), which reads in this case

$$|\psi_{t+dt}\rangle = e^{-\frac{i}{\hbar}\hat{H}dt} \prod_l \left((1 - m_l) + m_l \left(\frac{n_l \hat{n}_l}{\sqrt{\langle \hat{n}_l \rangle_t}} + \frac{(1 - n_l)(1 - \hat{n}_l)}{\sqrt{\langle 1 - \hat{n}_l \rangle_t}} \right) \right) |\psi_t\rangle \,. \tag{3.9}$$

Here, both $n_l = 0, 1$ and $m_l = 0, 1$ are binary random variables that are drawn independently. The probability to measure at a given time step on site l, i.e. for $m_l = 1$ is $\frac{\gamma dt}{2}$ in the limit of $dt \to 0$ to match the corresponding Lindblad equation of the QSD protocol. To keep it bounded for finite dt independently of the measurement-strength, we implement this probability numerically as $1 - e^{-\gamma dt/2}$. The QJ state update can be implemented in terms of the correlation matrix D_{mn}. In every time step, we first randomly select which sites are measured according to the distribution given by γ and dt. On all of these sites l, we then determine the probability to measure 1, given by $D_{ll} = \langle \hat{n}_l \rangle$. By another random number, we then determine if 1 or 0 is measured at

site l and if $n_l = 1$ is measured, we transform the correlation matrix according to

$$D_{mn} \to D_{mn} + \delta_{ml}\delta_{nl} - \frac{D_{ml}D_{ln}}{D_{ll}}. \tag{3.10}$$

If on the other hand, $n_l = 0$ is measured, we apply

$$D_{mn} \to D_{mn} - \delta_{ml}\delta_{nl} - \frac{(\delta_{ml} - D_{ml})(\delta_{ln} - D_{ln})}{1 - D_{ll}}. \tag{3.11}$$

Both these operations keep the particle number and the norm of the state untouched but implement projections onto single particle eigenstates on the site l. After this series of projections, we apply the Hamiltonian on both sites, which amounts to

$$D \to e^{-\frac{i}{\hbar}hdt} D e^{\frac{i}{\hbar}hdt}. \tag{3.12}$$

This concludes a single time-step of the simulation which is the iterated[16]. In Fig. 13 we show examples for quantum jump trajectories. To shine light on the question whether a

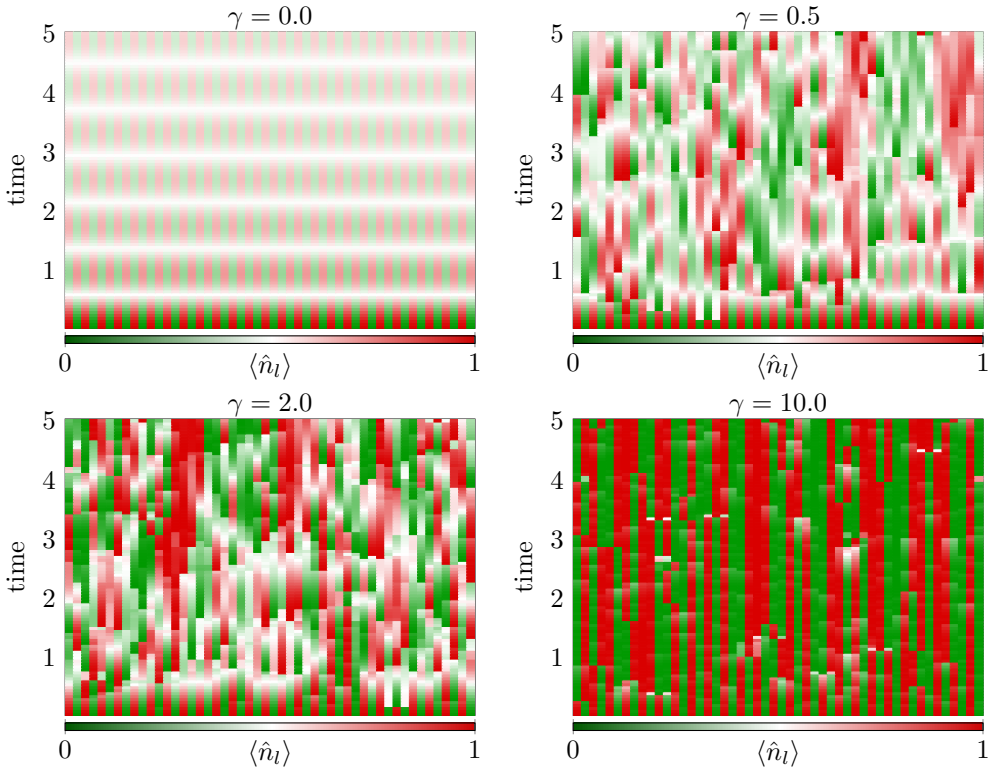

Figure 13: Single trajectories for the QJ protocol. They differ from the QSD trajectories in the sense that exact local eigenstates of $\hat{n}_l$ are more present due to the projective nature even in the case of weak measurements.

phase transition in this type of model exists or not, and if the type of protocol, QSD or

[16]We checked numerically that this protocol is numerically stable for many iterations, keeping the normalization and particle number conservation invariant for arbitrary dt. We take $dt = 0.05$ everywhere as both in the QSD and QJ protocol, $2dt$ or $dt/2$ does not change the quantitative behavior.

QJ, that is performed matters for the universal properties, we will reconsider the weak measurement protocol in this section. To do so, we perform an analytical treatment based on the replica trick introduced in Sec. 2.2.2 and an improved numerical analysis, both for the QSD and the QJ protocol.

3.2 Field theory approach

3.2.1 Functional integral for the microscopic model

Let us start the analytical approach by constructing the replica version of the fermionic Keldysh path integral to describe the original model of monitored fermions [69]. This approach is also straightforwardly suitable for generalizations as long as they are formulated in the language of spinless fermions. The derivation is closely following Refs. [28, 29, 154], generalizing the concepts to more than one replica. We introduce coherent states $|\psi\rangle$ such that $\hat{c}_l^{(r)}|\psi\rangle = \psi_l^{(r)}|\psi\rangle$ and $\langle\psi|\hat{c}_l^{(r)\dagger} = \langle\psi|\bar{\psi}_l^{(r)}$ where $\psi_l^{(r)}, \bar{\psi}_l^{(r)}$ are Grassmann numbers, and $\hat{c}_l^{(r)}, \hat{c}_l^{(r)\dagger}$ are the fermionic creation and annihilation operators on replica r in terms of which all operators can be formulated. This is done for every time-step and on the forward and backward Keldysh contour. Since all operators are even in the number of fermions, we may assume anti-commutation relations between the operators acting on different replicas without breaking the construction of the replica theory. As the measurement-operators are quadratic in fermion-operators, they only generate quartic terms in the action. Therefore, let us for a moment consider the replica action in absence of measurement (see App. A.2),

$$S_0 = \sum_r \int_{\omega,p} \bar{\psi} G_0^{-1} \psi, \qquad G_0^{-1} = \begin{pmatrix} 0 & P_A \\ P_R & P_K \end{pmatrix}, \tag{3.13}$$

with $P_R = P_A = \omega - \epsilon(p)$ and $P_K = 0$[17]. The matrix only acts on the Keldysh index $\alpha = c, q$. All terms appearing are evaluated at momentum p and frequency ω and $\epsilon(p) = -2J\cos(pa)$ is the dispersion relation of the fermions. Note that the inverse Green's function can become 0 here which means that we need to introduce a regularization in order to make correlation functions well defined. Dropping the interactions due to measurements for now, the action does not couple different replicas such that the physics is entirely the same as at $R = 1$ and we may use properties of single replica Keldysh field theory here, especially using initial conditions to fix the regularization. Correlation functions of this action can be computed by adding a source term and solving the Gaussian integral. This yields (see App. A.2) $G_K = 0$ and $G_R = G_A = (\omega - \epsilon(p))^{-1}$. This however needs to be regularized to recover the causality

[17] The definitions of the discussed objects follow [28, 29]

$G_R(t) \sim \theta(t)$. To fix this, consider the real time representation

$$G_R(t) = -i\langle \psi_c^{(r)}(t)\bar{\psi}_q^{(r)}(0)\rangle = \int_\omega \frac{e^{-i\omega t}}{\omega - \epsilon(p)}. \tag{3.14}$$

For $t < 0$, we solve the integral by closing the contour in the upper half plane. This has to vanish such that we shift the pole to the lower half plane as $\omega \to \omega + i0^+$. For $t > 0$, we can then close the contour in the upper half plane and obtain the finite result

$$G_{R/A}(\omega) = (\omega \pm i0^+ - \epsilon(p))^{-1} \qquad \to \qquad G_R(t) = \mp i\theta(\pm t)e^{-it\epsilon(p)\mp 0^+ t} \tag{3.15}$$

In absence of a regularization, the Keldysh Greens function vanishes as there is no contour-coupling term. To see how the regularization changes this, let us assume that we initialize the system in a thermal state at a temperature T. In this case, we use the fluctuation dissipation theorem for fermions,

$$G_K(\omega) = (1 - 2n(\omega))(G_R(\omega) - G_A(\omega)), \tag{3.16}$$

where $n(\omega) = 1/(e^{\beta\omega} + 1)$ is the occupation number of each mode, as given by the temperature. Since any finite measurement-rate drives the system into an infinite temperature state, independently of $\gamma > 0$, it is reasonable to assume that the system is initialized with $\beta = 0$ i.e. $n(\omega) = 1/2$. This is compatible with half filling since all modes are occupied with a probability of $1/2$. For the Keldysh Green's function, this simply implies $G_K = 0$ even with regularization, and therefore $P_K = 0$. The regularized quadratic action is therefore given by the bare inverse Greens function

$$G_0^{-1} = \delta_{r,r'} \begin{pmatrix} 0 & \omega - i0^+ - \epsilon(p) \\ \omega + i0^+ - \epsilon(p) & 0 \end{pmatrix}. \tag{3.17}$$

Next, let us consider the monitoring operator. It is better written in the real space representation. It is quadratic and has the property $\hat{n}_l^{(r)2} = \hat{n}_l^{(r)}$ such that we need to be careful with the normal ordering prescription (see App. A.2). We get the two additional contributions

$$S_{\mathcal{L}} = \frac{-i\gamma}{2} \sum_{r,l} \int_t \left(2n_+^{(r)}n_-^{(r)} - n_+^{(r)}n_+^{(r)} - n_-^{(r)}n_-^{(r)}\right), \tag{3.18}$$

and

$$S_{\mathcal{M}} = \frac{-i\gamma}{2} \sum_{r\neq r',l} \int_t \left(2n_+^{(r)}n_-^{(r')} + n_+^{(r)}n_+^{(r')} + n_-^{(r)}n_-^{(r')}\right), \tag{3.19}$$

which couples different replicas.

Guided by the observation that the replica-diagonal physics is trivial due to the

heating to an infinite temperature state, let us now integrate out the average mode over replicas perturbatively in γ to find the Gaussian theory describing the short-distance physics in terms of fermionic degrees of freedom. In order to do so, we perform a Fourier transformation in replica space,

$$\psi_{\sigma,l}^{(r)}(t) = \frac{1}{\sqrt{R}} \sum_{k=0}^{L-1} e^{2\pi i k r/R} \psi_{\sigma,l}^{(k)}(t), \tag{3.20}$$

$$\bar{\psi}_{\sigma,l}^{(r)}(t) = \frac{1}{\sqrt{R}} \sum_{k=0}^{L-1} e^{-2\pi i k r/R} \bar{\psi}_{\sigma,l}^{(k)}(t). \tag{3.21}$$

In order to separate the $k = 0$ from the other modes, let us introduce also

$$\psi_{\sigma,l}^{(0)}(t) = \frac{1}{\sqrt{R}} \psi_{\sigma,l}^{(k=0)}(t), \qquad \psi_{\sigma,l}^{(r,>)}(t) = \frac{1}{\sqrt{R}} \sum_{k=1}^{L-1} e^{2\pi i k r/R} \psi_{\sigma,l}^{(k)}(t), \tag{3.22}$$

$$\bar{\psi}_{\sigma,l}^{(0)}(t) = \frac{1}{\sqrt{R}} \bar{\psi}_{\sigma,l}^{(k=0)}(t), \qquad \bar{\psi}_{\sigma,l}^{(r,>)}(t) = \frac{1}{\sqrt{R}} \sum_{k=1}^{L-1} e^{-2\pi i k r/R} \bar{\psi}_{\sigma,l}^{(k)}(t). \tag{3.23}$$

In the quadratic part of the action, the terms remain decoupled,

$$S_0 = \sum_k \int_{\omega,p} \bar{\psi} G_0^{-1} \psi, \tag{3.24}$$

$$G_0^{-1} = \delta_{k,k'} \begin{pmatrix} 0 & \omega - i0^+ - \epsilon(p) \\ \omega + i0^+ - \epsilon(p) & 0 \end{pmatrix}. \tag{3.25}$$

However, the regularization fixing the correlation functions based on the assumption of an infinite temperature state only persists for the $k = 0$ mode as all other modes are affected by the replica-coupling term which leads to an effective cooling. In order to make this apparent, we perturbatively integrate out the $k = 0$ mode from the action, using that up to a non-physical normalizing prefactor,

$$\mathcal{Z} = \int \mathcal{D}\bar{\psi}^{(k>0)} \mathcal{D}\psi^{(k>0)} \langle e^{iS_\mathcal{L} + iS_\mathcal{M}} \rangle_{0,k=0} e^{iS_0[\psi^{(k>0)}, \bar{\psi}^{(k>0)}]}. \tag{3.26}$$

The action only containing $k > 0$ fields is therefore given by

$$S_{k>0} = S_0[\psi^{(k>0)}, \bar{\psi}^{(k>0)}] - i \log \langle e^{iS_\mathcal{L} + iS_\mathcal{M}} \rangle_{0,k=0} \tag{3.27}$$

We treat the interaction terms $S_\mathcal{L}, S_\mathcal{M}$ perturbatively as they are $\sim \gamma$ to obtain the

leading behavior for small monitoring strengths. This yields (see App. A.3)

$$\langle S_{\mathcal{L}} + S_{\mathcal{M}} \rangle_{0,k=0} = i\gamma \sum_{r,l} \int_t \left(n_+^{(r,>)} n_+^{(r,>)} + n_-^{(r,>)} n_-^{(r,>)} - 2(R-1)(n_+^{(r,>)} + n_-^{(r,>)}) \right) - \frac{i\gamma}{2} \sum_{r,r',l} \int_t \left(2n_+^{(r,>)} n_-^{(r',>)} + n_+^{(r,>)} n_+^{(r',>)} + n_-^{(r,>)} n_-^{(r',>)} \right) + \mathcal{O}(\gamma^2), \quad (3.28)$$

where $n_\sigma^{r,>} = \bar{\psi}_\sigma^{r,>} \psi_\sigma^{r,>}$. The only quadratic term appearing vanishes for $R \to 1$ such that in the properly normalized theory it disappears. Therefore, even after integrating out the $k = 0$ mode, the entanglement is dominated by the interaction term. We even find that the exact structure is preserved,

$$\langle S_{\mathcal{L}} + S_{\mathcal{M}} \rangle_{0,k=0} = S_{\mathcal{L}}[\psi^{(r,>)}, \bar{\psi}^{(r,>)}] + S_{\mathcal{M}}[\psi^{(r,>)}, \bar{\psi}^{(r,>)}] \quad (3.29)$$

i.e. integrating out the (0) fields amounts to just setting them to 0 to leading order in γ. Note however, that any $R \neq 1$ regularizes the quadratic part of the action, which reads now

$$S_{0,k>0} = \sum_{k>0} \int_{\omega,p} \bar{\psi} G_0^{-1} \psi, \quad (3.30)$$

$$G_0^{-1} = \delta_{k,k'} \begin{pmatrix} -2i\gamma(R-1) & \omega - i0^+ - \epsilon(p) \\ \omega + i0^+ - \epsilon(p) & -2i\gamma(R-1) \end{pmatrix}. \quad (3.31)$$

Note that this structure implies that the + and − contour decouple for the $k > 0$ modes while there is a coupling between the two contours for $k = 0$, and that in replica Fourier space, all replicas decouple, as illustrated in Fig. 14 From inversion of this matrix, we obtain the Greens functions

$$G_K = \frac{2i\gamma(R-1)}{(\omega - \epsilon(p))^2 + (0^+)^2 + 4\gamma^2(R-1)^2}, \quad G_{R/A} = \frac{\omega \pm i0^+ - \epsilon(p)}{(\omega - \epsilon(p))^2 + (0^+)^2 + 4\gamma^2(R-1)^2}. \quad (3.32)$$

Now, we may again study the fluctuation-dissipation theorem in the limit $0^+ \to 0$ and $R \to 1$. It turns out, that for both sides of the equation the order of limits does not matter and we find

$$G_K = i\pi\delta(\omega - \epsilon(p)), \qquad G_R - G_A = 2i\pi\delta(\omega - \epsilon(p)) \quad (3.33)$$

This means that in the replica limit $R \to 1$ and in absence of dissipation, $G_K \propto G_R - G_A$ which is characteristic for ground states. We therefore conclude that in the limit $\gamma \to 0$, all observables that are non-linear in the state are dominated by this ground state physics, which justifies an expansion around the ground state in the first place, prior

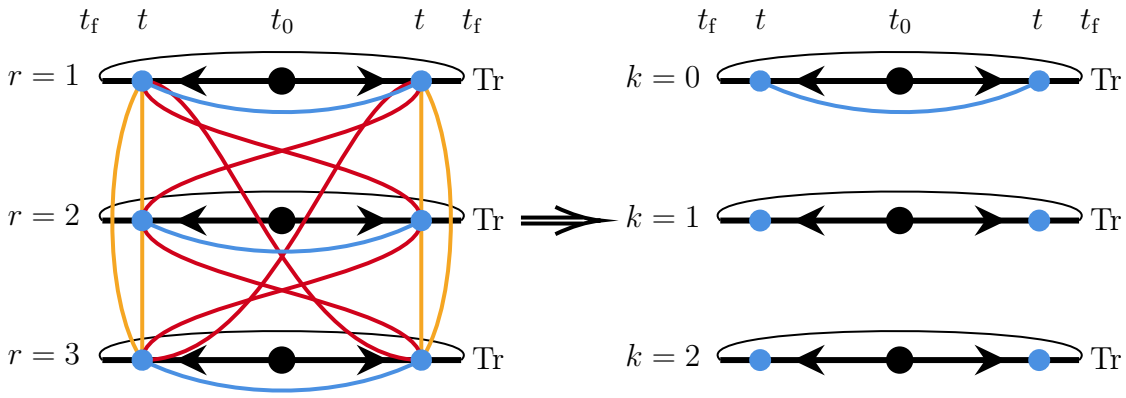

Figure 14: Illustration of the simplification of the replica theory when the Fourier transformation in replica space is performed. The thick black lines with arrows symbolize the forward and backward Keldysh contour in the time evolution of an individual replica of the quantum state from an initial state at $t = t_0$ (black circle) to a final time at $t = t_f$. The thin black lines symbolize the trace connecting the contours at this time. The coloured lines show all the couplings between fields at a given time t. In a generic monitored system, there are the usual Keldysh couplings (blue) on a single replica on the same and between the two contours. Due to the measurements, we also obtain a pairwise coupling between all replicas on the same (orange) and the opposite (red) contour. The Fourier transformation decouples the different replicas and there only remains a single replica with a coupling between the contours and $R - 1$ (here 2) replicas where the contours decouple. In the fermion model, we showed this perturbatively for weak measurement strength. After bosonization, this decoupling is exact.

to the replica construction. This is detailed in the following, using a bosonization approach, suitable for low-temperature, long distance physics in one dimension. The zero temperature property is recovered in this approach as well, where we can even show that it holds exactly to all orders in the measurement strength.

As an alternative to this approach, we might also use the fermionic path integral construction directly, using a Hubbard-Stratonovich decoupling to map the problem to a non-linear sigma model (see Ref. [98] for the 2D case and Ref. [69, 97] for projective measurements). However, throughout this thesis, we focus on the idea that we can absorb the infinite temperature behavior of the un-replicated model into a single mode of the replica model, which in turn establishes a zero temperature model for all other modes. This idea opens the toolbox of operatorial bosonization, which is very useful for a both quantitative and qualitative understanding of measurement-induced phenomena in fermion chains.

3.2.2 Bosonic replica path integral approach

Bosonization on a lattice Let us first recap the general bosonization scheme for fermions on a lattice [83, 84, 86, 87]. Consider a single type of fermions on a 1D lattice with lattice constant a described by the annihilation operators $\hat{c}_l$. We can write them

in Fourier representation as

$$\hat{c}_l = \mathcal{N} \sum_k e^{-ikal} \hat{c}_k. \tag{3.34}$$

The possible momenta k and the normalization are given by the general properties of the model: We have L/a lattice sites i.e. L/a different l. Periodicity in $al \to al + L$ constrains $e^{-ikL} = 1$ i.e. $k = \frac{2\pi n}{L}$ and n has to be integer. Besides that, we know that there can only be as many momentum states as real space states (both are finite) which means that there are only L/a different k, which are in principle free to choose. We choose $-\pi/a \leq k < \pi/a$ to satisfy that. To get fermionic commutation relations of the fermions, we need then to fix $\mathcal{N} = \sqrt{\frac{a}{L}}$. In a continuum formulation, we can still define $\hat{c}_l = \sqrt{\frac{a}{2\pi}} \hat{\psi}(al)$ where $\hat{\psi}(x)$ is a field operator. This is merely for notational convenience, in the end, we need to keep things discrete to obtain proper lattice properties.

In the Luttinger model [79–82], the main assumption is that there are two chiral modes that do not interact and therefore we can extend the momenta in both directions. If the lattice effects are to be kept, we do a decomposition into two different species as well, but they cannot be simply associated with particles moving to the left or the right. We define

$$\hat{c}_{k_F+q} = \hat{c}_{q,+} \tag{3.35}$$

$$\hat{c}_{-k_F-q} = \hat{c}_{q,-} \tag{3.36}$$

where $-k_F \leq q < k_F$, $q = 2\pi n/L$ and $k_F = \pi/2a$. The direction of the momenta q is chosen in this way because we then know that in the ground state all momenta $q < 0$ are occupied for both species. The fermionic commutation relations are preserved by that. The building blocks of the rigorous bosonization are that within the particle number eigenstate of the different species of fermions, i.e. $\left|\vec{N}\right\rangle$ with $\sum_q \hat{c}^\dagger_{q\pm} \hat{c}_{q\pm} \left|\vec{N}\right\rangle = N_\pm \left|\vec{N}\right\rangle$, all excitations are bosonic in nature. This is still true for a finite number of q values due to lattice effects, but the precise formulation becomes more complicated. In a first step, we assume that we indeed have two different species that do not couple. This means

$$\begin{aligned}
\hat{\psi}(x) &= \frac{1}{\sqrt{L}} \sum_{-2k_F \leq k < 2k_F} e^{-ikx} \hat{c}_k \\
&= \frac{1}{\sqrt{L}} e^{-ik_F x} \sum_{-k_F \leq k < k_F} e^{-ikx} \hat{c}_{k,+} + \frac{1}{\sqrt{L}} e^{ik_F x} \sum_{-k_F \leq k < k_F} e^{ikx} \hat{c}_{k,-} \\
&\approx \frac{1}{\sqrt{2\pi}} e^{-ik_F x} \underbrace{\sqrt{\frac{2\pi}{L}} \sum_{k=-\infty}^{\infty} e^{-ikx} \hat{c}_{k,+}}_{\hat{\psi}_+(x)} + \frac{1}{\sqrt{2\pi}} e^{ik_F x} \underbrace{\sqrt{\frac{2\pi}{L}} \sum_{k=-\infty}^{\infty} e^{ikx} \hat{c}_{k,-}}_{\hat{\psi}_-(-x)}
\end{aligned} \tag{3.37}$$

In the last step we neglected that the bandwidth is finite which means that we dropped

the periodicity in k due to the discreteness of the lattice. This means that if we neglect the influence of very large momenta $|k| > k_F$ i.e. we can split any excitation into a left- and a right-moving part, i.e. two chiral fermions. At larger momenta, this does not work any more and we would get chirality-breaking parts. To see how this modifies the representation of the fermions, consider the normal-ordered density of fermions in this representation

$$\begin{aligned}\hat{n}(x) &=: \hat{\psi}^\dagger(x)\hat{\psi}(x) : \\ &= \frac{1}{2\pi}(: \hat{\psi}_+^\dagger(x)\hat{\psi}_+(x) : + : \hat{\psi}_-^\dagger(-x)\hat{\psi}_-(-x) : \\ &\quad + e^{2ik_F x} : \hat{\psi}_+^\dagger(x)\hat{\psi}_-(-x) : + e^{-2ik_F x} : \hat{\psi}_-^\dagger(-x)\hat{\psi}_+(x) :) \qquad (3.38) \\ &= \frac{\hat{N}_+}{L} + \frac{\partial_x\hat{\phi}_+(x)}{2\pi} + \frac{\hat{N}_-}{L} + \frac{\partial_x\hat{\phi}_-(-x)}{2\pi} + \text{oscillating with } \pi/a \\ &\simeq n_0 - \frac{1}{\pi}\partial_x\hat{\phi}(x) \qquad (3.39)\end{aligned}$$

In the last step we used that we have a number-conserving model where the density of fermions i.e. $N_+ + N_-$ is fixed so that we can replace it by a number which gives a constant particle density which is not an operator any more. We also defined the combination $\hat{\phi}(x) = -\frac{1}{2}(\hat{\phi}_+(x) + \hat{\phi}_-(-x))$ which describes fluctuations of the density. The terms that mix the two different chiralities appear due to the fact that we can never totally decouple the left- and right moving part of the fermions. Next, we reintroduce the finite lattice spacing by giving the field ϕ an interpretation as a counting field. Bosonization can be understood using the idea that in 1D we can label all particles uniquely by counting them from left to right [83]. This means that we can define a smooth counting function $\phi_L(x)$ that takes the value $2\pi l$ at the position of the l-th particle, counting from the left. It must be therefore a monotonously growing function that is arbitrary in a system with localized particles, up to the positions x_l where the particles are located, where it takes the value $\phi_L(x_l) = 2\pi l$. For such localized particles, we can represent the local particle density as

$$n(x) = \sum_l \delta(x - x_l) = \sum_l |\partial_x\phi_L(x)|\delta(\phi_L(x) - 2\pi l) = \frac{\partial_x\phi_L(x)}{2\pi}\sum_l e^{il\phi_L(x)} \qquad (3.40)$$

In the last step we used the Poisson summation rule for the case of an infinite system where l runs from $-\infty$ to ∞ as we have infinitely many particles and we used that ϕ_L is monotonously growing across the wire. Since in the fermionic system of lattice spacing a, the particle number from one site to the next one can change maximally by 1, we know $0 \leq \phi_L(x+a) - \phi_L(x) \leq 2\pi$, in the continuum limit $a \to 0$ we get $0 \leq \partial_x\phi_L(x) \leq \frac{2\pi}{a}$ to leading order in a. In a system of constant density n_0, in the case of half filling $n_0 = \frac{1}{2a}$, the counting function would look like $\phi_L(x) = 2\pi n_0 x$. Besides that, there can

be deviations which are represented by a function $\phi(x)$ so that $\phi_L(x) = 2(\pi n_0 x - \phi(x))$. Hence the fluctuations of $\phi(x)$ are constrained to $\pi n_0 \geq \partial_x \phi(x) \geq \frac{1}{\pi}(n_0 - \frac{1}{a})$ and at half filling $|\partial_x \phi(x)| \leq \frac{\pi}{2a}$. Anything outside would correspond to faster oscillations than necessary to describe the lattice based system. We represent the particle number as

$$n(x) = \left(n_0 - \frac{1}{\pi}\partial_x \phi(x)\right) \sum_{l=-\infty}^{\infty} e^{2il(\pi n_0 x - \phi(x))}, \tag{3.41}$$

with some real function $\phi(x)$. We can identify $k_F = \pi n_0$ in the oscillating part and recognize that in the long-wavelength limit, we reproduce the result from the exact bosonization formulas presented above, namely that density fluctuations are best describes as the gradient of a field, which is of bosonic nature. Hence, we translate above expression to operators where $\hat{\phi}(x) = \hat{\phi}^\dagger(x)$ and $[\hat{\phi}(x), \hat{\phi}(x')] = 0$ since particle densities at different positions have to commute,

$$\hat{n}(x) = \left(n_0 - \frac{1}{\pi}\partial_x \hat{\phi}(x)\right) \sum_{l=-\infty}^{\infty} e^{2il(k_F x - \hat{\phi}(x))}. \tag{3.42}$$

We realize that due to the discreteness of the particle number on each lattice site, we need an infinite number of oscillating terms. Comparing with Eq.(3.39) we realize that the additional oscillating terms appear due to the finite lattice spacing. Within the Dirac model of unbound linear dispersion for both fermion species, bosonization [83] is exact and maps the Hamiltonian to

$$\hat{H} = \frac{v}{2\pi} \int dx \left[(\partial_x \hat{\phi})^2 + (\partial_x \hat{\theta})^2\right], \tag{3.43}$$

where $\hat{\theta}(x) = \hat{\theta}^\dagger(x)$ is the canonically conjugate operator $[\partial_x \hat{\theta}(x), \hat{\phi}(x')] = -i\pi\delta(x - x')$ and $v > 0$. This mapping is possible as long as the particles close to $k = k_F$ dominate the physics probed by the observables under consideration. Here this is the case as we have shown in the limit of weak measurements by demonstrating that observables that are non-linear in quantum trajectories are essentially determined by a zero temperature density operator.

We therefore found a way to represent both the Hamiltonian and the measurement-operator of the model of monitored free fermions with nearest neighbor hopping in terms of real bosonic operators. Let us now briefly comment on the observables that we need to compute in this bosonized framework. With the association $x = al$ with $a = 1$, we obtain for the connected density-density correlation function in the continuum limit

$$C_{l,l'} \to C(x, x') = \overline{\langle \hat{n}(x)\hat{n}(x')\rangle - \langle \hat{n}(x)\rangle\langle \hat{n}(x')\rangle}. \tag{3.44}$$

Plugging in the representation of $\hat{n}(x)$ in terms of the bosonic fields yields n_0^2 and $n_0\partial_x\hat{\phi}(x)$ and $n_0\cos 2l\hat{\phi}(x)$ terms that cancel out due to the connected structure of the correlation function. The remaining terms are therefore quadratic in the derivatives or they contain correlations of two cos terms. As we are interested in the long wavelength properties and the fields are strongly fluctuating, the contributions of the (bounded) cosines are irrelevant and we conclude

$$C(x,x') \simeq \frac{1}{\pi^2}\partial_x\partial_{x'}\left(\overline{\langle\hat{\phi}(x)\hat{\phi}(x')\rangle - \langle\hat{\phi}(x)\rangle\langle\hat{\phi}(x')\rangle}\right). \tag{3.45}$$

In terms of the replicated density operator this reads (for $r \neq r'$)

$$C(x,x') = \lim_{R\to 1}\frac{1}{\pi^2}\partial_x\partial_{x'}\,\mathrm{Tr}\left(\hat{\phi}^{(r)}(x)(\hat{\phi}^{(r)}(x') - \hat{\phi}^{(r')}(x'))\tilde{\rho}_R\right). \tag{3.46}$$

Based on this result and translation-invariance $C(x,x') = C(x-x')$, we also introduce the momentum-space representation as a useful observable

$$C(p) \equiv \int dx e^{ipx} C(x_0+x, x_0), \tag{3.47}$$

and the particle number fluctuation in a subsystem A, where we again use that the lattice spacing is set to $a = 1$,

$$C_A^{(2)} = \int_A dx \int_A dx' C(x,x'). \tag{3.48}$$

This is finally the leading contribution to the entanglement entropy in subsystem A,

$$S(A) \simeq \frac{\pi^2}{3} C_A^{(2)}. \tag{3.49}$$

Based on these definitions, we realize that the central observables defined above can be all deduced from the correlation function $C(x)$ or equivalently $C(p)$ which are computed in the path integral formalism in the following. Conveniently, this is also accessible in the numerical simulation of Monte Carlo wave functions to and in the non-linear sigma model approach, to which we compare the results.

Feynman Keldysh path integral Now that we rewrote the problem on the operator level in terms of bosonic degrees of freedom, let us construct a path integral description in order to solve the replicated Lindblad equation and compute the relevant correlation functions. Using that $\hat{\phi}$ and $\partial_x\hat{\theta}$ are conjugate variables, we can use a Feynman path integral construction which allows to obtain the action (see App. C.1),

all terms are functionals of $\phi_\pm^{(r)}(x,t), \theta_\pm^{(r)}(x,t)$)

$$S_R = \sum_r \left[S_V^{(r)} + S_H^{(r)} + S_{\mathcal{L}}^{(r)}\right] + \sum_{r\neq r'} S_{\mathcal{M}}^{(r,r')}, \tag{3.50}$$

where

$$S_V^{(r)} = -\frac{1}{\pi}\int_{t,x}\left(\phi_+^{(r)}\partial_x\partial_t\theta_+^{(r)} - \phi_-^{(r)}\partial_x\partial_t\theta_-^{(r)}\right), \tag{3.51}$$

$$S_H^{(r)} = -\frac{1}{\hbar}\int_t\left(H_+^{(r)} - H_-^{(r)}\right), \tag{3.52}$$

$$S_{\mathcal{L}}^{(r)} = -i\gamma\int_{t,x}\left(O_+^{(r)}O_-^{(r)} - \frac{1}{2}O_+^{(r)}O_+^{(r)} - \frac{1}{2}O_-^{(r)}O_-^{(r)}\right), \tag{3.53}$$

$$S_{\mathcal{M}}^{(r,r')} = -i\gamma\int_{t,x}\left(O_+^{(r)}O_-^{(r')} + \frac{1}{2}O_+^{(r)}O_+^{(r')} + \frac{1}{2}O_-^{(r)}O_-^{(r')}\right). \tag{3.54}$$

The measurement operator is here just the density $O(x) = n(x)$. Adding the $\pm$ index means that we replaced the operators by their eigenvalue on the $\pm$ Keldysh contour. Note that when taking the continuum limit, we need to replace the measurement rate by a measurement rate density $\gamma \to a\gamma$ where a is the lattice spacing since the original measurement operators are discrete. The dimension of γ in the field theory sense is therefore $(\text{time}\times\text{length})^{-1}$. To compute the expectation value of the trivially normal-ordered operator $\hat{\phi}^{(r)}(x)\hat{\phi}^{(r')}(x')$ at a fixed time t, we need to introduce it on both contours. As $\hat{\phi}$ commutes with itself, this yields

$$\operatorname{Tr}\hat{\phi}^{(r)}(x)\hat{\phi}^{(r')}(x')\tilde{\rho}_R(t) = \frac{1}{2}\int \mathcal{D}\Phi_\pm\mathcal{D}\Theta_\pm\phi_c^{(r)}(x,t)\phi_c^{(r)}(x',t)e^{iS_R}, \tag{3.55}$$

where we used the Keldysh rotation $\phi_{c/q}^{(r)} = \frac{\phi_+^{(r)}\pm\phi_-^{(r)}}{\sqrt{2}}$. Therefore we reformulated the problem of computing the correlation function $C(x,x')$ in the path integral formalism.

$$C(x,x') = \lim_{R\to 1}\frac{1}{2\pi^2}\partial_x\partial_{x'}\langle\phi_c^{(r)}(x,t)(\phi_c^{(r)}(x',t) - \phi_c^{(r')}(x',t))\rangle. \tag{3.56}$$

Here, $\langle\rangle$ denotes the expectation value in the path integral sense.

As argued above, the field θ does not appear in the measurement operator and the Hamiltonian is quadratic in θ. It also does not appear in the observables we intend to compute such that we can integrate it out to simplify the action. Up to the measurement-contribution, this yields the action

$$S_{0,H} = -\frac{1}{2\pi\upsilon}\int_{x,t}\sum_r\sum_\sigma\sigma\phi_\sigma^{(r)}(\partial_t^2 - v^2\partial_x^2)\phi_\sigma^{(r)}. \tag{3.57}$$

Alternatively we may write this action in momentum space using the convention

$$\phi_{\pm}^{(r)}(x,t) = \int_{-\infty}^{\infty} \frac{d\omega}{2\pi} \int_{-\infty}^{\infty} \frac{dp}{2\pi} e^{i(px+\omega t)} \phi_{\pm}^{(r)}(p,\omega), \tag{3.58}$$

and find

$$S_{0,H} = \frac{1}{2\pi v} \int_{p,\omega} \sum_{r} \sum_{\sigma} \sigma \phi_{\sigma}^{(r)*} (\omega^2 - v^2 p^2) \phi_{\sigma}^{(r)}, \tag{3.59}$$

where we use the short hand notation $\int_{p,\omega} = \int_{-\infty}^{\infty} \frac{d\omega}{2\pi} \int_{-\infty}^{\infty} \frac{dp}{2\pi}$. Note that after the transformation, the fields are complex with the constraint $\phi_{\pm}^{(r)*}(p,\omega) = \phi_{\pm}^{(r)}(-p,-\omega)$. Furthermore, we may use the replica transformation in replica space as well

$$\phi_{\sigma}^{(r)} = \frac{1}{\sqrt{R}} \sum_{k=0}^{R-1} e^{-i(2\pi k r/R)} \phi_{\sigma}^{(k)}, \tag{3.60}$$

with the equivalent property. The same definition applies equivalently to the real and momentum space representation of the field. We then find

$$S_{0,H} = \frac{1}{2\pi v} \int_{p,\omega} \sum_{k} \sum_{\sigma} \sigma \phi_{\sigma}^{(k)*} (\omega^2 - v^2 p^2) \phi_{\sigma}^{(k)}. \tag{3.61}$$

While the Fourier-transformation does not have an apparent effect here, it does in the measurement-related terms. Finally, we may apply the Keldysh rotation to check the symmetries known from the single replica case. It reads $\phi_{c/q}^{(r)} = (\phi_{+}^{(r)} \pm \phi_{-}^{(r)})/\sqrt{2}$ which equivalently translates to all Fourier transformations defined above. The action then reads

$$S_{0,H} = \frac{1}{2\pi v} \int_{p,\omega} \sum_{k} \begin{pmatrix} \phi_c^{(k)*} & \phi_q^{(k)*} \end{pmatrix} \begin{pmatrix} 0 & \omega^2 - v^2 p^2 \\ \omega^2 - v^2 p^2 & 0 \end{pmatrix} \begin{pmatrix} \phi_c^{(k)} \\ \phi_q^{(k)} \end{pmatrix}. \tag{3.62}$$

We observe that, up to the regularization fixing the temperature, this is just the R times copied Keldysh action of a Luttinger Liquid at thermal equilibrium. Here, we do not need to worry about the regularization as the measurement terms regularize the action. Now, we need to add the measurement operators to the action. All appearing terms have the form

$$\begin{aligned}
&-i\gamma \int_{x,t} n_{\sigma}^{(r)} n_{\sigma'}^{(r')} \\
&= -i\gamma \int_{x,t} \left(n_0 - \frac{1}{\pi} \partial_x \phi_{\sigma}^{(r)} \right) \sum_{l} e^{2il(\pi n_0 x - \phi_{\sigma}^{(r)})} \left(n_0 - \frac{1}{\pi} \partial_x \phi_{\sigma'}^{(r')} \right) \sum_{l} e^{2il'(\pi n_0 x - \phi_{\sigma'}^{(r')})} \\
&= -i\gamma \int_{x,t} \left(n_0 - \frac{1}{\pi} \partial_x \phi_{\sigma}^{(r)} \right) \left(n_0 - \frac{1}{\pi} \partial_x \phi_{\sigma'}^{(r')} \right) \sum_{l,l'} e^{2i(l-l')\pi n_0 x} e^{2i(l\phi_{\sigma}^{(r)} - l'\phi_{\sigma'}^{(r')})}
\end{aligned}$$

Note that the oscillating factor cancels for $l = l'$ so that only these terms survive. Also note that single derivative terms are forbidden by inversion symmetry and the product of oscillating terms with derivative terms is generically less relevant than either of the two terms. Furthermore, the constant term n_0^2 cancels out with the other terms in the action. Hence, the derivative term and the non-linearities decouple and we obtain

$$-i\gamma \int_{x,t} n_\sigma^{(r)} n_{\sigma'}^{(r')} \simeq -i\frac{\gamma}{\pi^2} \int_{x,t} \phi_\sigma^{(r)}(-\partial_x^2)\phi_{\sigma'}^{(r')} - i2n_0^2\gamma \int_{x,t} \sum_l \cos 2l(\phi_\sigma^{(r)} - \phi_{\sigma'}^{(r')}).$$

This means that we effectively measure 2 different observables with different RG relevance. Their microscopic relative strength is given by the particle density $n_0 = 1/2a = 1/2$ for half filling and formulating everything in units of the lattice spacing.

Adding measurements Ignoring the interacting part of the measurement action allows to derive a quadratic action of a gapless model describing monitored free fermions. After Fourier transformation, the Gaussian action reads

$$S_1 = -\frac{i\gamma}{\pi^2} \int_{p,\omega} p^2 \left(\phi_+^{(k=0)*}\phi_-^{(k=0)} - \frac{1}{2}\phi_+^{(k=0)*}\phi_+^{(k=0)} - \frac{1}{2}\phi_-^{(k=0)*}\phi_-^{(k=0)} \right) + \frac{i\gamma}{\pi^2} \int_{p,\omega} p^2 \sum_{k>0} \left(\phi_+^{(k)*}\phi_+^{(k)} + \phi_-^{(k)*}\phi_-^{(k)} \right). \quad (3.63)$$

This structure suggests to apply the Keldysh rotation in the $k = 0$ mode but keep the $\pm$ contour indices in the other sectors. Combining this result with the Hamiltonian yields

$$S_{0,H,1} = \underbrace{\frac{1}{2\pi v} \int_{p,\omega} \begin{pmatrix} \phi_c^{(k=0)*} & \phi_q^{(k=0)*} \end{pmatrix} \begin{pmatrix} 0 & \omega^2 - v^2p^2 \\ \omega^2 - v^2p^2 & \frac{2i\gamma v}{\pi}p^2 \end{pmatrix} \begin{pmatrix} \phi_c^{(k=0)} \\ \phi_q^{(k=0)} \end{pmatrix}}_{S_{0,H,1}^{(k=0)}[\phi^{(k=0)}]} + \sum_{k>0} \underbrace{\frac{1}{2\pi v} \sum_\sigma \int_{p,\omega} \phi_\sigma^{(k)*} \left(\sigma(\omega^2 - v^2p^2) + \frac{2i\gamma v}{\pi}p^2 \right) \phi_\sigma^{(k)}}_{S_{0,H,1}^{(k>0)}[\phi^{(k)}]}. \quad (3.64)$$

Crucially, the contour-coupling term only appears in the $k = 0$ sector where it induces the heating to the infinite temperature state. To demonstrate this, we compute the equal time correlation function of the fields (see App.C.3). Using again an infinitesimal dissipation $0^+ > 0$ as regularization ensuring causality yields that the retarded and advanced Green's function vanish at equal times, but

$$\langle \phi_c^{(k=0)*}(t,p)\phi_c^{(k=0)}(t,p')\rangle = 2\pi\delta(p-p')\frac{\gamma}{4(0^+)}. \quad (3.65)$$

Hence, the regularization does not cure the divergence when taking $0^+ \to 0$ and the Keldysh Green's function diverges for any finite measurement strength γ. Taking into account the possibility of actual finite dissipation of the ϕ fields, we conclude that the infinite-temperature state is characterized by $\gamma \gg 0^+$ where the measurement dominates over the dissipation. This is what we assume in the following. When we evaluate the non-linear terms due to measurement of $\hat{O}_2 = m \cos 2\hat{\phi}$, we need the equal time and equal position contribution

$$\left\langle \left(\phi_c^{(k=0)}(t,x)\right)^2 \right\rangle = \int \frac{dp}{2\pi} \frac{\gamma}{4(0^+)} = \frac{\gamma}{4a(0^+)}, \tag{3.66}$$

where a is the lattice spacing which regularizes the integral by introducing a finite phase space volume. The central result is here, that for any finite γ, the fluctuations become infinite which is associated with the infinite temperature state. We conclude the correlations on the Keldysh contour to be

$$\langle \phi_\sigma^{(k=0)}(t,x)\phi_{\sigma'}^{(k=0)}(t,x)\rangle = \frac{1}{2}\phi_c^{(k=0)}(t,x)\phi_c^{(k=0)}(t,x)\rangle = \frac{\gamma}{8a(0^+)}.$$

The important benchmark is here that all the correlation are positively infinite. As the behavior of the $k = 0$ mode is trivial, and it decouples from the rest of the action, we may integrate out $\phi_\sigma^{(k=0)}$ which means just to drop it. However, if we add the non-linearities emerging from the particle number measurement, this is not possible as they couple different k modes. As the behavior of the $k = 0$ mode is trivial, and it decouples from the rest of the action, we may integrate out $\phi_\sigma^{(k=0)}$ which means just to drop it. However, if we add the non-linear part of the measurement operator, this is not possible as it couples different k modes. Therefore, we integrate out the $k = 0$ fields perturbatively (see App. C.4). It even turns out, that only the leading order in the perturbative expansion is non-zero such that the remaining action after this is without further approximation

$$S[\phi] = \sum_{\sigma=\pm}\sum_{k>0} \frac{1}{2\pi v}\int_{p,\omega} \phi_\sigma^{(k)*}\left(\sigma(\omega^2 - v^2p^2) + \frac{2i\gamma v}{\pi}p^2\right)\phi_\sigma^{(k)} \\ - i\gamma n_0^2 \sum_{\sigma=\pm}\sum_{l=1}^{\infty}\sum_{r\neq r'}\int_{x,t} \cos 2l(\phi_\sigma^{(r)} - \phi_\sigma^{(r')}). \tag{3.67}$$

We obtained a replica Sine-Gordon model here. A direct Gaussian expansion of the cos term is not appropriate, but instead, we use perturbative RG to extract information about observables at large distances. This motivates to rewrite the action in terms of

complex flowing couplings as

$$S[\phi] = \sum_{\sigma=\pm} \frac{\sigma K_\sigma}{2\pi} \sum_{k>0} \int_{p,\omega} \phi_\sigma^{(k)*} \left(\frac{1}{\eta_\sigma} \omega^2 - \eta_\sigma p^2 \right) \phi_\sigma^{(k)} - \sum_{\sigma=\pm} \sum_{l=1}^{\infty} \sigma \lambda_{\sigma,l} \sum_{r \neq r'} \int_{x,t} \cos 2l(\phi_\sigma^{(r)} - \phi_\sigma^{(r')}). \quad (3.68)$$

The bare couplings can be read off as

$$K_\sigma = \sqrt{1 - \frac{2i\sigma\gamma}{\pi v}}, \qquad \eta_\sigma = v\sqrt{1 - \frac{2i\sigma\gamma}{\pi v}}, \qquad \lambda_{\sigma,l} = i\sigma\gamma n_0^2. \quad (3.69)$$

Starting with these microscopic values, we may now study the RG of this effective action. Before doing so however, it is useful to compute the relevant observables based on this action. The Gaussian part follows the structure shown in Fig. 14, such that we obtain equal and uncoupled theories for all $k > 0$ replicas. Since the couplings for all of these are renormalized in the exactly same way by the nonlinearity as shown below, we conclude that indeed all $k > 0$ modes decouple exactly and we can actually compute observables that are non-linear in the state based on an arbitrary choice of k as long as $k > 0$.

Observables on the Gaussian level At long distances, the cos term does not contribute to correlations functions as it is compact. Therefore, on a given scale in the RG flow where $K_\sigma, \eta_\sigma, \lambda_{\sigma,l}$ are given, we may compute correlations ignoring the non-linearity. Let us therefore take the Gaussian part of the action to compute the relevant observables. Note that the action decouples into independent and equal sectors for all k modes. This allows for an explicit formulation of the density-density correlation function derived above. We start from

$$C(x, x') = \lim_{R \to 1} \frac{1}{\pi^2} \partial_x \partial_{x'} \langle \phi_c^{(r)}(x,t)(\phi_c^{(r)}(x',t) - \phi_c^{(r')}(x',t)) \rangle, \quad (3.70)$$

where $r \neq r'$. Crucially, the construction of the replica field theory is symmetric under arbitrary exchanges $r \to r'$ such that we can rewrite $C(x, x')$ in terms of an average

over all choices of r and r' with $r \neq r'$,

$$\begin{aligned} C(x,x') &= \lim_{R\to 1} \frac{1}{\pi^2}\partial_x\partial_{x'} \left\langle \frac{1}{R}\sum_r \phi_c^{(r)}(x,t)(\phi_c^{(r)}(x',t) - \frac{1}{R-1}\sum_{r',r'\neq r} \phi_c^{(r')}(x',t)) \right\rangle \\ &= \lim_{R\to 1} \frac{1}{R(R-1)}\frac{1}{\pi^2}\partial_x\partial_{x'} \left\langle \sum_r \phi_c^{(r)}(x,t)\phi_c^{(r)}(x',t) - \sum_r \phi_c^{(r)}(x,t)\sum_{r'} \phi_c^{(r')}(x',t)) \right\rangle \\ &= \lim_{R\to 1} \frac{1}{R(R-1)}\frac{1}{\pi^2}\partial_x\partial_{x'} \left\langle \sum_k \phi_c^{(k)*}(x,t)\phi_c^{(k)}(x',t) - R\phi_c^{(k=0)*}(x,t)\phi_c^{(k=0)}(x',t) \right\rangle \\ &= \lim_{R\to 1} \frac{1}{R-1}\frac{1}{\pi^2}\partial_x\partial_{x'} \left\langle \sum_{k>0} \phi_c^{(k)*}(x,t)\phi_c^{(k)}(x',t) \right\rangle . \end{aligned} \tag{3.71}$$

In the last step we used the replica limit $R \to 1$. In the Gaussian action, we saw that the different $k > 0$ modes decouple and have equal correlation functions. This allows to replace $\sum_{k>0} = R - 1$ which cancels the prefactor and we can take the replica limit without encountering the divergence. We conclude

$$C(x,x') = \frac{1}{\pi^2}\partial_x\partial_{x'} \left\langle \phi_c^{(k>0)*}(x,t)\phi_c^{(k>0)}(x',t) \right\rangle , \tag{3.72}$$

where k is arbitrary. See Fig. 15 for a visualization of the transformation in replica space used to simplify the correlation function. Since the model is translation-invariant,

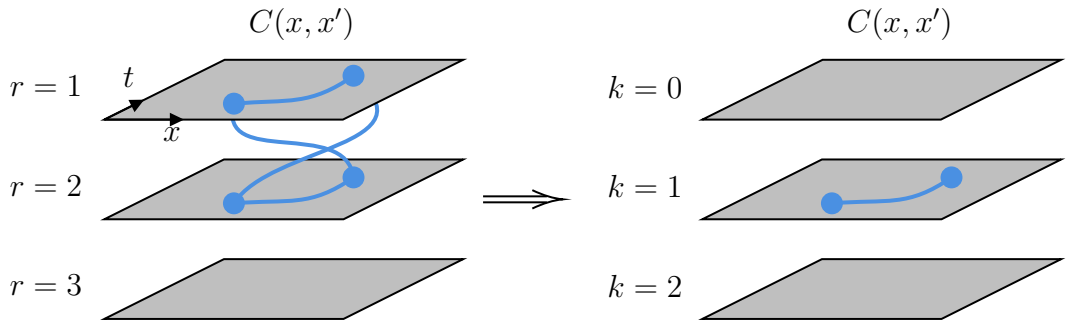

Figure 15: The correlation function $C(x,x')$ in involves terms connecting two arbitrary replicas. The Fourier transformation in replica space allows to write it terms of a single arbitrary replica with $k > 0$. As all $k > 0$ modes decouple and have the same action, it is enough to solve the problem for a single k replica.

we may also define the correlation function in momentum space,

$$C(p) = \int_x e^{ipx} C(x_0 + x, x_0) = \frac{p^2}{\pi^2}\int \frac{dp'}{2\pi} e^{i(p'-p)x_0} \left\langle \phi_c^{(k>0)*}(p,t)\phi_c^{(k>0)}(p',t) \right\rangle . \tag{3.73}$$

This motivates to solve the Gaussian integral and extract the correlation functions (see App. C.5) which yields

$$C(p) = \frac{c|p|}{2\pi}, \tag{3.74}$$

where $c = \mathrm{Re}\, 1/K_+$. Based on this result, we perform a Fourier transformation and find (for $x \neq 0$)

$$C(x) = \frac{c}{2\pi}\int_{-\infty}^{\infty}\frac{dp}{2\pi}e^{ipx}|p| \simeq \frac{c}{2\pi^2}\int_0^\infty dpp\cos pxe^{-ap} \simeq \frac{c}{2\pi^2}\frac{a^2-x^2}{(a^2+x^2)^2} \simeq -\frac{c}{2\pi^2x^2}. \tag{3.75}$$

We introduced $a > 0$ acting as a cutoff to obtain a finite result, using that the large momenta beyond $1/a$ correspond to distances $\sim a$, the lattice spacing. Mind that the bosonized description only works for long wavelength properties such that the short distance behavior needs to be cured by introducing appropriate short-distance or large momentum cutoffs. However, the regularization becomes important as soon as one integrates over short distances, which is needed for the second particle number cumulant of a subsystem A of length l. To avoid this subtlety, we compute the cumulant directly from the momentum space representation

$$C_A^{(2)} = \int_0^l dx\int_0^l dx' C(x-x') = \frac{2}{\pi}\int_0^\infty dp\frac{C(p)(1-\cos pl)}{p^2}. \tag{3.76}$$

Using the linear dependence of $C(p)$ yields

$$C_A^{(2)} = \frac{c}{\pi^2}\int_0^\infty dp\frac{1-\cos pl}{p}. \tag{3.77}$$

This integral is divergent in the UV. To cure this, we again introduce a large momentum cutoff $1/a$ due to the finite lattice spacing. This regularizes the integral to

$$C_A^{(2)} = \frac{c}{\pi^2}\int_0^{l/a} ds\frac{1-\cos s}{s} = \frac{c}{\pi^2}\left(\Gamma + \log(l/a) + \mathcal{O}((a/l)^2)\right), \tag{3.78}$$

where Γ is the Euler-Mascheroni constant. Setting $a = 1$ as we did after taking the continuum limit, we conclude that for $l \gg a(1)$

$$C_A^{(2)} \simeq \frac{c\Gamma}{\pi^2} + \frac{c}{\pi^2}\log(l). \tag{3.79}$$

This yields the leading term for the entanglement entropy

$$S(A) \simeq \frac{\pi^2}{3}C_A^{(2)} \simeq \frac{c\Gamma}{3} + \frac{c}{3}\log(l). \tag{3.80}$$

Here we recognize the typical entanglement entropy of a conformal field theory with central charge c [169–171], which motivated its definition in the first place. In particular, we find that $c = 1$ in absence of the measurement which indeed corresponds to free fermions. We may also read off the offset $s_0 = \frac{c\Gamma}{3}$. We therefore find that the only coupling emerging in the entanglement-entropy is the effective central charge c. It

undergoes an RG flow as we show below. The breakdown of the logarithmic scaling is signalled by a vanishing central charge. That means, that the entanglement becomes constant beyond the scale at which c vanishes.

3.2.3 Perturbative renormalization group for replica theory

Let us now turn to the renormalization group (RG) analysis to compute how the effective central charge c, determining the entanglement properties, behaves for large distances. We note that the Keldysh contours ($\sigma = \pm$) in the action (3.68) decouple exactly which means that we can treat both contour sectors separately. We can write the action for the forward time evolution ($\sigma = +$) as

$$iS = \frac{i}{2\pi}\sum_{k>0}\int_{\omega,p}\phi^{(k)*}\left(v\left(1-\frac{2i\gamma}{\pi v}\right)p^2-\frac{1}{v}\omega^2\right)\phi^{(k)} - \int_{x,t}\sum_{r,r'}\sum_{l}\lambda_l\cos 2l(\phi^{(r)}-\phi^{(r')}). \quad (3.81)$$

Due to the finite lattice spacing we introduce a short distance cutoff $a = 1$ which translates into a large momentum cutoff $\sim \Lambda = \pi/a$. In the temporal domain, we do not introduce a cutoff as we send $dt \to 0$ and assume that this cutoff does not matter and the frequency integrals are unbound. This allows to perform a Wick rotation $t \to it$ and re-scale space and time to eliminate v which gives the Euklidian action

$$S = \frac{1}{2\pi}\sum_{k>0}\int_{\omega,p}\phi^{(k)*}\left(K_1p^2+K_2\omega^2\right)\phi^{(k)} + i\int_{x,t}\sum_{r,r'}\sum_{l}\lambda_l\cos 2l(\phi^{(r)}-\phi^{(r')}). \quad (3.82)$$

Due to the complex cutoff structure, we formulate the action in terms of three flowing parameters with the bare values $K_1 = (1 - 2i\gamma/\pi v)$, $K_2 = 1$ and $\lambda_l = i\gamma n_0^2$. We split the fields into slow and fast modes according to

$$\phi_<^{(k)}(x,t) = \int_{-b\Lambda}^{b\Lambda}\frac{dp}{2\pi}e^{ipx}\int_{-\infty}^{\infty}\frac{d\omega}{2\pi}e^{i\omega t}\phi^{(k)}(p,\omega) = \int_<e^{i(px+\omega t)}\phi^{(k)}(p,\omega), \quad (3.83)$$

$$\phi_>^{(k)}(x,t) = \int_{b\Lambda<|p|<\Lambda}\frac{dp}{2\pi}e^{ipx}\int_{-\infty}^{\infty}\frac{d\omega}{2\pi}e^{i\omega t}\phi^{(k)}(p,\omega) = \int_>e^{i(px+\omega t)}\phi^{(k)}(p,\omega). \quad (3.84)$$

Now, we integrate out the fast modes perturbatively in λ_l to obtain an action for the slow modes,

$$S_< \simeq S_{0,<} + \langle\Delta S\rangle_{0,>} - \frac{1}{2}\left(\langle(\Delta S)^2\rangle_{0,>} - \langle\Delta S\rangle_{0,>}^2\right). \quad (3.85)$$

We need to evaluate the expectation value of the non-linearity using the previously computed correlation function on the Gaussian level[18][19] (see App. C.6):

$$\langle \Delta S \rangle_{0,>} = i \sum_l \lambda_l \int_{\mathbf{x}} \sum_{r,r'} \cos 2l\phi_<^{(r,r')} e^{-\frac{2l^2 s}{\sqrt{K_1 K_2}}}. \tag{3.86}$$

If we re-scale $\mathbf{x} \to \mathbf{x}/b$ to complete the RG step, we therefore find that the RG flow equations to linear order in the couplings λ_l is

$$\partial_s \lambda_l = 2\left(1 - \frac{l^2}{\sqrt{K_1 K_2}}\right)\lambda_l. \tag{3.87}$$

This flow equation can easily be solved

$$\lambda_l(s) = \gamma n_0^2 e^{2\left(1-\frac{l^2}{\sqrt{K_1K_2}}\right)s} \to |\lambda_l|(s) = \gamma n_0^2 e^{2\left(1-l^2\,\mathrm{Re}\,\frac{1}{\sqrt{K_1K_2}}\right)s} \tag{3.88}$$

Since at this level, K_1, K_2 are not renormalized, we plug in the bare value $\sqrt{K_1K_2} = \sqrt{1-\frac{2i\gamma}{\pi v}}$. There is then a closed expression for the real part,

$$\mathrm{Re}\,\frac{1}{\sqrt{K_1K_2}} = \mathrm{Re}\,\frac{1}{\sqrt{1-i(2\gamma/\pi v)}} = \sqrt{\frac{1+\sqrt{1+\left(\frac{2\gamma}{\pi v}\right)^2}}{2\left(1+\left(\frac{2\gamma}{\pi v}\right)^2\right)}} = 1 - \frac{3\gamma^2}{\pi^2 v^2} + \mathcal{O}((\gamma/v)^4). \tag{3.89}$$

Hence, for $\gamma \to 0$, the leading scaling behavior is

$$|\lambda_l|(s) = \begin{cases} \gamma n_0^2 e^{\frac{3\gamma^2 s}{\pi^2 v^2}} & l = 1 \\ \gamma n_0^2 e^{2(1-l^2)s} & l > 1 \end{cases}. \tag{3.90}$$

The $l = 1$ term is the only relevant one. For the second order calculation, we may therefore restrict ourselves to the leading perturbation $l = 1$ and set $\lambda_{l>1} = 0$ in the following second order calculation. Up to RG-irrelevant terms, we find (see App. C.6)

$$-\frac{1}{2}\left(\langle (\Delta S)^2 \rangle_{0,>} - (\langle \Delta S \rangle_{0,>})^2\right) = -\frac{4\lambda^2 I s}{\Lambda^4 \sqrt{K_1 K_2}} \sum_{k>0} \int_{\omega,p} \phi_<^{(k)*}(p^2+\omega^2)\phi_<^{(k)}, \tag{3.91}$$

where $I \approx 0.07805$ is an integration constant. Note that in the derivation of this expression, we needed to assume $K_1 = K_2 = 1$ such that the result is only valid in the vicinity of the BKT point. Since this point determines the critical behaviour, this does not obstruct the validity of the calculation, while is is actually important for the complex RG flow as we see later. Comparing to the original action and rescaling space

[18] $\phi^{(r,r')} = \phi^{(r)} - \phi^{(r')}$

[19] $\mathbf{x} = (x, t)$

and time $\mathbf{x} \to \mathbf{x}/b$ allows to restore the original action with new couplings

$$\lambda \to e^{2\left(1-1/\sqrt{K_1K_2}\right)s}\lambda + \mathcal{O}(\lambda^2), \tag{3.92}$$

$$K_1 \to K_1 - \frac{8\pi\lambda^2 I s}{\Lambda^4\sqrt{K_1K_2}} + \mathcal{O}(K_1-1, K_2-1), \tag{3.93}$$

$$K_2 \to K_2 - \frac{8\pi\lambda^2 I s}{\Lambda^4\sqrt{K_1K_2}} + \mathcal{O}(K_1-1, K_2-1). \tag{3.94}$$

This means that the flow equations are

$$\partial_s\lambda = 2\left(1-\frac{1}{\sqrt{K_1K_2}}\right)\lambda, \quad \partial_s K_1 = -\frac{8\pi\lambda^2 I}{\Lambda^4\sqrt{K_1K_2}}, \quad \partial_s K_2 = -\frac{8\pi\lambda^2 I}{\Lambda^4\sqrt{K_1K_2}}. \tag{3.95}$$

Note that K_1, K_2 renormalize the same way which allows to formulate the flow equations in terms of $K = \sqrt{K_1K_2}$ with the bare value $K = \sqrt{1-2i\gamma/\pi v}$ and $g = \lambda/vn_0^2$ with the bare value $g = \gamma/v$. This yields the flow equations

$$\partial_s g = 2\left(1-\frac{1}{K}\right)g, \qquad \partial_s K = -Ag^2/K, \tag{3.96}$$

where $A = \frac{8\pi n_0^4 v^2 I}{\Lambda^4}$. Note that this makes g, K dimensionless and the prefactor is indeed dimensionless. Reasonable cutoff scales are $\Lambda = \sqrt{v}\pi/a$ for the band width of the fermion model, or indeed $\Lambda = \sqrt{v}\pi/2a$ for the maximal distance from the Fermi edge. This difference makes a difference of a factor of $2^4 = 16$ for the size of the prefactor which means that the result is sensitive to the right choice of the cutoff. Still, the numerical value of the prefactor is small, $A = \frac{I}{2\pi^3} \approx\ll 1$, irrespective of this choice. Additionally, already did an expansion in small $K-1$ as we neglected the explicit K dependence of the integrals for the second order correction. Therefore, the second RG flow equation is actually only known up to the zeroth order in $K-1$ such that we replace $K = 1$ here. The flow equation for g is however exact in K. We may also re-scale g again, absorbing A into its bare value such that the RG flow equations read

$$\partial_s g = 2\left(1-\frac{1}{K}\right)g, \qquad \partial_s K = -g^2. \tag{3.97}$$

From the direct microscopic mapping, we obtained that we have an analytical expression for $K = \sqrt{1-2i\gamma/\pi v}$ while for g we may only assume that it is purely imaginary and linear in γ, while the scale is determined by non-universal microscopic properties. This result precisely reproduces what was found in Ref. [44]. The derivation presented here validates the RG result for an arbitrary replica number using the replica trick to avoid the appearance of terms that are non-linear in the state. We also did not assume any space-time equivalence but showed that the RG of spatial and temporal derivative terms behaves in exactly the same way. We now study the RG flow equations

numerically, extracting the scale-dependent central charge $c = \mathrm{Re}\, 1/K$ along the way. Depending on the choice of the microscopic couplings γ/v and A, we find two different qualitative behaviors (see Fig. 16). For $\gamma/v \lesssim 0.5$ and sufficiently small A, the RG

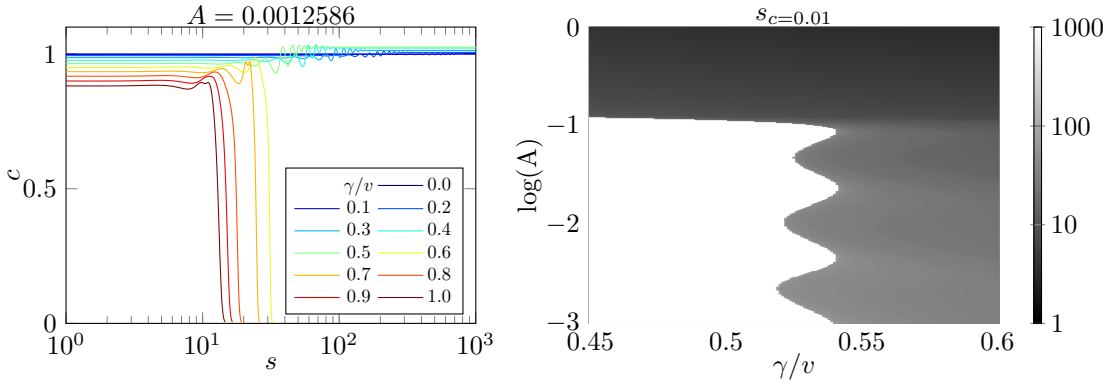

Figure 16: RG flow for the nearest neighbor hopping model, shown in terms of the effective central charge. If we use the parameter A obtained from the microscopic cutoff, we obtain a phase transition at $\gamma/v \approx 0.5$. For weaker measurement, the RG flow only weakly modifies c indicating a stable logarithmic entanglement scaling up to infinite systems. For stronger measurement, c drops to 0 at a finite length scale $L = ae^s$, signalling the transition to area law scaling. This transition vanishes if we take A by orders of magnitude larger than what we found by the microscopic mapping. Note that the length scale on which that happens is exponentially large close to the phase transition. In the RG we can easily describe scales up to $L = ae^{100}$ which is impossible in a numerical simulation.

flow only weakly modulates the effective central charge and we find that the system is in the area-law phase. For larger γ/v, the logarithmic phase is unstable, which we can see in the RG as a vanishing c beyond a certain length scale. This length scale is the correlation length, which in the present BKT scenario scales with the distance from the critical point as

$$\xi \sim e^{\frac{\alpha}{\sqrt{\gamma-\gamma_c}}}, \tag{3.98}$$

for $\gamma > \gamma_c$ where α and γ_c are non-universal parameters but the square root behavior is typical for the BKT flow. The critical point γ_c is found from the RG to be $\gamma_c \approx 0.5v$ but v non-trivially depends on the mapping of the fermionic Hamiltonian in bosonization.

Summarizing the analytical treatment of the nearest neighbor hopping model, we found that the system undergoes a phase transition at a finite measurement rate γ_c that non-trivially depends on the microscopic parameters of the original fermion model. The phase transition is of the BKT type which implies that the correlation length exponentially diverges at the critical point. This exponential length scale is particularly hard to investigate in finite system size numerical simulation which left room in the literature for different interpretations of the numerical data. Beyond that, we predict that in the strong measurement phase, the system has area law entanglement while in

the weak measurement phase it should obey conformal scaling. In the following, we check these statements numerically for both weak and strong measurements.

3.3 Monte Carlo wave functions

Informed by the analytic results in the replica formalism, we now test the predictions in finite system size numerics. To do so, we implement the QSD and QJ protocol as discussed in Sec. 3.1 and study trajectory averages in finite systems. A single run is always initialized in a randomly chosen half filled product state and then we evolve it according to the respective protocol for many trajectories in parallel, until the trajectory-average of the entanglement entropy which is computed along each trajectory reaches a stationary value up to weak fluctuations. Then, we continue evolving the state and compute the observables we are interested in repeatedly in a temporal distance given by the time that was needed to reach the stationary state. This allows to efficiently generate many statistically independent results for the trajectory-observables. We can straightforwardly estimate errors of the average from the number of samples and their mean square difference from the average of the ensemble.

Entanglement entropy First, let us consider the bipartite entanglement entropy as a function of the system size L and the length of the subsystem l, as discussed in Sec. 2.2.1. In a finite system with periodic boundary-conditions, a central prediction of a conformal field theory (CFT) is, that the entanglement-entropy has the functional dependence [169–171]

$$S(l, L) = s_0 + \frac{c}{3} \log\left(\frac{L}{\pi} \sin\frac{\pi l}{L}\right), \tag{3.99}$$

where c is the central charge and s_0 is an offset depending on the micrsocopic details. In the analytical part (see Sec. 3.2.2), we argued that for the QSD protocol, the replica theory is a Sine-Gordon model and that there is a phase where the non-linearity is irrelevant. Hence, the long-range physics of this model is predicted to behave as a non-Hermitian CFT with a continuously varying central charge. This implies that in the regime of validity of the effective long-wavelength model, the properties of a CFT are expected to surface. Indeed, we find in the numerical simulation according to the QSD protocol that the entanglement entropy in the stationary state is a function of the chord length $\frac{L}{\pi} \sin\frac{\pi l}{L}$ (see Fig. 17). The slope of the apparent logarithmic growth of the entanglement entropy however depends on the system size and it is not immediately clear from the simulations, whether it saturates or if it ultimately approaches 0, indicating an area law.

In contrast to these findings, for the QJ protocol we obtain a clear deviation from a functional dependence on the chord length as shown in Fig. 18. We also find clear evidence that the data approaches a constant value (i.e. area law) even for extremely

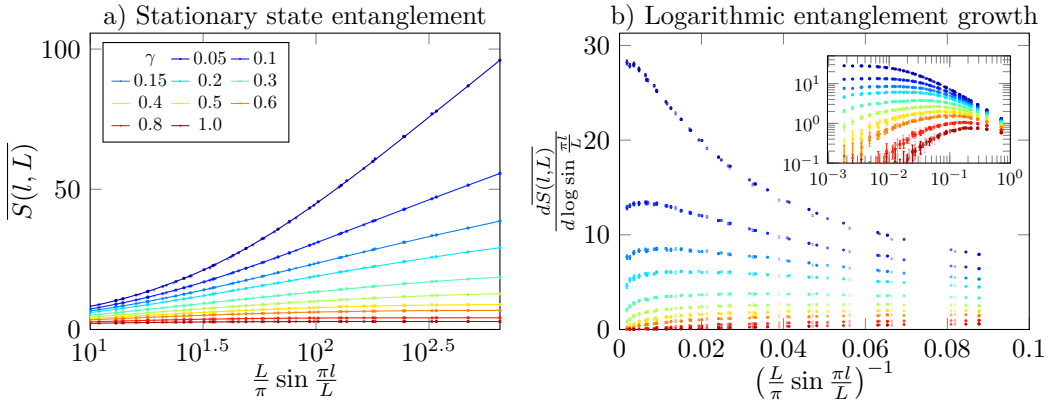

Figure 17: Entanglement entropy in the stationary state of the QSD protocol with a nearest neighbor hopping Hamiltonian for systems sizes up to $L = 2048$. We find a perfect matching of the data being a function of the cord length. To extract the slope of the entanglement growth, we numerically take the derivative with respect to the cord length. For small values of $\gamma \lesssim$, the derivative seems to saturate indicating a logarithmic scaling in the thermodynamic limit. The inset shows the same data on a logarithmic scale.

small measurement strength already at considerably much smaller systems, even though the corresponding QSD data suggests the presence of logarithmic scaling. We conclude that the QSD simulation is matches the analytical predictions from bosonization on that level, we we already see a clear discrepancy for the QJ protocol. In general, even though both protocol are unravelings for the same quantum master equation[20], the QJ protocol results in substantially reduced absolute size of the entanglement. This is rationalized by the drastic nature of projective measurements, erasing entanglement of a single site with the rest of the system in a single time-step.

This data for the entanglement entropy now provides a way to extract the effective central charge for a given system size fitting the data to Eq. (3.99) for $l = L/2 \pm n$ for $n = 1$ to $n = 4$, assuming logarithmic entanglement scaling at the largest distances resolvable for the given system size. In order to study whether the system undergoes a phase transition, we treat the fit parameter c as an order parameter: In the area law phase, c is expected to vanish upon increasing the system size while in the CFT phase, it saturates at a finite value. Therefore, we can perform a finite size scaling analysis of this order parameter, see Fig. 19. It turns out that the data for both QSD and QJ trajectories agrees with BKT essential scaling instead of the weak localization scaling $\xi \sim e^{\beta/\gamma}$. This provides further evidence for the existence of a BKT phase transition in this model. However, the critical measurement strength γ_c turns out to be very small, $\gamma_c < 0.1$ and we cannot confidently rule out $\gamma_c = 0$. Furthermore, the effective central charge in the logarithmic phase (should it exist) is very large, $\mathcal{O}(100)$. The bosonization approach lacks an explanation for this observation as it predicts $c = 1$ in

[20] We matched the notion of the measurement strength or rate in both cases to make this comparable

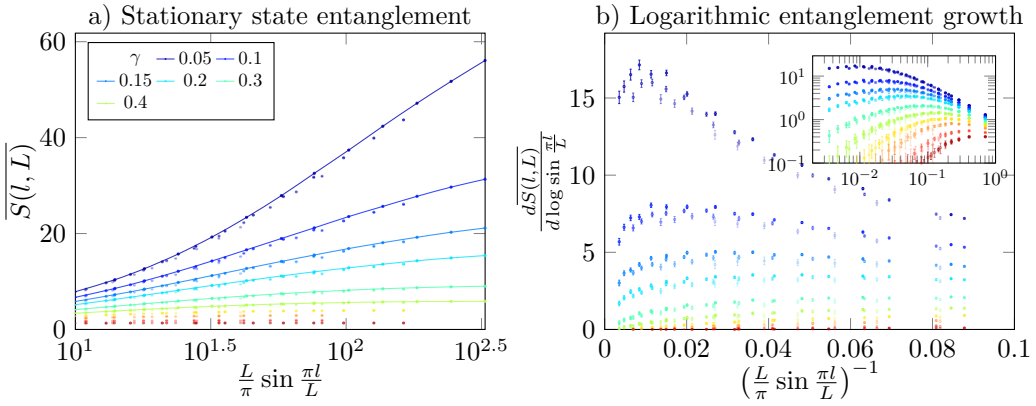

Figure 18: Entanglement entropy in the stationary state of the QJ protocol with a nearest neighbor hopping Hamiltonian for systems sizes up to $L = 1024$. There is a clear systematic discrepancy from a functional dependence of the data on the cord length for different system sizes. This indicates that the CFT prediction made for the QSD protocol does not apply here. Note that the deviation from a perfect data collapse is indeed not due to noise but instead systematic. To demonstrate this, we computed an estimate for standard deviation of the average and show error bars

the limit $\gamma \to 0$.

Extrapolation of the correlation function In order to get another estimate for the effective central charge, we additionally study $C(q)$, the numerical Fourier transformed of the density-density correlation function $C_{mn} = \overline{\langle \hat{n}_m \hat{n}_n \rangle - \langle \hat{n}_m \rangle \langle \hat{n}_n \rangle}$. In the case of free fermions, it can be directly related to the entanglement entropy (see Sec. 2.2.1, and Sec. 3.2.2). The advantage is, that we can compute this object in the simulations with very high precision and extrapolate the data to $q = 0$. The leading scaling behavior in the different phases (see Sec. 3.2.2, c.f. [69]) is expected to be

$$\frac{C(q)}{q} \to \begin{cases} 0 & \text{Area law} \\ \frac{c}{2\pi} & \text{CFT} \\ \infty & \text{Volume law} \end{cases} \tag{3.100}$$

where c is the central charge of the CFT. In the numerical simulation on a lattice, the momenta are periodic which is taken into account by plotting the data w.r.t. $\tilde{q} = 2\sin\frac{q}{2}$. Performing the simulation for large system sizes (see Fig. 20) shows, that extrapolations yield a finite effective central charge which varies with the system size. Based on this, we again perform a finite size scaling analysis of the effective central charge, shown in Fig. 21 Note that these results are obtained independently of the entanglement scaling and do not rely on an assumption of the functional dependence of the observable on the chord length, motivated by the CFT result [169, 170]. However, we obtain the same qualitative behavior and also good quantitative agreement for the central charge

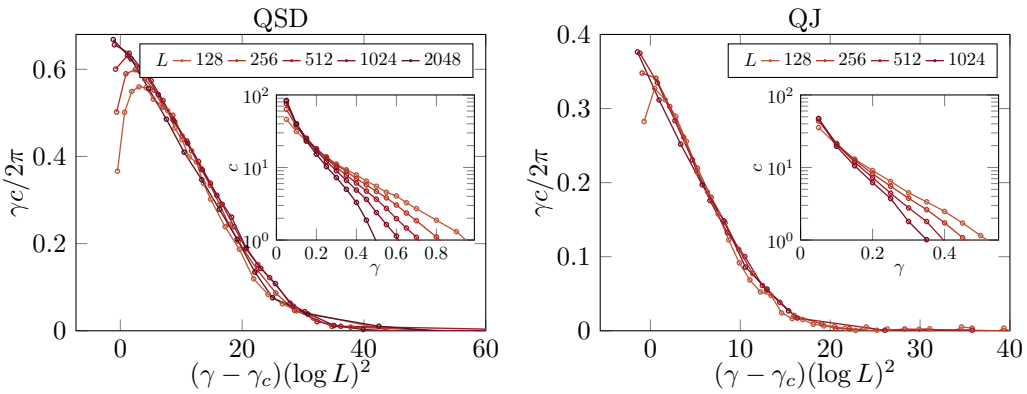

Figure 19: Scaling collapse of the central charge as extracted from a fit to the entanglement entropy as a function of the chord length. We obtain the best fit for $\gamma_c \approx 0.07, 0.08$ for QSD and QJ respectively. However, we also obtain a reasonably good data collapse for $\gamma_c \approx 0$. It is clear that the data collapse only works assuming $\xi \sim e^{\alpha/\sqrt{\gamma-\gamma_c}}$ which is the prediction from the BKT scenario, instead of $\xi \sim e^{\beta/\gamma}$, expected for weak localization. The insets show the unrescaled data.

data. We can therefore confirm that the method of operatorial bosonization correctly predicts the finite size scaling behavior and the existence of an extended range of scales with logarithmic entanglement scaling, while it lacks an explanation for the question why the apparent critical value is very small in the natural units of the problem, and why the effective central charge in the CFT phase is so large[21], $c = \mathcal{O}(100)$.

3.4 Conclusion

In this section, we investigated the question if one-dimensional free fermions with nearest neighbor hopping and local particle measurement undergo a phase transition at a finite measurement rate. To do so, we discussed that in the limit of weak measurements, where the strongly entangled phase is expected, non-linear observables in the density matrix can be characterized in terms of a theory at zero temperature. This can be seen on the level of lattice fermions and relies on the heating of the linearly averaged system to an infinite temperature state due to the repeated measurement. This yields an improved justification for the application of operatorial bosonization for this model: Ground state physics in one-dimensional quantum systems is characterized by a Sine-Gordon model. We derived this Sine-Gordon theory in a newly developed replica framework for the QSD protocol. The RG analysis of this model was done for an arbitrary number of replicas which allows to take the replica limit to characterize the phase transition of normalized replica density-operator, i.e. the physical object determining observables that are non-linear in the state. These considerations where done to put the result that this model undergoes a phase transition onto a more solid ground [44].

[21] The analytical prediction is $c \approx 1$.

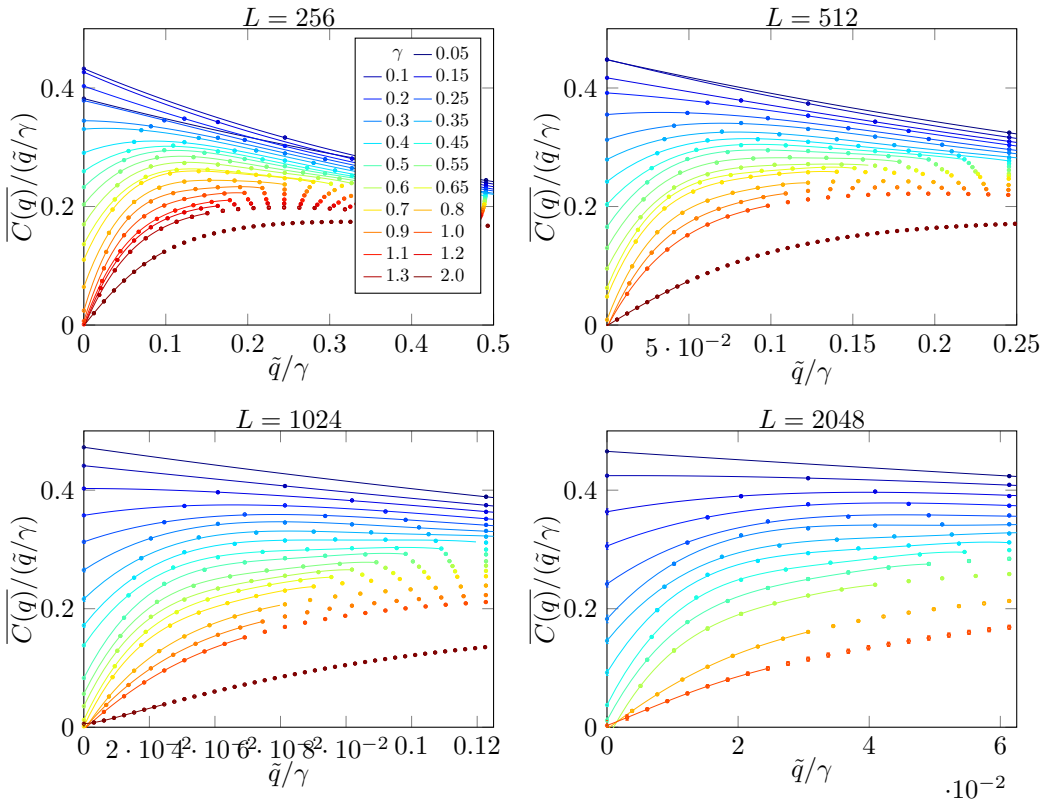

Figure 20: Scaling of the density-density correlation function for small momenta using the QSD protocol. To find an estimate for the thermodynamic limit, we extrapolate the data by a fourth order polynomial fit to the data points at the 8 smallest accessible momenta. The extrapolated data point at $\tilde{q} = 0$ is used as an order parameter to characterize the phase transition.

We also investigated specific predictions of that theory in numerical simulations and found that the Sine-Gordon model correctly predicts the finite size scaling behavior of the entanglement, in contrast to a non-linear sigma model approach put forward in Ref. [69] for the QJ protocol. Additionally, we put new bounds on the possible values of the critical measurement strength $\gamma_c < 0.1$ using a refined numerical analysis. While we cannot rule out that the existence of a finite critical point $\gamma_c > 0$ is an artifact of finite system sizes, we do find an extended regime of logarithmic scaling of the entanglement for weak measurements in such finite systems, relevant for experiments. It therefore remains of interest to study a protocol which makes the non-trivial behavior of this model accessible in experimental settings. In Sec. 5, we discuss ideas how to overcome the post-selection problem associated with measurement-induced dynamics in this system. Besides that, the ambiguity of the numerical results and the ongoing debate about the phase structure of this model motivates to study modifications that leave the system within the realm of applicability of the methods we discussed here, but add more structure to the phase diagram that can be studied numerically. Therefore, in the next section, we investigate the effect of long-range hopping which turns out to

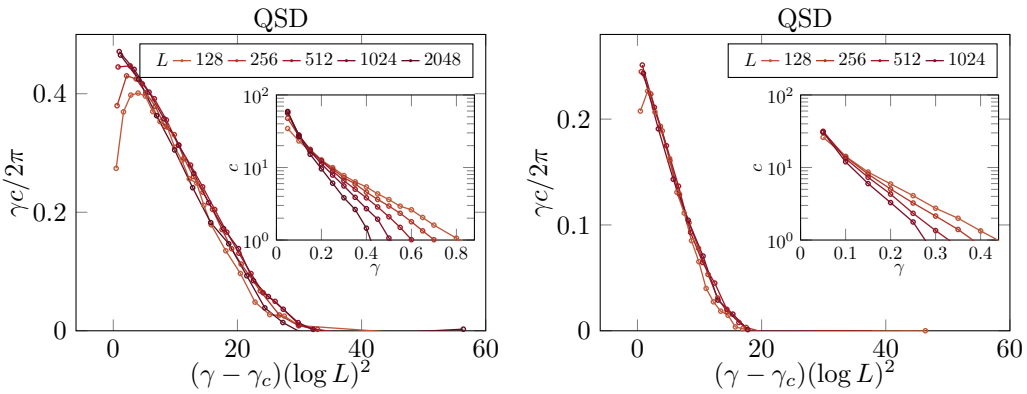

Figure 21: Scaling collapse of the central charge as extracted from the density auto correlation function $C(p)$ extrapolated in the limit $p \to 0$, see Fig. 20. We show data with $\gamma_c = 0.03$ for both QSD and QJ. We find a good quantitative agreement with the data directly obtained from the entanglement entropy.

induce a new phase [99, 128] that is predicted by the analytical framework developed in this section which coincides with numerical simulations. This also provides additional justification for the assumptions we made in the analytical treatment of the model with nearest neighbor hopping as we can make testable predictions using the bosonization approach.

4 Measurement-induced dark state phase transitions in long-ranged fermion systems

This section closely (in large parts word for word) follows the publication [99] and the associated supplemental material. The author of this thesis is a co-author of these manuscripts which is the result of a collaboration with M. Buchhold and S. Diehl. He conducted all numerical simulations which where discussed and interpreted in discussions with the other co-authors. He also derived the long-range term appearing in the bosonized action for this model and did the perturbative calculation that results in the modification to the non-Hermitian Sine-Gordon model. These computations where done under guidance by the other co-authors. He also contributed to the writing of the original manuscripts. All figures in section 4 are identical to those in Ref. [99]. The author made some changes to the manuscript to embed it into this thesis. In particular, we add more details to the analytical part and match the notation with the rest of this thesis by formulating the analysis in terms of the newly developed replica field theory method discussed in Sec. 2.2.2 and Sec. 3.2.2. This was specifically developed in preparation of this thesis.

4.1 Model and results

In the previous section, we investigated the question whether there exists a phase transition from an area-law $S \simeq L^0$ to an extended critical phase $S \simeq \log L$ induced by measurements. This scenario has been discussed in [44, 65, 68, 94, 172]. Besides that, in one dimensional quantum circuits [47–55] and also certain Hamiltonian systems [56–58] in one dimension, an entanglement transition from area-law to volume law $S \simeq L$ has been found.

This calls for the question, whether this is the exhaustive set of phases and phase transitions that can exist in monitored quantum dynamics. Promising candidates for exploring it are systems with long-ranged generators of dynamics: Long-ranged Hamiltonians are known to induce new phases in ground states, and to qualitatively modify the critical behavior at phase transitions [100–102]. The thus achieved redistribution of particles over large distances strongly modifies the entanglement dynamics and the spreading of correlations [104, 173, 174]. Experimental platforms for engineering such Hamiltonians range from trapped ions [103–106], cold atoms in cavities [107, 108], Rydberg atoms [109], and polar molecules [110].

In this work, we explore an elementary model of monitored, long-ranged dynamics: Free fermions with variably ranged hopping, characterized by an algebraic range exponent p (see Fig. 22a), competing with disentangling, local particle number measurements. As a main result, we demonstrate that the long-range entangling evolution

leads to the emergence of an unconventional dynamical phase, in which the entanglement entropy grows with the system size $S \sim L^b$ with $b = 3/2 - p$[22], faster than logarithmically but slower than the volume law of fully ergodic dynamics [175]. Furthermore, the phase features nonlinear density-density correlation functions, which follow an algebraic decay $\sim L^{-a}$ with $a = p + 1/2$. This phase is realized for exponents $1 < p < p_c = 3/2$, irrespective to the strength of measurement $\gamma > 0$: Local measurements cannot supersede the entanglement generated by long-range coherent hopping. This implies the existence of a tricritical point, where a conformally invariant phase with logarithmic entanglement growth, an area law phase, and the long-range phase meet (see Fig. 22b,c).

To establish these results, we employ a combination of numerical simulations [67, 68, 94] and an analytical replica field theory [44], in which the steady state under monitoring emerges as the dark state of an effective, non-Hermitian Sine-Gordon Hamiltonian or, equivalently as a zero temperature complex Sine-Gordon Keldysh action. The measurements then favor the evolution into an eigenstate of the measurement operators, i.e., a state with a fixed particle number $n_l = 0, 1$ at each site. This corresponds to a pinning of the density fluctuations. This mechanism competes with the long-range hopping, which establishes long-range coherent states, corresponding to a pinning of the conjugate phase. The analytical results align well with the numerical simulations, predicting the critical value of p and the scaling exponents in the long-range phase with high accuracy.

4.1.1 Microscopic model

We consider fermions on a ring of L sites (labeled s, m), which are created and annihilated by the operators, $\hat{c}_s^\dagger, \hat{c}_s$ with $\{\hat{c}_s, \hat{c}_m^\dagger\} = \delta_{s,m}$, $\hat{n}_s = \hat{c}_s^\dagger \hat{c}_s$. The long-range hopping Hamiltonian is

$$\hat{H} = -\sum_{s \neq m} h_{s,m} \hat{c}_s^\dagger \hat{c}_m, \quad h_{s,m} = |s - m|^{-p}. \tag{4.1}$$

Its range is set by the exponent p and decreases with larger p, reproducing nearest-neighbor hopping for $p \to \infty$ [44, 67, 68]. We consider $p > 1$, ensuring a well-defined thermodynamic limit with a non-singular fermion dispersion. This Hamiltonian generalizes the nearest neighbor hopping considered in Sec. 3 but leaves the applicability of the numerical approach untouched. The only change we have to do is to replace the hopping matrix h.

In order to implement measurement of the wave function, we consider the QSD protocol introduced in Sec. 2.1 and monitor the local particle number operator $\hat{n}_m = \hat{c}_m^\dagger \hat{c}_m$ with a rate γ according to (2.42). This equation is quadratic in $\hat{c}_s, \hat{c}_s^\dagger$ and number

[22] The numerical results match the analytical predictions with very high accuracy and we use the analytical identities for a, b, p_c here and in the following.

conserving, and can be efficiently simulated with Gaussian wave functions just as in the case of nearest neighbor hopping. We start from the half-filled Néel state, and evolve the system until a stationary state is reached. The random measurement outcomes

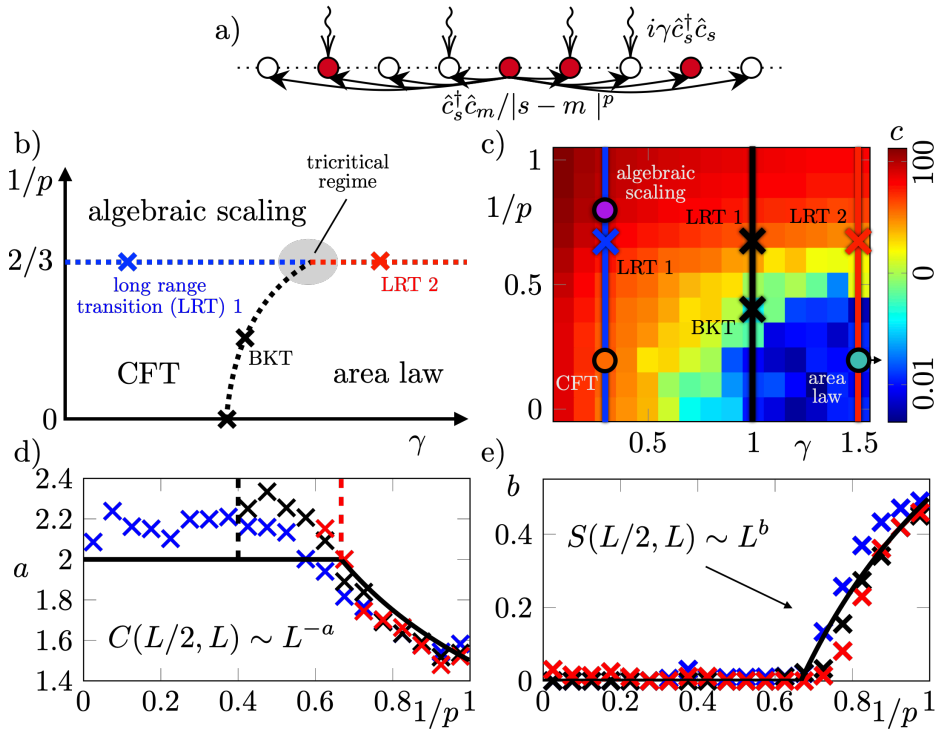

Figure 22: Phase characterization of conformally invariant ($\gamma = 0.3, p = 1.25$, orange), area-law ($\gamma = 2, p = 5$, light blue) and algebraic scaling phase ($\gamma = 0.3, p = 5$, purple). a) Half-system entanglement entropy and best fit using the ansatz $S = \frac{c}{3}\log\frac{L}{\pi} + s_0 + BL^b$. The entropy always grows slower than a volume law ($\sim L$, dashed line). b) The scaling exponent of the correlation function at opposite ends of the system is determined by fitting to $C = 1/\left[AL^a + DL\right]$ (dashed line $\sim L^{-2}$).

generate a large configurational entropy: each allowed measurement outcome appears with equal probability in the long-time limit. This is reflected in the conditioned density matrix $|\psi_t\rangle\langle\psi_t|$, whose trajectory average always yields a maximally mixed state $\overline{|\psi_t\rangle\langle\psi_t|} \sim \hat{1}$. The nontrivial quantum dynamics of individual wave functions $|\psi_t\rangle$, however, is encoded in nonlinear trajectory averages of $|\psi_t\rangle\langle\psi_t|$ [44, 55, 59, 176]. Examples are the entanglement entropy or conditioned correlation functions. This is detailed in Sec. 2.2.1. In order to access nonlinear observables analytically, we apply the *replica field theory* for MIPTs put forward in Ref. [44]. Details for this procedure can be found in Sec. 2.2.2 and for the nearest neighbor hopping case in Sec. 3. It introduces the product of two *replicated* density matrices $|\psi_t\rangle\langle\psi_t| \otimes |\psi_t\rangle\langle\psi_t|$, which allows us to separate the measurement randomness (accumulating it in an effective center-of-mass coordinate) from the inherent quantum evolution of the wave functions [44]. For fermions in one spatial dimension, the latter becomes particularly accessible due to bosonization. The quantum degrees of freedom are then mapped onto boson field

operators $\hat{\phi}_x, \hat{\theta}_x$, obeying the canonical commutation relation $[\hat{\phi}_y, \partial_x \hat{\theta}_x] = i\pi\delta(x-y)$. Here we extend the replica field theory to long-range hopping fermions (See Sec. 4.3).

4.1.2 Dark state phase structure

Based on the properties of the replica action, we qualitatively distinguish three phases (see Fig. 22b): (i) An area law phase for large monitoring ($\gamma \gtrapprox 1$) and short-ranged hopping ($p > 3/2$), (ii) a conformally invariant (CFT) phase for small but non-vanishing monitoring and short-ranged hopping ($p > 3/2$), and (iii) a novel algebraic scaling phase due to long-range hopping ($p < 3/2$). We show representative results for each phase in Fig. 23. Additionally, isolated at $\gamma = 0$, a volume law is realized, crossing over to small system sizes for $\gamma > 0$ [68].

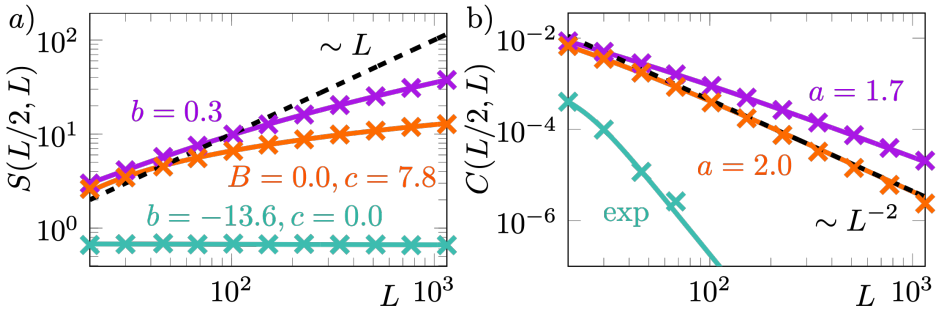

Figure 23: Phase characterization of conformally invariant ($\gamma = 0.3, p = 1.25$, orange), area-law ($\gamma = 2, p = 5$, light blue) and algebraic scaling phase ($\gamma = 0.3, p = 5$, purple). a) Half-system entanglement entropy and best fit using the ansatz $S = \frac{c}{3}\log\frac{L}{\pi} + s_0 + BL^b$. The entropy always grows slower than a volume law ($\sim L$, dashed line). b) The scaling exponent of the correlation function at opposite ends of the system is determined by fitting to $C = 1/\left[AL^a + DL\right]$ (dashed line $\sim L^{-2}$).

To obtain these results, we use a combination of numerical simulations that we discuss in Sec. 4.2, and an extension of the replica Keldysh field theory for the bosonized model, presented in Sec. 4.3.

4.2 Numerical simulations

Numerically, we combine two approaches to distinguish the three phases, and their boundaries. (1) Informed by logarithmic growth of the entanglement entropy in the CFT phase, $S(L/2, L) \sim \frac{c}{3}\log(L)$, we assume a logarithmic scaling of $S(L/2, L)$ and extract a size-dependent prefactor $c(L)$. In the area-law phase and in the CFT phase, $c(L)$ saturates as a function of the system size. In the algebraic phase it does not saturate, indicating faster than logarithmic growth of $S(l, L)$ on large distances (see Fig. 22c, Fig. 26a), allowing us to localize the phase boundaries. (2) We make a general ansatz for $S(L/2, L)$ and $C(L/2, L)$, including both algebraic and logarithmic scaling and compute the best fit as a function of L (see Fig. 23). For sufficiently large system

sizes (up to $L = 2048$), the fits then converge to *either* a logarithmic *or* an algebraic form. This yields consistent results for the scaling behavior in each regime, as well as for the scaling exponents and the location of the phase boundaries (see Fig. 22d,e). We further confirm these results by a third approach (see Fig. 24), where we vary the subsystem size l. First, we recall the properties of phases appearing in the short-range

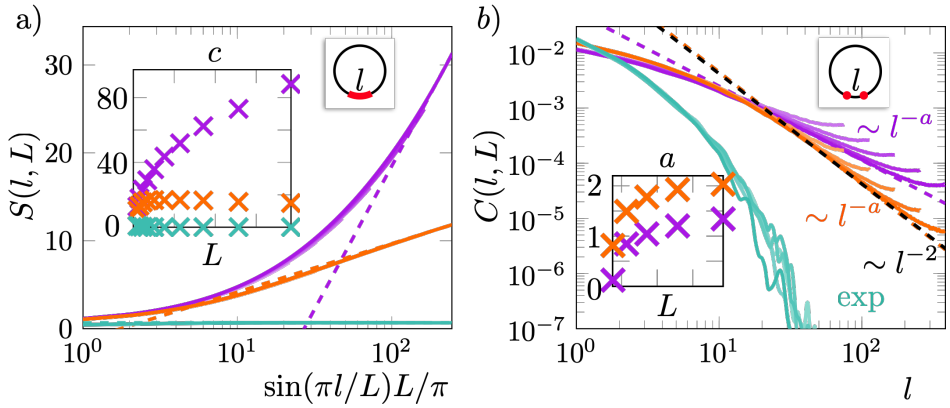

Figure 24: Further characterization of CFT ($\gamma = 0.3, p = 1.25$, orange), area-law ($\gamma = 2, p = 5$, light blue) and algebraic scaling phase ($\gamma = 0.3, p = 5$, purple) in terms of subsystem size dependent observables for different system sizes (different shades) up to $L = 770$. a) The collapse of the entanglement entropy onto a function of the conformally invariant combination $\frac{L}{\pi} \sin \frac{\pi l}{L}$ for different L breaks down in the algebraic scaling phase. Inset: L-dependence of the extracted effective central charge. Dashed lines: best fit under the assumption of a CFT at $L = 770$. b) Emergence of algebraic scaling of the correlation function at intermediate l for $L \to \infty$ in the CFT and the algebraic scaling phase. Fitting to the scaling regime yields the exponents indicated in the inset and (for $L = 770$) by dashed lines in the main plot (black dashed line $\sim l^{-2}$ for comparison).

hopping limit [68]. In the CFT-like regime (orange curves in Fig. 24 and Fig. 23), we observe an asymptotic scaling collapse of the entanglement entropy,

$$S(l, L) \simeq \frac{c}{3} \log \left[\frac{L}{\pi} \sin \frac{\pi l}{L} \right] + s_0, \tag{4.2}$$

familiar from a CFT with periodic boundary conditions in 1+1 dimensions [170, 171]. The effective central charge c can be extracted efficiently from the simulations (see Fig. 24a, inset) by fitting the data to Eq. (4.2) for $L/4 < l < 3L/4$, and depends in a continuous way on both the hopping range p and the monitoring strength γ (see Fig. 22c in the main text). However, the phase is stable against deviations from the nearest-neighbor hopping $p = \infty$. This result is supported by the asymptotic scaling collapse of the correlation function onto

$$C(l, L) \sim \left[\frac{L}{\pi} \sin \frac{\pi l}{L} \right]^{-2} \sim \frac{1}{l^2}, \frac{1}{L^2}, \tag{4.3}$$

in the same parameter-regime (see Fig. 24b) and Fig. 23b in the main text), in agreement with conformal scaling [170, 171].

Conversely, the area-law phase (light blue lines in Fig. 24 and Fig. 23) is characterized by asymptotically constant entanglement entropy, quantified by a vanishing effective central charge, and exponentially decaying correlation functions, both as functions of l and L. Applying the same procedure in the long-range hopping regime (purple curves in Fig. 24 and Fig. 23) reveals a breaking of this behavior in three ways: (i) $S(l, L)$ and $C(l, L)$ do not collapse onto a function of the scale-invariant combination $\frac{L}{\pi} \sin \frac{\pi l}{L}$, (ii) the extracted effective central charge does not approach a finite value for for $L \to \infty$ (see Fig. 26a), indicating algebraic scaling of the entanglement entropy, and (iii) the correlation function $C(l, L)$ decays algebraically, but slower than l^{-2} or L^{-2}. To extract the critical point, where the algebraic scaling sets in, and the exponents for both S and C in this regime, we use an ansatz to capture both conformal scaling and algebraic scaling, and finite size effects

$$S(L/2, L) = BL^b + \frac{c}{3} \log \frac{L}{\pi} + s_0, \quad C(L/2, L) = \frac{1}{AL^a + DL}. \tag{4.4}$$

Fitting B, b, c, s_0, A, a and D to the numerical data is sensitive to the phase transition. Especially the exponents a and b can be extracted quantitatively, signalling the algebraic scaling phase by $a < 2$ and $b > 0$ (cf. Fig. 1d,e in the main text). Comparing the exponents extracted in this way to $S(l, L) \sim l^b$ and $C(l, L) \sim l^{-a}$ in a scaling regime at intermediate l shows good agreement (cf. Fig. 24).

4.3 Bosonic Keldysh replica field theory

4.3.1 Replica action of the long-range hopping model

We show in this section how to bosonize the long-range hopping Hamiltonian and write the bosonic replica Keldysh action for this case. To do so, we represent the lattice fermions in terms of the real bosonic operators as [83]

$$\hat{c}_l^\dagger \to \hat{\psi}^\dagger(x) = \sqrt{\hat{n}(x)} e^{-i\hat{\theta}(x)}, \tag{4.5}$$

where $\hat{n}(x)$ is represented in terms of the counting field $\hat{\phi}(x)$, as shown in Sec. 3. In the continuum limit, the Hamiltonian can be written as

$$\hat{H} = -\int_{x,y}' \frac{\hat{\psi}^\dagger(x)\hat{\psi}(y)}{|x - y|^p}, \tag{4.6}$$

where $\int'$ denotes that short distances $|x-y| < a$, where a is the lattice spacing, are cut off. Note that the distributions from short distances $|x - y| \approx a$ can be captured by a

derivative expansion around the Fermi points, which yields the Dirac model to leading order. Subsequently, using the same construction and arguments as in Sec. 3, we again obtain the usual Luttinger liquid Hamiltonian [79–81]. Therefore, to study the effect of the slowly decaying hopping amplitudes, we focus on the large distance behavior of the Hamiltonian. At large distances $|x-y| \to \infty$, we may assume the density at sites x and y to be uncorrelated such that we replace $\hat{n} \approx n_0$ in this limit. For that reason, we consider the bosonized Hamiltonian

$$\hat{H} = \hat{H}_{\mathrm{sr}} + \hat{H}_{\mathrm{lr}}, \tag{4.7}$$

$$\hat{H}_{\mathrm{sr}} = \frac{v}{2\pi} \int dx \left[(\partial_x \hat{\phi})^2 + (\partial_x \hat{\theta})^2 \right], \tag{4.8}$$

$$\hat{H}_{\mathrm{lr}} = -\delta \int_{x,y}' |x-y|^{-p} \cos\Big(\hat{\theta}(x) - \hat{\theta}(y)\Big). \tag{4.9}$$

$\delta = n_0 > 0$ is the microscopic coupling of the long-range contribution. Note that v is expected to be modified due to short-range contributions beyond $|x-y| = 1$. This does not change the universal properties of the system but changes the non-universal critical point. Now, we include the long-range hopping Hamiltonian into the replica field theory framework. Since the short-range Hamiltonian and the measurement-term remain unchanged compared to Sec. 3, this only amounts to adding the following term

$$S_{\mathrm{lr}} = \delta \sum_{r=1}^{R} \sum_{\sigma=\pm} \int_{t,x,y}' \sigma |x-y|^{-p} \cos \theta^{(r)}_{\sigma,x,y}, \tag{4.10}$$

where we defined $\theta^{(r)}_{\sigma,x,y}(t) = \theta^{(r)}_{\sigma}(t,x) - \theta^{(r)}_{\sigma}(t,y)$. The addition of this term is not expected to prevent the linearly averaged density-operator from heating up to an infinite temperature state as this is driven by the unmodified measurements. Therefore, we proceed as before, performing a Fourier-transformation in replica space and integrating out the $k = 0$ mode. In contrast to the short-range contribution, S_{lr} does not decouple into independent k contributions such that we treat it perturbatively in δ, just like the measurement non-linearity in Sec. 3. In order to do so, we need to compute the correlation functions of $\theta^{(k)}_{\sigma}$ in the Gaussian approximation, in particular for $k = 0$, which means that in this case we cannot simply eliminate the θ fields as we did for the short-ranged model. However, we can simply re-introduce the θ fields and obtain the

Gaussian part of the action

$$S_0 = \frac{1}{2\pi}\int_{\omega,q} \Psi^{(k=0)\dagger} \begin{pmatrix} 0 & 0 & -vq^2 & \omega q \\ 0 & 0 & \omega q & -vq^2 \\ -vq^2 & \omega q & \frac{2i\gamma}{\pi}q^2 & 0 \\ \omega q & -vq^2 & 0 & 0 \end{pmatrix} \Psi^{(k=0)} + \sum_{k>0} \frac{1}{2\pi}\int_{\omega,q} \sum_{\sigma=\pm} \begin{pmatrix} \phi_\sigma^{(k)*} & \theta_\sigma^{(k)*} \end{pmatrix} \begin{pmatrix} -\sigma v q^2 + \frac{2i\gamma}{\pi}q^2 & \sigma\omega q \\ \sigma\omega q & -\sigma v q^2 \end{pmatrix} \begin{pmatrix} \phi_\sigma^{(k)} \\ \theta_\sigma^{(k)} \end{pmatrix} \quad (4.11)$$

Where $\Psi^{(k=0)} = \begin{pmatrix} \phi_c^{(k=0)} & \theta_c^{(k=0)} & \phi_q^{(k=0)} & \theta_q^{(k=0)} \end{pmatrix}^T$. We still find that all k modes decouple and that the $k = 0$ mode is qualitatively different from all the others. For the $k = 0$ mode we find the (now matrix valued) Green's functions

$$G_K^{(k=0)} = \frac{-2i\gamma v}{(\omega^2 - v^2q^2 - 0^{+2})^2 + 40^{+2}\omega^2} \begin{pmatrix} v^2q^2 & -\omega v q \\ -\omega v q & \omega^2 \end{pmatrix}, \quad (4.12)$$

$$G_{R/A}^{(k=0)} = \frac{i\pi}{(\omega \pm i0^+)^2 - v^2q^2} \begin{pmatrix} v & \frac{\omega \pm i0^+}{q} \\ \frac{\omega \pm i0^+}{q} & v \end{pmatrix}. \quad (4.13)$$

Here we again included an infinitesimal regularization $0^+ > 0$ ensuring causality. This means, that all correlations between classical fields at equal times diverge as the integral over ω diverges even with regularization, as the integral over ω scales as $\sim 1/0^+$ (see Sec. 3). On the other hand, for the retarded and advanced Greens function we may always close the contour such that the pole is not enclosed which means that they vanish at equal times. Using that, we can compute the expectation value of the long-range action over the $k = 0$ component exactly as for the measurement non-linearity above

$$\begin{aligned} \langle S_{\mathrm{lr}}\rangle_{k=0} &= \delta \int_{t,x,y}' \sum_{r=1}^{R}\sum_{\sigma=\pm} \sigma|x-y|^{-p} \left\langle \cos\left(\frac{1}{\sqrt{R}}\theta_{\sigma,x,y}^{(k=0)} + \frac{1}{\sqrt{R}}\sum_{k>0}\theta_{\sigma,x,y}^{(k)} e^{i2\pi kr/R}\right)\right\rangle_{k=0} \\ &= \delta \int_{t,x,y}' \sum_{r=1}^{R}\sum_{\sigma=\pm} \sigma|x-y|^{-p} \cos\left(\frac{1}{\sqrt{R}}\sum_{k>0}\theta_{\sigma,x,y}^{(k)} e^{i2\pi kr/R}\right) e^{-\frac{1}{2R}\langle\theta_{\sigma,x,y}^{(k=0)}\rangle_{k=0}} = 0 \end{aligned} \quad (4.14)$$

In contrast to the measurement non-linearity, in this cases there is no exact cancellation of terms over which the expectation value is taken such that the infinite fluctuations of the infinite temperature state are always present, rendering $\langle S_{\mathrm{lr}}\rangle_{k=0}$. Therefore, in this case a second order perturbative expansion in S_{lr} is needed to integrate out the $k = 0$ mode from this term. Therefore, the leading contribution in δ to the action after integrating out the $k = 0$ modes reads $\frac{i}{2}\langle S_{\mathrm{lr}}^2\rangle_{k=0}$. To simplify the expression, we use

that we can expand

$$\cos^2(a+b) = \cos^2 a \cos^2 b + \sin^2 a \sin^2 b - \sin a \cos a \sin b \cos b \tag{4.15}$$

where a represents the the $k=0$ field and b represents the $k>0$ fields and that for instance

$$\begin{aligned}\left\langle \cos \frac{1}{\sqrt{R}} \theta^{(k=0)}_{\sigma,x,y}(t) \cos \frac{1}{\sqrt{R}} \theta^{(k=0)}_{\sigma',x',y'}(t') \right\rangle_{k=0} =& \frac{1}{2} \left\langle \cos\left(\frac{1}{\sqrt{R}} \theta^{(k=0)}_{\sigma,x,y}(t) - \frac{1}{\sqrt{R}} \theta^{(k=0)}_{\sigma',x',y'}(t') \right) \right\rangle_{k=0} \\ &+ \frac{1}{2} \left\langle \cos\left(\frac{1}{\sqrt{R}} \theta^{(k=0)}_{\sigma,x,y}(t) + \frac{1}{\sqrt{R}} \theta^{(k=0)}_{\sigma',x',y'}(t') \right) \right\rangle_{k=0}.\end{aligned} \tag{4.16}$$

This term is only finite if the terms in the cos exactly cancel out such that the infinite fluctuations do not yield 0. This is only possible if $\sigma = \sigma'$ and precisely $t = t'$ and $x = x', y = y'$ for the first term and $x = y', y = x'$ for the second term. If these conditions are met, the fields cancel and the expectation value is 1. Otherwise, the infinite fluctuations let the expectation value of the cosine vanish and there is no contribution to the action. Therefore, in order to obtain a finite contribution to the replica action determining the non-linear observables such as entanglement entropy, we need to include a regularization in both space (lattice spacing a) and time (dt). Besides the $\cos^2$ term, there appears also the equivalent problem with $\sin^2$ and $\sin\cos$. For the $\sin^2$ part, the two contributions from matching the positions exactly cancel out, while in the $\sin\cos$ term all contributions vanish independently. Putting everything together yields

$$S^{(k>0)}_{\mathrm{lr}} = \frac{i}{2} \langle S^2_{\mathrm{lr}} \rangle_{k=0} + \mathcal{O}(\delta^3) \tag{4.17}$$

$$= i\Delta \sum_{\sigma=\pm} {\int_{t,x,y}}' |x-y|^{-2p} \left(\sum_{r=1}^{R} \cos\left(\frac{1}{R} \sum_s (\theta^{(r)}_{\sigma,x,y} - \theta^{(s)}_{\sigma,x,y}) \right) \right)^2 + \mathcal{O}(\delta^3) \tag{4.18}$$

where $\Delta = \frac{1}{2} dt a^2 n_0^2 > 0$. Note the doubling of the exponent describing the decay of the hopping matrix elements. Just as for the short-range contributions to the model, the Keldysh contours exactly decouple. We find again, that for the entire action (including the measurement non-linearity) the Keldysh contours decouple due to the infinite temperature state of the $k=0$ sector. This implies that we can understand the theory in terms of a non-Hermitian Hamiltonian as the action has the structure

$$S = -\int_t (H_+ - H_-^*). \tag{4.19}$$

Hence, remembering the construction of the path integral, we identify the non-Hermitian Hamiltonian $\hat{H}$ by replacing (normal-ordered) fields in H_+ by the corresponding oper-

ators. The observables obtained from the solution of the path integral derived above then coincide with the ones obtained from the dark state of the non-Hermitian Hamiltonian. In Ref. [99], we compute the observables along these lines, while we use the path-integral formulation throughout this thesis for consistency.

4.3.2 Phase structure and observables

Let us now take a step back and analyze the situation: We mapped the long-range hopping model to a bosonic replica field theory consisting of three different terms: (1) There is a gapless Gaussian contribution. In absence of non-linearities it is a conformal field theory with the hallmark of logarithmic entanglement scaling. (2) On top of that, we find a non-linearity due to the cos contribution to the measurement operator $\hat{n}_l$ in bosonized language. If this term is relevant, the counting field ϕ is gapped which signals an area-law phase. Both these cases have been discussed in detail in Sec. 3 both numerically and analytically. Between these two phases we identified a BKT phase transition. (3) In the presence of long-range hopping, another contribution is added to the action, which only emerges in second order perturbation theory and only acts on the phase fields. If this term is relevant, the phase is pinned instead of the fluctuations. Since the two degrees of freedom are conjugate to each other, this implies that a third phase emerges (two conjugate fields cannot be pinned simultaneously). In this phase, the non-linearity pinning the counting field ϕ is irrelevant while the long-range contribution is relevant which justifies an expansion in $\theta^{(r)}_{\sigma,x,y}$. Note that in this case, an expansion is only justified near *minima* of $\cos^2$ to keep the path integral well defined, i.e. for $\frac{1}{R}\sum_{s=1}^{R}(\theta^{(r)}_{\sigma,x,y} - \theta^{(s)}_{\sigma,x,y}) \approx \pi/2$. This occurs because the second order contribution appears in form of a dissipative term in this case and is important to obtain the correct sign for the observables. Up to an irrelevant constant and a prefactor $R \to 1$, this yields to quadratic order

$$\begin{aligned} S_{\mathrm{lr}}^{(k>0)} &= i\Delta \sum_{k>0}\sum_{\sigma=\pm}\int'_{t,x,y} |x-y|^{-2p}|\theta^{(k)}_{\sigma}(x) - \theta^{(k)}_{\sigma}(y)|^2 \\ &= 8i\Delta \sum_{k>0}\sum_{\sigma=\pm}\int_{\omega,q}\int_{a}^{L/2} dy y^{-2p}\sin^2\frac{qy}{2}\theta^{(k)*}_{\sigma}\theta^{(k)}_{\sigma} \\ &= 8i\Delta \sum_{k>0}\sum_{\sigma=\pm}\int_{\omega,q}\int_{|q|a}^{|q|L/2} dy \frac{\sin^2\frac{y}{2}}{y^{2p}}\theta^{(k)*}_{\sigma}|q|^{2p-1}\theta^{(k)}_{\sigma}. \end{aligned} \tag{4.20}$$

We introduced a finite system size L here to make sure that the integral over y is finite. Depending on p we can distinguish three different cases: For $p \leq 1/2$, the integral diverges in the infrared which means that the model is ill-defined. We do not further consider that case. If $p \geq 3/2$, the integral is divergent in the ultra-violet which is

regularized by the lattice spacing. The leading contribution in a reads in this case

$$S_{\mathrm{lr}}^{(k>0)} = \frac{2i\Delta a^{3-2p}}{2p-3} \sum_{k>0} \sum_{\sigma=\pm} \int_{\omega,q} \int_{qa}^{qL/2} dy \frac{\sin^2 \frac{y}{2}}{y^{2p}} \theta_\sigma^{(k)*} q^2 \theta_\sigma^{(k)}. \tag{4.21}$$

This means, that the long-range term adds a term to the action that has the same RG relevance as the original Gaussian action, even though with an imaginary prefactor due to its origin in second order perturbation theory. However, this means that the scaling behavior of the the observables remains unchanged independently of the precise value of p, while prefactors may indeed be changed. We conclude that in this regime, the long range hopping does not result in a new measurement-induced phase. Finally, for $1/2 < p < 3/2$, we can take the limit $L \to \infty$ and $a \to 0$ and obtain a finite number in the integral,

$$I_p = \int_0^\infty dy \frac{\sin^2 \frac{y}{2}}{y^{2p}} = \frac{\Gamma(2-2p)\sin \pi p}{4p-2}. \tag{4.22}$$

A plot of this function is shown in Fig. 25. This means that we obtain

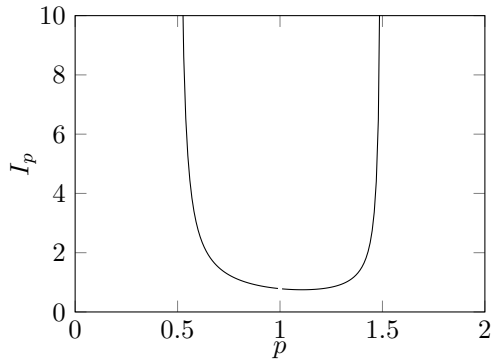

Figure 25: The integral I_p determines the dispersion in the Gaussian approximation. Only for $1/2 < p < 3/2$, it yields a finite number and both the ultraviolet and infrared behavior are regular.

$$S_{\mathrm{lr}}^{(k>0)} = 8i\Delta I_p \sum_{k>0} \sum_{\sigma=\pm} \int_{\omega,q} \theta_\sigma^{(k)*} |q|^{2p-1} \theta_\sigma^{(k)}. \tag{4.23}$$

Since $p < 3/2$, we find $2p-1 < 2$ such that this term dominates over the short-range contribution at short distances. This modified scaling results in a different scaling for correlation functions and entanglement which we associate with the emergence of an additional phase, driven by long-range hopping. As the original fermionic model is still Gaussian, even in presence of this additional, we again use that the relevant observables can all be obtained from the Keldysh greens function of the counting field, describing density fluctuations. To obtain them, we need to consider the Gaussian action for the $k > 0$ components, replacing the dispersion of the phase field by the dominant

long-range contribution,

$$S_0^{(k>0)} = \sum_{k>0} \frac{1}{2\pi} \int_{\omega,q} \begin{pmatrix} \phi_\sigma^{(k)*} & \theta_\sigma^{(k)*} \end{pmatrix} \begin{pmatrix} -\sigma v q^2 + \frac{2i\gamma}{\pi} q^2 & \sigma\omega q \\ \sigma\omega q & iA|q|^{2p-1} \end{pmatrix} \begin{pmatrix} \phi_\sigma^{(k)} \\ \theta_\sigma^{(k)} \end{pmatrix}, \quad (4.24)$$

where $A = 16\pi\Delta I_p > 0$. By solving the Gaussian integral, we find the Green's functions for the density counting field

$$G_{\sigma\sigma'}(\omega, q) = \delta_{\sigma\sigma'} \frac{-i\pi A|q|^{2p-3}}{\omega^2 + i\sigma v K_\sigma^2 A|q|^{2p-1}}, \quad (4.25)$$

where we introduced again the bare Luttinger parameter $K_\sigma = \sqrt{1 - \frac{2i\sigma\gamma}{\pi v}}$. The density-density correlation function is found in momentum space to be

$$C(q) = \frac{iq^2}{2\pi^2} \sum_{\sigma,\sigma'} \int \frac{d\omega}{2\pi} G_{\sigma\sigma'}(\omega, q) = \frac{\sqrt{A/v}}{2\pi} \operatorname{Re} \frac{1}{\sqrt{i}K^2} |q|^{p-1/2}. \quad (4.26)$$

This behavior smoothly connects to the linear momentum-dependence found in the Luttinger liquid phase at $p = 3/2$. A Fourier-transformation of this result shows that the correlation functions and the entanglement entropy acquire a p-dependent scaling exponent[23],

$$S(l) \sim B|l|^b + s_0, \quad b = \tfrac{3}{2} - p, \quad (4.27)$$

$$C(l) \sim A|l|^{-a}, \quad a = p + \tfrac{1}{2}. \quad (4.28)$$

This analytical estimate is confirmed by the numerical simulations very accurately, which is demonstrated in Figs. 22d,e, Fig. 23 (purple lines), and 24. These scaling exponents clearly differ from the volume-law $b = 1$, found for instance in monitored random circuits [50, 176, 178–183]. We find a slower growth of the entanglement entropy $b < 1/2$, matching the scaling relation $b = 2 - a$ (see Fig. 26b), implied by the Klich-Levitov formula [158] as discussed in Sec. 2.2.1.

4.3.3 Renormalization of the long-range action

Let us now study the different three different regimes shown in Fig. 22b using the renormalization group perspective. The area-law (i) and CFT (ii) regimes are established for the limit $p \to \infty$ (numerically in Refs. [68, 172] and analytically in Ref. [44] and also detailed in Sec. 3). In the following, we thus focus on the new algebraic regime (iii) and the phase transitions (i)↔(iii) and (ii)↔(iii). Canonical power counting of the

[23] Variable, measurement-induced exponents have also been reported in the time domain in Ref. [177].

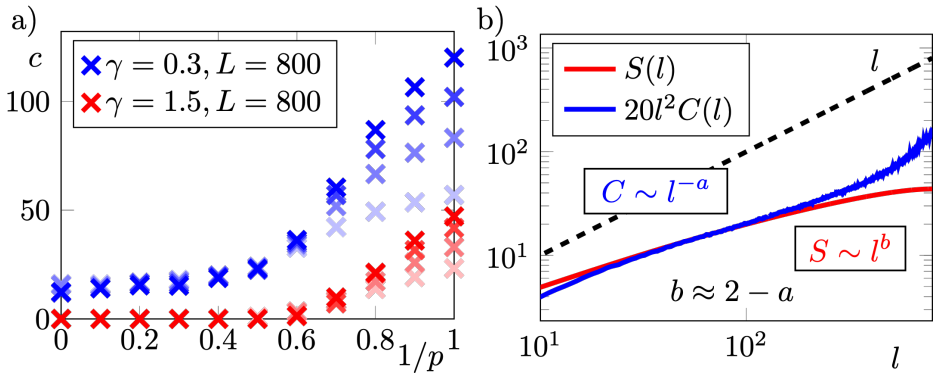

Figure 26: a) Effective central charge c determined from a fit at $l \in [L/4, 3L/4]$ for system sizes $L = 200, 400, 600, 800$. For $1/p \lesssim 0.6$, c saturates, while it diverges with L for $1 > 1/p \gtrsim 0.6$, indicating faster than log entanglement growth. b) Entanglement entropy and density-density correlation function deep in the algebraic scaling phase ($\gamma = 0.3, p = 1.25$) for $L = 1600$. At intermediate distances, where finite-size effects are negligible, the algebraic scaling matches the analytical prediction $b = 2 - a$.

cosine vertex yields the scaling dimension $[\Delta] = 3 - 2p$[24]. It shows that the long-range aspect of the hopping is irrelevant for $p > 3/2$, and explains why the algebraic phase is located at $p < 3/2$. The numerical simulations confirm the independence of the critical value $p_c = 3/2$ from the measurement strength $\gamma > 0$, shown in Fig. 22d,e. This implies that even frequent local measurements cannot overcome the entanglement generation of a long-ranged kinetic Hamiltonian, which we confirm analytically below.

The three different phases discussed above are separated from each other by three different types of phase transitions (illustrated in Fig. 22). Each phase transition features a characteristic competition between different parts of the action: the quadratic part $\sim K$ tends to balance the fluctuations of ϕ, θ, while the nonlinearities ($\sim \Delta, g$) suppress fluctuations of θ or ϕ. In order to reveal and analyze this competition, we investigate the perturbative renormalization group (RG) equations for K, Δ, g. Note that the leading order perturbative RG equations due to the measurement non-linearity have been obtained already in Sec. 3, where no long-range coupling term was generated. Therefore, we now exclusively focus on the renormalization effects of the long-range non-linearity. As it only depends on θ but not on ϕ, we may in this case integrate out ϕ and find the Euklidian action (restricting again only to the $\sigma = +$ contour as the

[24] Two spatial integrals, one temporal integral and the factor $|y|^{-2p}$, i.e., $dt\ dx\ dy y^{-2p}$ scale like b^{3-2p} with a distance b.

two contours decouple)

$$S = \sum_{k>0} \frac{1}{2\pi} \int_{\omega,q} \theta^{(k)*} \left(\frac{\omega^2}{vK^2} + vp^2 \right) \theta^{(k)} + i\Delta \int'_{t,x,y} |x-y|^{-2p} \left(\sum_r \cos\left(\frac{1}{R} \sum_s (\theta^{(r)}_{x,y} - \theta^{(s)}_{x,y}) \right) \right)^2, \quad (4.29)$$

where $K = \sqrt{1 - \frac{2i\gamma}{\pi v}}$. We can again re-scale space and time to eliminate v to make the equations dimensionless. We then absorb v into a redefinition Δ. We also note that the $\cos^2$ has a constant contribution that has no effect but re-scales differently from the cos such that we proceed with

$$S = \underbrace{\sum_{k>0} \frac{1}{2\pi} \int_{\omega,q} \theta^{(k)*} \left(\frac{\omega^2}{K_1} + \frac{p^2}{K_2} \right) \theta^{(k)}}_{S_0} \underbrace{-i\Delta \int'_{t,x,y} |x-y|^{-2p} \left(\sum_r \cos\left(\frac{1}{R} \sum_s (\theta^{(r)}_{x,y} - \theta^{(s)}_{x,y}) \right) \right)^2}_{\Delta S}. \quad (4.30)$$

We again allow for an space-time asymmetric RG flow and define microscopic couplings $K_1 = 1 - \frac{2i\gamma}{\pi v}$ and $K_2 = 1$. The RG equations are again obtained by introducing a cutoff $\Lambda \sim \pi/a$ and integrating out fields with momenta $b\Lambda < p < \Lambda$, followed by rescaling space and time. First, we integrate out the fast modes $\theta_>$ out perturbatively. The resulting action reads to leading order in Δ

$$S_< \simeq S_{0,<} + \langle \Delta S \rangle_{0,>}, \quad (4.31)$$

where we simply replace the cutoff in $S_{0,<}$ using $\Lambda \to b\Lambda$. The fast mode expectation value is discussed in App. C.7. Using a proper (complex) rescaling of the coupling Δ to absorb the microscopic details and defining $K = \sqrt{K_1 K_2}$, we obtain the first order RG equations

$$\partial_s \Delta = (3 - 2p - K)\Delta, \quad (4.32)$$

$$\partial_s K = -K^2 \Delta. \quad (4.33)$$

Similar equations have been obtained in Ref. [102] for the ground state of a Hermitian, long-range interacting XXZ-chain. Here, however, all couplings are complex, and the canonical scaling dimension of the long-range coupling Δ is modified compared to the Hermitian case [102] by replacing $p \to 2p$. The quantum phase transitions observed here thus represent a generalization of ground state phase transitions in unitary

systems, to dark state MIPTs.

The RG equations (4.32),(4.33) yield several insights: (a) For $p > 3/2$, the long-range hopping $\sim \Delta$ is always irrelevant and any initial $\Delta \neq 0$ decays to zero exponentially fast ($\mathrm{Re}(K) \geq 0$ is required for stability). In this case, the monitored long-range hopping dynamics are effectively reduced to a nearest neighbor hopping model. This short-ranged model undergoes a Berezinskii-Kosterlitz-Thouless (BKT) transition from a critical to an area law phase as a function of the measurement strength. This scenario is discussed in detail in Refs. [44, 68] and Sec. 3. (b) For $p \leq 3/2$, the long-range hopping is relevant and strongly enhances fluctuations of ϕ. This can be seen already on the level of first order RG equations: any $|\Delta| > 0$ enforces a rapid decrease of K in Eq. (4.33)[25]. This confirms the result from canonical power counting. (c) Although Eq. (4.32) is reminiscent of a conventional Sine-Gordon model (here for a p-dependent canonical scaling dimension), the transition between the critical and the long-range phase does not match the BKT paradigm. The reason is the linear appearance of Δ in Eq. (4.33), obtained at first order perturbation theory. It gives rise to an unconventional transition, which is characteristic for long-range coupled systems [102]. (d) A similar argument applies for the transition from the area law to the long-range phase. This transition arises from the direct competition between the two cosine terms. For a short-ranged Sine-Gordon model, this gives rise to a sequence of universality classes depending on the factor in the nonlinearities, including the Ising and parafermionic ones [184]. However, due to Eq. (4.33), this is again different for the long-range model, where a transition of this type has not yet been characterized.

4.4 Conclusion

Long-range dynamics leads to a novel measurement induced sub-volume phase with a maximum entanglement growth exponent $S \sim \sqrt{L}$. Despite the enhanced entangling effect of long range hoppings, the system does not reach a volume law characteristic of an ergodic phase. Indeed, a volume law is typically associated with excited or generic states, located in the middle of the spectrum of a Hamiltonian. Here, the trajectory wave functions evolve to states that bear strong similarities to ground states. In fact, it is intriguing to notice the similarity of the phase structure to the ground state phase diagram of long-range interacting spin models in one dimension [102], where the density pinning effect of measurements is replaced by nearest neighbor interactions. This suggests a persistence of quantum ground state dynamics in the trajectory wave function, which is reflected in the effective *cooling* towards measurement-induced dark states in the replica formalism. These findings show that the replica Keldysh field theory approach [44] that we developed in Sec. 3 for the short-ranged model is indeed able to

[25] For a conventional Sine-Gordon model with short-range nonlinearity, the renormalization of K starts at the level of second order perturbation theory.

make testable predictions for variants of that model. This evidence motivates to apply this to other monitored systems where numerical simulations are more challenging, for instance due to interactions. In the next section, we will return to one of the original big questions of the field of measurement-induced phase transitions: how can we observe them in NISQ devices without exponential overhead? In order to make progress here, we propose to add feedback to the protocol in order to transform the MIPT in free fermions into an absorbing state phase transition that reveals the phase transition on the level of linearly averaged observables.

5 Revealing measurement-induced phase transitions of fermions by pre-selection

In this section, we present an approach to overcome the post-selection problem, as it is discussed in Sec. 2.3, called 'pre-selection'. This section is based on a revision of the pre-print [127] which is expected to be published after submission of this thesis. It is the result of a collaboration with M. Buchhold and S. Diehl. Significant parts of this section word for word follow the revised manuscript. The most significant novelty of the material presented here, as compared to the pre-print [127], is the addition of results from tensor-network simulations supporting the results. Additionally, some changes are made to logically embed the results into this thesis. The author of this thesis is a co-author of [127]. He performed all numerical simulations. In particular, he developed the matrix product state based implementation of measurement-induced dynamics for interacting systems from scratch. The results of the numerical simulations where discussed with the other co-authors. The analytical part was developed in collaboration with M. Buchhold. Specifically, the author of this thesis constructed the microscopic bosonization. He also contributed to the draft of the manuscript and did significant adaptions to fit the content into this thesis.

The common feature of all MIPTs is that the dynamics of the system is driven by measurements [47–53, 55, 65, 68, 92, 94, 178, 179]. This means that the measurements make the experimenter acquire knowledge about the quantum system by just performing the experiment. Ironically, despite this fact, MIPTs remain hard to detect (see Sec. 2.3): Constructing witnesses of the transition from quantum mechanical observables requires many identical copies of the same wave function in an experiment. However, the random occurrence of measurement outcomes (e.g. $\uparrow$ or $\downarrow$ in a qubit measurement) pushes the ensemble of measurement trajectories into a maximally mixed state, erasing all information on individually prepared wave functions. Detecting generalized entanglement measures such as Rényi entropies [185, 186] is subject to the same reproducibility bottleneck. In principle, the information gained from the measurements could be used to remedy the situation: post-selecting on trajectories with the same measurement outcomes generates an ensemble of identical pure states from which observables can be extracted. This problem is, however, exponentially costly [49] (see Sec. 2.3), unless special conditions are met [113].

5.1 Concept of pre-selection

In this work, we show how MIPTs of fermions can be made observable, via replacing post-selection by *pre-selection*. The core idea is to break the measurement degeneracy: we replace the random outcome state by a unique target wave function, which repre-

sents one of the exponentially many possible measurement outcomes [128]. When the target state features an extensive order parameter, the MIPT coincides with an ordering transition on the level of the density matrix and becomes observable by standard means. Pre-selection equips the dynamics with a directionality in Hilbert space, which is designed such that the stationary critical properties of the target state, particularly its entanglement, represent the entire ensemble.

Besides being a tool to reveal MIPTs, the phenomenology established below reveals that this scheme grants access to an intriguing new class of *quantum absorbing state phase transitions* [129–132].

The concept of pre-selection is general and applicable to a large class of MIPTs. We elaborate it here for fermion models with a $U(1)$-symmetry from particle number conservation. We demonstrate it for both interacting and non-interacting setups and for continuous and projective measurements. All approaches share in common to give quantitative access to the universal properties of the underlying MIPT. We emphasize a key asset of pre-selection: the scheme can be chosen such that no parallel simulation of the wave function is required.

The goal is to pull the MIPT to the observable level by modifying the dynamics such that it uncovers a phase transition in the density matrix $\hat{\rho}$, averaged over the measurement outcomes (see Sec. 2.3). In general, the update of $\hat{\rho}$ in a time step dt can be written as a dynamical Kraus map

$$\hat{\rho}_{t+dt} = \mathcal{X}[\hat{\rho}_t]dt, \tag{5.1}$$

with a time-local, completely positive, and trace preserving generator $\hat{\mathcal{X}}$, describing the evolution of the conditioned density-operator $|\psi\rangle\langle\psi|$, averaged over trajectories, $\hat{\rho} = \overline{|\psi\rangle\langle\psi|}$. Depending on the specific protocol, the average is taken over the outcomes of weak measurements (QSD) or locations of projective measurements and their respective outcomes (QJ). We focus on repeated measurement of mutually commuting operators $[\hat{O}_l, \hat{O}_{l'}] = 0$ with the same rate γ for all lattice sites l. Each $\hat{O}_l$ has eigenvalues $\{\lambda_1, \lambda_2\}$[26] and spans a two-dimensional Hilbert space $\{|\lambda_1\rangle, |\lambda_2\rangle\}$:

$$\hat{O}_l = \lambda_1 \hat{P}_l + \lambda_2(\hat{1} - \hat{P}_l), \text{ with } \hat{P}_l = |\lambda_1\rangle\langle\lambda_2| \text{ and } \hat{P}_l^2 = \hat{P}_l. \tag{5.2}$$

We start with the generator for the unmodified unitary[27] and measurement evolution, which we denote by $\mathcal{X}^{(0)}$. It has exactly one dynamical fixed point – the maximally mixed state $\hat{\rho} \propto \hat{1}$ – obeying $\mathcal{X}^{(0)}[\hat{1}] = 0$. This is verified in the temporal continuum

[26] This restricts us to binary measurement-outcomes. However these are relevant to many systems that are considered in the literature since spin or particle number in fermion systems are binary observables.

[27] For example due to a Hamiltonian.

limit $dt \to 0$, where $\mathcal{X}^{(0)}$ takes Lindblad form (for a derivation, see Sec. 2.1),

$$\hat{\mathcal{X}}^{(0)}[\hat{\rho}] = -i[\hat{H}^{(0)}, \hat{\rho}] - \frac{\gamma}{2}\sum_l [\hat{P}_l, [\hat{P}_l, \hat{\rho}]]. \tag{5.3}$$

This holds for general operators $\hat{O}_l$. Below, we consider fermions on a one-dimensional lattice (with sites l) and measurements of the particle number $\hat{O}_l = \hat{n}_l$, i.e., $(\lambda_{1,2} = 0, 1)$ and $\hat{P}_l = 1 - \hat{n}_l$. The Hamiltonian will implement nearest neighbor hopping, $\hat{H}^{(0)} = -\sum_l \hat{c}_l^\dagger \hat{c}_{l+1} + \text{h.c.}$, i.e. we will study the model discussed in Sec. 3 and Refs. [44, 68, 69].

In order to make the phase transition of this model observable, we will introduce modifications of the generator $\mathcal{X}^{(0)} \to \mathcal{X}$ such that the following three conditions are obeyed:

(c1) There exists a *dark state* $\hat{\rho}_D = |D\rangle\langle D|$ of the modified generator, i.e., $\hat{\mathcal{X}}[\hat{\rho}_D] = 0$, where $|D\rangle$ is an eigenstate of all measurement operators $\hat{O}_l$. This is our target state.

(c2) The unique stationary solution of $\partial_t \hat{\rho} = \mathcal{X}[\hat{\rho}]$ is $\hat{\rho} = \hat{\rho}_D$.

(c3) $\hat{\mathcal{X}}$ preserves all the symmetries of $\hat{\mathcal{X}}^{(0)}$ and all modifications are irrelevant in the renormalization group (RG) sense.

Condition (c1) pre-selects one representative eigenstate $|D\rangle$ of the measurement outcomes. A convenient choice of $|D\rangle$ equips it with an extensive order parameter, which eases experimental detection in many-body systems. Without loss of generality[28], we will from now on assume that the target state $|D\rangle$ corresponds to measurement outcomes corresponding to $\hat{P}_l$ and thus is stabilized by $\hat{P}_l\hat{\rho}_D = \hat{\rho}_D$. For local measurements, $\hat{\rho}_D$ is area law entangled. (c2) introduces a directionality in the evolution: iterating the dynamical map $\mathcal{X}$ ultimately filters out the state $\hat{\rho}_D$. In particular, the maximally mixed state ceases to be a dynamical fixed point of the averaged evolution. (c3) ensures that the modified dynamics is consistent with the original MIPT, and does not alter its universality class. This criterion is general but its implementation requires a case-by-case study: determining RG irrelevant modifications to the evolution requires knowledge on the universality class of the MIPT – and its corresponding field theory. For the fermion models studied here, this is the case: the RG fixed point is a non-unitary Luttinger Liquid as argued in Sec. 3.2.2 and Ref. [44]. We illustrate the possibility to find such a modified strategy obeying (c1-c3) introducing feedback: if a certain measurement outcome is obtained, then depending on the compatibility with the target state $|D\rangle$ a suitable state update is selected. We expose two principal strategies to implement this goal, which we dub 'classical-' and 'quantum feedback'.

[28] We may perform a particle hole transformation locally to ensure this.

They are illustrated in Fig. 27 for the toy model consisting of only two sites (i.e. two levels).

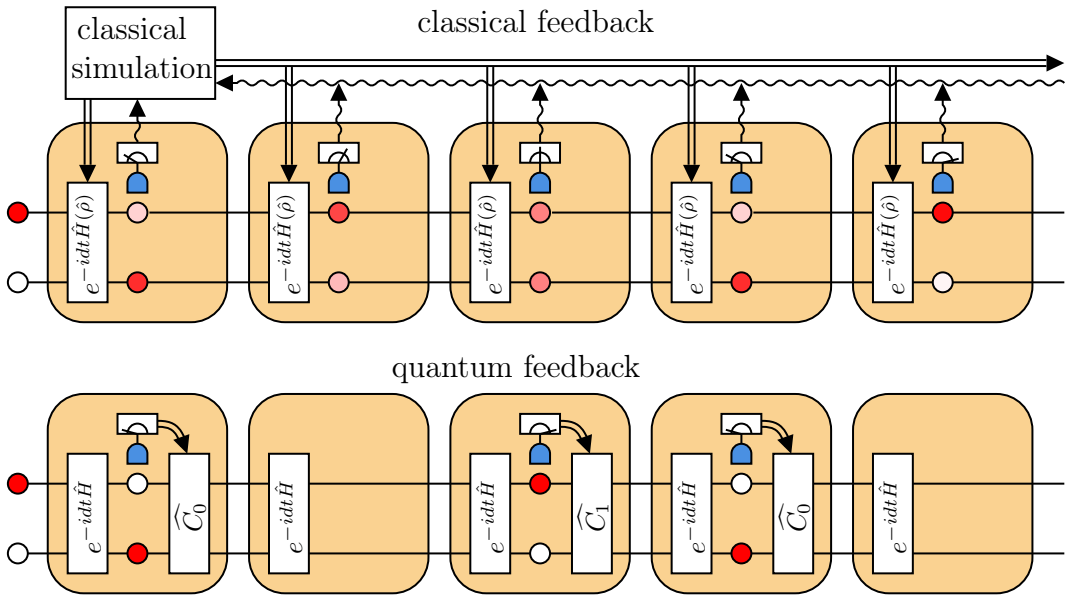

Figure 27: Illustration of the classical and quantum feedback protocols with time running to the right and orange boxes indicating a single time-step dt. In the classical feedback protocol, weak measurements extract information from the system, which is then used as input (wiggled lines) for a classical simulation, determining the right choice for the hopping strengths r_l at each time-step. This information is then fed back into the experimental setup (double lines) such that the Hamiltonian is changed. In the quantum feedback protocol, the binary measurement outcome of the projective measurements is directly used to apply the right unitary correction operator $\hat{C}$. This simple 'IF-THEN' clause does not require a classical simulation during the experiment.

In the 'classical feedback' strategy the structure of the Hamiltonian $\hat{H}^{(0)}$ and the measurement-projections $\hat{P}_l$ remains unchanged. Instead we condition the 'classical' parameters in the Hamiltonian on the detected state $\hat{H}^{(0)} \to \hat{H}[\hat{\rho}]$. The evolution then becomes non-linear in the state and steering in Hilbert space is achieved, indeed akin to feedback [133, 177, 187].

Opposed to that, in the 'quantum feedback' strategy, 'wrong' measurement results are corrected immediately [188, 189] by modifying the projection onto $\hat{1} - \hat{P}_l$ with a unitary correction $\hat{C}_l$ (see Fig. 27):

$$\hat{L}_l^{(0)} = \hat{1} - \hat{P}_l \to \hat{L}_l = \hat{C}_l(\hat{1} - \hat{P}_l) \text{ with } [\hat{C}_l, \hat{P}_l] \neq 0. \tag{5.4}$$

Hence, the evolution remains linear in the state, but the Hermitian projectors transform to non-Hermitian Lindblad operators $\hat{L}_l$, implementing the desired directionality in Hilbert space. To ensure that the unitary evolution does not spoil the dark state condition, we also need to modify the Hamiltonian to feature $|D\rangle$ as an eigenstate.

How does a phase transition manifest, if the dark state is the unique stationary

solution for all choices of parameters? An insight can be gained by drawing a link to dynamical systems undergoing an *absorbing state phase transition* (ASPT) (see Fig. 28), like directed percolation [190, 191]. These host the classical analogue of a global dark state – the absorbing state. The ASPT is a critical point separating two distinct dynamical regimes: In the *absorbing phase* the stationary dark state is dynamically stable and is reached from any initial state in finite time. In the *active phase*, the dark state is dynamically unstable and will only be reached on times $\log(t) \sim L$ exponentially large in the system size L [190]. Here we implement a quantum-mechanical ASPT. It separates an absorbing phase in which the pre-selection scheme is effective and $\hat{\rho}_t \to \hat{\rho}_D$, from an active phase, where pre-selection fails and $\hat{\rho}_t \to \hat{1}/\operatorname{Tr}\hat{1}$ (see Fig. 28).

Let us now connect this to MIPTs. Wave functions undergoing Hamiltonian dynamics subject to local measurements display two different dynamical phases: for weak (rare) measurements, the Hamiltonian scrambles information and each initial wave function evolves into a (sub-) extensively entangled state. For strong (frequent) measurements, each wave function enters a quantum Zeno regime and obeys area law entanglement. Despite their different entanglement structure, the wave functions in both phases are subject to randomness in space and time, and their ensemble always approaches a maximally mixed state. In the presence of pre-selection, a unique dark state is introduced. The presence of the dark state does not affect the dynamics in the weak measurement phase, but due to feedback, it acts as an attractor of disentangled wave functions in the quantum Zeno regime. Each disentangled wave function evolves towards the dark state, making the ensemble a pure, disentangled state. In the following, we illustrate each pre-selection scheme for the MIPT of monitored fermions [68]. The baseline model consists of a (free) fermion Hamiltonian, which describes hopping on a half-filled chain of length L

$$\hat{H}^{(0)} = \sum_l \hat{h}_l r_l, \tag{5.5}$$

with $\hat{h}_l = \hat{c}_l^\dagger \hat{c}_{l+1} + \text{h.c.}$, and $r_l = 1$ (units are set by $\hat{H}^{(0)}$). The Hamiltonian competes with measurements, either weak-continuous [139, 151] or projective, of the local densities $\hat{n}_l$ with a constant rate γ. The competition manifests in

$$[\hat{n}_l, \hat{h}_l] \neq 0, \tag{5.6}$$

and drives a MIPT between two different entanglement phases [44, 68] (see also Sec. 3): for small rates γ (weak measurements), each wave function is scrambled and approaches a state with logarithmic entanglement growth, reminiscent of a conformally invariant, quantum critical state. For large γ (strong measurements) a quantum Zeno regime

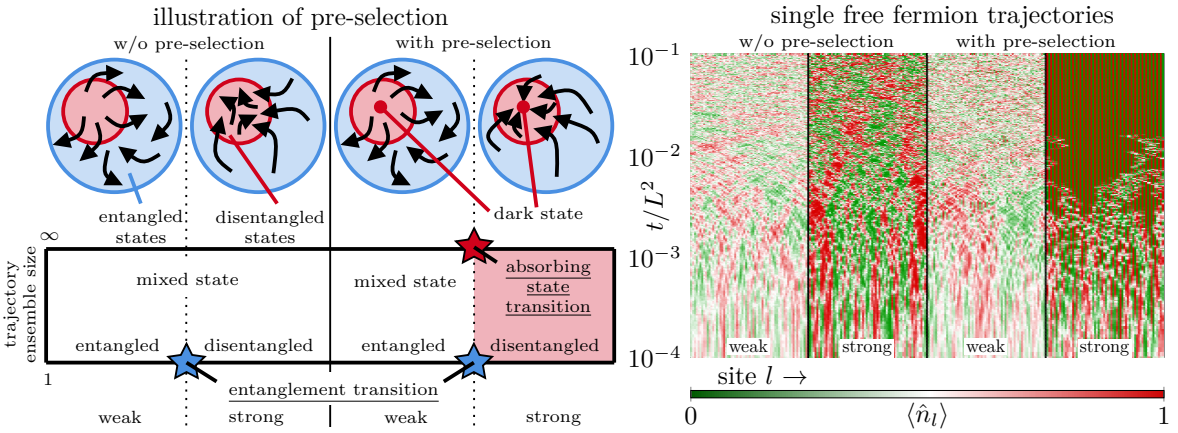

Figure 28: Pre-selection concept. While the information about a MIPT is lost in the ensemble average, pre-selection adds a dark state that is only a stable attractor in the weakly entangled phase which makes the transitions visible in terms of an order parameter. This is demonstrated for free fermions with the classical feedback protocol: With pre-selection, we find an ordered Néel state after times $\sim L^2$ that can be clearly distinguished from the disordered state by a single measurement of all particle number positions.

manifests with area law entangled wave functions close to instantaneous eigenstates of $\{\hat{n}_l\}$. Both regimes are separated by a MIPT in the BKT class [44, 172].

In the following, we use the classical and quantum feedback strategy to demonstrate the pre-selection phenomenology applied to this model. Let us start with the classical feedback.

5.2 Classical feedback

5.2.1 Dynamical protocol

The classical scheme makes the Hamiltonian

$$\hat{H}^{(0)} \rightarrow \hat{H}[\hat{\rho}] \text{ via } r_l \rightarrow r_l[\hat{\rho}], \tag{5.7}$$

state-dependent but leaves the structure of $\hat{H}, \hat{P}_l$ unmodified. Condition (c1) requires $[\hat{H}[\hat{\rho}_D], \hat{\rho}_D] = 0$ for the dark state. A suitable choice is the Néel state $|D\rangle = |010101\ldots\rangle$, populating either the even or the odd sites of the chain, see Fig. 28. The state-dependence of $r_l[\hat{\rho}]$ can be conveniently implemented by

$$r_l[\hat{\rho}] = 2 - (\lfloor\langle\hat{n}_{l-1}\rangle\rfloor - \lfloor\langle\hat{n}_l\rangle\rfloor)^2 - (\lfloor\langle\hat{n}_{l+1}\rangle\rfloor - \lfloor\langle\hat{n}_{l+2}\rangle\rfloor)^2,$$

where $\lfloor\ldots\rfloor$ indicates rounding to the nearest integer. This choice fulfills (c2) since $[\hat{H}[\hat{\rho}], \hat{\rho}] \neq 0$ for any other eigenstate $|\{n_m\}_m\rangle$ of all $\hat{n}_l$ such that $\hat{n}_l |\{n_m\}_m\rangle =$

$n_l |\{n_m\}_m\rangle$ but $|\{n_m\}_m\rangle \neq |D\rangle$. This conditions the couplings r_l on the instantaneous expectation values $\langle \hat{n}_l \rangle$ of the measured operators, given a state $\hat{\rho}$. In an experiment, these can be obtained by simulating the instantaneous state $\hat{\rho}$ (assuming that it can be efficiently simulated) or be extracted from the measurement outcomes, for instance by applying an appropriate noise filter [192] (see below).

An intuitive understanding is found in the limiting cases: (i) For weak measurements, the operators $\hat{h}_l$ scramble the observables $\hat{n}_l$. The state becomes translation invariant $\langle \hat{n}_l \rangle = 1/2$ and $r_l[\hat{\rho}] \to 1$ is effectively state-independent. This means that in this regime, the modification does not alter the original dynamics (ii) For strong measurements, $\hat{\rho}$ enters a quantum Zeno regime, where $\langle \hat{n}_l \rangle \hat{\rho} \sim \hat{n}_l \hat{\rho}$. We can thus promote

$$r_l[\hat{\rho}] \to \hat{r}_l \equiv 2 - (\hat{n}_{l-1} - \hat{n}_l)^2 - (\hat{n}_{l+1} - \hat{n}_{l+2})^2, \tag{5.8}$$

to an operator with $r_l[\hat{\rho}]\hat{\rho} = \hat{r}_l \hat{\rho}$. A directed evolution towards $\hat{\rho}_D$ is implemented when the product $\hat{h}_l \hat{r}_l$ is non-Hermitian, which is true here as $[\hat{h}_l, \hat{r}_l] \neq 0$. Both limits, (i) and (ii), allow us to effectively eliminate the state dependence in $\hat{H}[\hat{\rho}]$, yielding two types of Hamiltonians $\hat{H}_{w,s}$: for weak measurements $\hat{H}_w \equiv \hat{H}^{(0)}$ is unmodified by pre-selection. For strong measurements $\hat{H}_s \equiv \sum_l \hat{h}_l \hat{r}_l$ is non-Hermitian and steers towards $\hat{\rho}_D$ as demonstrated in Fig. 28. Beyond that, an analytical treatment of the phase transition is out of the scope of this work since it would require solving a non-linear equation of motion for the many-body density operator. This requires additional method development. Therefore, we focus here on numerical simulations that are efficient due to the Gaussianity of all appearing operators. For the quantum feedback protocol, this will be reverted: Here we can use standard Keldysh field theory due to the linearity of the state evolution, while the numerical simulation becomes challenging due to the need to add interactions in this protocol as we discuss in Sec. 5.3.

5.2.2 Numerical simulations

For the numerical simulation (see Fig. 29, Fig. 30), we need to be more specific about the model now: We implement the dynamics using the QSD protocol, i.e. weak measurements. The only modification that is made compared to the protocol described in Sec. 3.3 is, that the hopping matrix $h \to h(U)$ now depends on the current state matrix U, as $r_l(\hat{\rho}) = r_l(\{\langle \hat{n}_s \rangle\}_s) = r_l(\{(UU^\dagger)_{ss}\}_s)$. In particular, the modified dynamics is still non-interacting and particle number conserving such that we use the same parametrization in terms of Gaussian states at half filling. Note that along each trajectory, the weak measurement protocol makes the measurement currents $J_{l,t}$ experimentally accessible at each time step. These are related to the instantaneous measurement readouts

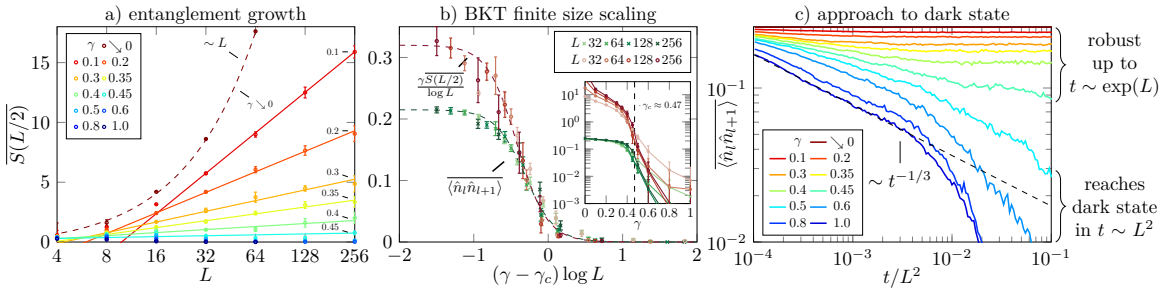

Figure 29: Absorbing state phase transition of monitored free fermions with classical pre-selection. a) Growth of the half-chain entanglement entropy $S(L/2)$ with system size L at $t = 0.1L^2$. b) Finite size scaling of the entanglement entropy and the ensemble averaged density-density correlation function $\langle \hat{n}_l \hat{n}_{l+1} \rangle$, extracted after an evolution time of $t = 0.1L^2$. The inset shows the unrescaled data, with dashed lines as guides to the eye. c) Evolution of the order parameter to the dark state. The error bars in a) and b) represent the statistical error from fitting the data between times $t = L^2/10$ and $t = 1.2L^2/10$ by linear regression.

via

$$J_{l,t} = \langle \hat{n}_l \rangle_t + \frac{dW_{l,t}}{2dt\sqrt{\gamma}}. \tag{5.9}$$

Hence, given that the initial state is known, we can infer the Wiener increment $dW_{l,t}$ from the expectation value computed from a numerical simulation at every time-step and the measurement read-out such that the numerical simulation of a given trajectory is *deterministic*. This means, that we can in principle compute the expectation value $\langle \hat{n}_l \rangle_t$ during the experiment and therefore find appropriate r_l to implement the post-selection method. In the numerical simulation presented here, we assume this scenario to be realized.

For a more complex wave function evolution, which cannot be efficiently simulated in real time, one could refer to alternative schemes. For instance one may estimate the instantaneous expectation values $\langle \hat{L}_l^{(0)} \rangle$ directly from the measurement outcomes $J_{l,t}$ by applying appropriate filtering. Examples for advanced filtering schemes are Kalman [193] or low pass filters [192], which can represent an alternative way to resolve MIPTs in the classical feedback scheme. Alternatively, the quantum feedback variants do not require the classical inputs.

Each trajectory is initialized in a random, half-filled product state (e.g. $|01101\rangle$), which is evolved under an unconditioned Hamiltonian ($r_l = 1$) for a period $t = -5$ to $t = 0$ to reach an entangled initial wave function at $t = 0$. Then, the classical pre-selection scheme is applied as described above. During the evolution, we compute the entanglement entropy to benchmark with the non-linear observables relevant for MIPTs, the order parameter $\langle \hat{n}_l \hat{n}_{l+1} \rangle$ and the ensemble purity $\tau \equiv \mathrm{tr}\hat{\rho}^2$ (see below). Each observable reaches a (quasi-) stationary plateau at times $t \sim \mathcal{O}(L^2)$, as we show

in Fig. 29c). The evolution of the order parameter $\langle \hat{n}_l \hat{n}_{l+1} \rangle$ displays a characteristic behavior in the two different regimes: for strong measurements, the dark state is reached after an algebraic time scale $t \sim L^2$ resulting from the diffusive redistribution of number-conserved particles under strong measurements. The initial relaxation follows a power law decay $\sim t^{-1/3}$ of the order parameter. In the weak measurement regime, the order parameter saturates on a plateau, which is robust up to exponentially long time scales $t \sim \exp(L)$ in the system size. This phenomenology in the dynamics gives a further parallel to absorbing state transitions, and to purification transitions [178]. Throughout this work, we set the stationary values to be reached at $t = 0.1L^2$, which turns out to yield consistent and converged expectation values, shown in Fig. 29a),b), see also Fig. 30a). The observables at this timescale are extracted by averaging over

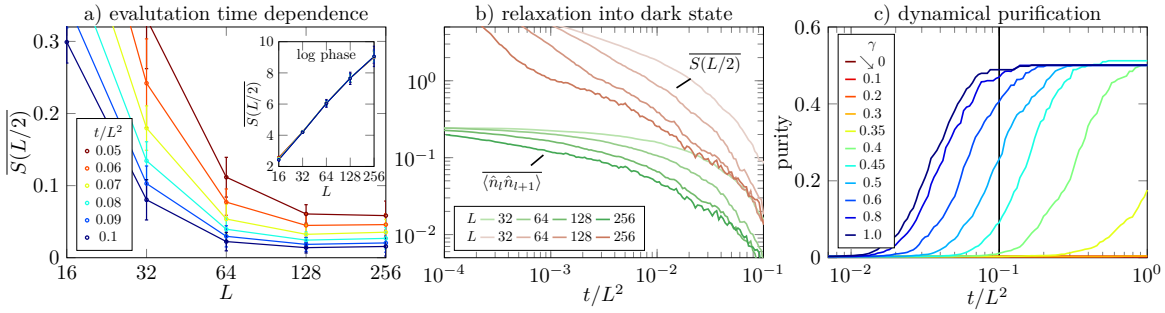

Figure 30: Classical pre-selection dynamics. a) In the area-law phase ($\gamma = 0.6$), the entanglement-entropy has a finite value for $L \to \infty$ at timescales $\sim L^2$. The precise value depends on γ (not shown) and the precise choice of the observation time. In the logarithmic phase (inset), this dependence disappears at large L due to the formation of a exponentially long-lived plateau value for all observables. b) The reaction-diffusion timescale L^2 emerges when comparing the time-evolution for different system sizes in the absorbing phase ($\gamma = 0.6$). Studying $t = 0.1L^2$ appears to be a reasonable choice to efficiently distinguish the different regimes. c) For strong measurements the trajectory ensemble purifies at the same timescale, while weak measurements leave it fully mixed for exponentially long times. The final purity is 1/2 due to the degeneracy of the target state in the classical pre-selection setup.

$\mathcal{O}(1/L)$ different trajectories (denoted by an overbar). Each result is then also time-averaged over the period $t = L^2/10$ to $t = 1.2L^2/10$ and fitted by linear regression, yielding the error estimates shown in Fig. 29a),b). The data shown there demonstrates the MIPT with pre-selection: In the weak measurement phase ($\gamma \lesssim 0.47$), the entanglement grows logarithmically $S(L/2) \sim \frac{c_{\text{eff}}}{3} \log L$, and it becomes constant in the strong measurement phase, $c_{\text{eff}} = 0$, since the entanglement entropy in the Néel state is exactly zero and in the approach to the Néel state, typical states at finite time obey area law scaling, see Fig. 30a). In the limit of vanishing measurement strength, a volume-law growth of the entanglement is observed (Fig. 29a)). A scaling collapse (Fig. 29b)) reveals that both the entanglement entropy and the ensemble order parameter indicate a phase transition at the same critical measurement strength $\gamma_c \approx 0.47$. Here, the

arbitrarily small values of $S(L/2)$ and $\langle \hat{n}_l \hat{n}_{l+1} \rangle$ for $\gamma > 0.47$ at late times reduce the uncertainty in determining γ_c compared to the unmodified MIPT (see Sec. 3.3). The data displays an exponential divergence of the correlation length $\log \xi \sim |\gamma - \gamma_c|^{-1}$. Note that this behavior does not coincide with the finding from the unmodified model where the BKT essential scaling $\log \xi \sim |\gamma - \gamma_c|^{-1/2}$ was found. However, the exponential scaling demonstrates the connection of the absorbing state phase transition in the ensemble average and the entanglement transition on the level of individual trajectories. At the critical point and in the thermodynamic limit, both the order parameter and the entanglement entropy undergo a discontinuous jump from $\langle \hat{n}_l \hat{n}_{l+1} \rangle \approx 0.21$ or $c_{\text{eff}} \approx 2.0$ to zero.

These results demonstrate that the entanglement scaling is inherited in the pre-selected case, but now accompanied by a phase transition for the order parameter $\sum_l \langle \hat{n}_l \hat{n}_{l+1} \rangle$, which can be probed in experiments, e.g., from measurements of the density distribution. The critical behavior is governed by the essential scaling of a BKT transition.

To further support this result, we also study the purity τ. For a pure state we have $\hat{\rho}^2 = \hat{\rho}$ and the purity is $\tau = 1$. Generally, the purity is proportional to the number of quantum states that contribute to the stationary ensemble, $\tau \sim |\mathcal{H}_{ss}|^{-1}$, where $\mathcal{H}_{ss}$ is the Hilbert space of stationary wave functions. Without pre-selection, the stationary state is maximally mixed $\hat{\rho} \sim \hat{1}$ and thus $\tau \sim \exp(-L)$ decays exponentially with the system size. When pre-selection is applied, and when the system reaches an absorbing state, $\tau = 1/N_D$, where N_D is the number of possible dark states (2 in this case). When $\hat{\rho}$ is a statistical mixture of N independently measured wave functions $\left|\psi^{(l)}\right\rangle$, i.e., $\hat{\rho} = \frac{1}{N} \sum_{l=1}^{N} \left|\psi^{(l)}\right\rangle \left\langle\psi^{(l)}\right|$, then

$$\tau = \frac{1}{N^2} \sum_{l,l'=1}^{N} |\langle \psi^{(l)} | \psi^{(l')} \rangle|^2. \tag{5.10}$$

In Fig. 30c) we show the purity of monitored free fermions undergoing a MIPT with pre-selection for a system of $L = 64$ sites. At the critical point, it jumps from $\tau \sim 0$ in the weak monitored phase to $\tau = 1/2$ in the strongly measured, absorbing phase. This is precisely the degeneracy of the two Néel states.

To summarize, we numerically studied the classical feedback protocol and found that the universal behavior at the phase transition is not modified on the level of observables that are also accessible in the underlying MIPT, such as entanglement and purification. The effect of the feedback is to transform the MIPT into a quantum ASPT where the BKT transition is visible in linearly averaged observables. We demonstrated this here for the Néel order parameter. To give further evidence for the proposed strategy being useful in making MIPT visible, let us now discuss the complementary

quantum feedback strategy.

5.3 Quantum feedback

5.3.1 Dynamical protocol

In the quantum feedback scheme, we modify the Hamiltonian in Eq. (5.5) such that the Néel state is again a dark state,

$$\hat{H}^{(0)} \to \hat{H} = \sum_l (\hat{h}_{l+1} + \hat{h}_{l-2})\hat{Q}_l, \qquad \hat{Q}_l = \begin{cases} \hat{n}_l & l \text{ odd} \\ 1 - \hat{n}_l & l \text{ even.} \end{cases} \tag{5.11}$$

The directionality is implemented by an IF-THEN condition acting right after a 'wrong' (incompatible with target dark state) measurement result $\hat{n}_{l\,\mathrm{odd}} \to 1$ or $\hat{n}_{l\,\mathrm{even}} \to 0$ has been obtained. Wrong results can be corrected by applying a quasi-local unitary gate operation $\hat{C}_l$ with $[\hat{C}_l, \hat{L}^{(0)}] \neq 0$. Here we take randomly with equal probability one of

$$\hat{C}_l^{+} = \exp\Big(-i\tfrac{\pi}{2}\hat{h}_l\Big), \qquad \hat{C}_l^{-} = \exp\Big(-i\tfrac{\pi}{2}\hat{h}_{l-1}\Big). \tag{5.12}$$

These are chosen such that when acting on a product state of sites l and $l \pm 1$, they exchange the occupation number of these two states. If both sites are occupied or empty, nothing happens but if they are different, this brings the state closer to the target state. Here, we use the QJ protocol to be able to obtain a simple correction rule based on binary measurement-outcomes. The principle of the steering towards the dark state is this: if a 'right' measurement result has been recorded, the projector $\hat{Q}_l$ evolves the state towards $\hat{\rho}_D$. If a 'wrong' measurement result has been recorded, the state is projected by $\hat{Q}_l = \hat{1} - \hat{P}_l$ away from $\hat{\rho}_D$. We then rotate it back onto the dark state by the unitary $\hat{C}_l^{\pm}$,

$$\text{'right'} : \hat{\rho} \to \frac{\hat{P}_l\hat{\rho}\hat{P}_l}{\langle \hat{P}_l \rangle}, \qquad \text{'wrong'} : \hat{\rho} \to \frac{\hat{C}_l^{\pm}\hat{Q}_l\hat{\rho}\hat{Q}_l\hat{C}_l^{\pm\dagger}}{\langle \hat{Q}_l \rangle}. \tag{5.13}$$

Based on these simple update-rules we can redo the derivation of the Lindblad master equation from a projective measurement protocol, shown in Sec. 2.1. In absence of the correction, it reads

$$\partial_t\hat{\rho} = -i[\hat{H}, \hat{\rho}] + \frac{\gamma}{2}\sum_l \left(\hat{P}_l\hat{\rho}\hat{P}_l + \hat{Q}_l\hat{\rho}\hat{Q}_l - \hat{\rho}\right). \tag{5.14}$$

Here we used that the measurement dynamics is invariant under $\hat{n}_l \leftrightarrow 1 - \hat{n}_l$. The correction operator acts after projection onto the eigenstate that is incompatible with

the target state. This yields

$$\partial_t \hat{\rho} = -i[\hat{H}, \hat{\rho}] + \frac{\gamma}{4} \sum_l \sum_{\sigma=\pm} \left(\hat{P}_l \hat{\rho} \hat{P}_l + \zeta_{l,\sigma} \hat{C}_l^\sigma \hat{Q}_l \hat{\rho} \hat{Q}_l \hat{C}_l^{\sigma\dagger} - \hat{\rho} \right). \tag{5.15}$$

Here, $\zeta_{\sigma,l}$ is a binary random variable which takes for every lattice site and every time-step independently equal probability the values 0 or 1. This ensures that we do not implement a breaking of inversion symmetry on the averaged level. Taking the trajectory average over these choices of the correction operators yields the Lindblad master equation

$$\partial_t \hat{\rho} = -i[\hat{H}, \hat{\rho}] \underbrace{-\frac{\gamma}{2} \sum_l [\hat{n}_l, [\hat{n}_l, \hat{\rho}]]}_{\mathcal{D}\hat{\rho}} + \underbrace{\frac{\gamma}{4} \sum_l \sum_{\sigma=\pm} \left(\hat{L}_l^\sigma \hat{\rho} \hat{L}_l^{\sigma\dagger} - \hat{Q}_l \hat{\rho} \hat{Q}_l \right)}_{\mathcal{F}\hat{\rho}}, \tag{5.16}$$

where we introduced Lindblad operators

$$L_l^\sigma = \hat{C}_l^\sigma \hat{Q}_l. \tag{5.17}$$

$\mathcal{D}$ corresponds to the measurement process. This leads to the diffusion dynamics known from the unmodified problem, which means that all terms in the density-operator that are off-diagonal in the particle number basis decay. The new term $\mathcal{F}$ that emerges due to the feedback acts only if the occupation at site l is definite and different from the target state, in which case a correction is applied. If the correction has no effect, this term also vanishes. Preservation of the trace is ensured by the unitarity of $\hat{C}_l^\pm$. Since the Néel state is also an eigenstate of $\hat{H}$ due to the modification ($\hat{P}_l \left|D\right\rangle = 0$), the master equation (5.16) turns the fermion MIPT in individual wave functions into an absorbing state transition for the ensemble: The repeated application of both $\hat{H}$ and $\hat{L}_l^\pm$ pushes any initial state into the Néel state $\hat{\rho}_D$. Active and inactive phases are distinguished by the characteristic time scale at which $\hat{\rho}_D$ is reached. This can be discussed on the level of a mean-field approach.

5.3.2 Mean-field dynamics

In the limit of strong measurements ($\gamma \gg 1$), the state $\hat{\rho}$ is nearly diagonal in the fermion number basis after a time $\mathcal{O}(1/\gamma)$ as projections act local and dominate over the entangling Hamiltonian. Based on this, the modified Lindblad operators cause a diffusive motion of defects, i.e. local configurations that do not coincide with the dark state, which stops once the Néel state is reached. This does not happen on the microscopic time-scale due to the conservation of particle number. Defects can only disappear by annihilating with other defects. Therefore, in this limit the Néel state is expected to be reached on time scales $t \sim L^2$ with system size L, exactly as

in the classical feedback protocol. This is confirmed by a mean-field analysis of the Lindbladian for a homogeneous system of infinite size. We find it convenient to use a particle-hole transformation $\hat{c}_l \leftrightarrow \hat{c}_l^\dagger$ on even sites. After this transformation, the dark state is the vacuum $|00000\ldots\rangle$. Hence, a natural order-parameter is the particle number $\hat{n}_l$: It vanishes everywhere in the dark state while it is finite for every other state. Therefore, we describe the dynamics of the state towards the dark state in terms of an evolution of the trajectory average $n = \overline{\langle \hat{n}_l \rangle}$ which, on the mean field level is approximated as a constant in space but a function of time.

The particle-hole transformation modifies the Hamiltonian to

$$\hat{H} = \sum_l \hat{n}_l (-1)^l (\hat{c}_{l-2}\hat{c}_{l-1} + \hat{c}_{l-1}^\dagger \hat{c}_{l-2}^\dagger + \hat{c}_{l+1}^\dagger \hat{c}_{l+2}^\dagger + \hat{c}_{l+2}\hat{c}_{l+1}). \tag{5.18}$$

After the transformation, the number conservation (in terms of the new degrees of freedom) is broken. Instead, we now find that the hopping can only annihilate or generate pairs of excitations on neighboring sites if there already is an excitation nearby. Combining this to the dynamics due to measurement and feedback yields

$$\partial_t \hat{\rho} = -i[\hat{H}, \rho] - \frac{\gamma}{2} \sum_l \left(\{\hat{n}_l, \hat{\rho}\} - \hat{n}_l \hat{\rho} \hat{n}_l - \frac{1}{2} \sum_{\sigma=\pm} \hat{L}_l^\sigma \hat{\rho} \hat{L}_l^{\sigma\dagger} \right), \tag{5.19}$$

where

$$\hat{L}_l^\pm = \hat{n}_l (1 - \hat{n}_{l\pm1}) - i(-1)^l \hat{c}_l \hat{c}_{l\pm1} \tag{5.20}$$

Based on this model, we now study the directed motion of the state towards the dark state. We anticipate, that in the strong measurement limit, after sufficiently long times, we will be close to the dark state such that the excitation density is low and excitations are only weakly correlated. This allows a mean field treatment, neglecting long-range correlations and decoupling correlators using Wicks theorem. Considering correlations up to nearest neighbors yields the mean-field time evolution (for a derivation see App. D.1)

$$\partial_t n = n(4K - \gamma n), \qquad \partial_t K = 4n - \gamma K, \tag{5.21}$$

with the additional mean field $K = i(-1)^l \langle \hat{c}_l \hat{c}_{l+1} - \hat{c}_{l+1}^\dagger \hat{c}_l^\dagger \rangle$. The time-evolution for the density is quadratic in the mean fields due to the particle-number conservation: local particle excitations can only be generated or annihilated if two excitations meet. In contrast, the evolution for K is linear as it is not conserved. For that reason, K undergoes a much faster evolution than n. Let us therefore make the the ansatz of constant n to solve for K which yields that $K - 4n/\gamma \sim e^{-\gamma t}$. Since n evolves

algebraically, we plug in the approached stationary value $K = 4n/\gamma$ which yields

$$\partial_t n = \frac{n^2}{\gamma}(4^2 - \gamma^2) \qquad \rightarrow \qquad n(t) = \frac{1}{\frac{1}{n(t=0)} - \frac{4^2-\gamma^2}{\gamma}t}. \tag{5.22}$$

Since $n > 0$ is the excitation density, we can distinguish 3 cases: (i) For $\gamma > 4$, we never hit the pole and the excitation density vanishes $n \sim t^{-1}$. This slow decay justifies the separation of scales used in the discussion above a posteriori. (ii) For $\gamma = 4$, the time dependence vanishes and we get $n(t) = n(t = 0) = const.$ (iii) For $\gamma < 4$, the time-evolution hits the pole at $t = \gamma/n(t = 0)(4^2 - \gamma^2)$ and the excitation density diverges, signalling that the dark state is unstable and the approximation breaks down. In this case, we cannot drop higher order terms in n for stability. If we keep them (see App. D.1), we find another stationary state $n = \frac{\gamma^2-16}{\gamma^2-32}$ ($\gamma < 4$ in this case) and $K = \frac{\gamma n}{4}$. This means, that the defect density in the long-time limit on the discussed mean-field level goes continuously to 0 at the critical point $\gamma = 4$ and nicely connects to $n = \frac{1}{2}$ i.e. a totally disordered system in absence of measurements. We demonstrate this also by solving the mean field equations numerically, see Fig. 31.

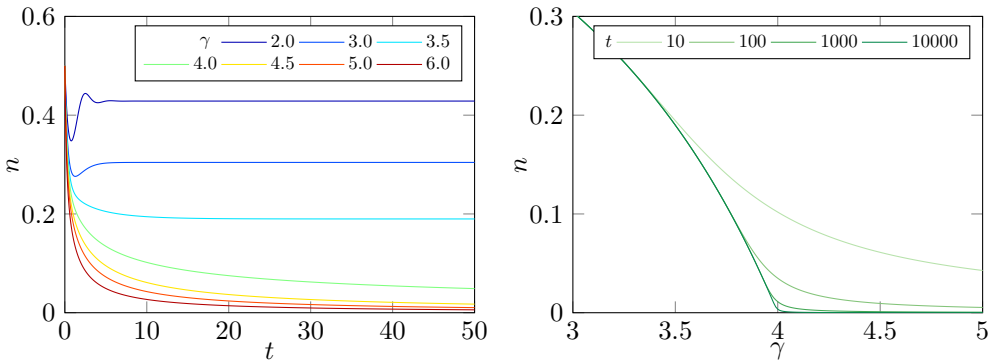

Figure 31: Time evolution of the defect density in the quantum feedback protocol in mean field approximation, initialized with $n = 0.5$ and $K = 0$. The transition between active and inactive phase becomes sharp at late times. In mean field, the active phase is stable until infinite times as we effectively assume an infinite system. In a real finite system, the defect density ultimately goes to 0 for any finite γ on an exponential timescale in L in the active phase and an algebraic time-scale in the absorbing phase. Both effects are not present on the mean field level.

This discussion shows that we get a dark state phase transition on the mean-field level at $\gamma = 4$[29]. For strong measurements, there is an algebraic approach to the Néel state which is well described in a classical picture as the dynamics is dominated by the diffusion of single defects. This corresponds to an area law phase. For weak measurements on the other hand, the enhanced superposition of particles leads to a

[29]The precise value that is predicted does not depend on whether we apply the correction on every site or on every other site, and it also does not depend on whether we correct randomly in both directions or always to the left or right.

drastic enlargement of the accessible Hilbert space, and a slowing down of the relaxation towards the Néel state. It can only be reached on time scales growing with the size of the Hilbert space $t \sim \exp(L)$. In the mean-field equations, this is revealed by the emergence of a second stationary solution: an active state with $\langle \hat{P}_l \rangle = \frac{16-\gamma^2}{32-\gamma^2}$ for $\gamma < 4$. While the Néel state remains stationary, any other initial configuration approaches the active state, whose lifetime diverges in the $L \to \infty$ limit. This confirms the phenomenology of an absorbing state phase transition.

5.3.3 Bosonization

In order to examine the long-wavelength dynamics beyond mean-field, we work in the spatial continuum limit, which for number-conserving fermion dynamics amounts to the bosonization framework [44], discussed also in Sec. 3.2.2 and Sec. 4.3. This approach is applicable assuming that the system is in the active phase, where the stationary state is far away from the Néel state such that the density is distributed constantly and the correction is irrelevant. The emergence of Néel order here signals the critical point. This justifies an expansion around a state of constant density which on the level of operators motivates the bosonization on a lattice,

$$\hat{c}_l^\dagger \to \sqrt{\hat{n}(x)} e^{-i\hat{\theta}(x)}, \qquad \hat{n}(x) = \left(n_0 - \frac{1}{\pi} \partial_x \hat{\phi}(x) \right) \sum_{l=-\infty}^{\infty} e^{2il(\pi n_0 x - \hat{\phi}(x))} \tag{5.23}$$

where $x = al$ and a is the lattice spacing and $n_0 = 1/2a$ is the density. The Hamiltonian can be conveniently rewritten as[30]

$$\hat{H} = \sum_l (1 - (-1)^l (\hat{n}_{l+2} - \hat{n}_{l-1}))(\hat{c}_l^\dagger \hat{c}_{l+1} + \hat{c}_{l+1}^\dagger \hat{c}_l). \tag{5.24}$$

If the density is constant, we can approximate $\hat{n}_{l+2} - \hat{n}_{l-1} \approx 0$ which just yields the original Hamiltonian, which in bosonization yields the unmodified Luttinger liquid Hamiltonian,

$$\hat{H}_0 = \frac{v}{2\pi} \int_x \left((\partial_x \hat{\phi})^2 + (\partial_x \hat{\theta})^2 \right). \tag{5.25}$$

If there is a tendency towards Néel order in the state, we obtain the following non-linear term (see App. D.2),

$$\Delta \hat{H} = g \int_x \cos 2\hat{\phi}, \tag{5.26}$$

where $g \in \mathbb{R}$ is a coupling that signals an instability towards the Néel state if it is relevant in the RG sense. Besides that, only derivative terms or oscillating factors that

[30] Here we work again in the original representation of the fermions, undoing the particle-hole transformation.

do not contribute at large distances appear. Therefore, the long wavelength effective Hamiltonian ins $\hat{H} = \hat{H}_0 + \Delta\hat{H}$. Since all terms are normal-ordered, we can straightforwardly translate this into a Keldysh path integral via the Feynman construction as discussed in Sec. 3.2.2. Besides that, the dephasing term $\mathcal{D}$ can be bosonized just as before. It drives the system into an infinite temperature state which is not obstructed of Hamiltonian terms of any kind. Therefore, $\Delta\hat{H}$ is irrelevant in absence of the feedback term that induced direction in Hilbert space, $\mathcal{F}$. The appearing terms locally are $\sim \hat{L}_l^{\pm}\hat{\rho}\hat{L}_l^{\pm\dagger} - \hat{Q}_l\hat{\rho}\hat{Q}_l$ with $\hat{L}_l^{\pm} = \hat{C}_l^{\pm}\hat{Q}_l$. Bosonization of this object is tedious as the preservation of the trace is only ensured by the unitarity of the correction operator, which is easily lost in approximations. Therefore, let us discuss the correction operator on the level of symmetries of the problem. We start by recalling that any non-Hermitian operator $\hat{L} \neq \hat{L}^{\dagger}$ can be decomposed into a Hermitian and an anti-Hermitian contribution $\hat{L} = \hat{L}^H + i\hat{L}^A$ with $(\hat{L}^H)^{\dagger} = \hat{L}^H$ and $(\hat{L}^A)^{\dagger} = \hat{L}^A$. When acting with a Hermitian operator from the left and the right onto a density operator, $\hat{L}^H\hat{\rho}\hat{L}^H$, this needs to be compensated by an anti-commutator in the Lindblad equation to ensure the preservation of probability. The resulting contribution will again be of the form of a pure noise term just like the measurement. The same applies for the application of $\hat{L}^A$ from both sides. Therefore, we absorb these contributions into the dephasing couplings and retain only

$$\mathcal{F}\hat{\rho} = -\frac{i\gamma}{4}\sum_l\sum_{\sigma=\pm}\left(\hat{L}_l^{\pm A}\hat{\rho}\hat{L}_l^{\pm H} - \hat{L}_l^{\pm H}\hat{\rho}\hat{L}_l^{\pm A}\right). \tag{5.27}$$

The correction operators can be written as

$$\hat{C}_l^{+} = (1-(\hat{n}_l - \hat{n}_{l+1})^2) - i\hat{h}_l, \qquad \hat{C}_l^{-} = (1-(\hat{n}_l - \hat{n}_{l+1})^2) - i\hat{h}_{l-1}. \tag{5.28}$$

Based on this, let us now discuss the symmetries of the model in terms of the fermions and the bosonized fields. The original model in absence of feedback conserves the particle number. This corresponds to a $U(1)$ symmetry which in terms of the bosonized operators reads $\hat{\theta} \to \hat{\theta} + b$ where b is an arbitrary real number. This conservation law is not broken by the feedback operator $\hat{L}_l^{\pm}$ such that we need to obey this symmetry. Besides that, the compact nature of the density counting field enforces the symmetry $\hat{\phi} \to \hat{\phi} + \pi m$ for integer m as two configurations that are related by such a global shift describe the same state. This allows for contributions of the form $\sim \cos 2m\hat{\phi}$. The alternating pattern of the correction operators indeed gives rise to the leading contribution, the Néel order $\sim \cos 2\hat{\phi}$, as we also saw in the perturbation to the Hamiltonian $\Delta\hat{H}$. Even though the translation invariance of the microscopic model is broken down from $x \to x+a$ to $x \to x+2a$, the coarse grained model obeys infinitesimal translation invariance $x \to x + \delta$. Finally, the original model has inversion symmetry, $l \leftrightarrow -l$

i.e. $x \leftrightarrow -x$ in the continuum. This symmetry is explicitly broken by the individual correction operators $\hat{C}_l^{\pm}$ as

$$\sum_l \hat{C}_l^{\pm}\hat{Q}_l\hat{\rho}\hat{Q}_l\hat{C}_l^{\pm} \to \sum_l \hat{C}_{-l}^{\mp}\hat{Q}_{-l}\hat{\rho}\hat{Q}_{-l}\hat{C}_{-l}^{\mp} = \sum_l \hat{C}_l^{\mp}\hat{Q}_l\hat{\rho}\hat{Q}_l\hat{C}_l^{\mp}. \tag{5.29}$$

Note that the + and − correction exchange their role under inversion. We work in the fine-tuned case that correction operators in both directions are applied with equal rate such that the sum of both contributions is again inversion symmetric. Hence, the inversion symmetry of the problem is retained. In bosonization, the inversion symmetry corresponds to simultaneous transformation of both operators, $\hat{\phi}(x) \to -\hat{\phi}(-x)$ and $\hat{\theta}(x) \to \hat{\theta}(-x)$. We conclude that all symmetries of the coarse grained measurement model are unaffected by the quantum feedback protocol. For that reason, we can construct the potential terms that appear in the dissipative part of the master equation (5.27). We need to find Hermitian operators occuring in $\hat{L}_l^H$ and $\hat{L}_l^A$ that, in combination of both terms, obey all symmetries.

Due to the shift-invariance of both fields, massive fields are ruled out. Instead, to zeroth order in derivatives, there can only emerge $\cos 2\hat{\phi}$ (and higher harmonics). On top of that, we may add derivative terms $\partial_x\hat{\phi}$ and $\partial_x\hat{\theta}$ up to quadratic order in derivatives, as higher derivatives are less relevant in the RG sense. Trivially, the Hermitian operator might also be constant. However, choosing either $\hat{L}_l^H$ or $\hat{L}_l^A$ constant yields the usual commutator structure which renormalizes the Hamiltonian. The terms appearing like that have the same form as the Hamiltonian due to the symmetries but the relative size of $\sim (\partial_x\hat{\phi})^2$ and $\sim (\partial_x\hat{\theta})^2$ terms are not expected to be equal since the problem is interacting due to the feedback. It is therefore expected that the feedback shifts the Luttinger liquid parameter by a real number that depends on the measurement strength γ. Therefore, we expect an altered critical measurement strength which is observed in the numerical simulation, see Fig. 34, where the critical point is found for comparably larger measurement rate. In this sense, the feedback stabilizes the strongly entangled phase.

Besides these, non-trivial operators may act from both sides on the state. If the same operator acts from both sides, the two contributions to $\mathcal{F}$ cancel out. The only term remaining that is quadratic and contains up to two derivatives reads $\int_x \partial_x\hat{\phi}\hat{\rho}\partial_x\hat{\theta}$. It however breaks inversion symmetry and cannot appear because of that. Therefore, all dissipative contributions need to contain the cos non-linearity. The combination of $\cos 2\hat{\phi}$ with $\partial_x\hat{\phi}$ vanishes due to the additional − sign that $\hat{\phi}$ obtains under inversion. In contrast, the phase field does not generate a − sign under inversion and therefore, we finally identify the steering term in bosonization,

$$\mathcal{F}\hat{\rho} = i\kappa \int_x \left((\partial_x\hat{\theta})\hat{\rho}\cos\left(2\hat{\phi}\right) - \cos\left(2\hat{\phi}\right)\hat{\rho}(\partial_x\hat{\theta}) \right), \tag{5.30}$$

where $\kappa > 0$ is a coupling constant that vanishes in the absence of feedback. The first derivative term here is no boundary term and also does not break the microscopic symmetries due to being conditioned on the relevance of the Néel order instability. However it is globally crucial as it enables directed evolution into the dark state once the non-linearity becomes relevant, which coincides with the BKT transition on the replica level, where the corresponding operator appears as well.

This can be discussed on the level of the Keldysh action for a single replica. We found, that in absence of the feedback, only the quadratic part of the measurement is present and θ can be integrated out exactly. Due to the feedback, we obtain the additional action[31]

$$\Delta S = \int_{x,t} \sum_{\sigma} \sigma \left[-g \cos(2\phi_\sigma) + \kappa (\partial_x \theta_\sigma) \cos 2(\phi_{-\sigma}) \right]. \tag{5.31}$$

The Hamiltonian term does not depend on θ such that integrating out θ is trivial while we need to redo the computation in App. C.2. It amounts to a shift of the time-derivative of $\partial_t \phi_\sigma \to \partial_t \phi_\sigma + \pi\kappa \cos 2\phi_{-\sigma}$. This yields the action

$$S = \frac{1}{2\pi v} \int_{x,t} \sum_{\sigma} \sigma \left[(\partial_t \phi_\sigma + \pi\kappa \cos 2\phi_{-\sigma})^2 - v^2 (\partial_x \phi_\sigma)^2 - g \cos 2\phi_\sigma \right] + \frac{i\gamma}{2\pi^2} \int_{x,t} (\partial_x \phi_+ - \partial_x \phi_-)^2. \tag{5.32}$$

To get an interpretation of this result, we rewrite it in terms of a Langevin equation [154] by first performing the Keldysh rotation and expanding in quantum fields to quadratic order. This yields[32]

$$S = \int_{x,t} -2\phi_q \left((\partial_t^2 - \partial_x^2)\phi_c - 4\pi\kappa \sin\left(\sqrt{2}\phi_c\right) \left(\partial_t \phi_c + \sqrt{2}\pi\kappa \cos\sqrt{2}\phi_c + \frac{\sqrt{8}g}{4\pi\kappa} \right) \right) + \int_{x,t} \frac{i\gamma v}{\pi} (\partial_x \phi_q)^2. \tag{5.33}$$

The quadratic contribution corresponds to noise as we can see by rewriting

$$\begin{aligned} e^{-\frac{\gamma v}{\pi} \int_{x,t} (\partial_x \phi_q)^2} &= e^{-\frac{\gamma v}{\pi} \int_{p,\omega} p^2 \phi_q^* \phi_q} \\ &= \int \mathcal{D}\xi e^{-\int_{p,\omega} \frac{\pi}{\gamma v p^2} \xi^* \xi} e^{2i \int_{\omega,p} \xi^* \phi_q} \\ &= \int \mathcal{D}\xi e^{-\int_{p,\omega} \frac{\pi}{\gamma v p^2} \xi^* \xi} e^{2i \int_{t,x} \xi \phi_q}, \end{aligned} \tag{5.34}$$

where ξ is a real field. The Gaussian is now interpreted as an integral over noise

[31] We suppress the replica index as we consider $R = 1$ here.
[32] We re-scaled the quantum fields by a factor $2\pi v$.

realizations where the noise is correlated with $\overline{\xi_{-p}\xi_p} = \frac{\gamma v p^2}{\pi}$ and enters the action according to

$$S = \int_{x,t} -2\phi_q \left((\partial_t^2 - \partial_x^2)\phi_c - 4\pi\kappa \sin\sqrt{2}\phi_c \left(\partial_t \phi_c + \sqrt{2}\pi\kappa \cos\sqrt{2}\phi_c + \frac{\sqrt{8}g}{4\pi\kappa} \right) - \xi \right) \tag{5.35}$$

Finally, taking the semi-classical limit and studying the saddle point equation yields the stochastic time-evolution of the classical field. It is related to the classical density counting field by $\phi_c = \sqrt{2}\phi$ due to the Keldysh rotation that was used. This yields the Langevin equation

$$(\partial_t^2 - \partial_x^2)\phi - 4\pi\kappa \sin 2\phi \left(\partial_t \phi + \pi\kappa \cos 2\phi + \frac{g}{2\pi\kappa} \right) = \frac{\xi}{\sqrt{2}}. \tag{5.36}$$

Without pre-selection ($g = \kappa = 0$), this equation describes a conventional Luttinger liquid subject to heating or dephasing in the density $\sim \hat{n}_l$ [38]. This term yields fluctuations $\sim p^2$ for each momentum mode p and pushes the system into a maximally mixed state. Adding the modification to the Hamiltonian ($g \neq 0$) only adds a potential term that however cannot prevent the fluctuation from heating as there is no mechanism counteracting the heating. Adding the feedback ($\kappa \neq 0$) however adds a first derivative term such that ϕ experiences cooling once the non-linear operator $\cos 2\phi$ becomes relevant, i.e. $\kappa \neq 0$ on large distance scales. Whenever nonzero, the cooling term dominates over the noise and pushes the system into the absorbing state. This can be studied, considering the homogeneous solutions of the Langevin equation. As they are homogeneous, they are not affected by the noise such that the mean field evolves deterministically. A non-zero g does not qualitatively change the picture such that we assume $g = 0$ now. The flow of the counting field is visualized in Fig. 32. It shows, that the only stable fixed point (up to shifts by π) is at $\phi = -\pi/4$ which corresponds to the Néel state that is the dark state of the original model. The other fixed points correspond to the constant density state and the opposite Néel state. The constant density state is a hyperbolic fixed point and the opposite Néel state is repulsive. Hence, in bosonization we also recover the directed motion towards the dark state conditioned on the relevance of the instability itself, signalling the area law phase of the original model.

Overall, this gives rise of a new type of absorbing state phase transition, where the order parameter ϕ remains gapless both in the spectrum as well as in the noise in the entire active phase. The absorbing state phase transition corresponds to a generation of a mass scale in the spectrum according to the BKT mechanism, which steers the state into the noiseless configuration $\phi_c = \text{const.}$, i.e. at momentum $p = 0$, which is blind to the noise $\sim p^2$ in Fourier space.

It is instructive to compare the present version of an absorbing state phase tran-

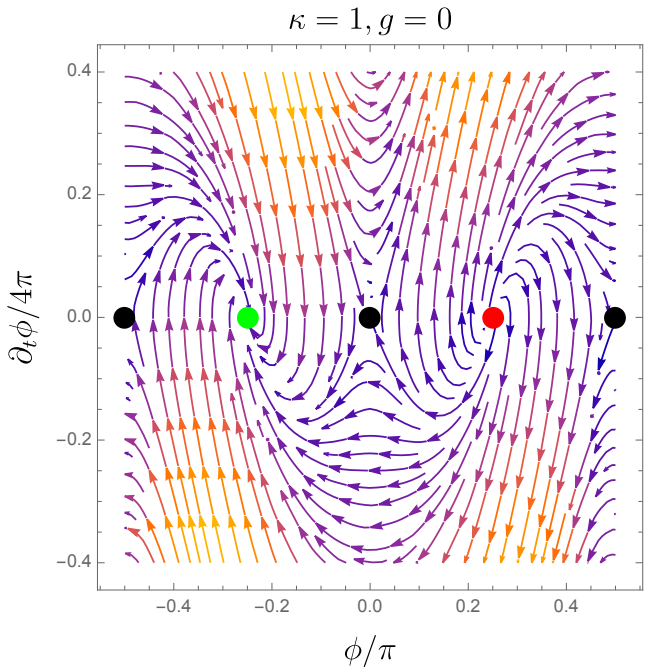

Figure 32: Flow of the mean density counting field ϕ over time. The feedback term κ lets a generic initial system state flow into a unique fixed point which corresponds to the dark state (green). The other fixed points of the dynamics are hyperbolic (black) or repulsive (red) and correspond to a fine tuned state that is unstable under contributions from higher harmonics.

sitions to more conventional, classical variants. A paradigmatic example in the latter context is directed percolation, which we consider here for definiteness. The overarching common feature is the existence of a dark or absorbing state of the full master equation. Also common is a suppressed noise level in the vicinity of the dark state, which vanishes in the dark state itself, creating its 'dark' or 'absorbing' property. This is responsible for the existence of genuine phase transitions in $1+1$ dimensions, which can have no counterpart at finite temperature thermal equilibrium, where the noise level is flat and non-zero. However, differences are present in the incarnations of the suppressed noise level: In the case discussed above, there is a dark state at $p = 0$, while in the vicinity, there is an additive noise level which scales $\sim p^2$ as indicated above. This scaling of the noise level equips the system with an effectively $1+1$ dimensional phase space, analogous to a quantum problem at $T = 0$ [194], and thus enabling a quantum phase transition (for comparison, a noise level scaling $\sim p^0$ would reduce the problem to an effectively $1+0$ dimensional, classical one). In contrast, in classical absorbing state transitions, the dark state is realized by a noise which is multiplicative but scales $\sim p^0$, i.e., the noise level scales with the order parameter field of the absorbing state transition. Therefore, it vanishes identically in the inactive phase, while being proportional to the order parameter in the active phase.

To summarize, in bosonization, the irrelevance of the modifications leads to $\hat{H} \approx$

$\hat{H}^{(0)}$ and $\hat{L}_l \approx \hat{L}_l^{(0)}$ up to (globally crucial) gradient terms. Quantitatively, the dynamics is described by a non-Hermitian sine-Gordon theory, which predicts the absorbing state transition to be BKT. This complements analytically our numerical results for the classical scheme (Fig. 33). In particular, the term describing the noise level in the effective theory is RG irrelevant, reflecting the existence of a dark state and preserving the scaling behavior characteristic of a $1+1$ dimensional quantum BKT scenario.

5.3.4 Numerical simulation

To demonstrate the discussed behavior, we implement the quantum feedback scheme numerically and study the dynamics in finite systems. Due to the interacting nature of both $\hat{L}_l^{\pm}$ and $\hat{H}$ this cannot be done using Gaussian states, in contrast to the classical feedback scheme, so that we implement a time-evolution block-decimation (TEBD) [195–198] algorithm based on a matrix product state (MPS) representation [122]. Initializing the system in a random product state leads to weak entanglement throughout the time-evolution in both phases, as long as we avoid very weak measurement rates. Therefore we may simulate systems beyond the scope of exact diagonalization. To implement the TEBD algorithm, we need to rewrite the state update due to feedback in every time-step (choosing again $dt = 0.05$) in terms of local gate operations in a system with open boundary conditions (as opposed to periodic boundary conditions in the classical feedback scheme), see Fig. 33a). The state is first updated by applying a series of 3-local operations of the form $e^{-i\hat{n}_i \hat{h}_{i\pm1,i\pm2} dt/2}$ from trotterization of the Hamiltonian time-step $e^{-i\hat{H}dt}$ using a truncation of the MPS at a finite bond-dimension in each step. After that, all gates are again applied in opposite order. The splitting is done to reduce trotterization errors. After that, we apply the measurement and feedback operation (see Fig. 27) by extracting the probabilities of the measurement outcomes of $\hat{n}_l$ for a set of randomly (rate $1 - e^{-\gamma dt}$)[33] chosen sites l and according to this distribution, we apply first a local projection operator onto the state, normalize and in case of an outcome that is not compatible with the target state, we apply the correction operator $\hat{C}_{l,l\pm1}$ ($\pm$ chosen randomly) which is a 2-local object, after which we truncate the MPS at the given bond-dimension. After such a time-step we extract the entanglement entropy and the observable order parameter $\langle \hat{n}_l \hat{n}_{l+1} \rangle$. These steps are implemented using the ITensors.jl package [197, 198] and we repeat them up to times $0.1L^2$, repeating the whole process in independent trajectories. The stochastic nature of the trajectories leads to noisy data while a finite bond dimension yields a systematic error (see Fig. 33b)). Therefore, we need to perform a scaling analysis in terms of both the system size and the bond dimension to analyze the absorbing state phase transition. In App. B.2 we discuss the role of the bond dimension in more detail.

[33] Note a different definition by a factor of 2 compared to the classical feedback simulations and the analytical approach.

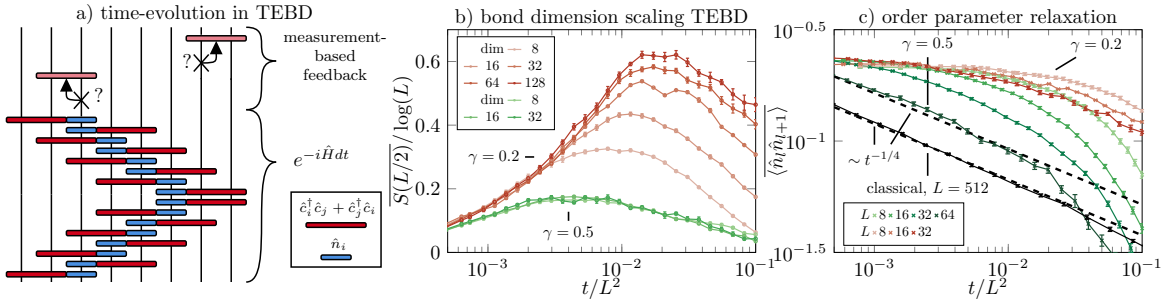

Figure 33: a) Discrete representation of the quantum feedback protocol that is implemented using TEBD. b) Impact of the maximal bond dimension in TEBD in the different phases: For strong measurement, entanglement is low and a small bond dimension is enough to capture the entanglement bottleneck at intermediate times while for weak measurement, a large bond dimension is required. We show data for $L = 32$ here. c) The time-evolution towards the target state, as characterized by the order parameter. In the absorbing phase, we observe a power-law decay with an exponent of $\approx 1/4$ (dashed line) different to the classical pre-selection setting and the target state is reached in the reaction-diffusion time-scale L^2. This is compared to the (time-rescaled) results of a classical simulation in the semi-classical limit of the model, where much larger system-sizes are available (see App. D.3). For rare measurement, the large entropy barrier masks the formation of a long-lived plateau as we are restricted to rather small system sizes but there is a clear trend towards this scenario. The bond dimension is chosen such that the observables at $t = 0.1L^2$ remain unchanged when doubling the bond dimension.

Besides that point, we observe the phenomenology of an absorbing state phase transition just like in the classical feedback scenario: For strong measurements, at system goes into the dark state in algebraic time $t \sim L^2$ according to a power law, while for weak measurements, an active phase emerges that is stabilized by the system size (see Fig. 33c)). This is also reflected in the entanglement, supporting the pre-selection phenomenology (see Fig. 28) in this model: The absorbing state corresponds to the weakly entangled phase while the active phase is strongly entangled (see Fig. 33b)). In fact, the entanglement entropy is logarithmic in the system size (see Fig. 34b)) indicating a CFT phase matching the unmodified model. Besides that, we may perform a finite size scaling analysis for both the entanglement and the order parameter in the quasi-stationary state which indicates a qualitative change at $\gamma \approx 0.35$ between an active phase with logarithmic entanglement scaling and a finite order parameter at $t = 0.1L^2$ and a phase with a drastically reduced order parameter and entanglement, indicating an absorbing phase. This confirms the existence of a phase transition for both at the same critical measurement strength (see Fig. 34c)). The results shown in Fig. 34 qualitatively match the picture found in the classical feedback numerics and the field theory analysis, indicating a phase transition at $\gamma_c \approx 0.35$ between an area law entangled, absorbing phase and a logarithmic active phase at the reaction-diffusion timescale $\sim L^2$.

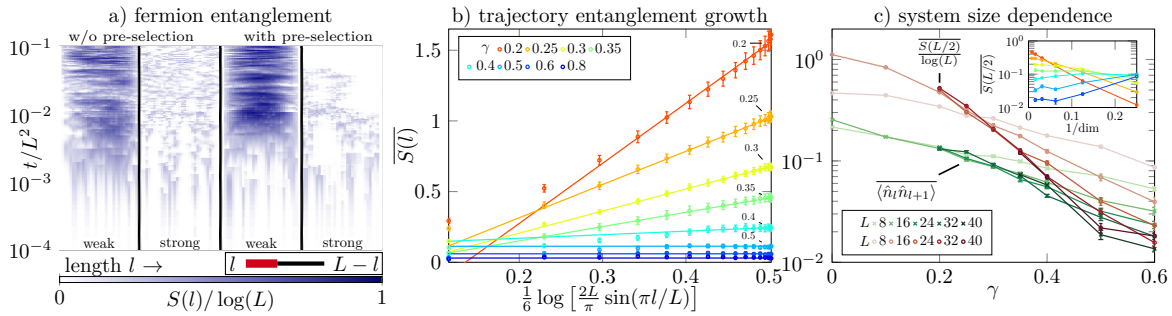

Figure 34: Entanglement-entropy in a single trajectory depending on the position l of the bi-partition of the state into a subsystem of length l and its compliment in a system with open boundary conditions, starting from a random product state with half filling. The full Hamiltonian of the quantum pre-selection scheme with measurements (left columns) results in a qualitatively different entanglement between rare $\gamma = 0.2$ and frequent $\gamma = 0.5$ measurement and a quick saturation of the behavior. Including the active feedback (right columns, see Fig. 27) has no drastic effect on the entanglement scaling up to the considered time $0.1L^2$ for rare measurements (c.f. classical feedback data, Fig. 28) while all entanglement is gone for frequent measurements as the target-state is reached at this timescale. b) The entanglement scaling at the timescale $t = 0.1L^2$ and $L = 32$ with subsystem l size in the trajectory average shows a logarithmic growth for $\gamma \lesssim 0.35$ and area law for $\gamma \gtrsim 0.35$. c) Finite system size analysis for both the entanglement and the ensemble order parameter. Inset: In particular for the comparison of different system-sizes, a proper analysis of the the bond-dimension cutoff in the MPS approximation is crucial and we obtain the data by extrapolating from finite bond-dimension data (colorcode like in b), $L = 32$).

5.4 Conclusion

Pre-selection reveals the physical meaning of MIPTs in terms of quantum absorbing state phase transitions in representative wave functions. This result is rationalized by the individual measurement trajectories hosting the same information as the entire ensemble in a large system. In this sense, it parallels post-selection, but it avoids an exponential overhead. On the practical side, this opens up a clear path towards experimental observability of MIPTs in controlled quantum platforms. We demonstrated this connection for spinless fermions in one dimension and a trivial target state without entanglement. We argued that this proof of principle suffices to lift the MIPT of BKT type in free fermions under monitoring, which is still debated, to the level of observability in terms of an order parameter. On the theory side, it also opens up an entirely different direction: the availability of adaptive quantum circuits [124, 125] enables a controlled physical realization of quantum absorbing state phase transitions with potentially novel non-equilibrium universality classes in the quantum regime. While we demonstrated the tight connection of stationary behaviors of MITPs and pre-selected scenarios, a particular challenge is posed by exploring their mutual relation in terms of dynamics.

6 Conclusion and outlook

In this thesis, we discussed various aspects of the dynamics of monitored fermions in one dimension. This system constitutes the ideal platform to study measurement-induced phenomena in the presence of a conservation law due to the fact that it can be efficiently simulated and that the equilibrium counterpart is an extremely well studied system. We established a systematic field theoretical framework for this specific model, discussing especially the effective cooling of the relative modes ($k > 0$) in replica space, induced by the heating of a single mode ($k = 0$) to an infinite temperature state. This mechanism was used to make numerically testable predictions for the specific model, both with short- and long-ranged dynamics. Especially for the long-ranged case, we found striking numerical evidence confirming the non-trivial predictions of our replica Keldysh field theory approach.

One crucial technical insight is that for these models, the Keldysh contours for relative modes ($k > 0$) in replica space decouple such that a description in terms of a non-Hermitian Hamiltonian captures the essential physics of the problem. Even though the $k = 0$ mode behaves so differently from all the others, in Abelian bosonization, the replica exchange symmetry is not broken. In disordered systems [199, 200], as well as in the non-linear sigma model approach [69] to this model however, such a spontaneous replica symmetry breaking is fundamental. This calls for the question, what the precise difference of replica theory for disorder and measurement problems is. Is there spontaneous replica symmetry breaking in measurement problems as well? How would that be observable in numerical simulations?

Besides the mechanisms described within the framework of the replica trick, a better understanding of this framework itself might also be useful: mathematically speaking, the replica trick requires taking a limit that is not well defined as we extrapolate from a discrete subset of points to another one. While this is anyways widely accepted for the treatment of disordered systems, a deeper mathematical understanding requires a well defined method which further backs the results we obtained. For that reason, it is worth wile to explore the super-symmetric approach to disorder problems [159–162] in the case of measurement-induced dynamics.

After establishing this theoretical framework for measurement-induced phases and phase transitions, another promising direction is to study related models and investigate the true realm of universality of the fermionic model. For instance, without changing the effective action, we may break Gaussianity of the states by adding interactions, or the integrability of the Hamiltonian by considering a disordered potential. While the effective replica model is not changed by this type of modification, the numerical treatment is more tedious. However, there is evidence [201–203] suggesting that indeed the logarithmically entangled phase can even be stabilized by these perturbations. How

general is that?

The replica method we developed to study conservation laws in MIPTs is not restricted to the specific case of particle number conservation. In contrast, it should be seen as a tool to investigate a wide range of models with different symmetries. It will be interesting to explore the whole range of applicability of this method. In particular, we would like to study models that describe experimentally realized systems where measurements can be performed, such as Rydberg arrays [204–206]. This brings us closer to an experimental observation of measurement-induced phenomena in many body quantum systems.

Very recently, another angle is taken when looking at measurement-induced phenomena and, more generally, synthetic quantum matter. Besides entanglement, we may study the so-called magic [207, 208] or even the full complexity [7, 209] of states. The complexity of a state measures, how many local unitary operations are at least needed in order to prepare that state. This is closely related amount of quantum information the state contains. The idea is, that a complex quantum state is hard to (even approximately) store on a classical computer. Hence, complex states are of particular relevance when we want to realize quantum supremacy in NISQ devices. Therefore, it would be useful to better understand the complexity of states generated by measurement-induced dynamics.

Complexity itself is hard to extract, even numerically, for a given state. Instead, we have looked in this thesis into one way, how states can be non-classical: by being entangled. The entanglement entropy can be understood as a measure, how large the bond dimension of an MPS needs to be to approximately store the state on a classical computer. Therefore, it is related to complexity. However, there are strongly entangled states that can be efficiently classically simulated, namely stabilizer states which are the outcomes of Clifford circuits [210]. Therefore, another measure for complexity is the non-stabilizerness of states (also called magic) [211, 212] of a state, which can be numerically quantified [213]. It has been shown numerically, that magic can undergo phase transitions [214–218], just like entanglement, but in very different scenarios and with very different representations of the states, compared to the fermion model.

While the physics of entanglement in monitored Hamiltonian systems becomes more and more understood (and is discussed in this thesis), a general understanding of complexity in field theory is lacking. Therefore, it would be very interesting to define measures of magic and complexity on the level of replica Keldysh field theory or a generalization thereof, and understand universal critical phenomena in terms of these. We know, that non-interacting systems such as free fermions are not complex, even though highly entangled, as they can be efficiently simulated using Gaussian states. This works even for volume law states in the absence of measurements. Therefore, an interesting starting point would be to add interactions here and identify the relevant

observables that quantify the corresponding complexity.

We also discussed ways to overcome the post-selection problem that monitored dynamics generically faces, obstructing experimental observability. In particular, this motivated to study different ways of implementing pre-selection using feedback of measurement results into the dynamics. The very recently demonstrated experimental possibility to adjust the unitary gates in NISQ devices to measurement read-outs in run time of a single experiment [124, 125] further motivates to study such a type of dynamics. There is a lot of room to explore different protocols that make use of this technological advancement.

In particular, we may study universal properties of state preparation by active steering [134]. The directionality in Hilbert space induced by feedback makes it natural to study quantum absorbing state phase transitions and investigate the role of entanglement in these. How does the fact that a steered system is inherently quantum-mechanical affect the critical behavior? Is there a fundamental difference between classical and quantum absorbing state phase transitions? Note, that in the scenarios we discussed in this thesis, the dark state is a product state (the Néel state) such that, at least in the absorbing phase, a classical understanding suffices. For instance, in the semi-classical limit of the quantum feedback scheme, we numerically find the same critical behavior as in the full quantum model. Therefore, to answer the questions posed above, the implementation of dark states with entanglement such as topologically ordered pure [219, 220] or mixed states [221–223] is promising. A opportune example system for that is the Kitaev chain [224].

An even more exploratory direction to investigate is the combination of measurement-only circuits with active feedback. Can we steer a system purely by applying the right measurements depending on the measurement outcomes of previous measurements? What are the connected phases and phase transitions?

Finally, let us return to the originally stated goal of the field to realize a universal quantum computer or at least an efficient scalable quantum simulator. It is to a large degree an experimental and engineering problem to improve the hardware of NISQ devices even further. Nevertheless, we hope that a better understanding of the universal behavior of quantum systems under the typical dynamics realized in these devices enables more efficient schemes both for the preparation of states as well as quantum error correction. Therefore, it will be exciting to investigate the precise connections of quantum absorbing state phase transitions and, more generally, measurement-induced dynamics with quantum error correction and quantum steering. These questions will be of huge relevance once even larger noisy quantum simulators exist, where the laws of quantum thermodynamics govern the possibilities and limitations of quantum computing.

Appendices

Appendix A Theory of free fermions under continuous monitoring

A.1 Derivation of the replica quantum master equation for the QSD protocol

Here we derive the replica master equation for the weak measurement protocol, Eq. (2.70) from the main text. The exact time-evolution of the replicated density operator is

$$\tilde{\rho}_{R,t+dt} = \left(e^{-\frac{i}{\hbar}\hat{H}dt}\right)^{\otimes R} \overline{\hat{P}^{\otimes 2R}}(t, \tilde{\rho}_{R,t}) \left(e^{\frac{i}{\hbar}\hat{H}dt}\right)^{\otimes R}, \tag{A.1}$$

where

$$\overline{\hat{P}^{\otimes 2R}}(t, \tilde{\rho}_{R,t}) = \int \mathcal{D}J_t \left(\otimes_{r=1}^{R} \hat{P}(\{J_{\alpha,t}\}_\alpha)\right) \tilde{\rho}_{R,t} \left(\otimes_{r=1}^{R} \hat{P}(\{J_{\alpha,t}\}_\alpha)\right). \tag{A.2}$$

To get the deterministic time-evolution of the R replicated non-normalized density operator $\tilde{\rho}_{R,t}$, we need to apply the generalized projector from both sides and average over all measurement outcomes. Let us first define the corresponding operator acting on a single replica

$$\hat{P}^{(r)}(\{J_{\alpha,t}\}_\alpha) = \prod_\alpha \left(\frac{2\gamma_\alpha dt}{\pi}\right)^{1/4} e^{-\gamma_\alpha dt (J_\alpha - \hat{O}_\alpha^{(r)})^2}. \tag{A.3}$$

When the system is replicated, this acts on every replica and we obtain the R replica generalized projector

$$\hat{P}_R(\{J_{\alpha,t}\}_\alpha) = \prod_r \hat{P}^{(r)}(\{J_{\alpha,t}\}_\alpha). \tag{A.4}$$

Note that while the operator $\hat{O}_\alpha^{(r)}$ depends on the chosen replica, the observed current does not, which induces a coupling between the different replicas in the time-evolution. Since all measurement operators commute $[\hat{O}_\alpha^{(r)}, \hat{O}_{\alpha'}^{(r')}] = 0$ mutually, the we may sum over α in the end and drop the index for simplicity. The problem then simplifies to the

average

$$\begin{aligned}
&\int dJ \left(\prod_{r=1}^{R} \hat{P}^{(r)}(J)\right) \tilde{\rho}_R \left(\prod_{r=1}^{R} \hat{P}^{(r)}(J)\right) \\
&= \left(\frac{2\gamma dt}{\pi}\right)^{R/2} \int dJ e^{-\gamma dt \sum_{r=1}^{R} (J-\hat{O}^{(r)})^2} \tilde{\rho}_R e^{-\gamma dt \sum_{r=1}^{R} (J-\hat{O}^{(r)})^2} \\
&= \left(\frac{2\gamma dt}{\pi}\right)^{R/2} \int dJ e^{-\gamma dt \sum_{r=1}^{R} \left[(J-\hat{O}_-^{(r)})^2 + (J-\hat{O}_+^{(r)})^2\right]} \tilde{\rho}_R,
\end{aligned} \tag{A.5}$$

where the index $\pm$ indicates that the operator acts on $\tilde{\rho}_R$ from either side. Introducing the replica-summed operator $\overline{O}^R = \sum_r \hat{O}^{(r)}$ we find

$$\begin{aligned}
&\left(\frac{2\gamma dt}{\pi}\right)^{R/2} \int dJ e^{-\gamma dt \left(2J^2 - 2J\left(\overline{O_+}^R + \overline{O_-}^R\right) + \left(\overline{O_+^2}^R + \overline{O_-^2}^R\right)\right)} \tilde{\rho}_R \\
=&\frac{1}{\sqrt{R}} \left(\frac{2\gamma dt}{\pi}\right)^{\frac{R-1}{2}} e^{\frac{1}{2}\gamma dt \left[\left(\overline{O_+}^R + \overline{O_-}^R\right)^2 - 2\left(\overline{O_+^2}^R + \overline{O_-^2}^R\right)\right]} \tilde{\rho}_R.
\end{aligned} \tag{A.6}$$

In the very end, we are only interested in the limit $R \to 1$. While keeping the R copies of all operators and states, the explicit appearance in the normalization does not matter for the structure of the master equation and therefore we already take the limit there. This is necessary because otherwise, the result is not properly differentiable in dt due to the lack of normalization of the state update. Using the right replica limit allows then expanding in short dt which yields (adding the index α again)

$$\tilde{\rho}_R + dt \sum_\alpha \gamma_\alpha \left[\overline{O_\alpha}^R \tilde{\rho}_R \overline{O_\alpha}^R - \frac{1}{2}\left\{2\overline{O_\alpha^2}^R - \left(\overline{O_\alpha}^R\right)^2, \tilde{\rho}_R\right\}\right] + \mathcal{O}(dt^2). \tag{A.7}$$

Adding the Hamiltonian contribution yields the replica master equation

$$\partial_t \tilde{\rho}_R = -\frac{i}{\hbar}[\overline{H}^R, \tilde{\rho}_R] + \sum_\alpha \gamma_\alpha \left[\overline{O_\alpha}^R \tilde{\rho}_R \overline{O_\alpha}^R - \frac{1}{2}\left\{2\overline{O_\alpha^2}^R - \left(\overline{O_\alpha}^R\right)^2, \tilde{\rho}_R\right\}\right].$$

This result does not assume any additional properties about the observables $\hat{O}_\alpha$ and is therefore fully general. If we take $R = 1$ exactly everywhere, we may use $\overline{O_\alpha^2}^R = \hat{O}_\alpha^2 = \left(\overline{O_\alpha}^R\right)^2$ such that we obtain a simplification in the anti-commutator revealing the ordinary Lindblad quantum master equation. For $R > 1$ however, we find that $\left(\overline{O_\alpha}^R\right)^2$ contains products of operators acting on different replicas, introducing a coupling between the replicas. Expanding again in the replica index yields the generalized Lindblad equation (2.70).

A.2 Fermionic path integral construction

The overlap of two fermionic coherent states is

$$\langle\psi_A|\psi_B\rangle = e^{\sum_{r,l}\bar{\psi}^{(r)}_{i,A}\psi^{(r)}_{l,B}} \equiv e^{\bar{\psi}_A\psi_B}. \tag{A.8}$$

We construct a resolution of unity in terms of this object as

$$1 = \int d\bar{\psi}d\psi e^{-\sum_{r,l}\bar{\psi}^{(r)}_l\psi^{(r)}_i}\,|\psi\rangle\,\langle\psi| \equiv \int d\bar{\psi}d\psi e^{-\bar{\psi}\psi}\,|\psi\rangle\,\langle\psi| \tag{A.9}$$

This allows to construct the trace of the R times replicated non-normalized density operator at some final time t_N as

$$\begin{aligned}\mathcal{Z}_R = \operatorname{Tr}\tilde{\rho}_R(t_N) &= \int d\bar{\psi}_N d\psi_N e^{-\bar{\psi}_N\psi_N}\,\langle\psi_N|\,\tilde{\rho}_R(t_N)\,|-\psi_N\rangle \\ &= \int_{\psi_{+,N}=-\psi_{-,N},\bar{\psi}_{+,N}=-\bar{\psi}_{-,N}} d\bar{\psi}_{+,N}d\psi_{+,N}d\bar{\psi}_{-,N}d\psi_{-,N}e^{\bar{\psi}_{+,N}\psi_{-,N}}\,\langle\psi_{+,N}|\,\tilde{\rho}_R(t_N)\,|\psi_{-,N}\rangle\end{aligned} \tag{A.10}$$

Based on this, we use a temporal discretization $t_n = t_0 + n\Delta t$ to rewrite $\tilde{\rho}_R(t_N) = (1 + \Delta t\mathcal{L}_R)\tilde{\rho}_R(t_{N-1})$ repeatedly, adding resolutions of unity on both sides. Finally sending $\Delta t \to 0$ yields the path integral

$$\mathcal{Z}_R = \int \mathcal{D}\bar{\psi}_\pm\mathcal{D}\psi_\pm e^{iS_R[\psi_\pm,\bar{\psi}_\pm]}, \tag{A.11}$$

$$S_R[\psi_\pm,\bar{\psi}_\pm] = \sum_{l,r,\sigma=\pm}\int_t \bar{\psi}^{(r)}_{\sigma,l}(t)i\sigma\partial_t\psi^{(r)}_{\sigma,l}(t) - i\int_t \mathcal{L}_R(\psi_\pm(t),\bar{\psi}_\pm(t)), \tag{A.12}$$

$$\mathcal{L}_R(\psi_\pm,\bar{\psi}_\pm) = \frac{\langle\psi_+|\,\mathcal{L}_R(|\psi_+\rangle\,\langle-\psi_-|)\,|-\psi_-\rangle}{\langle\psi_+|\psi_+\rangle\,\langle-\psi_-|-\psi_-\rangle}. \tag{A.13}$$

As we are interested in the stationary state, we send $t_0 \to -\infty$ and $t_N \to \infty$. Here, $\mathcal{L}_R$ is the generator of the time-evolution of the non-normalized density operator, see Eq. (2.70). The initial state fixes the conserved quantities under this evolution which are fixed by a proper regularization of the theory. This can be done because the role of initial conditions in the Keldysh construction is simply to fix the regularization as it only affects the boundary conditions of the path integral. It is now useful to rewrite the action in momentum space[34] using

$$\psi^{(r)}_l(t) = \int_{-\pi/a}^{\pi/a}\frac{dp}{2\pi}\int_{-\infty}^{\infty}\frac{d\omega}{2\pi}e^{ipal}e^{-i\omega t}\psi^{(r)}_{p,\omega} \equiv \int_{p,\omega} e^{ipal-i\omega t}\psi^{(r)}_{p,\omega}, \tag{A.14}$$

$$\bar{\psi}^{(r)}_l(t) = \int_{-\pi/a}^{\pi/a}\frac{dp}{2\pi}\int_{-\infty}^{\infty}\frac{d\omega}{2\pi}e^{-ipal}e^{i\omega t}\bar{\psi}^{(r)}_{p,\omega} \equiv \int_{p,\omega} e^{-ipal+i\omega t}\bar{\psi}^{(r)}_{p,\omega}, \tag{A.15}$$

[34] $a = 1$ is the lattice spacing, introduced here to fix the right dimensions.

and equivalently on the level of operators such that the anti-commutation relations are preserved,

$$\{\hat{\psi}_p, \hat{\psi}^\dagger_{p'}\} = 2\pi\delta(p-p'). \tag{A.16}$$

The Hamiltonian is given as

$$\hat{H} = -J\sum_l \hat{c}^\dagger_l \hat{c}_{l+1} + \text{h.c} = -2J\int_p \cos(pa)\hat{\psi}^\dagger_p\hat{\psi}_p = \int_p \epsilon(p)\hat{\psi}^\dagger_p\hat{\psi}_p, \tag{A.17}$$

where we identify the dispersion $\epsilon(p) = -2J\cos(pa)$ This is trivially normal ordered and we can simply replace operators by fields. We introduced a coupling constant J to fix the dimensionality. In the numerical simulation we picked $J=-1$ but the sign does not matter as we can shift the momenta by π/a and redefine the boundaries of the first Brillouin zone which removes the sign. The term that we need to add to the action is therefore simply

$$-\frac{\sigma}{\hbar}\sum_{r,\sigma}\int_{p,\omega}\epsilon(p)\bar{\psi}^{(r)}_\sigma\psi^{(r)}_\sigma. \tag{A.18}$$

This yields the free theory in absence of the monitoring, which dominates the short distance physics of the problem[35]. After a Keldysh rotation $\psi^{(r)}_{c/q} = (\psi^{(r)}_+ \pm \psi^{(r)}_-)/\sqrt{2}$, $\bar{\psi}^{(r)}_{c/q} = (\bar{\psi}^{(r)}_+ \pm \bar{\psi}^{(r)}_-)/\sqrt{2}$, this yields the bare action (3.13) from the main text. We can now add a source term and solve the Gaussian integral

$$\mathcal{Z}[J,\bar{J}] \equiv \int \mathcal{D}\bar{\psi}\mathcal{D}\psi e^{\int_{\omega,p}\bar{\psi}iG_0^{-1}\psi + i\bar{J}\psi + i\bar{\psi}J} \tag{A.19}$$

$$= \int \mathcal{D}\bar{\psi}\mathcal{D}\psi e^{\int_{\omega,p}(\bar{\psi}-\bar{J}iG_0)iG_0^{-1}(\psi - iG_0J) + \bar{J}iG_0J} \tag{A.20}$$

$$= \mathcal{Z}e^{\int_{\omega,p}\bar{J}iG_0J}. \tag{A.21}$$

Based on this, we can take functional derivatives with respect to $J, \bar{J}$ to generate the correlation functions,

$$\langle\psi\bar{\psi}\rangle_0 = \frac{1}{\mathcal{Z}}\int\mathcal{D}\bar{\psi}\mathcal{D}\psi\psi\bar{\psi}e^{iS_0} = \frac{1}{\mathcal{Z}}\left(\frac{\delta}{\delta J}\frac{\delta}{\delta\bar{J}}\mathcal{Z}[J,\bar{J}]\right)_{J=\bar{J}=0} = iG_0 \tag{A.22}$$

The general form of the inverse Keldysh greens function obeying the symmetries of the Keldysh action for a normalized density operator, obtained in the limit $R\to 1$ is

$$G_0^{-1} = \begin{pmatrix} 0 & P_A \\ P_R & P_K \end{pmatrix}, \tag{A.23}$$

[35]Let us take $\hbar = 1$ from now. It sets the scale for the Hamiltonian coupling J

such that the Green's function is

$$G_0 = \begin{pmatrix} G_K & G_R \\ G_A & 0 \end{pmatrix} = \begin{pmatrix} -P_R^{-1} P_K P_A^{-1} & P_K^{-1} \\ P_A^{-1} & 0 \end{pmatrix}. \tag{A.24}$$

In absence of the measurements, we simply have $P_R = P_A = \omega + 2J\cos pa$ as discussed in the main text.

Next, let us consider the monitoring operator. It is better written in the real space representation. It is quadratic and has the property $\hat{n}_l^{(r)2} = \hat{n}_l^{(r)}$ such that we need to be careful with the normal ordering prescription. Due to the structure of the regularization of the action, we only obtain a causally well defined action if we do not use this property but instead normal order $\hat{L}_l = \hat{L}_l^{(r)\dagger} = \hat{n}_l^{(r)}$, evaluate the operators $\hat{L}_l^{(r)}$ and $\hat{L}_l^{(r)\dagger}$ separately at slightly different times and then take the limit of continuous times only after doing the calculations. [28, 29, 154]. This yields for the Lindblad term diagonal in replica space

$$S_{\mathcal{L}} = \frac{-i\gamma}{2} \sum_{r,l} \int_t \left(2 n_+^{(r)} n_-^{(r)} - n_+^{(r)} n_+^{(r)} - n_-^{(r)} n_-^{(r)} \right). \tag{A.25}$$

Note that we also find in the replica construction that the $\bar{\psi}_+$ fields are evaluated slightly later, than the ψ_+ field in n_+ since the creation operator is acting to the left, i.e. on a later time step than the annihilation operator. For the $-$ fields, this order is reverted. For the replica-coupling term, the temporal regularization of the particle number operator acting on a single contour does not change anything since the different particle number operators act on different replicas. Here we find

$$S_{\mathcal{M}} = \frac{-i\gamma}{2} \sum_{r \neq r', l} \int_t \left(2 n_+^{(r)} n_-^{(r')} + n_+^{(r)} n_+^{(r')} + n_-^{(r)} n_-^{(r')} \right). \tag{A.26}$$

We understand the different appearing terms in the presence of a regularization as

$$n_+^{(r)} n_-^{(r')} = \bar{\psi}_+^{(r)}(t + (0^+)) \psi_+^{(r)}(t) \bar{\psi}_-^{(r')}(t) \psi_-^{(r')}(t + 0^+), \tag{A.27}$$

$$n_+^{(r)} n_+^{(r')} = \bar{\psi}_+^{(r)}(t + 3(0^+)) \psi_+^{(r)}(t + 2(0^+)) \bar{\psi}_+^{(r')}(t + 0^+) \psi_+^{(r')}(t), \tag{A.28}$$

$$n_-^{(r)} n_-^{(r')} = \bar{\psi}_-^{(r)}(t - 3(0^+)) \psi_-^{(r)}(t - 2(0^+)) \bar{\psi}_-^{(r')}(t - 0^+) \psi_-^{(r')}(t). \tag{A.29}$$

This means that in fact all fields in a coupling term are in fact evaluated at slightly different times which makes the evaluation of replica coupling terms unambiguous. Note that the $\pm$ correlation vanishes due to the infinite temperature as we show below such that the replica coupling term is regularized as well.

A.3 Elimination of the infinite temperature mode

Here we show how to integrate out the $k = 0$ mode from the fermionic action perturbatively for small γ. We need to compute

$$S_{k>0} = S_0[\psi^{(k>0)}, \bar{\psi}^{(k>0)}] + \langle S_{\mathcal{L}} + S_{\mathcal{M}} \rangle_{0,k=0} + \mathcal{O}(\gamma^2) \tag{A.30}$$

To evaluate this expectation value, we use the infinite temperature property. To do so, we need the correlation functions in the $\pm$ basis. The non-vanishing correlation functions are (using $G_K = 0$ and that all k modes decouple)

$$\langle \psi_\sigma(p,\omega)\bar{\psi}_{\sigma'}(p',\omega')\rangle_0 = 2\pi\delta(\omega-\omega')2\pi\delta(p-p')\frac{1}{2}(\sigma i G_A + \sigma' i G_R) \tag{A.31}$$

The difference $G_R - G_A$ vanishes up to the regularization. Therefore, all inter-contour couplings vanish and we only get

$$\langle \psi_\sigma(p,\omega)\bar{\psi}_{\sigma'}(p',\omega')\rangle_0 = 2\pi\delta(\omega-\omega')2\pi\delta(p-p')\delta_{\sigma\sigma'}\frac{i\sigma(\omega-\epsilon(p))}{(\omega-\epsilon(p))^2+(0^+)^2}. \tag{A.32}$$

A Fourier transformation to real time yields in the limit $0^+ \to 0$

$$\langle \psi_\sigma(p,t)\bar{\psi}_{\sigma'}(p',t')\rangle_0 = 2\pi\delta(p-p')\delta_{\sigma\sigma'}\sigma\mathrm{sgn}(t-t')e^{-i\epsilon(p)(t-t')} \tag{A.33}$$

At equal positions, we can compute the correlation function in a closed form,

$$\begin{aligned}\langle \psi_{\sigma,l}(t)\bar{\psi}_{\sigma',l}(t')\rangle_0 &= \delta_{\sigma\sigma'}\sigma\mathrm{sgn}(t-t')\int_p e^{2iJ\cos(pa)(t-t')} \\ &= \delta_{\sigma\sigma'}\sigma\mathrm{sgn}(t-t')J_0(2J(t-t')),\end{aligned} \tag{A.34}$$

where $J_0(x)$ is the Bessel function of first kind, where $J_0(0) = 1$. This simplifies the correlation function at almost equal times to

$$\langle \bar{\psi}_{\sigma,l}(t)\psi_{\sigma',l}(t\pm 0^+)\rangle_0 = \mp\sigma\delta_{\sigma\sigma'} \tag{A.35}$$

This can now be used to evaluate the interaction term, which yields

$$\begin{aligned}\langle n_\sigma^{(r)} n_{\sigma'}^{(r')}\rangle_{0,k=0} = \langle \bar{\psi}_\sigma^{(0)}\psi_\sigma^{(0)}\bar{\psi}_{\sigma'}^{(0)}\psi_{\sigma'}^{(0)}\rangle_{0,k=0} + \bar{\psi}_\sigma^{(r,>)}\psi_\sigma^{(r,>)}\bar{\psi}_{\sigma'}^{(r',>)}\psi_{\sigma'}^{(r',>)} \\ + \langle \bar{\psi}_\sigma^{(0)}\psi_\sigma^{(0)}\bar{\psi}_{\sigma'}^{(r',>)}\psi_{\sigma'}^{(r',>)}\rangle_{0,k=0} + \delta_{\sigma,\sigma'}\langle \bar{\psi}_\sigma^{(0)}\psi_\sigma^{(r,>)}\bar{\psi}_{\sigma'}^{(r',>)}\psi_{\sigma'}^{(0)}\rangle_{0,k=0} \\ + \langle \bar{\psi}_\sigma^{(r,>)}\psi_\sigma^{(r,>)}\bar{\psi}_{\sigma'}^{(0)}\psi_{\sigma'}^{(0)}\rangle_{0,k=0} + \delta_{\sigma,\sigma'}\langle \bar{\psi}_\sigma^{(r,>)}\psi_\sigma^{(0)}\bar{\psi}_{\sigma'}^{(0)}\psi_{\sigma'}^{(r',>)}\rangle_{0,k=0}.\end{aligned} \tag{A.36}$$

In this reordering, we used that we only get finite expectation values if there is an equal number of annihilation and creation fields in a term. The first term is just a constant that can be absorbed into normalization of the path integral. The second term is the interaction term between fields that are non-diagonal in the replica basis. The last four terms generate a quadratic contribution to the $k \neq 0$ action. To evaluate them, we need to consider the normalization prescription discussed above, for the individual replica coupling terms. We obtain

$$\langle n_+^{(r)} n_-^{(r')} \rangle_{0,k=0} = n_+^{(r,>)} n_-^{(r',>)} + n_+^{(r,>)} + n_-^{(r',>)} \tag{A.37}$$

$$\langle n_+^{(r)} n_+^{(r')} \rangle_{0,k=0} = n_+^{(r,>)} n_+^{(r',>)} + n_+^{(r,>)} + n_+^{(r',>)} - \bar{\psi}_+^{(r',>)} \psi_+^{(r,>)} + \bar{\psi}_+^{(r,>)} \psi_+^{(r',>)} \tag{A.38}$$

$$\langle n_-^{(r)} n_-^{(r')} \rangle_{0,k=0} = n_-^{(r,>)} n_-^{(r',>)} + n_-^{(r,>)} + n_-^{(r',>)} - \bar{\psi}_-^{(r',>)} \psi_-^{(r,>)} + \bar{\psi}_-^{(r,>)} \psi_-^{(r',>)} \tag{A.39}$$

The relative sign between the replica coupling terms appears because in the first term, we need to commute two of the $>$ fields but we do not change the position or temporal order of the (0) fields, while in the other case, the $>$ fields are in normal order and we need to commute two of the (0) fields which means that also their temporal order is inverted, which gives an additional sign that cancels out again. While they trivially disappear for $r = r'$, they cancel out when summing over $r \neq r'$ by a simple relabelling. This results in Eq. (3.28) of the main text.

Appendix B Numerical simulations

B.1 Gaussian states for QSD

We parametrize the state $|\psi\rangle$ of a half-filled one-dimensional fermionic chain that is evolving according to a non-interacting and particle-number conserving dynamics in the form [67, 167],

$$|\psi\rangle = \prod_{j=1}^{L/2} \left(\sum_{l=1}^{L} U_{lj} \hat{c}_l^\dagger \right) |0\rangle \,. \tag{B.1}$$

The operator

$$\hat{d}_j^\dagger = \sum_{l=1} U_{lj} \hat{c}_l^\dagger, \tag{B.2}$$

creates a single fermion in a a state given by a column of the matrix $U = \{U_{lj}\}_{lj}$ as its single particle wave function. The many-body state is given by the successive creation of single particles. The anti-commutation relations read

$$\{\hat{d}_i^\dagger, \hat{d}_j\} = (U^\dagger U)_{ij}. \tag{B.3}$$

For the single particle states to be distinct single particle states, we therefore demand $U^\dagger U = 1$ due to the Pauli principle. In this case, the many-body state is normalized,

$$\begin{aligned}
\langle\psi|\psi\rangle &= \langle 0|\, \hat{d}_{L/2}\hat{d}_{L/2-1}\dots\hat{d}_2\hat{d}_1\hat{d}_1^\dagger\hat{d}_2^\dagger\dots\hat{d}_{L/2-1}^\dagger\hat{d}_{L/2}^\dagger\, |0\rangle \\
&= \langle 0|\, \hat{d}_{L/2}\hat{d}_{L/2-1}\dots\hat{d}_2((U^\dagger U)_{11} - \hat{d}_1^\dagger\hat{d}_1)\hat{d}_2^\dagger\dots\hat{d}_{L/2-1}^\dagger\hat{d}_{L/2}^\dagger\, |0\rangle \\
&= \langle 0|\, \hat{d}_{L/2}\hat{d}_{L/2-1}\dots\hat{d}_2\hat{d}_2^\dagger\dots\hat{d}_{L/2-1}^\dagger\hat{d}_{L/2}^\dagger\, |0\rangle \\
&= \langle 0|0\rangle = 1.
\end{aligned} \tag{B.4}$$

Additionally, we can compute expectation values of fermion bilinears using $\{\hat{c}_n, \hat{d}_j^\dagger\} = U_{nj}$,

$$\begin{aligned}
D_{mn} &= \langle \hat{c}_m^\dagger \hat{c}_n \rangle \\
&= \langle 0|\, \hat{d}_{L/2}\hat{d}_{L/2-1}\dots\hat{d}_2\hat{d}_1\hat{c}_m^\dagger\hat{c}_n\hat{d}_1^\dagger\hat{d}_2^\dagger\dots\hat{d}_{L/2-1}^\dagger\hat{d}_{L/2}^\dagger\, |0\rangle \\
&= \sum_{k,k'=1}^{L/2} (-1)^{k+k'} U_{mk}^* U_{nk'} \langle 0| \left(\prod_{j\neq k} \hat{d}_j \right) \left(\prod_{j'\neq k'} \hat{d}_{j'}^\dagger \right) |0\rangle \\
&= \sum_{k,k'=1}^{L/2} (-1)^{k+k'} U_{mk}^* U_{nk'} \delta_{k,k'} = \sum_k U_{mk}^* U_{nk} = (U^* U^T)_{mn}
\end{aligned} \tag{B.5}$$

Here we used again that the states $\hat{d}_j$ are orthonormal. Note that up to complex conjugation, this yields $D = UU^\dagger$. However, complex conjugation drops out of all observables as they need to be real. In particular, we find for the particle density

$\langle \hat{n}_l \rangle = (UU^\dagger)_{ll}$. Additionally, the simple structure of the state also allows to evaluate expectation values of arbitrary operators. Let us demonstrate this for the next higher order operator that is particle-number conserving[36]

$$\begin{aligned}
\langle \hat{c}_a^\dagger \hat{c}_b^\dagger \hat{c}_c \hat{c}_d \rangle &= \sum_{k_a,k_d=1}^{L/2} (-1)^{k_a+k_d} U^*_{ak_a} U_{dk_d} \langle 0| \left(\prod_{j\neq k_a} \hat{d}_j \right) \hat{c}_b^\dagger \hat{c}_c \left(\prod_{j'\neq k_d} \hat{d}_{j'}^\dagger \right) |0\rangle \\
&= \sum_{k_a\neq k_b, k_c\neq k_d}^{L/2} (-1)^{k_a+k_b+k_c+k_d} U^*_{ak_a} U_{dk_d} U^*_{bk_b} U_{ck_c} \langle 0| \left(\prod_{j\neq k_a,k_b} \hat{d}_j \right) \left(\prod_{j'\neq k_c,k_d} \hat{d}_{j'}^\dagger \right) |0\rangle \\
&= \sum_{k_a\neq k_b, k_c\neq k_d} (-1)^{k_a+k_b+k_c+k_d} U^*_{ak_a} U_{dk_d} U^*_{bk_b} U_{ck_c} (\delta_{k_ak_d}\delta_{k_bk_c} - \delta_{k_ak_c}\delta_{k_bk_c}) \\
&= (U^*U^T)_{ad}(U^*U^T)_{bc} - (U^*U^T)_{ac}(U^*U^T)_{bd} = D_{ad}D_{bc} - D_{ac}D_{bd}.
\end{aligned} \tag{B.6}$$

Hence, Wick's theorem applies to all states $|\psi\rangle$ of this form. Therefore, we also call them Gaussian states. To see, that this parametrization is actually useful in the case of QSD for free fermions with particle number measurement, consider the action of $(\epsilon \to 0)$,

$$\begin{aligned}
e^{i\epsilon \hat{c}_n^\dagger \hat{c}_m} |\psi\rangle &= (1 + i\epsilon \hat{c}_n^\dagger \hat{c}_m + \mathcal{O}(\epsilon^2)) \prod_{j=1}^{L/2} \left(\sum_{l=1}^{L} U_{lj} \hat{c}_l^\dagger \right) |0\rangle \\
&= \left(\sum_{l=1}^{L} U_{l1} \hat{c}_l^\dagger \right) (1 + i\epsilon \hat{c}_n^\dagger \hat{c}_m + \mathcal{O}(\epsilon^2)) \prod_{j=2}^{L/2} \left(\sum_{l=1}^{L} U_{lj} \hat{c}_l^\dagger \right) |0\rangle \\
&\quad + \left(i\epsilon U_{m1} \hat{c}_n^\dagger + \mathcal{O}(\epsilon^2) \right) \prod_{j=2}^{L/2} \left(\sum_{l=1}^{L} U_{lj} \hat{c}_l^\dagger \right) |0\rangle \\
&= |\psi\rangle + i\epsilon \sum_{k=1}^{L/2} \prod_{j=1}^{L/2} \left(\sum_{l=1}^{L} \left((1-\delta_{kj}) U_{lj} + \delta_{kj}\delta_{nl} U_{mj} \right) \hat{c}_l^\dagger \right) |0\rangle + \mathcal{O}(\epsilon^2) \\
&= \prod_{j=1}^{L/2} \left(\sum_{l=1}^{L} (U_{lj} + i\epsilon \delta_{nl} U_{mj}) \hat{c}_l^\dagger \right) |0\rangle + \mathcal{O}(\epsilon^2)
\end{aligned} \tag{B.7}$$

In this way, we found a way to express exponential of bilinears if there is a small prefactor,

$$\begin{aligned}
e^{i\epsilon \sum_{n,m} A_{nm} \hat{c}_n^\dagger \hat{c}_m} |\psi\rangle &= e^{\epsilon \sum_{n,m} A_{nm} \hat{c}_n^\dagger \hat{c}_m} \prod_{j=1}^{L/2} \left(\sum_{l=1}^{L} U_{lj} \hat{c}_l^\dagger \right) |0\rangle \\
&= \prod_{j=1}^{L/2} \left(\sum_{l=1}^{L} \left(U_{lj} + i\epsilon \sum_m A_{lm} U_{mj} \right) \hat{c}_l^\dagger \right) |0\rangle + \mathcal{O}(\epsilon^2)
\end{aligned} \tag{B.8}$$

[36] All non-particle number conserving operators have a trivially vanishing expectation value.

Hence, to linear order in ϵ, we can write the action of such an operator in terms of an update of the single particle states as

$$|\psi\rangle \to e^{i\epsilon \sum_{n,m} A_{nm}\hat{c}_n^\dagger \hat{c}_m}|\psi\rangle \qquad \hat{=} \qquad U \to e^{i\epsilon A}U + \mathcal{O}(\epsilon^2). \tag{B.9}$$

Where $A = \{A_{nm}\}_{nm}$ and $U = \{A_{lj}\}_{lj}$ are matrices. To linear order in ϵ, we therefore find that a Hermitian matrix $A = \hat{A}^\dagger$ leaves the normalization unaffected as $U^\dagger e^{-i\epsilon A^\dagger} e^{i\epsilon A} U = U^\dagger U = 1$. However, higher orders in ϵ break the orthonormalization condition such that after every application of such an operator, we need to normalize the state, even if a Hamiltonian time-evolution step is applied. On top of that, non-hermitian time-evolution operators, such as projections or generalized projections, break this property explicitly and we need to orthonormalize after every time-step. The generalized projector corresponding to weak measurement of $\hat{n}_l$ reads

$$\begin{aligned}
\hat{P}_l(J_l) &= \left[\frac{2\gamma dt}{\pi}\right]^{1/4} e^{-\gamma dt(J_l - \hat{n}_l)^2} \\
&= \left[\frac{2\gamma dt}{\pi}\right]^{1/4} e^{-\gamma dt\left(\langle \hat{n}_l\rangle + \frac{dW_l}{2\sqrt{\gamma dt}} - \hat{n}_l\right)^2} \\
&= \left[\frac{2\gamma dt}{\pi}\right]^{1/4} e^{-\gamma dt\left(\langle \hat{n}_l\rangle + \frac{dW_l}{2\sqrt{\gamma dt}}\right)^2} e^{\left(\gamma dt(2\langle \hat{n}_l\rangle - 1) + \sqrt{\gamma dt}\xi_l\right)\hat{n}_l}
\end{aligned} \tag{B.10}$$

Where we used that the readout current is a Gaussian random variable which is parametrized by normalized Gaussian white noise $\overline{\xi_l} = 0$, $\overline{\xi_l \xi_m} = \delta_{lm}$. This has precisely the form we discussed above for $dt \to 0$, up to the normalization. Since $\hat{P}_l$ only acts on the l-th site, up to the normalization, the measurement of all lattice sites acts as

$$U \to \mathrm{diag}(\{e^{-\gamma dt(2\langle \hat{n}_l\rangle - 1) + \sqrt{\gamma dt}\xi_l}\}_l)U + \mathcal{O}(\epsilon^2) \tag{B.11}$$

The Hamiltonian has the form $\hat{H} = \sum_{n,m} h_{n,m}\hat{c}_n^\dagger \hat{c}_m$ where for nearest neighbor hopping we find $h_{nm} = \delta_{n,m+1} + \delta_{n,m-1}$, imposing periodic boundary conditions. Hence, we implement a single time-step up to normalization and higher orders in dt as

$$U \to e^{-\frac{i}{\hbar}h}\mathrm{diag}(\{e^{-\gamma dt(2\langle \hat{n}_l\rangle - 1) + \sqrt{\gamma dt}\xi_l}\}_l)U. \tag{B.12}$$

B.2 TEBD for quantum feedback

Here we give more details on the numerical implementation of the quantum feedback protocol. Just like in the case of Gaussian states, we simulate individual trajectories generated by Hamiltonian, measurement and feedback to be able to access the pure state entanglement. Therefore, we need to perform a trajectory average again. Due to the computationally more demanding states that we need to describe due to the

interacting nature of the problem, we need to carefully estimate the stochastic error due to the finite amount of trajectories. This allows to distinguish the stochastic from a systematic error that we obtain from limiting the bond dimension, as discussed below. To get an error estimate, we generate mini-batches of $768/L$ trajectories, average the observables within the mini-batch and then compute the mean and standard error of the mean over several batches until we obtain reasonable accuracy for each point in time. This procedure is repeated for various different cutoffs for the bond dimension of the matrix product state and we perform a finite bond dimension analysis to extract the proper behavior in the limit of infinite bond dimension (see the inset in Fig. 34c) and Fig. 33b)). The systematic error appearing over time can be most clearly studied looking at the control observable of the number of particles in the system: The breakdown of the MPS representation is signalled by the breaking of this conservation law in the simulations, as shown in Fig. 35. We find, especially for weak measurements, the

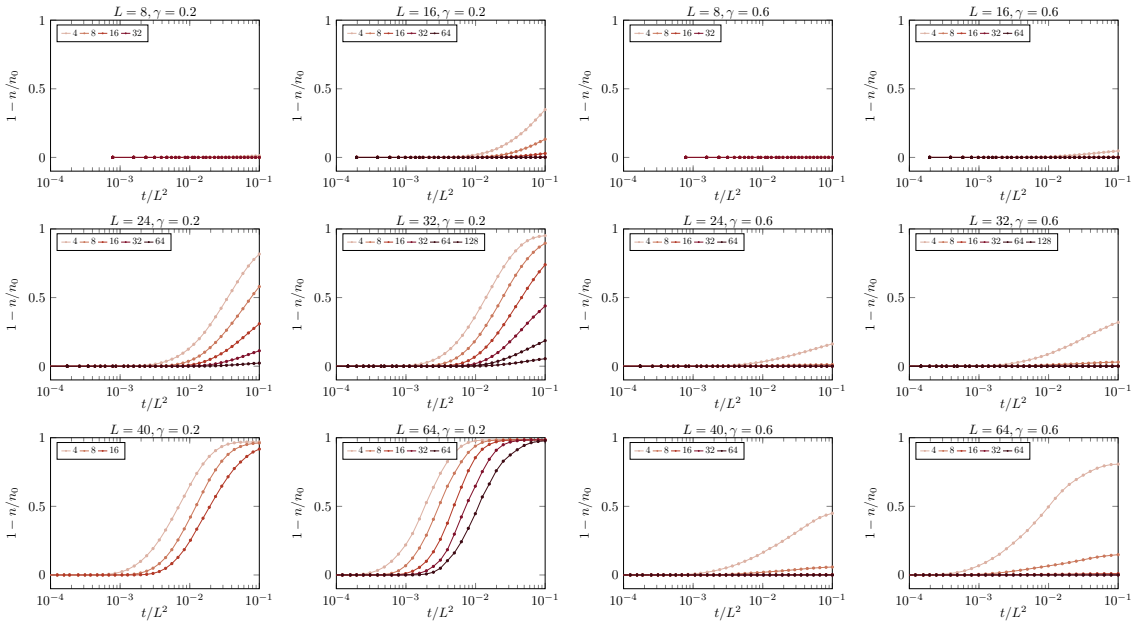

Figure 35: Evolution of the particle density n in the system in TEBD with finite bond dimension (different colors). The implemented model conserves the particle number exactly but the truncation of the bond dimension leads to a decay of the number of particles at late times as a numerical artifact. For weak measurements, and small systems, this does not lead to a problem while for larger systems and weaker measurement i.e. a larger entanglement bottleneck, the simulation can only be trusted at short times.

TEBD algorithm fails to properly implement the particle number conservation at late times. This occurs as the entanglement is peaked at intermediate times: With a system initialized in a product state, at short times the Hamiltonian generates a growth of entanglement before, at late times the feedback steers any finite system into the dark state that is again a product state. Therefore, in between there is a large entanglement regime for weak measurements that cannot be sufficiently well described by a MPS

with small bond dimension. Therefore, the limitation of the simulation is mainly due to this entanglement bottleneck that we show in Fig. 36. The same large error at late

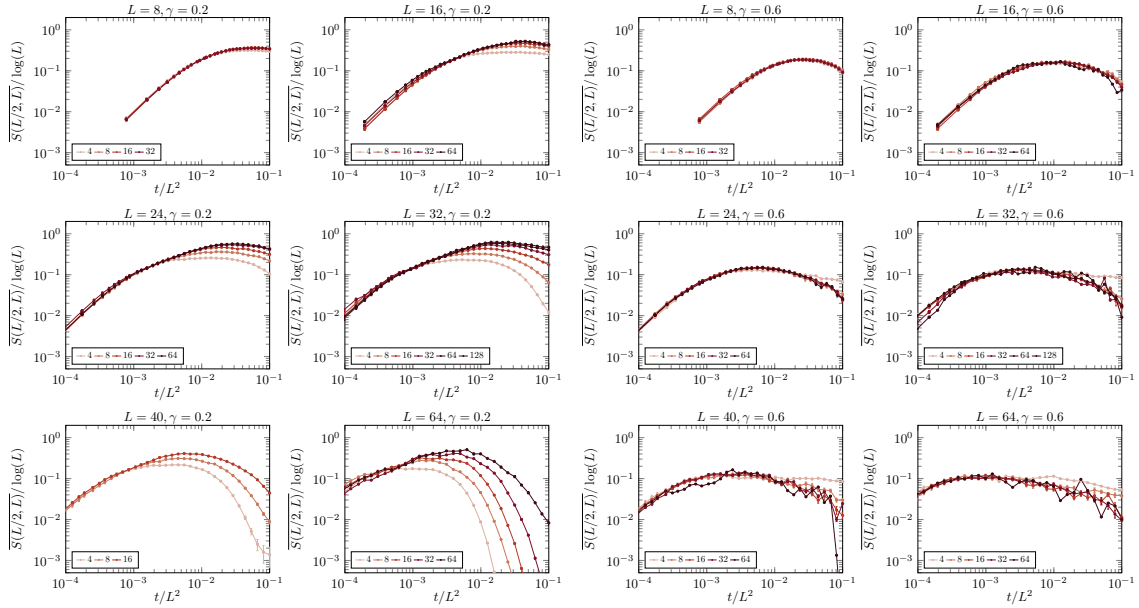

Figure 36: Simulations with a bond dimension that is chosen too small cannot capture the peak of the entanglement at intermediate times which leads to the breaking of the particle number conservation signalled also by a strongly reduced entanglement at late times. This is an issue for weak measurements while in the strongly measured phase, the entanglement bottleneck is well described even using small bond dimensions.

times also affects the order parameter, as shown in Fig. 37. As we are interested in the quasi-stationary state at $t = 0.1L^2$, we need to infer the results at this point in time that we would obtain for an infinite bond dimension. This is done by simulating the system for a set of finite bond dimensions until the observables at $t = 0.1L^2$ start to saturate. Then, we extrapolate from the data to infinite bond dimension. If, for a given system size and measurement rate, no saturation is seen within the range of numerically accessible bond dimension, we cannot give a reasonable estimate for the observables. Examples for the dependence of the order parameter on the bond dimension are shown in Fig. 38. Based on the extrapolations in bond dimension, we can then study the system size dependence of the quasi-stationary observables to describe the absorbing state phase transition as discussed in the Sec. 5.3.4.

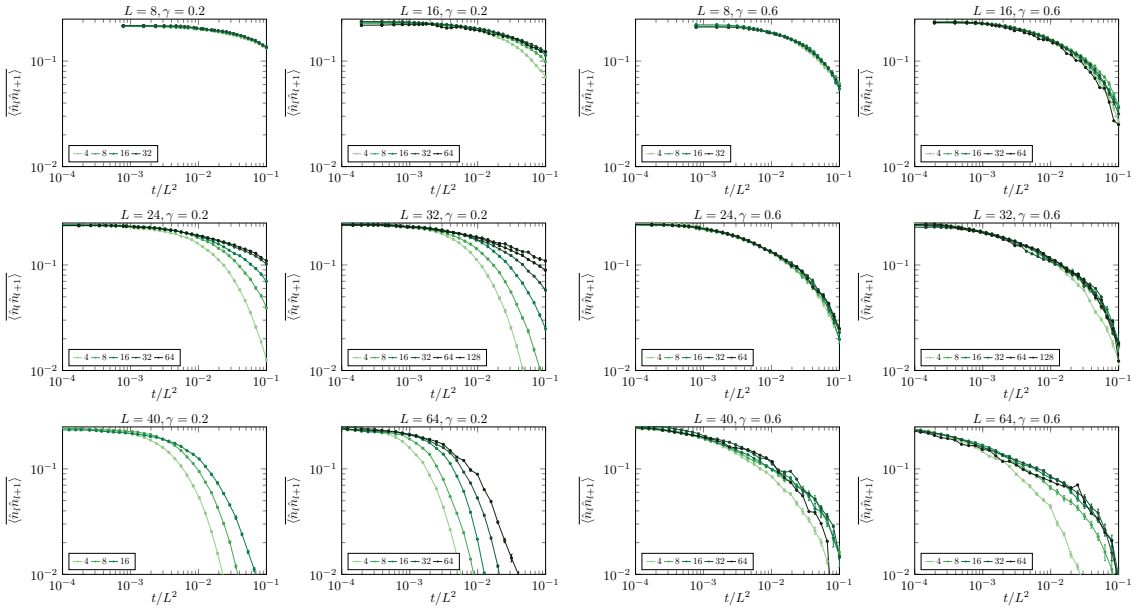

Figure 37: The entanglement bottleneck yields systematic errors for the order parameter at late times, mainly due to the broken conservation of the particle number for finite bond dimension.

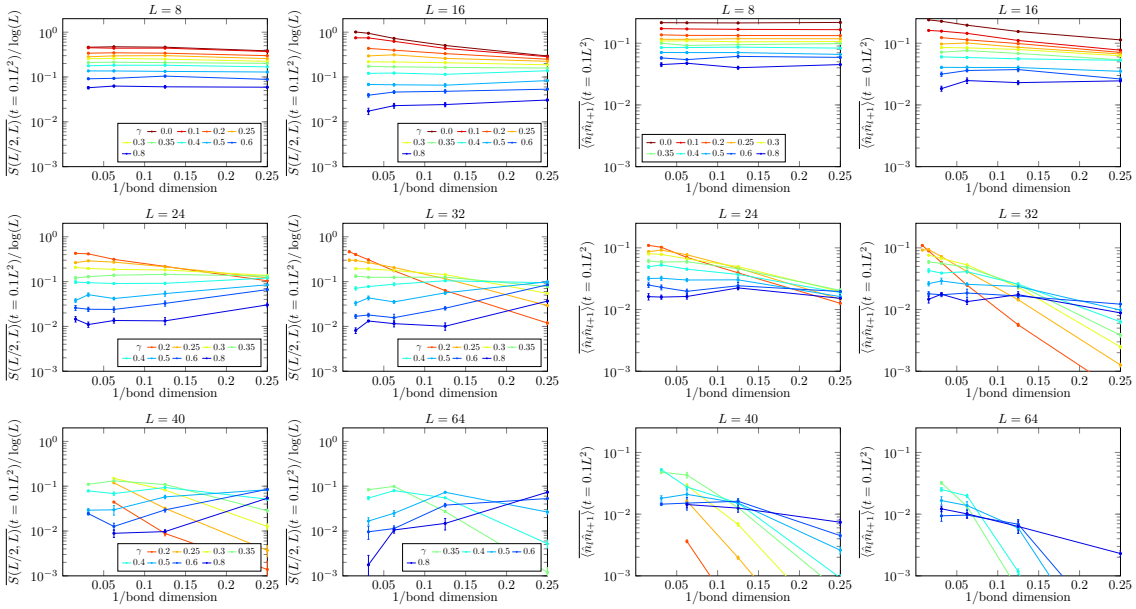

Figure 38: Dependence of the quasi-stationary state observables at $t = 0.1L^2$ on the bond dimension. For strong measurement and small systems we see a quick saturation while large systems and weak measurements do not result in a saturation for accessible bond dimensions such that we cannot give a prediction that does not suffer from a systematic error.

Appendix C Bosonic Keldysh replica field theory

C.1 Feynman Keldysh path-integral construction

We start from the replicated model written in terms of the hermitian operators $\hat{\phi}^{(r)}(x)$ and $\hat{\theta}^{(r)}(x)$ with $[\hat{\phi}^{(r)}(x), \partial_{x'}\hat{\theta}^{(r')}(x')] = i\pi\delta(x-x')\delta_{r,r'}$ which motivates to introduce another set of operators $\hat{\pi}^{(r)}(x) = \frac{1}{\pi}\partial_x\hat{\theta}^{(r)}(x)$ such that $\hat{\phi}^{(r)}$ and $\hat{\pi}^{(r)}$ are conjugate variables. Hence, we may use the Feynman Keldysh path integral construction, using 'position' and 'momentum' eigenstates

$$\hat{\phi}^{(r)}(x)\,|\Phi\rangle = \phi^{(r)}(x)\,|\Phi\rangle\,, \qquad \hat{\pi}^{(r)}(x)\,|\Pi\rangle = \pi^{(r)}(x)\,|\Pi\rangle \tag{C.1}$$

with the overlap

$$\langle\Phi|\Pi\rangle = \langle\Pi|\Phi\rangle^* = e^{i\sum_{r=1}^{R}\int dx\phi^{(r)}(x)\pi^{(r)}(x)}. \tag{C.2}$$

Using a proper integral measure, we find resolutions of unity

$$1 = \int d\Phi\,|\Phi\rangle\,\langle\Phi|\,, \qquad 1 = \int d\Pi\,|\Pi\rangle\,\langle\Pi|\,. \tag{C.3}$$

Using the same integral measure, we may write the trace of the R-replicated non-normalized density operator at some final time t_N as

$$\begin{aligned}
\mathcal{Z}_R(t_N) &= \mathrm{Tr}\,\tilde{\rho}_R(t_N) = \int d\Phi_N\,\langle\Phi_N|\,\tilde{\rho}_R(t_N)\,|\Phi_N\rangle \\
&= \int d\Phi_N d\Pi_N\,\langle\Phi_N|\Pi_N\rangle\,\langle\Pi_N|\,\tilde{\rho}_R(t_N)\,|\Phi_N\rangle \\
&= \int_{\Phi_{+,N}=\Phi_{-,N},\Pi_{+,N}=\Pi_{-,N}} d\Phi_{+,N}d\Pi_{+,N}d\Phi_{-,N}d\Pi_{-,N} \\
&\quad \times e^{i\sum_{r=1}^{R}\int dx\phi^{(r)}_{+,N}(x)\pi^{(r)}_{+,N}(x)}\,\langle\Pi_{+,N}|\,\tilde{\rho}_R(t_N)\,|\Phi_{-,N}\rangle\,.
\end{aligned} \tag{C.4}$$

Now, we use a temporal discretization $t_n = t_0 + n\Delta t$ to rewrite $\tilde{\rho}_R(t_N) = (1 + \Delta t\mathcal{L}_R)\tilde{\rho}_R(t_{N-1})$ repeatedly, adding resolutions of unity on both sides. Finally sending $\Delta t \to 0$ yields the path integral

$$\mathcal{Z}_R = \int \mathcal{D}\Phi_\pm\mathcal{D}\Pi_\pm e^{iS_R[\Phi_\pm,\Pi_\pm]}, \tag{C.5}$$

$$\begin{aligned}
S_R[\Phi_\pm,\Pi_\pm] &= \int_{t,x}\sum_{r=1}^{R}[-\Phi_+^{(r)}\partial_\tau\Pi_+^{(r)} - \Pi_-^{(r)}\partial_t\Phi_-^{(r)}] \\
&\quad - i\int_t \mathcal{L}_R(\Phi_\pm(\tau),\Pi_\pm(\tau)),
\end{aligned} \tag{C.6}$$

$$\mathcal{L}_R(\Phi_\pm,\Pi_\pm) = \frac{\langle\Pi_+|\,\mathcal{L}_R(|\Phi_+\rangle\,\langle\Pi_-|)\,|\Phi_-\rangle}{\langle\Pi_+|\Phi_+\rangle\,\langle\Pi_-|\Phi_-\rangle}. \tag{C.7}$$

Integrals over t always run from t_0 where the initial state is fixed, to t_N, the time at which the trace is taken at. As we are interested in stationary states, we may send $t_0 \to -\infty$ and $t_N \to \infty$. Note that eigenstates of $\hat{\pi}^{(r)}(x)$ are also eigenstates of $\hat{\theta}^{(r)}(x)$ and, up to a rescaling of the integral measure, we may equivalently evaluate the path integral over the corresponding eigenvalues $\theta_{\pm}^{(r)}(x)$. Hence, the normal ordering prescription in the Hamiltonian is to bring the θ fields to the left of the ϕ fields. The other terms in $\mathcal{L}_R$ only depend on $\hat{\phi}^{(r)}(x)$ since they appear due to measurement of the density and the local particle number operator $\hat{n}^{(r)}(x)$ does not depend on the phase operator $\hat{\theta}^{(r)}(x)$. Therefore the normal ordering is trivial for the other terms and we find Eq. (3.50).

C.2 Integrating out θ

The field θ does not appear in the measurement operator and the Hamiltonian of the nearest neighbor hopping model is simply given by

$$\hat{H} = \frac{v}{2\pi} \int_x \left[(\partial_x \hat{\phi})^2 + (\partial_x \hat{\theta})^2 \right]. \tag{C.8}$$

It is therefore quadratic in θ and we may integrate out θ exactly from the general R-replica Keldysh action without even considering the measurement terms. In this case, the action is found using Eq. (3.50) to be

$$S_{0,H} = -\frac{1}{2\pi} \sum_r \sum_{\sigma=\pm} \sigma \int_{t,x} \left[\phi_\sigma^{(r)} \partial_x \partial_t \theta_\sigma^{(r)} + \theta_\sigma^{(r)} \partial_x \partial_t \phi_\sigma^{(r)} - \frac{v}{\hbar} \phi_\sigma^{(r)} \partial_x^2 \phi_\sigma^{(r)} - \frac{v}{\hbar} \theta_\sigma^{(r)} \partial_x^2 \theta_\sigma^{(r)} \right]. \tag{C.9}$$

Note that the effect of $\hbar$ is essentially to act as a unit in which we measure v. We set it $\hbar = 1$ by choosing appropriate units and recover the general form by $v \to v/\hbar$ where necessary. The action decouples the different σ and r components. Integrating out $\theta_\sigma^{(r)}$ is therefore done for all components individually (all fields have the contour index σ and the replica index r, suppressed for short notation)

$$\begin{aligned}
\int \mathcal{D}\theta e^{iS} &= \int \mathcal{D}\theta e^{\frac{i\sigma v}{2\pi} \int_{x,t} \left[\theta \partial_x^2 \theta - \frac{1}{v} \theta \partial_x \partial_t \phi - \frac{1}{v} \phi \partial_x \partial_t \theta + \phi \partial_x^2 \phi \right]} \\
&= \int \mathcal{D}\theta e^{\frac{i\sigma v}{2\pi} \int_{x,t} \left[(\theta - f) \partial_x^2 (\theta - f) + f \partial_x^2 \theta + \theta \partial_x^2 f - f \partial_x^2 f - \frac{1}{v} \theta \partial_x \partial_t \phi - \frac{1}{v} \phi \partial_x \partial_t \theta + \phi \partial_x^2 \phi \right]} \\
&= \int \mathcal{D}\theta e^{\frac{i\sigma v}{2\pi} \int_{x,t} \left[(\theta - f) \partial_x^2 (\theta - f) + \phi \partial_x^2 \phi - f \partial_x^2 f \right]}
\end{aligned} \tag{C.10}$$

We now fix f such that $\partial_x f = \frac{1}{v} \partial_t \phi$ and shift the fields $\theta(x,t) = \tilde{\theta}(x,t) + \frac{1}{v} \int_{x_0}^{x} dy \partial_t \tilde{\phi}(y,t)$ and $\phi(x,t) = \tilde{\phi}(x,t)$. Note that $\frac{\delta \phi(x,t)}{\delta \tilde{\theta}(x',t')} = 0$. Therefore, the Jacobi matrix of the transformation is of block-triangular form. The blocks on the diagonal are unit matrices

if one discretizes space such that the determinant is one and therefore we find $\int \mathcal{D}\phi\mathcal{D}\theta = \int \mathcal{D}\tilde{\phi}\mathcal{D}\tilde{\theta}$ for this transformation and we may equivalently just shift f away from the θ term. This means

$$\int \mathcal{D}\theta e^{iS} = \int \mathcal{D}\theta e^{\frac{i\sigma v}{2\pi}\int_{x,t}\left[\theta\partial_x^2\theta+\phi\partial_x^2\phi-\frac{1}{v^2}\phi\partial_t^2\phi\right]} \tag{C.11}$$

Therefore, the integral over θ can just be absorbed into the normalization of the integral and we obtain the action in terms of ϕ alone.

C.3 Fluctuations in the infinite temperature state

Here we compute the correlation functions of $k = 0$ fields using the Gaussian measurement action 3.64. This is done again in real space to demonstrate the effect of the fields being real. $\phi_{c/q}^{(k=0)}(x,t) = \frac{1}{\sqrt{R}}\sum_r \phi_{c/q}^{(r)}(x,t)$ is real because all fields $\phi_{c/q}^{(r)}(x,t)$ are real. The Keldysh path integral therefore has the structure

$$\mathcal{Z} = \int \mathcal{D}e^{-\frac{1}{2}\int_{p,\omega}\phi^*(-iG^{-1})\phi} = \int \mathcal{D}e^{-\frac{1}{2}\int_{x,t}\phi(-iG^{-1})\phi}, \tag{C.12}$$

$$G^{-1} = \frac{1}{\pi v}\begin{pmatrix} 0 & \omega^2 - v^2p^2 \\ \omega^2 - v^2p^2 & \frac{2i\gamma v}{\pi} \end{pmatrix} \to \frac{1}{\pi v}\begin{pmatrix} 0 & -\partial_t^2 + v^2\partial_x^2 \\ -\partial_t^2 + v^2\partial_x^2 & \frac{2i\gamma v}{\pi} \end{pmatrix} \tag{C.13}$$

Note that we define the Green's function without the factor of 2 in front. Next, we add a real source term J and use that the partition function is normalized in the replica limit $R \to 1$ which allows to solve the Gaussian integral

$$\mathcal{Z}[J] = \int \mathcal{D}e^{-\frac{1}{2}\int_{x,t}\phi(-iG^{-1})\phi+\int_{x,t}J^T\phi} = e^{\frac{1}{2}J^TiGJ}. \tag{C.14}$$

Now, we can take functional derivatives w.r.t. J and generate the correlation functions. After returning to momentum space, we can perform the inversion and we find

$$\begin{aligned}\langle\phi_{c/q}^{(k=0)*}(\omega,p)\phi_{c/q}^{(k=0)}(\omega',p')\rangle &= iG \\ &= i2\pi\delta(p-p')2\pi\delta(\omega-\omega')\frac{-\pi v}{(\omega^2-v^2p^2)^2}\begin{pmatrix} \frac{2i\gamma v}{\pi}p^2 & -(\omega^2-v^2p^2) \\ -(\omega^2-v^2p^2) & 0 \end{pmatrix}.\end{aligned} \tag{C.15}$$

To get the occupation number of the modes, we are interested in the result at equal times, i.e.

$$\begin{aligned}\langle\phi_{c/q}^{(k=0)*}(t,p)\phi_{c/q}^{(k=0)}(t,p')\rangle = 2\pi\delta(p-p')\int\frac{d\omega}{2\pi}\frac{-\pi iv}{(\omega^2-v^2p^2)^2} \\ \times\begin{pmatrix} \frac{2i\gamma v}{\pi}p^2 & -(\omega^2-v^2p^2) \\ -(\omega^2-v^2p^2) & 0 \end{pmatrix}.\end{aligned} \tag{C.16}$$

All components of the integral are not convergent. To regularize, we may use the usual $\omega \to \omega \pm i0^+$ in the retarded/advanced sector introducing an infinitesimal dissipation $0^+ > 0$. This renders the frequency-integral finite and we obtain

$$\langle \phi_{c/q}^{(k=0)*}(t,p)\phi_{c/q}^{(k=0)}(t,p')\rangle = 2\pi\delta(p-p')\int \frac{d\omega}{2\pi}\frac{-\pi i v}{((\omega+i0^+)^2-v^2p^2)((\omega-i0^+)^2-v^2p^2)} \times \begin{pmatrix} \frac{2i\gamma v}{\pi}p^2 & -((\omega+i0^+)^2-v^2p^2) \\ -((\omega-i0^+)^2-v^2p^2) & 0 \end{pmatrix}. \quad \text{(C.17)}$$

Including this regularization, the frequency-integral can be done. On the off-diagonals, the result is zero as the functions only have poles in either the upper or the lower half plane and we may close the contour in the other half plane. Therefore, the only contribution at equal times comes from the *cc* correlation function which reads

$$\langle \phi_{c}^{(k=0)*}(t,p)\phi_{c}^{(k=0)}(t,p')\rangle = 2\pi\delta(p-p')\int \frac{d\omega}{2\pi}\frac{2\gamma v^2p^2}{(\omega^2-v^2p^2-(0^+)^2)^2+4(0^+)^2\omega^2}. \quad \text{(C.18)}$$

The integrand now has 4 poles, $\omega = \pm 2i0^+ \pm pv$ i.e. 2 in both half planes. Therefore, we need to close the contour around two of the poles. We choose the upper half plane to find

$$\int \frac{d\omega}{2\pi}\frac{1}{(\omega^2-v^2p^2-(0^+)^2)^2+4(0^+)^2\omega^2} = \oint_{z=pv+2i(0^+)}\frac{dz}{2\pi i}\frac{i}{(\omega^2-v^2p^2-(0^+)^2)^2+4(0^+)^2\omega^2} + \oint_{z=-pv+2i(0^+)}\frac{dz}{2\pi i}\frac{i}{(\omega^2-v^2p^2-(0^+)^2)^2+4(0^+)^2\omega^2} = \frac{1}{8(0^+)p^2v^2}. \quad \text{(C.19)}$$

This yields Eq. (3.65).

C.4 Integrating out the infinite temperature mode

The bosonized replica Keldysh partition function (3.50) of monitored free fermions takes the form

$$\mathcal{Z}_R = \int \mathcal{D}\phi^{(k=0)}\mathcal{D}\phi^{(k>0)} e^{i\sum_{k>0} S_{0,H,1}^{(k)}[\phi^{(k)}]+iS_2[\phi]} e^{iS_{0,H,1}^{(k=0)}[\phi^{(k=0)}]}, \quad \text{(C.20)}$$

where $S_2[\phi]$ contains the non-linear terms emerging due to the non-linear measurement operator $\hat{O}_2 = m\cos 2\hat{\phi}$. In this section, we treat this term as a perturbation as the cosine is bound and we found that the absolute fields are strongly fluctuating due to the heating to an infinite temperature state (see App. C.3). In this way, we compute the most relevant contribution to the replica coupling action describing non-linear

observables. Therefore, we find

$$\begin{aligned}\mathcal{Z}_R &\approx \int \mathcal{D}\phi^{k>0}\mathcal{D}\phi^{k=0}(1+i\Delta S_2[\phi])e^{iS^{(k=0)}_{0,H,1}[\phi^{(k=0)}]}e^{i\sum_{k>0}S^{k>0}_{0,H,1}[\phi^{(k)}]} \\ &\approx \int \mathcal{D}\phi^{k>0}(1+i\langle S_2[\phi]\rangle_{S^{(k=0)}_{0,H,1}})e^{i\sum_{k>0}S^{(k>0)}_{0,H,1}[\phi^{(k)}]} \\ &\approx \int \mathcal{D}\phi^{k>0}\exp\left\{i\langle S_2[\phi]\rangle_{S^{(k=0)}_{0,H,1}} + i\sum_{k>0}S^{k>0}_{0,H,1}[\phi^{(k)}]\right\}, \end{aligned} \tag{C.21}$$

where $\langle\dots\rangle_{S^{(k=0)}_{0,H,1}}$ denotes the expectation value over the infinite temperature state of the replica-averaged mode $k=0$, as derived above. Repeating this calculation to the next order yields the expansion

$$S^{k>0}[\phi^{k>0}] = \sum_{k>0}S^{k>0}_{0,H,1}[\phi^{(k)}] + \langle S_2[\phi]\rangle_{S^{(k=0)}_{0,H,1}} - \frac{1}{2}\left(\langle (S_2[\phi])^2\rangle_{S^{(k=0)}_{0,H,1}} - \langle S_2[\phi]\rangle^2_{S^{(k=0)}_{0,H,1}}\right) + \dots \tag{C.22}$$

Let us first just discuss the expansion to first order. All terms that appear in S_2 are of the form $\cos 2l(\phi^{(r)}_\sigma - \phi^{(r')}_{\sigma'})$, where $\sigma,\sigma' = \pm$ and r,r' arbitrary replica indices, and they are local in space and time. We use the Fourier transformation in replica space and that fluctuations of the $k=0$ mode diverge to obtain

$$\left\langle \cos\frac{2l}{\sqrt{R}}(\phi^{(k=0)}_\sigma - \phi^{(k=0)}_{\sigma'})\right\rangle_{S^{(k=0)}_{0,H,1}} = e^{-\frac{2l^2}{R}\left\langle\left(\phi^{(k=0)}_\sigma - \phi^{(k=0)}_{\sigma'}\right)^2\right\rangle_{S^{(k=0)}_{0,H,1}}} = \delta_{\sigma\sigma'}, \tag{C.23}$$

$$\left\langle \sin\frac{2l}{\sqrt{R}}(\phi^{(k=0)}_\sigma - \phi^{(k=0)}_{\sigma'})\right\rangle_{S^{(k=0)}_{0,H,1}} = 0. \tag{C.24}$$

Therefore, we can simplify

$$\left\langle \cos 2l(\phi^{(r)}_\sigma - \phi^{(r')}_{\sigma'})\right\rangle_{S^{(k=0)}_{0,H,1}} = \delta_{\sigma\sigma'}\cos 2l(\phi^{(r)}_\sigma - \phi^{(r')}_{\sigma'}), \tag{C.25}$$

which does not depend on the $k=0$ mode any more because this term just gives a constant whenever $r=r'$. This cancels out the Lindblad term entirely and due to the vanishing contour-coupling, the action drastically simplifies to

$$\langle S_2[\phi]\rangle_{S^{(k=0)}_{0,H,1}} = -i\gamma n_0^2\int_{x,t}\sum_{l=1}^{\infty}\sum_{\sigma=\pm}\sum_{r\neq r'}\cos 2l(\phi^{(r)}_\sigma - \phi^{(r')}_\sigma) \tag{C.26}$$

Looking at the second order term, we realize that besides measure 0 contributions from $x = y, t = \tau$ that vanish under integration, we find

$$\left\langle \cos 2l(\phi_\sigma^{(r)}(x,t) - \phi_{\sigma'}^{(r')}(x,t)) \cos 2m(\phi_\rho^{(u)}(y,\tau) - \phi_{\rho'}^{(u')}(y,\tau)) \right\rangle_{S_{0,H,1}^{(k=0)}}$$
$$= \delta_{\sigma\sigma'}\delta_{\rho\rho'} \cos 2l(\phi_\sigma^{(r)}(x,t) - \phi_{\sigma'}^{(r')}(x,t)) \cos 2m(\phi_\rho^{(u)}(y,\tau) - \phi_{\rho'}^{(u')}(y,\tau)). \quad \text{(C.27)}$$

Therefore

$$\langle (S_2[\phi])^2 \rangle_{S_{0,H,1}^{(k=0)}} = \langle S_2[\phi] \rangle_{S_{0,H,1}^{(k=0)}}^2, \quad \text{(C.28)}$$

which means that the second order perturbative correction to the $k > 0$ modes vanishes. The same structure repeats at higher order perturbation theory which means that in the infinite temperature state of the Gaussian theory, we may integrate the $k = 0$ mode out *exactly*. This yields the action (3.67)

C.5 Observables of the Sine-Gordon action

Here we compute the Keldysh Greens function from the action (3.68). To do so, remember that the fields are real in the original replica diagonal formulation. To take this into account when solving the path integral, we rewrite the (normalized) Keldysh partition function including real source terms $J_\sigma^{(r)}$ with the constraint (the $k = 0$ mode has been integrated out such that we do not couple it to a source term) $\sum_r J_\sigma^{(r)} = 0$

$$\begin{aligned}
\mathcal{Z}[J] &= \int \mathcal{D}\phi e^{-\frac{1}{2}\sum_{k>0,\sigma}\int_{\omega,p}\phi_\sigma^{(k)*}(-iG_\sigma^{(-1)})\phi_\sigma^{(k)} + \sum_{k>0,\sigma}\int_{x,t} J_\sigma^{(k)*}\phi_\sigma^{(k)}} \\
&= \prod_{k>0,\sigma} \int \mathcal{D}\phi e^{-\frac{1}{2}\int_{x,t}\phi_\sigma^{(k)*}(-iG_\sigma^{(-1)})\phi_\sigma^{(k)} + \int_{x,t} J_\sigma^{(r)}\phi_\sigma^{(r)}} \\
&= \prod_{k,\sigma} \int \mathcal{D}\phi e^{-\frac{1}{2}\int_{x,t}\phi_\sigma^{(k)*}(-iG_\sigma^{(-1)})\phi_\sigma^{(k)} + \int_{x,t} J_\sigma^{(r)}\phi_\sigma^{(r)}} \\
&= \int \mathcal{D}\phi e^{-\frac{1}{2}\sum_{k,\sigma}\int_{\omega,p}\phi_\sigma^{(k)*}(-iG_\sigma^{(-1)})\phi_\sigma^{(k)} + \sum_{k,\sigma}\int_{x,t} J_\sigma^{(k)*}\phi_\sigma^{(k)}} \\
&= \int \mathcal{D}\phi e^{-\frac{1}{2}\sum_{r,\sigma}\int_{\omega,p}\phi_\sigma^{(r)}(-iG_\sigma^{(-1)})\phi_\sigma^{(r)} + \sum_{r,\sigma}\int_{x,t} J_\sigma^{(r)}\phi_\sigma^{(r)}} \\
&= e^{\frac{1}{2}\sum_{r,\sigma}\int_{x,t}\phi_\sigma^{(r)} iG_\sigma \phi_\sigma^{(r)}}.
\end{aligned} \quad \text{(C.29)}$$

In between, we multiplied by 1 reintroducing the field $\phi^{(k=0)}$ which has no physical meaning here but is just used to compute the integral. The important point is here, that the result is still a real Gaussian integral with the corresponding factor of 2. We can read off the correlation function,

$$\langle \phi_\sigma^{(k>0)*}(p,\omega)\phi_{\sigma'}^{(k'>0)}(p',\omega')\rangle = 2\pi\delta(\omega-\omega')2\pi\delta(p-p')\delta_{\sigma\sigma'}\delta_{kk'}\frac{\pi i}{\sigma K_\sigma}\frac{1}{\frac{\omega^2}{\eta_\sigma} - p^2\eta_\sigma}. \quad \text{(C.30)}$$

We are interested in the correlations at equal times, i.e.

$$\langle \phi_\sigma^{(k>0)*}(t,p)\phi_{\sigma'}^{(k'>0)}(t,p')\rangle = 2\pi\delta(p-p')\delta_{\sigma\sigma'}\delta_{kk'}\int\frac{d\omega}{2\pi}\frac{\sigma\pi i\eta_\sigma/K_\sigma}{\omega^2-p^2\eta_\sigma^2}. \tag{C.31}$$

The poles of the integral are at $\pm\sqrt{p^2\eta_\sigma^2}$. As we see later, η_σ is not renormalized and due to $\operatorname{sgn}\operatorname{Im}\eta_\sigma = -\sigma$, we find that the $-\sigma$ solution is in the upper half plane. Therefore, when closing the contour in the upper half plane, we have to integrate counter-clockwise around the pole at $\omega = -\sqrt{p^2\eta_\sigma^2}$. This yields for the integral

$$\langle \phi_\sigma^{(k>0)*}(t,p)\phi_{\sigma'}^{(k'>0)}(t,p')\rangle = 2\pi\delta(p-p')\delta_{\sigma\sigma'}\delta_{kk'}\frac{\pi}{2K_\sigma|p|} \tag{C.32}$$

Therefore, we can read off the correlation function in momentum space, trivially taking the limit $R\to 1$, and with $c = \operatorname{Re}1/K_+$ we obtain Eq. (3.74) from the main text.

C.6 Details on the renormalization of the Sine-Gordon model

In order to renormalize the action (3.82), we need the correlation function

$$\begin{aligned}
G_{>/<}(x,t) &= \left\langle\left(\phi_{>/<}^{(r)}(x,t)-\phi_{>/<}^{(r')}(x,t)\right)\left(\phi_{>/<}^{(r)}(0,0)-\phi_{>/<}^{(r')}(0,0)\right)\right\rangle_0\\
&= \frac{1}{R}\sum_{k>0,k'>0}\left(e^{-i\frac{2\pi kr}{R}}-e^{-i\frac{2\pi kr'}{R}}\right)\left(e^{i\frac{2\pi k'r}{R}}-e^{i\frac{2\pi k'r'}{R}}\right)\left\langle\phi_{>/<}^{(k)*}(x,t)\phi_{>/<}^{(k')}(0,0)\right\rangle_0\\
&= \frac{1}{R}\sum_{k'>0}(2-e^{2\pi ik'(r-r')/R}-e^{-2\pi ik'(r-r')/R})\left\langle\phi_{>/<}^{(k>0)*}(x,t)\phi_{>/<}^{(k>0)}(0,0)\right\rangle_0\\
&= \frac{1}{R}\sum_{k'=0}^{R-1}(2-e^{2\pi ik'(r-r')/R}-e^{-2\pi ik'(r-r')/R})\left\langle\phi_{>/<}^{(k>0)*}(x,t)\phi_{>/<}^{(k>0)}(0,0)\right\rangle_0\\
&= 2(1-\delta_{r,r'})\left\langle\phi_{>/<}^{(k>0)*}(x,t)\phi_{>/<}^{(k>0)}(0,0)\right\rangle_0\\
&= 2(1-\delta_{r,r'})\int_{>/<}e^{i(px+\omega t)}\int_{>/<}e^{i(p'0+\omega'0)}\left\langle\phi_{>/<}^{(k>0)*}(p,\omega)\phi_{>/<}^{(k>0)}(p',\omega')\right\rangle_0\\
&= 2(1-\delta_{r,r'})\int_{>/<}\frac{\pi e^{i(px+\omega t)}}{K_1p^2+K_2\omega^2}.
\end{aligned}\tag{C.33}$$

We used here that the Gaussian theory decouples k modes and that is does not explicitly depend on k. Therefore, it does not matter, for which particular choice of $k>0$ the expectation value is computed, and we can add the $k=0$ term (which vanishes) to recover the fact that the expectation value needs to be real. By that mechanism, the explicit dependence on R drops out and we obtain a finite contribution to the RG flow equations in that limit. Knowing that the correlation function obviously vanishes for $r=r'$, we leave out the Kronecker delta and evaluate the integral separately, writing

only the leading order in s

$$\begin{aligned} G_>(x,t) &= 2\int_{b\Lambda<p<\Lambda}\frac{dp}{2\pi}\int_{-\infty}^{\infty}\frac{d\omega}{2\pi}\frac{\pi e^{i(px+\omega t)}}{K_1p^2+K_2\omega^2} \\ &= \frac{s}{\pi}\cos\Lambda x\int_{-\infty}^{\infty}d\omega\frac{e^{i\omega t}}{K_2\omega^2+K_1\Lambda^2} \\ &= \frac{s\cos\Lambda x e^{-\sqrt{\frac{K_1}{K_2}}\Lambda|t|}}{\sqrt{K_1K_2}}, \end{aligned} \tag{C.34}$$

and

$$\begin{aligned} G_<(x,t) &= 2\int_{-\Lambda}^{\Lambda}\frac{dp}{2\pi}\int_{-\infty}^{\infty}\frac{d\omega}{2\pi}e^{i(px+\omega t)}\frac{\pi e^{i(px+\omega t)}}{K_1p^2+K_2\omega^2} \\ &= \frac{1}{\sqrt{K_1K_2}}\int_0^{\Lambda}\frac{dp}{p}\cos pxe^{-\sqrt{\frac{K_1}{K_2}}p|t|} \\ &= \frac{\sqrt{K_1K_2}|t|}{K_1t^2+K_2x^2}\left(1-\cos\Lambda xe^{-\sqrt{\frac{K_1}{K_2}}\Lambda|t|}\right)+\frac{K_2x}{K_2x^2+K_1t^2}\sin\Lambda xe^{-\sqrt{\frac{K_1}{K_2}}\Lambda|t|}. \end{aligned} \tag{C.35}$$

This yields

$$\begin{aligned} \langle\Delta S\rangle_{0,>} &= i\sum_l\lambda_l\int_{\mathbf{x}}\sum_{r\neq r'}\left\langle\cos 2l(\phi_<^{(r,r')}+\phi_>^{(r,r')})\right\rangle_{0,>} \\ &= i\sum_l\lambda_l\int_{\mathbf{x}}\sum_{r,r'}\cos 2l\phi_<^{(r,r')}e^{-2l^2\left\langle\left(\phi_>^{(r,r')}\right)^2\right\rangle_{0,>}} \\ &= i\sum_l\lambda_l\int_{\mathbf{x}}\sum_{r,r'}\cos 2l\phi_<^{(r,r')}e^{-2l^2G_>(0,0)} \\ &= i\sum_l\lambda_l\int_{\mathbf{x}}\sum_{r,r'}\cos 2l\phi_<^{(r,r')}e^{-\frac{2l^2s}{\sqrt{K_1K_2}}}. \end{aligned} \tag{C.36}$$

For the second order perturbative correction, consider

$$\begin{aligned} -\frac{1}{2}\left(\langle(\Delta S)^2\rangle_{0,>}-\left(\langle\Delta S\rangle_{0,>}\right)^2\right) \\ = \frac{\lambda^2}{2}\sum_{r\neq r'}\sum_{u\neq u'}\int_{\mathbf{x},\mathbf{y}}\left\langle\cos 2\phi^{(r,r')}(\mathbf{x})\cos 2\phi^{(u,u')}(\mathbf{y})\right\rangle_{0,>} \\ -\frac{\lambda^2}{2}\sum_{r\neq r'}\sum_{u\neq u'}\int_{\mathbf{x},\mathbf{y}}\left\langle\cos 2\phi^{(r,r')}(\mathbf{x})\right\rangle_{0,>}\left\langle\cos 2\phi^{(u,u')}(\mathbf{y})\right\rangle_{0,>}. \end{aligned} \tag{C.37}$$

The locality of the model implies that no long-range coupled terms are generated which allows to expand in $\mathbf{x}-\mathbf{y}$ later on. In leading order, we simply generate an additional term ΔS^2 which is less relevant than ΔS itself and therefore dropped. On the other

hand, the spatial symmetry prohibits odd terms in $\mathbf{x}-\mathbf{y}$, and products of oscillating functions and derivative terms are less relevant than the derivative terms themselves. The only combinations where a non-oscillating term is generated at second order are $r=u, r'=u'$ and $r=u', r'=u$ which allows to eliminate one of the sums which just generates a factor of 2.

$$-\frac{1}{2}\left(\langle(\Delta S)^2\rangle_{0,>}-(\langle\Delta S\rangle_{0,>})^2\right)\simeq\lambda^2\sum_{r\neq r'}\int_{\mathbf{x},\mathbf{y}}\left\langle\cos 2\phi^{(r,r')}(\mathbf{x})\cos 2\phi^{(r,r')}(\mathbf{y})\right\rangle_{0,>} - \lambda^2\sum_{r\neq r'}\int_{\mathbf{x},\mathbf{y}}\left\langle\cos 2\phi^{(r,r')}(\mathbf{x})\right\rangle_{0,>}\left\langle\cos 2\phi^{(r,r')}(\mathbf{y})\right\rangle_{0,>}. \quad \text{(C.38)}$$

When we expand the cos terms, we need to compute all combinations

$$\left\langle\cos 2\phi_>^{(r,r')}(\mathbf{x})\cos 2\phi_>^{(r,r')}(\mathbf{y})\right\rangle_{0,>}=\frac{1}{2}\sum_{\sigma=\pm}\left(e^{-2\left\langle\left(\phi_>^{(r,r')}(\mathbf{x})-\sigma\phi_>^{(r,r')}(\mathbf{y})\right)^2\right\rangle_{0,>}}\right) \quad \text{(C.39)}$$

$$\left\langle\sin 2\phi_>^{(r,r')}(\mathbf{x})\sin 2\phi_>^{(r,r')}(\mathbf{y})\right\rangle_{0,>}=\frac{1}{2}\sum_{\sigma=\pm}\sigma\left(e^{-2\left\langle\left(\phi_>^{(r,r')}(\mathbf{x})-\sigma\phi_>^{(r,r')}(\mathbf{y})\right)^2\right\rangle_{0,>}}\right) \quad \text{(C.40)}$$

$$\left\langle\sin 2\phi_>^{(r,r')}(\mathbf{x})\cos 2\phi_>^{(r,r')}(\mathbf{y})\right\rangle_{0,>}=\left\langle\cos 2\phi_>^{(r,r')}(\mathbf{x})\sin 2\phi_>^{(r,r')}(\mathbf{y})\right\rangle_{0,>}=0. \quad \text{(C.41)}$$

Expanding and using translation-invariance yields

$$\left\langle\cos 2\phi_>^{(r,r')}(\mathbf{x})\cos 2\phi_>^{(r,r')}(\mathbf{y})\right\rangle_{0,>}=\cosh 4\left\langle\phi_>^{(r,r')}(\mathbf{x})\phi_>^{(r,r')}(\mathbf{y})\right\rangle_{0,>}e^{-4\left\langle\left(\phi_>^{(r,r')}\right)^2\right\rangle_{0,>}} \quad \text{(C.42)}$$

$$\left\langle\sin 2\phi_>^{(r,r')}(\mathbf{x})\sin 2\phi_>^{(r,r')}(\mathbf{y})\right\rangle_{0,>}=\sinh 4\left\langle\phi_>^{(r,r')}(\mathbf{x})\phi_>^{(r,r')}(\mathbf{y})\right\rangle_{0,>}e^{-4\left\langle\left(\phi_>^{(r,r')}\right)^2\right\rangle_{0,>}}. \quad \text{(C.43)}$$

For the second order perturbative result this yields

$$-\frac{1}{2}\left(\langle(\Delta S)^2\rangle_{0,>}-(\langle\Delta S\rangle_{0,>})^2\right)= \frac{\lambda^2}{2}\sum_{r\neq r'}\sum_{\sigma=\pm}\int_{\mathbf{x},\mathbf{y}}e^{-4G_>(\mathbf{0})}\left(e^{4\sigma G_>(\mathbf{x}-\mathbf{y})}-1\right) \cos 2\left(\phi_<^{(r,r')}(\mathbf{x})-\sigma\phi_<^{(r,r')}(\mathbf{y})\right) \quad \text{(C.44)}$$

Note that the fast mode correlation functions are $\mathcal{O}(s)$, both the local and the non-local one. Therefore, we can already at this point expand in s which yields

$$-\frac{1}{2}\left(\langle(\Delta S)^2\rangle_{0,>}-(\langle\Delta S\rangle_{0,>})^2\right)= \\ 2\lambda^2\sum_{r\neq r'}\sum_{\sigma=\pm}\sigma\int_{\mathbf{x},\mathbf{y}}G_>(\mathbf{x}-\mathbf{y})\cos 2\left(\phi_<^{(r,r')}(\mathbf{x})-\sigma\phi_<^{(r,r')}(\mathbf{y})\right) \quad \text{(C.45)}$$

By locality we know that the fast mode correlation function is peaked around 0 and vanishes at large distances. Therefore it makes sense to expand $\sigma\phi_<^{(r,r')}(\mathbf{y})\simeq\sigma\phi_<^{(r,r')}(\mathbf{x})+(\mathbf{y}-\mathbf{x})\nabla\phi_<^{(r,r')}(\mathbf{x})$. The term with $\sigma=-$ is dominated by the zeroth order contribution which generates a term $\sim\cos 4\phi_<^{(r,r')}$ which is less relevant than $\cos 2\phi_<^{(r,r')}$ and therefore ignored throughout the calculation. On the other hand, for $\sigma=+$, the constant contribution vanishes and we can expand the cosine in derivatives. This is slightly more complicated than one might assume at first glance because of the strong fluctuations of the field ϕ which makes the direct expansion in derivatives ill-defined. This can be cured using

$$\begin{aligned}
&\cos 2\left(\phi_<^{(r,r')}(\mathbf{y})-\phi_<^{(r,r')}(\mathbf{x})\right)\\
=&\frac{\cos 2\left(\phi_<^{(r,r')}(\mathbf{y})-\phi_<^{(r,r')}(\mathbf{x})\right)}{\left\langle\cos 2\left(\phi_<^{(r,r')}(\mathbf{y})-\phi_<^{(r,r')}(\mathbf{x})\right)\right\rangle_0}\left\langle\cos 2\left(\phi_<^{(r,r')}(\mathbf{y})-\phi_<^{(r,r')}(\mathbf{x})\right)\right\rangle_0\\
=&\frac{\cos 2\left(\phi_<^{(r,r')}(\mathbf{y})-\phi_<^{(r,r')}(\mathbf{x})\right)}{\left\langle\cos 2\left(\phi_<^{(r,r')}(\mathbf{y})-\phi_<^{(r,r')}(\mathbf{x})\right)\right\rangle_0}e^{-2\left\langle\left(\phi_<^{(r,r')}(\mathbf{y})-\phi_<^{(r,r')}(\mathbf{x})\right)^2\right\rangle_0}\\
=&\left(1-2\left((\mathbf{y}-\mathbf{x})\nabla\phi_<^{(r,r')}(\mathbf{x})\right)^2+\dots\right)e^{-4\left\langle\phi_<^{(r,r')}(\mathbf{x})\left(\phi_<^{(r,r')}(\mathbf{x})-\phi_<^{(r,r')}(\mathbf{y})\right)\right\rangle_0}\\
=&\left(1-2\left((\mathbf{y}-\mathbf{x})\nabla\phi_<^{(r,r')}(\mathbf{x})\right)^2+\dots\right)e^{-4(G_<(\mathbf{0})-G_<(\mathbf{y}-\mathbf{x}))}
\end{aligned} \quad \text{(C.46)}$$

This means that after we absorbed the divergent fluctuations using the Gaussian expectation value, we can safely expand (Giamarchi) in derivatives, which cures the integral appearing later. The constant term can be absorbed into the definition of the path integral while the derivative term generates an additional contribution to the Gaussian part of the action and renormalizes K_1, K_2. We find

$$-\frac{1}{2}\left(\langle(\Delta S)^2\rangle_{0,>}-(\langle\Delta S\rangle_{0,>})^2\right)=-4\lambda^2\sum_{r\neq r'}\int_{\mathbf{x},\mathbf{x}'}G_>(\mathbf{x}')e^{-4F_<(\mathbf{x}')}\left(\mathbf{x}'\nabla\phi_<^{(r,r')}(\mathbf{x})\right)^2. \quad \text{(C.47)}$$

We used the translation-invariance to decouple the two integrals and used the functions

$$G_>(x,t)=\frac{s\cos\Lambda x e^{-\sqrt{\frac{K_1}{K_2}}\Lambda|t|}}{\sqrt{K_1K_2}}, \quad \text{(C.48)}$$

and

$$\begin{aligned} F_<(x,t) = G_>(0,0) - G_>(x,t) &= \int_< \frac{2\pi(1-e^{i(px+\omega t)})}{K_1 p^2 + K_2 \omega^2} \\ &= \frac{1}{\pi}\int_0^\Lambda dp \int_{-\infty}^{\infty} d\omega \frac{1-\cos pxe^{i\omega t}}{K_1 p^2 + K_2\omega^2} \\ &= \frac{1}{\sqrt{K_1 K_2}} \int_0^\Lambda \frac{dp}{p}\left(1-\cos pxe^{-\sqrt{\frac{K_1}{K_2}}p|t|}\right). \end{aligned} \tag{C.49}$$

Since both $G_>$ and $F_<$ are symmetric under inversion $t \to -t$ or $x \to -x$, we only need to compute the integral for the ∂_x^2 and the ∂_t^2 term separately. Let us start with the spatial term,

$$\begin{aligned} &\int_{-\infty}^{\infty} dx \int_{-\infty}^{\infty} dt x^2 G_>(x,t) e^{-4F_<(x,t)} \\ =& s\int_{-\infty}^{\infty} dx \int_{-\infty}^{\infty} dt x^2 \frac{s\cos\Lambda x e^{-\sqrt{\frac{K_1}{K_2}}\Lambda|t|}}{\sqrt{K_1K_2}} e^{-\frac{4}{\sqrt{K_1K_2}}\int_0^\Lambda \frac{dp}{p}\left(1-\cos pxe^{-\sqrt{\frac{K_1}{K_2}}p|t|}\right)} \\ =& \frac{s}{\sqrt{K_1K_2}\Lambda^4}\int_{-\infty}^{\infty} dx \int_{-\infty}^{\infty} dt x^2 \cos x e^{-\sqrt{\frac{K_1}{K_2}}|t|} e^{-\frac{4}{\sqrt{K_1K_2}}\int_0^1 \frac{dp}{p}(1-\cos px)e^{-\sqrt{\frac{K_1}{K_2}}p|t|}}. \end{aligned} \tag{C.50}$$

In general, this is a function of K_1 and K_2. As we are mainly interested in the vicinity of the BKT point at $K_1 = K_2 = 1$, we plug this into the integrals to get the leading contribution. The remaining integral can then be numerically evaluated, and we can do the same for the temporal integral, which yields

$$\int_{-\infty}^{\infty} dx \int_{-\infty}^{\infty} dt x^2 G_>(x,t) e^{-4F_<(x,t)} \simeq \frac{Is}{\Lambda^4\sqrt{K_1K_2}}, \tag{C.51}$$

where

$$I = 4\int_0^{\infty} dx \int_0^{\infty} dt x^2 \cos x e^{-t} e^{-4\int_0^1 \frac{dp}{p}(1-\cos px)e^{-pt}} \approx 0.07805. \tag{C.52}$$

replacing $x^2 \to t^2$ yields the same numerical value up to the fifth digit. We conclude Eq. (3.91) from the main text.

C.7 renormalization of the long-range term

To compute the expectation value of the non-linearity, we need to evaluate

$$\begin{aligned}
&\left\langle \left(\frac{1}{\sqrt{R}} \sum_{k>0} \theta^{(k)}_{x,y,>} \left(e^{i2\pi kr/R} \pm e^{i2\pi kr'/R} \right) \right)^2 \right\rangle_{0,>} \\
=&\frac{1}{R} \sum_{k,k'>0} \left\langle \theta^{(k)*}_{x,y,>} \theta^{(k')}_{x,y,>} \right\rangle_{0,>} \left(e^{i\frac{2\pi r(k-k')}{R}} + e^{i\frac{2\pi r'(k-k')}{R}} \pm e^{i\frac{2\pi(rk-r'k')}{R}} \pm e^{i\frac{2\pi(r'k-rk')}{R}} \right) \\
=&\frac{1}{R} \sum_{k>0} \left\langle \theta^{(k)*}_{x,y,>} \theta^{(k)}_{x,y,>} \right\rangle_{0,>} (2 \pm e^{i\frac{2\pi k(r-r')}{R}} \pm e^{i\frac{2\pi k(r-r')}{R}}) \\
=&\frac{1}{R} \sum_{k'=0}^{R-1} \left\langle \theta^{(k>0)*}_{x,y,>} \theta^{(k>0)}_{x,y,>} \right\rangle_{0,>} (2 \pm e^{i\frac{2\pi k'(r-r')}{R}} \pm e^{i\frac{2\pi k'(r-r')}{R}}) \\
=&2(1 \pm \delta_{r,r'}) \left\langle \theta^{(k>0)*}_{x,y,>} \theta^{(k>0)}_{x,y,>} \right\rangle_{0,>} .
\end{aligned} \tag{C.53}$$

We used here that the Gaussian theory decouples into independent and equal replica momentum sectors for $k > 0$. This yields

$$\begin{aligned}
&\left\langle \cos\left(\frac{1}{R} \sum_s (\theta^{(r)}_{x,y,>} - \theta^{(s)}_{x,y,>}) \right) \cos\left(\frac{1}{R} \sum_{s'} (\theta^{(r')}_{x,y,>} - \theta^{(s')}_{x,y,>}) \right) \right\rangle_{0,>} \\
&\qquad = e^{-\left\langle \theta^{(k>0)*}_{x,y,>} \theta^{(k>0)}_{x,y,>} \right\rangle_{0,>}} \cosh \delta_{r,r'} \left\langle \theta^{(k>0)*}_{x,y,>} \theta^{(k>0)}_{x,y,>} \right\rangle_{0,>} .
\end{aligned} \tag{C.54}$$

Which is finite for $s \to 0$ independently of r, r'. In contrast, we obtain

$$\begin{aligned}
&\left\langle \sin\left(\frac{1}{R} \sum_s (\theta^{(r)}_{x,y,>} - \theta^{(s)}_{x,y,>}) \right) \sin\left(\frac{1}{R} \sum_{s'} (\theta^{(r')}_{x,y,>} - \theta^{(s')}_{x,y,>}) \right) \right\rangle_{0,>} \\
&\qquad = -e^{-\left\langle \theta^{(k>0)*}_{x,y,>} \theta^{(k>0)}_{x,y,>} \right\rangle_{0,>}} \sinh \delta_{r,r'} \left\langle \theta^{(k>0)*}_{x,y,>} \theta^{(k>0)}_{x,y,>} \right\rangle_{0,>} .
\end{aligned} \tag{C.55}$$

Which vanishes in the limit $s \to 0$ and therefore just yields a sub-leading contribution. The combination of sin and cos vanishes exactly for any s such that we obtain (neglecting sub-leading terms in s)

$$\begin{aligned}
&\left\langle \left(\sum_r \cos\left(\frac{1}{R} \sum_s (\theta^{(r)}_{x,y} - \theta^{(s)}_{x,y}) \right) \right)^2 \right\rangle_{0,>} \\
&\qquad = \left(\sum_r \cos\left(\frac{1}{R} \sum_s (\theta^{(r)}_{x,y,<} - \theta^{(s)}_{x,y,<}) \right) \right)^2 e^{-\left\langle \theta^{(k>0)*}_{x,y,>} \theta^{(k>0)}_{x,y,>} \right\rangle_{0,>}} .
\end{aligned} \tag{C.56}$$

Importantly, the found rescaling factor does not depend on the replica number and it does not vanish in the limit $R \to 1$. Using translation-invariance and inversion-

symmetry, we find

$$\langle\theta^{(k>0)*}_{x,y,>}\theta^{(k>0)}_{x,y,>}\rangle_{0,>} = 2\langle\hat{\theta}^{(k>0)*}_{x,>}\hat{\theta}^{(k>0)}_{x,>}\rangle_{0,>} - 2\langle\hat{\theta}^{(k>0)*}_{x,>}\hat{\theta}^{(k>0)}_{y,>}\rangle_{0,>}. \tag{C.57}$$

The correlation function can be computed from the Gaussian theory, implementing a cutoff in real space and evaluating the integral over time exactly. This yields

$$\begin{aligned}\langle\hat{\theta}^{(k>0)*}_{x,>}\hat{\theta}^{(k>0)}_{y,>}\rangle_{0,>} &= \int_{>}\frac{\pi e^{ip(y-x)}}{\frac{\omega^2}{K_1}+\frac{p^2}{K_2}} \\ &= s\Lambda K_1\cos(\Lambda(y-x))\int_{-\infty}^{\infty}\frac{d\omega}{2\pi}\frac{1}{\omega^2+(K_1/K_2)\Lambda^2} \\ &= \frac{1}{2}s\sqrt{K_1K_2}\cos(\Lambda(y-x)).\end{aligned} \tag{C.58}$$

Hence,

$$e^{-\langle\theta^{(k>0)*}_{x,y,>}\theta^{(k>0)}_{x,y,>}\rangle_{0,>}} = e^{-s\sqrt{K_1K_2}(1-\cos\Lambda(y-x))}. \tag{C.59}$$

Just as in the construction of the model, we may now separate the short- and long-distance behavior of this rescaling factor: Considering large distances $|y-x|\to\infty$, and the limit $s\to 0$, the cos just describes fast oscillations on a small scale, which does not contribute to the long-range coarse-grained field theory description at such scales. On the other hand, for short distances, the oscillations indeed become relevant since the shortest distances in the problem are indeed given by the cutoff scale $1/\Lambda$. Therefore, we separate the expression according to

$$e^{-\langle\theta^{(k>0)*}_{x,y,>}\theta^{(k>0)}_{x,y,>}\rangle_{0,>}} \simeq e^{-s\sqrt{K_1K_2}} + s\sqrt{K_1K_2}\cos\Lambda(y-x). \tag{C.60}$$

Consider first only the first term. It is constant and therefore provides a multiplicative renormalization of the coupling Δ. The RG step is to re-scale space $x\to xe^s$ and time $t\to te^s$ while the fields are not re-scaled to keep the Gaussian part of the action scale-invariant up to corrections due to non-linearities. This results in a total rescaling

$$\Delta\to\Delta e^{(3-2p-\sqrt{K_1K_2})}, \tag{C.61}$$

and therefore the flow-equation

$$\partial_s\Delta = (3-2p-\sqrt{K_1K_2})\Delta \tag{C.62}$$

The short-range contribution on the other hand generates an additional term which comes from the increased cutoff. It yields an additive renormalization of the Gaussian part of the spatial derivative term. To obtain that, we perform a derivative-expansion

in the cos using the suppression of long-distance terms due to the prefactor, i.e.

$$\begin{aligned}
&\sum_r \cos\left(\frac{1}{R}\sum_s((\theta_y^{(r)}-\theta_x^{(r)})-((\theta_y^{(s)}-\theta_x^{(s)}))\right)\\
=&\sum_r \cos\left(\frac{1}{\sqrt{R}}\sum_{k>0}(\theta_y^{(k)}-\theta_x^{(k)})e^{i\frac{2\pi kr}{R}}\right)\\
=&\sum_r \cos\left(\frac{1}{\sqrt{R}}\sum_{k>0}((y-x)\partial_x\theta_x^{(k)}+\mathcal{O}((y-x)^2))e^{i\frac{2\pi kr}{R}}\right)\\
=&\sum_r\left(1-\frac{(y-x)^2}{2R}\sum_{k,k'>0}\left(\partial_x\theta_x^{(k)*}\right)\left(\partial_x\theta_x^{(k')}\right)e^{-i\frac{2\pi(k-k')r}{R}}\right)+\mathcal{O}((y-x)^2))\\
=&R-\frac{(y-x)^2}{2}\sum_{k>0}\left(\partial_x\theta_x^{(k)*}\right)\left(\partial_x\theta_x^{(k)}\right)+\mathcal{O}((y-x)^2))
\end{aligned}\tag{C.63}$$

This can be now plugged into the action and we can perform the rescaling of space and time which yields, up to an irrelevant constant the following additional term in the action

$$2is\Delta\sqrt{K_1K_2}\Lambda^{2(p-1)}\int_{x,t}\underbrace{\int_{a\Lambda}^{\infty}dy y^{2(1-p)}\cos y}_{J_p}\left(\partial_x\theta_x^{(k)*}\right)\left(\partial_x\theta_x^{(k)}\right).\tag{C.64}$$

We dropped the higher order terms in the derivative expansion here. Note that the integral J_p only exists for $p>1$. Since the RG shall describe the vicinity of the phase transition which was identified to be at $p=3/2$, this is not a problem here. Using $\Lambda=\pi/a$ as UV cutoff yields $J_p<0$. Using a Fourier-transformation shows that this yields a additive renormalization of K_2,

$$\frac{1}{K_2}\to\frac{1}{K_2}+4\pi is\Delta\sqrt{K_1K_2}\Lambda^{2(p-1)}J_p\tag{C.65}$$

Which yields the flow equation

$$\partial_s\frac{1}{K_2}=4\pi i\Delta\sqrt{K_1K_2}\Lambda^{2(p-1)}J_p\tag{C.66}$$

To cast this into a form compatible with the BKT transition discussed in Sec. 3.2.2, we may rewrite both flow equations in terms of the combination $K=\sqrt{K_1K_2}$, which yields

$$\partial_s K=-2\pi i\Delta\Lambda^{2(p-1)}J_pK^2\Delta\tag{C.67}$$

Re-scaling the coupling Δ finally results in the equations (4.32) and (4.33) from the main text.

Appendix D Preselection

D.1 Derivation of mean-field time-evolution

Here we derive the time evolution of the mean field local excitation density $n = \langle \hat{n}_l \rangle$ in in the quantum feedback protocol after the particle-hole transformation. To compute this quantity, consider the time evolution of some operator $\hat{A}$ with expectation value $A = \langle \hat{A} \rangle$. We use just the cyclic property of the trace to obtain

$$\begin{aligned}\partial_t A &= \partial_t \langle \hat{A} \rangle = \partial_t \operatorname{Tr} \hat{A}\hat{\rho} \\ &= -i\langle [\hat{A}, \hat{H}] \rangle - \frac{\gamma}{2} \sum_l \langle \{\hat{n}_l, \hat{A}\} \rangle + \frac{\gamma}{2} \sum_l \langle \hat{n}_l \hat{A} \hat{n}_l \rangle + \frac{\gamma}{4} \sum_{l,\sigma=\pm} \langle \hat{L}_{l\sigma}^\dagger \hat{A} \hat{L}_{l,\sigma} \rangle. \end{aligned} \tag{D.1}$$

This is still exact. In the next step, we perform a mean-field calculation under the assumption that we are close to the dark state, with a few excitations that can move. If the excitation density is low, we may decouple expectation values using the Wick theorem.

First approximation: purely local If one is very close to the dark state, the excitation density is so low that non-local expectation values $\langle \hat{c}_l^\dagger \hat{c}_m \rangle$ and $\langle \hat{c}_l \hat{c}_m \rangle$ for $l \neq m$ can be neglected. Under these assumptions, the only relevant term in the mean-field calculation is $\langle \hat{n}_l \rangle = n$ since $\langle \hat{c}_l^2 \rangle = \langle \hat{0} \rangle$ trivially for fermions. We also assumed that the question whether l is even or odd does not matter for the mean-field calculation which is justified a posteriori. For the time-evolution, we need the expectation value of

$$\begin{aligned}[\hat{n}_l, \hat{H}] &= \sum_m (-1)^m \left([\hat{n}_l, \hat{n}_m \hat{c}_{m-2} \hat{c}_{m-1}] + [\hat{n}_l, \hat{n}_m \hat{c}_{m+2} \hat{c}_{m+1}] + \text{h.c} \right) \\ &= \sum_m (-1)^m \left(\hat{n}_m [\hat{n}_l, \hat{c}_{m-2} \hat{c}_{m-1}] + \hat{n}_m [\hat{n}_l, \hat{c}_{m+2} \hat{c}_{m+1}] - \text{h.c.} \right) \\ &= (-1)^l \left((\hat{n}_{l-1} + \hat{n}_{l+2}) \hat{c}_{l+1} \hat{c}_l + (\hat{n}_{l+1} + \hat{n}_{l-2}) \hat{c}_{l-1} \hat{c}_l \right) - \text{h.c.}, \end{aligned} \tag{D.2}$$

using standard commutator algebra. To evaluate the expectation value, we use Wicks theorem for fermionic operators as we are close to a Gaussian state (the trivial vacuum state). The terms that we have here have the form $\langle \hat{n}_A \hat{c}_B \hat{c}_C \rangle \approx \langle \hat{n}_A \rangle \langle \hat{c}_B \hat{c}_C \rangle - \langle \hat{c}_A^\dagger \hat{c}_B \rangle \langle \hat{c}_A \hat{c}_C \rangle + \langle \hat{c}_A^\dagger \hat{c}_C \rangle \langle \hat{c}_A \hat{c}_B \rangle$. This means that under the mean-field decoupling described above, all terms cancel since they all are $\sim \langle \hat{c}_l \hat{c}_{l+d} \rangle$ with $d = 1, 2$ i.e. not completely local. This means that the Hamiltonian does not appear at all to lowest order in the expansion:

$$\langle [\hat{n}_l, \hat{H}] \rangle \approx 0 + \text{non-local correlations} \approx 0. \tag{D.3}$$

The second term in the expansion,

$$\begin{aligned}
&-\sum_m \langle \{\hat{n}_l, \hat{n}_m\} - \hat{n}_m \hat{n}_l \hat{n}_m \rangle \\
=&-\sum_m \langle \hat{n}_l \hat{n}_m \rangle \approx -\langle \hat{n}_l \rangle - \sum_{m \neq l} \langle \hat{n}_l \rangle \langle \hat{n}_m \rangle + \text{ non-local correlations} \\
\approx&- n - (L-1)n^2, \qquad \text{(D.4)}
\end{aligned}$$

in the thermodynamic Limit. For the correction term we find

$$\begin{aligned}
&\frac{1}{2}\sum_{m,\pm} \langle \hat{L}^\dagger_{m,\pm} \hat{n}_l \hat{L}_{m,\pm} \rangle \\
=&\frac{1}{2}\sum_{m,\pm} \langle (\hat{n}_m(1-\hat{n}_{m\pm1}) + i(-1)^m \hat{c}^\dagger_{m\pm1}\hat{c}^\dagger_m)\hat{n}_l(\hat{n}_m(1-\hat{n}_{m\pm1}) - i(-1)^m \hat{c}_m \hat{c}_{m\pm1}) \rangle \\
=&\frac{1}{2}\sum_{m,\pm} \langle \hat{n}_m(1-\hat{n}_{m\pm1})\hat{n}_l + \hat{c}^\dagger_{m\pm1}\hat{c}^\dagger_m \hat{n}_l \hat{c}_m \hat{c}_{m\pm1} \rangle. \qquad \text{(D.5)}
\end{aligned}$$

Above simplification is exact as the cross-terms vanish since for $m = l$ or $m = l \pm 1$ we have the cancellation $\hat{c}^\dagger_l \hat{n}_l = 0$ or $\hat{n}_l \hat{c}_l = 0$ and if they are not equal, the creation operators commute with $\hat{n}_l$ and annihilate $\hat{n}_m$. Therefore, the mixed term vanishes. To simplify, we need to consider four different cases for a given l, $l = m, l = m+1, l = m-1$ and anything else. For $m = l$, the second term in the equation always drops as $\hat{n}_l \hat{c}_l = \hat{c}^\dagger_l \hat{c}^2_l = 0$ and the first term decouples to $\frac{1}{2}\sum_\pm \langle \hat{n}_l(1-\hat{n}_{l\pm1}) \rangle = n(1-n)$ as we neglect non-local correlations again. The second case $m = l-1$ gives $\frac{1}{2}\langle \hat{n}_l \hat{n}_{l-1} \rangle = \frac{1}{2}n^2$ and equivalently for $m = l+1$ we get $\frac{1}{2}\langle \hat{n}_l \hat{n}_{l+1} \rangle = \frac{1}{2}n^2$. Finally, the cases $m \neq l, l\pm$ gives $(L-3)n^2$. All together, we find

$$\frac{1}{2}\sum_{m,\pm} \langle \hat{L}^\dagger_{m,\pm} \hat{n}_l \hat{L}_{m,\pm} \rangle = -3n^2 + n + Ln^2. \qquad \text{(D.6)}$$

Putting everything together, we get a closed equation for the excitation density time evolution:

$$\partial_t n = -\gamma n^2. \qquad \text{(D.7)}$$

On this level of approximation, we therefore always find that the dark state is reached in algebraic time. To discuss the breakdown of the mean-field approach due to the presence of the Hamiltonian (which drops out completely at this level), we need to consider non-local correlations.

Next order: nearest-neighbor correlations To make the Hamiltonian appear in the mean-field evolution, we now include nearest-neighbor correlations as well. To do

that, we reconsider the expectation value

$$\langle[\hat{n}_l, \hat{H}]\rangle = (-1)^l\langle(\hat{n}_{l-1} + \hat{n}_{l+2})\hat{c}_{l+1}\hat{c}_l + (\hat{n}_{l+1} + \hat{n}_{l-2})\hat{c}_{l-1}\hat{c}_l\rangle + \text{c.c.}, \tag{D.8}$$

with the mean-field decoupling $\langle\hat{n}_A\hat{c}_B\hat{c}_C\rangle = \langle\hat{n}_A\rangle\langle\hat{c}_B\hat{c}_C\rangle - \langle\hat{c}_A^\dagger\hat{c}_B\rangle\langle\hat{c}_A\hat{c}_C\rangle + \langle\hat{c}_A^\dagger\hat{c}_C\rangle\langle\hat{c}_A\hat{c}_B\rangle$. The first of these three terms always contains only nearest-neighbor correlations while the other two always also contain next to nearest order correlations, which we neglect again. This means, that the Hamiltonian term simplifies to

$$-i\langle[\hat{n}_l, \hat{H}]\rangle \approx -2in(-1)^l\langle\hat{c}_{l+1}\hat{c}_l + \hat{c}_{l-1}\hat{c}_l - \text{h.c.}\rangle, \tag{D.9}$$

We therefore introduce a second mean field, $K = i(-1)^l\langle\hat{c}_l\hat{c}_{l+1} - \hat{c}_{l+1}^\dagger\hat{c}_l^\dagger\rangle$. This mean field encodes the occupation of the target state as the Hamiltonian was defined with always positive amplitudes. We could also take two different mean-fields for the even and odd sites but an alternating definition captures the essential physics of the dark state transition on the mean-field level. Using this definition, we obtain

$$-i\langle[\hat{n}_l, \hat{H}]\rangle \approx 4Kn \tag{D.10}$$

Next, we reconsider the dissipative part to study nearest neighbor contributions. First

$$\begin{aligned}
&-\sum_m\langle\{\hat{n}_l, \hat{n}_m\} - \hat{n}_m\hat{n}_l\hat{n}_l\rangle \\
&= -\sum_m\langle\hat{n}_l\hat{n}_m\rangle = -\langle\hat{n}_l\rangle - \sum_{m\neq l}\langle\hat{n}_m\hat{n}_l\rangle \\
&\approx -\langle\hat{n}_l\rangle - \sum_{m\neq l}\Big(\langle\hat{n}_l\rangle\langle\hat{n}_l\rangle - \langle\hat{c}_l^\dagger\hat{c}_m^\dagger\rangle\langle\hat{c}_l\hat{c}_m\rangle + \langle\hat{c}_l^\dagger\hat{c}_m\rangle\langle\hat{c}_l\hat{c}_m^\dagger\rangle\Big) \\
&\approx -n - (L-1)n^2.
\end{aligned} \tag{D.11}$$

We can again neglect the off-diagonal terms as they all have the form (off-diagonal^2 which is negligible compared to diagonal $\times$ off-diagonal. This means that we do not have to introduce additional mean-fields for these additional terms. The same is true for the off-diagonal terms in the $\hat{L}\hat{n}\hat{L}$ term which are of order diagonal^2 $\times$ off-diagonal. This means, that for the description of the excitation density, we only need to know the evolution of the off-diagonal mean field K. The total time-evolution for the mean field density is therefore

$$\partial_t n = n(4K - \gamma n) \tag{D.12}$$

This still fulfills the necessary condition that $n = 0$ i.e. the dark state is indeed a dark state on the mean-field level.

Evolution of the off-diagonal mean field To get a closed set of mean-field equations, we next consider the time-evolution of the off-diagonal mean field in terms of densities and itself. This has the form

$$\partial_t K = \left\langle -i[\hat{K}_l, \hat{H}] - \gamma \sum_m \left(\{\hat{n}_m, \hat{K}_l\} - \hat{n}_m \hat{K}_l \hat{n}_m - \frac{1}{2} \sum_{\sigma=\pm} \hat{L}^\dagger_{l\sigma} \hat{K}_l \hat{L}_{l\sigma} \right) \right\rangle \tag{D.13}$$

First, we study the Hamiltonian part:

$$\begin{aligned} &- i\langle[\hat{K}_l, \hat{H}]\rangle \\ &= \sum_m (-1)^{m+l} \langle [\hat{c}_l \hat{c}_{l+1} - \hat{c}^\dagger_{l+1} \hat{c}^\dagger_l, \hat{n}_m (\hat{c}_{m-2} \hat{c}_{m-1} + \hat{c}^\dagger_{m-1} \hat{c}^\dagger_{m-2} + \hat{c}^\dagger_{m+1} \hat{c}^\dagger_{m+2} + \hat{c}_{m+2} \hat{c}_{m+1})] \rangle. \end{aligned} \tag{D.14}$$

To simplify this term, note that terms with a different number of creation and annihilation operators can only give rise to off-diagonal terms since $\hat{c}_l^2 = 0$. To lowest order approximation, we compute only local contributions as, in cases they do not vanish, non-local contributions are smaller close to the target state. Hence, we get

$$\begin{aligned} &- i\langle[\hat{K}_l, \hat{H}]\rangle \approx \sum_m (-1)^{m+l} \left(\langle [\hat{c}_l \hat{c}_{l+1}, \hat{n}_m (\hat{c}^\dagger_{m-1} \hat{c}^\dagger_{m-2} - \hat{c}^\dagger_{m+1} \hat{c}^\dagger_{m+2})] \rangle \right) + \text{c.c} \\ &= \sum_m (-1)^{m+l} \langle (\delta_{l+1,m} \hat{c}_l - \delta_{l,m} \hat{c}_{l+1}) \hat{c}_m \hat{c}^\dagger_{m-1} \hat{c}^\dagger_{m-2} \rangle + \langle (\delta_{l+1,m} \hat{c}_l - \delta_{l,m} \hat{c}_{l+1}) \hat{c}_m \hat{c}^\dagger_{m+1} \hat{c}^\dagger_{m+2} \rangle \\ &\quad + \sum_m (-1)^{m+l} \langle \hat{n}_m ([\hat{c}_l \hat{c}_{l+1}, \hat{c}^\dagger_{m-1} \hat{c}^\dagger_{m-2}] + [\hat{c}_l \hat{c}_{l+1}, \hat{c}^\dagger_{m+1} \hat{c}^\dagger_{m+2}]) \rangle + \text{c.c.} \end{aligned} \tag{D.15}$$

The first line of this result vanishes under the present approximation since it only produces off-diagonal terms. The second one does not:

$$\begin{aligned} &- i\langle[\hat{K}_l, \hat{H}]\rangle \\ &\quad \approx \sum_m (-1)^{m+l} \langle \hat{n}_m \left(\delta_{m,l+2} (1 - \hat{n}_l - \hat{n}_{l+1}) + \delta_{m,l-2} (1 - \hat{n}_l - \hat{n}_{l+1}) \right) \rangle + \text{c.c.} \end{aligned} \tag{D.16}$$

Taking now only the local contributions in the mean-field decoupling, we obtain

$$-i\langle[\hat{K}_l, \hat{H}]\rangle \approx 4n(1 - 2n). \tag{D.17}$$

We see that the excitation density has a back action on the off-diagonal correlations via the Hamiltonian, which vanishes in the absence of excitations. It remains open to compute the action of the dissipation on the second mean field. Let us start with the

anti-commutator

$$\sum_m \{\hat{n}_m, \hat{K}_l\} = i(-1)^l \sum_m \{\hat{n}_m, \hat{c}_l \hat{c}_{l+1}\} - i(-1)^l \sum_m \{\hat{n}_m, \hat{c}^\dagger_{l+1} \hat{c}^\dagger_l\}$$
$$= 2i(-1)^l \left(\hat{c}_l \hat{c}_{l+1} + \sum_{m \neq l, l+1} \hat{n}_m \hat{c}_l \hat{c}_{l+1} \right) + \text{h.c.}. \tag{D.18}$$

Taking the expectation value gives in the second term only the contribution $\langle \hat{n}_m \rangle \langle \hat{c}_l \hat{c}_{l+1} \rangle$ since we neglect any next to nearest neighbor contributions. Therefore

$$\sum_m \langle \{\hat{n}_m, \hat{K}_l\} \rangle \approx 2i(-1)^l (1 + (L-2)n) \langle \hat{c}_l \hat{c}_{l+1} \rangle + \text{c.c} \approx 2(1 + (L-2)n)K. \tag{D.19}$$

Along the same lines, we get

$$\sum_m \langle \hat{n}_m \hat{K}_l \hat{n}_m \rangle = LnK. \tag{D.20}$$

Finally,

$$\frac{1}{2} \sum_{m,\sigma} \langle \hat{L}^\dagger_{m\sigma} \hat{K}_l \hat{L}_{m\sigma} \rangle = i(-1)^l \frac{1}{2} \sum_{m,\sigma} \langle \hat{n}_m (1 - \hat{n}_{m+\sigma}) \hat{c}_l \hat{c}_{l+1} \hat{n}_m (1 - \hat{n}_{m+\sigma}) \rangle$$
$$+ \frac{1}{2} \sum_{m\sigma} (-1)^{l+m} \langle \hat{n}_m (1 - \hat{n}_{m+\sigma}) \hat{c}_l \hat{c}_{l+1} \hat{c}_m \hat{c}_{m+\sigma} - \hat{c}^\dagger_{m+\sigma} \hat{c}^\dagger_m \hat{c}_l \hat{c}_{l+1} \hat{n}_m (1 - \hat{n}_{m+\sigma}) \rangle$$
$$+ i(-1)^l \frac{1}{2} \sum_{m\sigma} \langle \hat{c}^\dagger_{m+\sigma} \hat{c}^\dagger_m \hat{c}_l \hat{c}_{l+1} \hat{c}_m \hat{c}_{m+\sigma} \rangle + \text{c.c.}. \tag{D.21}$$

The first line can be simplified by noting that it vanishes for $\sigma = +$ if $m = l$ or $m = l = 1$, it simplifies to $\hat{n}_{l-1} \hat{c}_l \hat{c}_{l+1}$ for $l = -1$ i.e. nK and in all other cases, the dominant contribution is $n(1-n)K$. For $\sigma = -1$, we get the same term again so that we have in total $(n + (L-3)n(1-n))K$ from the first line. The second line can be neglected as the non-zero contributions have at most the form $\hat{c}^\dagger \hat{c} \hat{c} \hat{c}^\dagger \hat{c} \hat{c}$ with appropriate indices. Under mean-field decoupling, this always gives quadratic terms in non-local correlations $\sim nK^2$ which we neglect compared to terms $\sim nK$. The third term vanishes if $m = l, l+1, l-\sigma, l+1-\sigma$ (3 cases) and otherwise we find $n^2 K$. This means that all together

$$\frac{1}{2} \sum_{m,\sigma} \langle \hat{L}^\dagger_{m\sigma} \hat{K}_l \hat{L}_{m\sigma} \rangle \approx (n + (L-3)n(1-n) + (L-3)n^2)K = (L-2)nK \tag{D.22}$$

The total time-evolution for K simplifies to

$$\partial_t K \approx 4n(1-2n) - \gamma(1-n)K. \tag{D.23}$$

Since we are working in the limit where $n \ll 1$, to leading order we find the time-evolution (5.21).

D.2 Quantum feedback Hamiltonian in bosonization

The perturbation to the Hamiltonian is discussed in the continuum limit,

$$\begin{aligned}
\Delta\hat{H} &= -\sum_l (-1)^l (\hat{n}_{l+2} - \hat{n}_{l-1})(\hat{c}_l^\dagger \hat{c}_{l+1} + \hat{c}_{l+1}^\dagger \hat{c}_l) \\
&= -\sum_l (-1)^l \hat{n}_l \left(\hat{c}_{l+1}^\dagger \hat{c}_{l+2} + \hat{c}_{l+2}^\dagger \hat{c}_{l+1} + \hat{c}_{l-1}^\dagger \hat{c}_{l-2} + \hat{c}_{l-2}^\dagger \hat{c}_{l-1}\right) \\
&= -a \int dx \cos(2k_F x) \hat{\psi}^\dagger(x)\hat{\psi}(x) \left(\hat{\psi}^\dagger(x+a)\hat{\psi}(x+2a) + (a \leftrightarrow -a) + \text{h.c.}\right) \\
&= -a \sum_{s=\pm} \int dx \cos(2k_F x) \hat{\psi}^\dagger(x)\hat{\psi}(x)\hat{\psi}^\dagger(x+sa)\hat{\psi}(x+2sa) + \text{h.c.}. \qquad \text{(D.24)}
\end{aligned}$$

Here we introduced $k_F = \pi/2a = \pi n_0$. Since the hopping commutes with the density, we just have to study a single term. We only retain the leading order in derivatives which means that in direct comparison with the density, we can drop the explicit dependence on the derivative in the definition of the bosonized fields. This gives:

$$\begin{aligned}
&- a \int dx \cos(2k_F x) \hat{\psi}^\dagger(x)\hat{\psi}(x)\hat{\psi}^\dagger(x+as)\hat{\psi}(x+2as) \\
=& -\frac{1}{2} a n_0^2 \sum_{l,l',l''} \int dx \cos(2k_F x) e^{2il(k_F x - \hat{\phi}(x))} e^{i(2l'+1)(k_F(x+sa) - \hat{\phi}(x+sa))} \\
&\times e^{-i\hat{\theta}(x+sa)} e^{i\hat{\theta}(x+2sa)} e^{i(2l''+1)(k_F(x+2sa) - \hat{\phi}(x+2sa))} \\
=& \frac{isan_0^2}{2} \sum_{l,l',l''} (-1)^{l''} \int dx \cos(2k_F x) e^{2il(k_F x - \hat{\phi}(x))} e^{i(2l'+1)(k_F(x+sa) - \hat{\phi}(x+sa))} \\
&\times e^{i(2l''+1)(k_F(x+2sa) - \hat{\phi}(x+2sa))} e^{-i\hat{\theta}(x+sa)} e^{i\hat{\theta}(x+2sa)} \\
=& \frac{-s^2 an_0^2}{2} \sum_{l,l',l''} (-1)^{l'+l''} \int dx \cos(2k_F x) e^{2il(k_F x - \hat{\phi}(x))} e^{i(2l'+1)(k_F x - \hat{\phi}(x+sa))} \\
&\times e^{i(2l''+1)(k_F(x+2sa) - \hat{\phi}(x+2sa))} e^{-i\hat{\theta}(x+sa)} e^{i\hat{\theta}(x+2sa)} \\
=& \frac{s^2 an_0^2}{2} \sum_{l,l',l''} (-1)^{l'+l''} \int dx \cos(2k_F x) e^{2il(k_F x - \hat{\phi}(x))} e^{i(2l'+1)(k_F x - \hat{\phi}(x+sa))} \\
&\times e^{i(2l''+1)(k_F x - \hat{\phi}(x+2sa))} e^{-i\hat{\theta}(x+sa)} e^{i\hat{\theta}(x+2sa)} \qquad \text{(D.25)}
\end{aligned}$$

Note that the sign s appears quadratic and therefore drops out so that we get the same for both directions. At this point, we have separated $\hat{\phi}$ and $\hat{\theta}$ using the point splitting given by the lattice discreteness so that we can safely take the limit $a \to 0$ in the operators $\hat{\phi}$ i.e. do a derivative expansion that is cut off at leading order. For the

field $\hat{\phi}$ we have to be a bit more careful because of the alternating sum. Still doing this yields

$$
\begin{aligned}
&- a \int dx \cos(2k_F x) \hat{\psi}^\dagger(x) \hat{\psi}(x) \hat{\psi}^\dagger(x+as) \hat{\psi}(x+2as) \\
&\simeq \frac{an_0^2}{2} \sum_{l,l',l''} (-1)^{l'+l''} \int dx \cos(2k_F x) e^{2i(1+l+l'+l'')(k_F x - \hat{\phi}(x))} \\
&= \frac{an_0^2}{4} \sum_{l,l',l''} (-1)^{l'+l''} \int dx \left(e^{2ik_F x} e^{2i(1+l+l'+l'')(k_F x - \hat{\phi}(x))} + e^{-2ik_F x} e^{2i(1+l+l'+l'')(k_F x - \hat{\phi}(x))} \right) \\
&\simeq \frac{an_0^2}{4} \sum_{l',l''} (-1)^{l'+l''} \int dx \left(e^{2i\hat{\phi}(x)} + e^{-2i\hat{\phi}(x)} \right) \\
&= \frac{an_0^2}{2} \sum_{l',l''} (-1)^{l'+l''} \int dx \cos 2\hat{\phi}(x),
\end{aligned}
\tag{D.26}
$$

where we again dropped all oscillating terms which removes the sum over l. The result is not well defined as it contains a divergent sum which comes from a missing regularization. However, it is clear how the dependence on $\hat{\theta}(x)$ neglecting all derivatives looks like. Therefore we identify the perturbation (5.26). This is the only newly emerging term that does not contain derivatives and does not explicitly depend on oscillating factors of x.

D.3 Semiclassical limit of quantum pre-selection

The feedback quantum master equation (5.16) obeys a well-defined semi-classical limit when the dynamics is dominated by measurements, i.e., for $\gamma \gg 1$. In this limit, the double commutator $\sim [\hat{n}_l, [\hat{n}_l, \hat{\rho}]]$, i.e. the dephasing, dominates and quickly pushes the system into a state $\hat{\rho} \to \hat{\rho}_D$, which is diagonal in the particle number basis. A general state $\hat{\rho}$ in the particle number basis has the form $\hat{\rho} = \sum_{\vec{n},\vec{m}} \rho_{\vec{n},\vec{m}} |\vec{n}\rangle \langle\vec{m}|$ with (complex) amplitudes $\rho_{\vec{n},\vec{m}}$. Its diagonal elements are $\hat{\rho}_D \equiv \sum_{\vec{n}} \rho_{\vec{n},\vec{n}} |\vec{n}\rangle \langle\vec{n}|$. In the presence of dephasing, the off-diagonal elements decay exponentially in time, following $\rho_{\vec{n},\vec{m}} \sim e^{-\frac{\gamma}{2}||\vec{n}-\vec{m}||^2 t}$. The diagonal elements $\rho_{\vec{n},\vec{n}}$ are not affected by the dephasing. They can be interpreted as the probability distribution for configurations of $L/2$ classical, hard-core particles in a system of size L.

Adding the Hamiltonian evolution $\sim i[\hat{H}, \hat{\rho}]$ and the feedback $\sim p\mathcal{F}\hat{\rho}$ has two different effects: (i) the Hamiltonian evolution leads to the hopping of particles by coupling diagonal and off-diagonal matrix elements. (ii) the feedback evolution does not couple the diagonal and off-diagonal elements but instead yields a directed hopping on both the diagonal and the off-diagonals simultaneously. In the limit where $\gamma \gg 1$, it is thus useful to parameterize the state $\hat{\rho}$ in terms of a power series $\hat{\rho} = \hat{\rho}^D + \frac{1}{\gamma}\hat{\rho}^O_{1/\gamma} + \mathcal{O}(1/\gamma^2)$ and treat the Hamiltonian evolution perturbatively. Assuming in addition

$p \ll 1$[37] yields the well-defined perturbative expansion

$$\partial_t \hat{\rho}^D = -p\gamma \mathcal{F} \hat{\rho}^D - \frac{i}{\gamma} \mathcal{P}[\hat{H}, \hat{\rho}^O_{1/\gamma}] + \mathcal{O}(p/\gamma, 1/\gamma^2), \tag{D.27}$$

$$\tfrac{1}{\gamma} \partial_t \hat{\rho}^O_{1/\gamma} = -\sum_l [\hat{n}_l, [\hat{n}_l, \hat{\rho}^O_{1/\gamma}]] - i[\hat{H}, \hat{\rho}^D]. \tag{D.28}$$

with $\mathcal{P}$ being the projector onto the diagonal in the particle number basis. The second equation describes the exponential decay of the of the off-diagonal elements. We solve it in the quasi-stationary limit by setting $\partial_t \hat{\rho}^O_{1/\gamma} = 0$. This yields

$$\partial_t \hat{\rho}^D = -p\gamma \mathcal{F} \hat{\rho}^D - \frac{1}{2\gamma} \mathcal{P} i[\hat{H}, [\hat{H}, \hat{\rho}^D]] + \mathcal{O}(p/\gamma, 1/\gamma^2). \tag{D.29}$$

It involves only diagonal terms, which can be parametrized by the probability distribution $\rho(\vec{n}) \equiv \rho_{\vec{n},\vec{n}}$. The probability of swapping the occupation number at two neighboring sites $n_l \leftrightarrow n_{l+1}$ in a time step dt is then given by

$$\begin{aligned} \rho(n_l \leftrightarrow n_{l+1}) =& \gamma dt \Big(\frac{p}{2} (1 - (-1)^l (n_l - n_{l+1})) \\ &+ \frac{1}{\gamma^2} (1 - (-1)^l (n_{l+2} - n_{l-1}))^2 \Big). \end{aligned} \tag{D.30}$$

These state updates can be efficiently simulated: it requires L bits to store the current state and we may therefore study the dynamics of the underlying model in the strong measurement limit $\gamma \gg 1, 1/p$. Besides that, the resulting master equation is an interesting classical reaction diffusion model by itself. Therefore, we perform a numerical analysis of eq. (D.30). We absorb one of the parameters into a re-scaled time $t \to t/(p\gamma + 4/\gamma)$, leaving just a single parameter $r = 1/p\gamma^2$ in the model as a tuning parameter. This rescaling allows to tune through $r \in [0, \infty)$ for a fixed time-discretization dt in the new units, always obeying $\gamma \gg 1, 1/p$ using a proper choice of γ and p. We identify the strong measurement regime with $p = 1$ of the original model with $r \ll 1$ but $r \neq 0$. In this limit, the results are consistent with the MPS simulations for strong measurements in Fig. 33. In particular, we find that the order parameter decays $\sim t^{-1/4}$ after a $\mathcal{O}(1)$ initialization time up to $t \sim L^2$, consistent with the evolution of the true quantum state in the absorbing phase. At larger $r \approx 1.45$ we numerically observe a phase transition to a long-lived active phase (see Fig. 39) with an order-parameter finite size scaling consistent with the BKT scenario.

[37] Only after a small fraction of the measurement, the correction operation is applied.

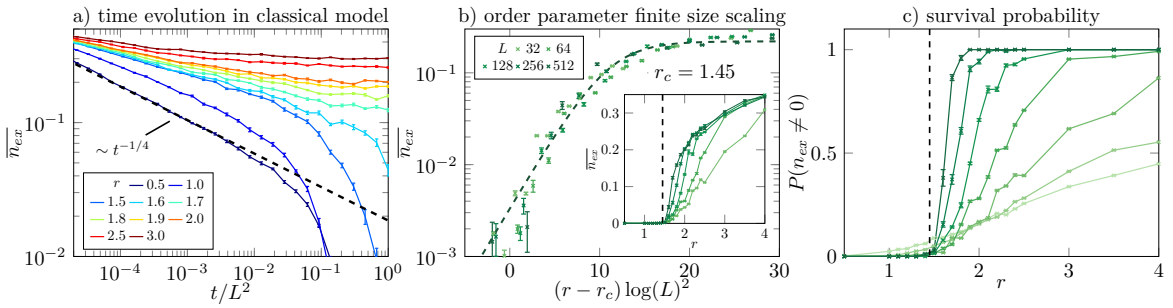

Figure 39: Numerical study of the classical limit. a) Trajectory-averaged time evolution of a random initial state towards the dark state of the classical stochastic model derived in the strong measurement limit of the quantum pre-selection scheme ($L = 512$) quantified by the order parameter $n_{ex} = \frac{1}{L}\sum_{l \text{ odd}} n_l + \frac{1}{L}\sum_{l \text{ even}}(1 - n_l)$. At $r \approx 1.5$ we find a change of the dynamics between an absorbing (decay $\sim t^{-1/4}$) and an active behavior at timescales $\sim L^2$, just like in the classical and quantum pre-selection schemes (see Fig. 29c) and Fig. 33c)). b) Evaluating systems of various sizes at $t = L^2$ allows to perform a scaling collapse of the order parameter, indicating an absorbing state phase transition with signatures of the BKT scenario at $r \approx 1.45$. Inset: un-rescaled data. c) The probability to have excitations left in the system in a given trajectory at $t = L^2$, i.e. the probability of being in any other state than the absorbing state $P(n_{ex} \neq 0)$ drastically changes its behavior and jumps from 0 to 1 at the phase transition.

References

[1]D. Castelvecchi, "Quantum computers ready to leap out of the lab in 2017", Nature **541**, 9–10 (2017).

[2]F. Arute, K. Arya, R. Babbush, D. Bacon, J. Bardin, R. Barends, R. Biswas, S. Boixo, F. Brandao, D. Buell, B. Burkett, Y. Chen, J. Chen, B. Chiaro, R. Collins, W. Courtney, A. Dunsworth, E. Farhi, B. Foxen, A. Fowler, C. M. Gidney, M. Giustina, R. Graff, K. Guerin, S. Habegger, M. Harrigan, M. Hartmann, A. Ho, M. R. Hoffmann, T. Huang, T. Humble, S. Isakov, E. Jeffrey, Z. Jiang, D. Kafri, K. Kechedzhi, J. Kelly, P. Klimov, S. Knysh, A. Korotkov, F. Kostritsa, D. Landhuis, M. Lindmark, E. Lucero, D. Lyakh, S. Mandrà, J. R. McClean, M. McEwen, A. Megrant, X. Mi, K. Michielsen, M. Mohseni, J. Mutus, O. Naaman, M. Neeley, C. Neill, M. Y. Niu, E. Ostby, A. Petukhov, J. Platt, C. Quintana, E. G. Rieffel, P. Roushan, N. Rubin, D. Sank, K. J. Satzinger, V. Smelyanskiy, K. J. Sung, M. Trevithick, A. Vainsencher, B. Villalonga, T. White, Z. J. Yao, P. Yeh, A. Zalcman, H. Neven, and J. Martinis, "Quantum supremacy using a programmable superconducting processor", Nature **574**, 505–510 (2019).

[3]Q. Xu, J. P. B. Ataides, C. A. Pattison, N. Raveendran, D. Bluvstein, J. Wurtz, B. Vasic, M. D. Lukin, L. Jiang, and H. Zhou, "Constant-overhead fault-tolerant quantum computation with reconfigurable atom arrays", Nature Physics (2024).

[4]M. W. Johnson, M. H. S. Amin, S. Gildert, T. Lanting, F. Hamze, N. Dickson, R. Harris, A. J. Berkley, J. Johansson, P. Bunyk, E. M. Chapple, C. Enderud, J. P. Hilton, K. Karimi, E. Ladizinsky, N. Ladizinsky, T. Oh, I. Perminov, C. Rich, M. C. Thom, E. Tolkacheva, C. J. S. Truncik, S. Uchaikin, J. Wang, B. Wilson, and G. Rose, "Quantum annealing with manufactured spins", Nature **473**, 194–198 (2011).

[5]J. Preskill, "Quantum computing in the nisq era and beyond", Quantum **2**, 79 (2018).

[6]A. Montanaro, "Quantum algorithms: an overview", npj Quantum Information **2** (2016).

[7]M. A. Nielsen and I. L. Chuang, *Quantum computation and quantum information: 10th anniversary edition* (Cambridge University Press, 2010).

[8]P. W. Shor, "Polynomial-time algorithms for prime factorization and discrete logarithms on a quantum computer", SIAM Journal on Computing **26**, 1484–1509 (1997).

[9]N. Gisin, G. Ribordy, W. Tittel, and H. Zbinden, "Quantum cryptography", Reviews of Modern Physics **74**, 145–195 (2002).

[10]L. K. Grover, "Quantum mechanics helps in searching for a needle in a haystack", Physical Review Letters **79**, 325–328 (1997).

[11]T. Kadowaki and H. Nishimori, "Quantum annealing in the transverse ising model", Phys. Rev. E **58**, 5355–5363 (1998).

[12]J. Preskill, "Quantum computing and the entanglement frontier", ArXiv:1203.5813 (2012).

[13]B. M. Terhal, "Quantum error correction for quantum memories", Rev. Mod. Phys. **87**, 307–346 (2015).

[14]D. Gottesman, "An introduction to quantum error correction and fault-tolerant quantum computation", ArXiv:0904.2557 (2009).

[15]R. P. Feynman, "Simulating physics with computers", International Journal of Theoretical Physics **21**, 467–488 (1982).

[16]G. Kurizki, P. Bertet, Y. Kubo, K. Mølmer, D. Petrosyan, P. Rabl, and J. Schmiedmayer, "Quantum technologies with hybrid systems", Proceedings of the National Academy of Sciences **112**, 3866–3873 (2015).

[17]H. Weimer, M. Müller, I. Lesanovsky, P. Zoller, and H. P. Büchler, "A rydberg quantum simulator", Nature Physics **6**, 382–388 (2010).

[18]J. T. Barreiro, M. Müller, P. Schindler, D. Nigg, T. Monz, M. Chwalla, M. Hennrich, C. F. Roos, P. Zoller, and R. Blatt, "An open-system quantum simulator with trapped ions", Nature **470**, 486–491 (2011).

[19]C. Monroe, W. Campbell, L.-M. Duan, Z.-X. Gong, A. Gorshkov, P. Hess, R. Islam, K. Kim, N. Linke, G. Pagano, P. Richerme, C. Senko, and N. Yao, "Programmable quantum simulations of spin systems with trapped ions", Reviews of Modern Physics **93** (2021).

[20]A. Einstein, "Quantentheorie des einatomigen idealen gases", Sitzungsberichte der Preussischen Akademie der Wissenschaften **1** (1924).

[21]M. H. Anderson, J. R. Ensher, M. R. Matthews, C. E. Wieman, and E. A. Cornell, "Observation of bose-einstein condensation in a dilute atomic vapor", Science **269**, 198–201 (1995).

[22]K. B. Davis, M. O. Mewes, M. R. Andrews, N. J. van Druten, D. S. Durfee, D. M. Kurn, and W. Ketterle, "Bose-einstein condensation in a gas of sodium atoms", Phys. Rev. Lett. **75**, 3969–3973 (1995).

[23]C. Gross and I. Bloch, "Quantum simulations with ultracold atoms in optical lattices", Science **357**, 995–1001 (2017).

[24]P. Scholl, M. Schuler, H. J. Williams, A. A. Eberharter, D. Barredo, K.-N. Schymik, V. Lienhard, L.-P. Henry, T. C. Lang, T. Lahaye, A. M. Läuchli, and A. Browaeys, "Quantum simulation of 2d antiferromagnets with hundreds of rydberg atoms", Nature **595**, 233–238 (2021).

[25]Y. Cao, J. Romero, J. P. Olson, M. Degroote, P. D. Johnson, M. Kieferová, I. D. Kivlichan, T. Menke, B. Peropadre, N. P. D. Sawaya, S. Sim, L. Veis, and A. Aspuru-Guzik, "Quantum chemistry in the age of quantum computing", Chemical Reviews **119**, 10856–10915 (2019).

[26]S. Diehl, A. Micheli, A. Kantian, B. Kraus, H. P. Büchler, and P. Zoller, "Quantum States and Phases in Driven Open Quantum Systems with Cold Atoms", Nature Physics **4**, 878–883 (2008).

[27]M. Müller, S. Diehl, G. Pupillo, and P. Zoller, "Engineered open systems and quantum simulations with atoms and ions", in *Advances in atomic, molecular, and optical physics*, Vol. 61, edited by P. Berman, E. Arimondo, and C. Lin, Advances In Atomic, Molecular, and Optical Physics (Academic Press, 2012), pp. 1–80.

[28]L. M. Sieberer, M. Buchhold, and S. Diehl, "Keldysh field theory for driven open quantum systems", Reports on Progress in Physics **79**, 096001 (2016).

[29]L. M. Sieberer, M. Buchhold, J. Marino, and S. Diehl, "Universality in driven open quantum matter", ArXiv:2312.03073 (2023).

[30]S. Diehl, E. Rico, M. A. Baranov, and P. Zoller, "Topology by dissipation in atomic quantum wires", Nature Physics **7**, 971–977 (2011).

[31]R. Lin, R. Rosa-Medina, F. Ferri, F. Finger, K. Kroeger, T. Donner, T. Esslinger, and R. Chitra, "Dissipation-engineered family of nearly dark states in many-body cavity-atom systems", Phys. Rev. Lett. **128**, 153601 (2022).

[32]M. A. Norcia, W. B. Cairncross, K. Barnes, P. Battaglino, A. Brown, M. O. Brown, K. Cassella, C.-A. Chen, R. Coxe, D. Crow, J. Epstein, C. Griger, A. M. W. Jones, H. Kim, J. M. Kindem, J. King, S. S. Kondov, K. Kotru, J. Lauigan, M. Li, M. Lu, E. Megidish, J. Marjanovic, M. McDonald, T. Mittiga, J. A. Muniz, S. Narayanaswami, C. Nishiguchi, R. Notermans, T. Paule, K. A. Pawlak, L. S. Peng, A. Ryou, A. Smull, D. Stack, M. Stone, A. Sucich, M. Urbanek, R. J. M. van de Veerdonk, Z. Vendeiro, T. Wilkason, T.-Y. Wu, X. Xie, X. Zhang, and B. J. Bloom, "Midcircuit qubit measurement and rearrangement in a ^{171}Yb atomic array", Phys. Rev. X **13**, 041034 (2023).

[33]T. Graham, L. Phuttitarn, R. Chinnarasu, Y. Song, C. Poole, K. Jooya, J. Scott, A. Scott, P. Eichler, and M. Saffman, "Midcircuit measurements on a single-species neutral alkali atom quantum processor", Physical Review X **13** (2023).

[34]J. M. Koh, S.-N. Sun, M. Motta, and A. J. Minnich, "Measurement-induced entanglement phase transition on a superconducting quantum processor with mid-circuit readout", Nature Physics **19**, 1314–1319 (2023).

[35]M. DeCross, E. Chertkov, M. Kohagen, and M. Foss-Feig, "Qubit-reuse compilation with mid-circuit measurement and reset", Phys. Rev. X **13**, 041057 (2023).

[36]S. Wolff, J.-S. Bernier, D. Poletti, A. Sheikhan, and C. Kollath, "Evolution of two-time correlations in dissipative quantum spin systems: aging and hierarchical dynamics", Phys. Rev. B **100**, 165144 (2019).

[37]S. Wolff, A. Sheikhan, and C. Kollath, "Numerical evaluation of two-time correlation functions in open quantum systems with matrix product state methods: a comparison", SciPost Phys. Core **3**, 10 (2020).

[38]D. Poletti, J.-S. Bernier, A. Georges, and C. Kollath, "Interaction-induced impeding of decoherence and anomalous diffusion", Phys. Rev. Lett. **109**, 045302 (2012).

[39]H. Pichler, A. J. Daley, and P. Zoller, "Nonequilibrium dynamics of bosonic atoms in optical lattices: decoherence of many-body states due to spontaneous emission", Phys. Rev. A **82**, 063605 (2010).

[40]A. J. Daley, "Quantum trajectories and open many-body quantum systems", Advances in Physics **63**, 77–149 (2014).

[41]S. F. Edwards and P. W. Anderson, "Theory of spin glasses", Journal of Physics F: Metal Physics **5**, 965 (1975).

[42]V. J. Emery, "Critical properties of many-component systems", Phys. Rev. B **11**, 239–247 (1975).

[43]G. Grinstein and A. Luther, "Application of the renormalization group to phase transitions in disordered systems", Phys. Rev. B **13**, 1329–1343 (1976).

[44]M. Buchhold, Y. Minoguchi, A. Altland, and S. Diehl, "Effective theory for the measurement-induced phase transition of dirac fermions", Phys. Rev. X **11**, 041004 (2021).

[45]J. Von Neumann, *Mathematische grundlagen der quantenmechanik* (Springer, 1932).

[46]L. Amico, R. Fazio, A. Osterloh, and V. Vedral, "Entanglement in many-body systems", Rev. Mod. Phys. **80**, 517–576 (2008).

[47]B. Skinner, J. Ruhman, and A. Nahum, "Measurement-induced phase transitions in the dynamics of entanglement", Phys. Rev. X **9**, 031009 (2019).

[48]Y. Li, X. Chen, and M. P. A. Fisher, "Quantum zeno effect and the many-body entanglement transition", Phys. Rev. B **98**, 205136 (2018).

[49]Y. Li, X. Chen, and M. P. A. Fisher, "Measurement-driven entanglement transition in hybrid quantum circuits", Phys. Rev. B **100**, 134306 (2019).

[50]M. J. Gullans and D. A. Huse, "Dynamical purification phase transition induced by quantum measurements", Phys. Rev. X **10**, 041020 (2020).

[51]S. Choi, Y. Bao, X.-L. Qi, and E. Altman, "Quantum error correction in scrambling dynamics and measurement-induced phase transition", Phys. Rev. Lett. **125**, 030505 (2020).

[52]C.-M. Jian, Y.-Z. You, R. Vasseur, and A. W. W. Ludwig, "Measurement-induced criticality in random quantum circuits", Phys. Rev. B **101**, 104302 (2020).

[53]R. Fan, S. Vijay, A. Vishwanath, and Y.-Z. You, "Self-organized error correction in random unitary circuits with measurement", Phys. Rev. B **103**, 174309 (2021).

[54]Y. Li and M. P. A. Fisher, "Statistical mechanics of quantum error correcting codes", Phys. Rev. B **103**, 104306 (2021).

[55]A. Nahum, S. Roy, B. Skinner, and J. Ruhman, "Measurement and entanglement phase transitions in all-to-all quantum circuits, on quantum trees, and in landau-ginsburg theory", PRX Quantum **2**, 010352 (2021).

[56]Y. Fuji and Y. Ashida, "Measurement-induced quantum criticality under continuous monitoring", Phys. Rev. B **102**, 054302 (2020).

[57]S.-K. Jian, C. Liu, X. Chen, B. Swingle, and P. Zhang, "Measurement-induced phase transition in the monitored sachdev-ye-kitaev model", Phys. Rev. Lett. **127**, 140601 (2021).

[58]E. V. H. Doggen, Y. Gefen, I. V. Gornyi, A. D. Mirlin, and D. G. Polyakov, "Generalized quantum measurements with matrix product states: entanglement phase transition and clusterization", Physical Review Research **4** (2022).

[59]A. Nahum, J. Ruhman, S. Vijay, and J. Haah, "Quantum entanglement growth under random unitary dynamics", Phys. Rev. X **7**, 031016 (2017).

[60]S. Kirkpatrick, "Percolation and conduction", Rev. Mod. Phys. **45**, 574–588 (1973).

[61]P. Sierant, M. Schirò, M. Lewenstein, and X. Turkeshi, "Measurement-induced phase transitions in $(d+1)$-dimensional stabilizer circuits", Phys. Rev. B **106**, 214316 (2022).

[62]X. Turkeshi, R. Fazio, and M. Dalmonte, "Measurement-induced criticality in (2+1)-dimensional hybrid quantum circuits", Phys. Rev. B **102**, 014315 (2020).

[63]A. Lavasani, Y. Alavirad, and M. Barkeshli, "Topological order and criticality in (2+1)D monitored random quantum circuits", Phys. Rev. Lett. **127**, 235701 (2021).

[64]O. Lunt, M. Szyniszewski, and A. Pal, "Measurement-induced criticality and entanglement clusters: a study of one-dimensional and two-dimensional clifford circuits", Phys. Rev. B **104**, 155111 (2021).

[65]M. Ippoliti, M. J. Gullans, S. Gopalakrishnan, D. A. Huse, and V. Khemani, "Entanglement phase transitions in measurement-only dynamics", Phys. Rev. X **11**, 011030 (2021).

[66]K. Klocke and M. Buchhold, "Majorana loop models for measurement-only quantum circuits", Physical Review X **13** (2023).

[67]X. Cao, A. Tilloy, and A. D. Luca, "Entanglement in a fermion chain under continuous monitoring", SciPost Phys. **7**, 024 (2019).

[68]O. Alberton, M. Buchhold, and S. Diehl, "Entanglement transition in a monitored free-fermion chain: from extended criticality to area law", Phys. Rev. Lett. **126**, 170602 (2021).

[69]I. Poboiko, P. Pöpperl, I. V. Gornyi, and A. D. Mirlin, "Theory of free fermions under random projective measurements", Phys. Rev. X **13**, 041046 (2023).

[70]S. Sachdev and J. Ye, "Gapless spin-fluid ground state in a random quantum heisenberg magnet", Phys. Rev. Lett **70**, 3339 (1993).

[71]A. Altland and B. Simons, *Condensed matter field theory* (Cambridge University Press, 2006).

[72]E. Noether, "Invarianten beliebiger Differentialausdrücke.", Nachr. Ges. Wiss. Göttingen, Math.-Phys. Kl. **1918**, 37–44 (1918).

[73]K. G. Wilson, "The renormalization group: critical phenomena and the kondo problem", Rev. Mod. Phys. **47**, 773–840 (1975).

[74]J. Zinn-Justin, *Quantum Field Theory and Critical Phenomena* (Oxford University Press, 2002).

[75]P. C. Hohenberg and B. I. Halperin, "Theory of dynamic critical phenomena", Rev. Mod. Phys. **49**, 435–479.

[76]R. Daviet, C. P. Zelle, A. Rosch, and S. Diehl, "Nonequilibrium criticality at the onset of time-crystalline order", Phys. Rev. Lett. **132**, 167102 (2024).

[77]C. P. Zelle, R. Daviet, A. Rosch, and S. Diehl, "Universal phenomenology at critical exceptional points of nonequilibrium $O(N)$ models", ArXiv:2304.09207 (2023).

[78]F. Evers and A. D. Mirlin, "Anderson transitions", Reviews of Modern Physics **80**, 1355–1417 (2008).

[79]S.-i. Tomonaga, "Remarks on Bloch's Method of Sound Waves applied to Many-Fermion Problems", Progress of Theoretical Physics **5**, 544–569 (1950).

[80]J. M. Luttinger, "An Exactly Soluble Model of a Many-Fermion System", Journal of Mathematical Physics **4**, 1154–1162 (1963).

[81]F. D. M. Haldane, "'luttinger liquid theory' of one-dimensional quantum fluids. i. properties of the luttinger model and their extension to the general 1d interacting spinless fermi gas", Journal of Physics C: Solid State Physics **14**, 2585 (1981).

[82]D. C. Mattis and E. H. Lieb, "Exact Solution of a Many-Fermion System and Its Associated Boson Field", Journal of Mathematical Physics **6**, 304–312 (1965).

[83]T. Giamarchi, *Quantum Physics in One Dimension* (Oxford University Press, 2003).

[84]A. O. Gogolin, A. A. Nersesyan, and A. M. Tsvelik, *Bosonization and strongly correlated systems* (Cambridge University Press, 1999).

[85]M. Mintchev and P. Sorba, "Luttinger liquid in a non-equilibrium steady state", Journal of Physics A: Mathematical and Theoretical **46**, 095006 (2013).

[86]D. Sénéchal, "An introduction to bosonization", ArXiv:9908262 (1999).

[87]J. von Delft and H. Schoeller, "Bosonization for beginners — refermionization for experts", Annalen der Physik **510**, 225–305 (1998).

[88]L. Venkataraman, Y. S. Hong, and P. Kim, "Electron transport in a multichannel one-dimensional conductor: molybdenum selenide nanowires", Phys. Rev. Lett. **96**, 076601 (2006).

[89]V. L. Berezinskiĭ, "Destruction of Long-range Order in One-dimensional and Two-dimensional Systems having a Continuous Symmetry Group I. Classical Systems", Soviet Journal of Experimental and Theoretical Physics **32**, 493 (1971).

[90]V. L. Berezinskiĭ, "Destruction of Long-range Order in One-dimensional and Two-dimensional Systems Possessing a Continuous Symmetry Group. II. Quantum Systems", Soviet Journal of Experimental and Theoretical Physics **34**, 610 (1972).

[91]J. M. Kosterlitz and D. J. Thouless, "Ordering, metastability and phase transitions in two-dimensional systems", Journal of Physics C Solid State Physics **6**, 1181–1203 (1973).

[92]M. Szyniszewski, A. Romito, and H. Schomerus, "Entanglement transition from variable-strength weak measurements", Phys. Rev. B **100**, 064204 (2019).

[93]M. Szyniszewski, A. Romito, and H. Schomerus, "Universality of entanglement transitions from stroboscopic to continuous measurements", Phys. Rev. Lett. **125** (2020).

[94]X. Turkeshi, A. Biella, R. Fazio, M. Dalmonte, and M. Schiró, "Measurement-induced entanglement transitions in the quantum ising chain: from infinite to zero clicks", Phys. Rev. B **103**, 224210 (2021).

[95]M. Szyniszewski, O. Lunt, and A. Pal, "Disordered monitored free fermions", Phys. Rev. B **108**, 165126 (2023).

[96]B. Ladewig, S. Diehl, and M. Buchhold, "Monitored open fermion dynamics: exploring the interplay of measurement, decoherence, and free hamiltonian evolution", Phys. Rev. Res. **4**, 033001 (2022).

[97]I. Poboiko, I. V. Gornyi, and A. D. Mirlin, "Measurement-induced phase transition for free fermions above one dimension", Phys. Rev. Lett. **132**, 110403 (2024).

[98]K. Chahine and M. Buchhold, "Entanglement phases, localization and multifractality of monitored free fermions in two dimensions", ArXiv:2309.12391 (2023).

[99]T. Müller, S. Diehl, and M. Buchhold, "Measurement-induced dark state phase transitions in long-ranged fermion systems", Phys. Rev. Lett. **128**, 010605 (2022).

[100]A. Campa, T. Dauxois, D. Fanelli, and S. Ruffo, *Physics of long-range interacting systems* (Oxford University Press, 2014).

[101]A. Dutta and J. K. Bhattacharjee, "Phase transitions in the quantum ising and rotor models with a long-range interaction", Phys. Rev. B **64**, 184106 (2001).

[102]M. F. Maghrebi, Z.-X. Gong, and A. V. Gorshkov, "Continuous symmetry breaking in 1d long-range interacting quantum systems", Phys. Rev. Lett. **119**, 023001 (2017).

[103]J. W. Britton, B. C. Sawyer, A. C. Keith, C.-C. J. Wang, J. K. Freericks, H. Uys, M. J. Biercuk, and J. J. Bollinger, "Engineered two-dimensional ising interactions in a trapped-ion quantum simulator with hundreds of spins", Nature **484**, 489–492 (2012).

[104]P. Richerme, Z.-X. Gong, A. Lee, C. Senko, J. Smith, M. Foss-Feig, S. Michalakis, A. V. Gorshkov, and C. Monroe, "Non-local propagation of correlations in quantum systems with long-range interactions", Nature **511**, 198–201 (2014).

[105]P. Jurcevic, B. P. Lanyon, P. Hauke, C. Hempel, P. Zoller, R. Blatt, and C. F. Roos, "Quasiparticle engineering and entanglement propagation in a quantum many-body system", Nature **511**, 202–205 (2014).

[106]J. Zhang, G. Pagano, P. W. Hess, A. Kyprianidis, P. Becker, H. Kaplan, A. V. Gorshkov, Z.-X. Gong, and C. Monroe, "Observation of a many-body dynamical phase transition with a 53-qubit quantum simulator", Nature **551**, 601–604 (2017).

[107]R. Landig, L. Hruby, N. Dogra, M. Landini, R. Mottl, T. Donner, and T. Esslinger, "Quantum phases from competing short- and long-range interactions in an optical lattice", Nature **532**, 476–479 (2016).

[108]F. Mivehvar, F. Piazza, T. Donner, and H. Ritsch, "Cavity qed with quantum gases: new paradigms in many-body physics", Advances in Physics **70**, 1–153 (2021).

[109]P. Schauß, M. Cheneau, M. Endres, T. Fukuhara, S. Hild, A. Omran, T. Pohl, C. Gross, S. Kuhr, and I. Bloch, "Observation of spatially ordered structures in a two-dimensional rydberg gas", Nature **491**, 87–91 (2012).

[110]B. Yan, S. A. Moses, B. Gadway, J. P. Covey, K. R. A. Hazzard, A. M. Rey, D. S. Jin, and J. Ye, "Observation of dipolar spin-exchange interactions with lattice-confined polar molecules", Nature **501**, 521–525 (2013).

[111]J. C. Hoke, M. Ippoliti, E. Rosenberg, D. Abanin, R. Acharya, T. I. Andersen, M. Ansmann, F. Arute, K. Arya, A. Asfaw, J. Atalaya, J. C. Bardin, A. Bengtsson, G. Bortoli, A. Bourassa, J. Bovaird, L. Brill, M. Broughton, B. B. Buckley, D. A. Buell, T. Burger, B. Burkett, N. Bushnell, Z. Chen, B. Chiaro, D. Chik, J. Cogan, R. Collins, P. Conner, W. Courtney, A. L. Crook, B. Curtin, A. G. Dau, D. M. Debroy, A. Del Toro Barba, S. Demura, A. Di Paolo, I. K. Drozdov, A. Dunsworth, D. Eppens, C. Erickson, E. Farhi, R. Fatemi, V. S. Ferreira, L. F. Burgos, E. Forati, A. G. Fowler, B. Foxen, W. Giang, C. Gidney, D. Gilboa, M. Giustina, R. Gosula, J. A. Gross, S. Habegger, M. C. Hamilton, M. Hansen, M. P. Harrigan, S. D. Harrington, P. Heu, M. R. Hoffmann, S. Hong, T. Huang, A. Huff, W. J. Huggins, S. V. Isakov, J. Iveland, E. Jeffrey, Z. Jiang, C. Jones, P. Juhas, D. Kafri, K. Kechedzhi, T. Khattar, M. Khezri, M. Kieferová, S. Kim, A. Kitaev, P. V. Klimov, A. R. Klots, A. N. Korotkov, F. Kostritsa, J. M. Kreikebaum, D. Landhuis, P. Laptev, K.-M. Lau, L. Laws, J. Lee, K. W. Lee, Y. D. Lensky, B. J. Lester, A. T. Lill, W. Liu, A. Locharla, O. Martin, J. R. McClean, M. McEwen, K. C. Miao, A. Mieszala, S. Montazeri, A. Morvan, R. Movassagh, W. Mruczkiewicz, M. Neeley, C. Neill, A. Nersisyan, M. Newman, J. H. Ng, A. Nguyen, M. Nguyen, M. Y. Niu, T. E. O'Brien, S. Omonije, A. Opremcak, A. Petukhov, R. Potter, L. P. Pryadko, C. Quintana, C. Rocque, N. C. Rubin, N. Saei, D. Sank, K. Sankaragomathi, K. J. Satzinger, H. F. Schurkus, C. Schuster, M. J. Shearn, A. Shorter, N. Shutty, V. Shvarts, J. Skruzny, W. C. Smith, R. Somma, G. Sterling, D. Strain, M. Szalay, A. Torres, G. Vidal, B. Villalonga, C. V. Heidweiller, T. White, B. W. K. Woo, C. Xing, Z. J. Yao, P. Yeh, J. Yoo, G. Young, A. Zalcman, Y. Zhang, N. Zhu, N. Zobrist, H. Neven, R. Babbush, D. Bacon, S. Boixo, J. Hilton, E. Lucero, A. Megrant, J. Kelly, Y. Chen, V. Smelyanskiy, X. Mi, V. Khemani, and P. Roushan, "Measurement-induced entanglement and teleportation on a noisy quantum processor", Nature **622**, 481–486 (2023).

[112]M. J. Gullans and D. A. Huse, "Scalable probes of measurement-induced criticality", Phys. Rev. Lett. **125**, 070606 (2020).

[113]C. Noel, P. Niroula, D. Zhu, A. Risinger, L. Egan, D. Biswas, M. Cetina, A. V. Gorshkov, M. J. Gullans, D. A. Huse, and C. Monroe, "Measurement-induced quantum

phases realized in a trapped-ion quantum computer", Nature Physics **18**, 760–764 (2022).

[114]H. Dehghani, A. Lavasani, M. Hafezi, and M. J. Gullans, "Neural-network decoders for measurement induced phase transitions", Nature Communications **14** (2023).

[115]S. J. Garratt and E. Altman, "Probing post-measurement entanglement without post-selection", ArXiv:2305.20092 (2023).

[116]J. Y. Lee, W. Ji, Z. Bi, and M. P. A. Fisher, "Decoding measurement-prepared quantum phases and transitions: from ising model to gauge theory, and beyond", ArXiv:2208.11699 (2022).

[117]Y. Li and M. P. A. Fisher, "Decodable hybrid dynamics of open quantum systems with $\mathbb{Z}_2$ symmetry", Physical Review B **108** (2023).

[118]S. J. Garratt, Z. Weinstein, and E. Altman, "Measurements conspire nonlocally to restructure critical quantum states", Phys. Rev. X **13**, 021026 (2023).

[119]S. Aaronson and D. Gottesman, "Improved simulation of stabilizer circuits", Phys. Rev. A **70**, 052328 (2004).

[120]S. Bravyi and D. Gosset, "Improved classical simulation of quantum circuits dominated by clifford gates", Phys. Rev. Lett. **116**, 250501 (2016).

[121]R. Orús, "Tensor networks for complex quantum systems", Nature Reviews Physics **1**, 538–550 (2019).

[122]P. Silvi, F. Tschirsich, M. Gerster, J. Jünemann, D. Jaschke, M. Rizzi, and S. Montangero, "The Tensor Networks Anthology: Simulation techniques for many-body quantum lattice systems", SciPost Phys. Lect. Notes, 8 (2019).

[123]H.-P. Breuer and F. Petruccione, *The theory of open quantum systems* (Oxford University Press, 2010).

[124]M. Iqbal, N. Tantivasadakarn, T. M. Gatterman, J. A. Gerber, K. Gilmore, D. Gresh, A. Hankin, N. Hewitt, C. V. Horst, M. Matheny, T. Mengle, B. Neyenhuis, A. Vishwanath, M. Foss-Feig, R. Verresen, and H. Dreyer, "Topological order from measurements and feed-forward on a trapped ion quantum computer", ArXiv:2302.01917 (2023).

[125]M. Foss-Feig, A. Tikku, T.-C. Lu, K. Mayer, M. Iqbal, T. M. Gatterman, J. A. Gerber, K. Gilmore, D. Gresh, A. Hankin, N. Hewitt, C. V. Horst, M. Matheny, T. Mengle, B. Neyenhuis, H. Dreyer, D. Hayes, T. H. Hsieh, and I. H. Kim, "Experimental demonstration of the advantage of adaptive quantum circuits", ArXiv:2302.03029 (2023).

[126]C. K. Andersen, A. Remm, S. Lazar, S. Krinner, J. Heinsoo, J.-C. Besse, M. Gabureac, A. Wallraff, and C. Eichler, "Entanglement stabilization using ancilla-based parity detection and real-time feedback in superconducting circuits", npj Quantum Information **5** (2019).

[127]M. Buchhold, T. Müller, and S. Diehl, "Revealing measurement-induced phase transitions by pre-selection", ArXiv:2208.10506 (2022).

[128]T. Iadecola, S. Ganeshan, J. H. Pixley, and J. H. Wilson, "Dynamical entanglement transition in the probabilistic control of chaos", arXiv:2207.12415 (2022).

[129]M. Marcuzzi, M. Buchhold, S. Diehl, and I. Lesanovsky, "Absorbing state phase transition with competing quantum and classical fluctuations", Phys. Rev. Lett. **116**, 245701 (2016).

[130]I. Lesanovsky, K. Macieszczak, and J. P. Garrahan, "Non-equilibrium absorbing state phase transitions in discrete-time quantum cellular automaton dynamics on spin lattices", Quantum Science and Technology **4**, 02LT02 (2019).

[131]F. Carollo and I. Lesanovsky, "Nonequilibrium dark space phase transition", Phys. Rev. Lett. **128**, 040603 (2022).

[132]F. Carollo, E. Gillman, H. Weimer, and I. Lesanovsky, "Critical behavior of the quantum contact process in one dimension", Phys. Rev. Lett. **123**, 100604 (2019).

[133]H. M. Wiseman and G. J. Milburn, "Quantum theory of optical feedback via homodyne detection", Phys. Rev. Lett. **70**, 548–551 (1993).

[134]S. Morales, Y. Gefen, I. Gornyi, A. Zazunov, and R. Egger, "Engineering unsteerable quantum states with active feedback", Phys. Rev. Res. **6**, 013244 (2024).

[135]D. A. Puente, F. Motzoi, T. Calarco, G. Morigi, and M. Rizzi, "Quantum state preparation via engineered ancilla resetting", Quantum **8**, 1299 (2024).

[136]R. Christie, J. Eastman, R. Schubert, and E.-M. Graefe, "Quantum-jump vs stochastic schrödinger dynamics for gaussian states with quadratic hamiltonians and linear lindbladians", Journal of Physics A: Mathematical and Theoretical **55**, 455302 (2022).

[137]G. Lindblad, "On the generators of quantum dynamical semigroups", Commun.Math. Phys. **48**, 119–130 (1976).

[138]A. Kossakowski, "On quantum statistical mechanics of non-Hamiltonian systems", Reports on Mathematical Physics **3**, 247–274 (1972).

[139]N. Gisin and I. C. Percival, "The quantum-state diffusion model applied to open systems", Journal of Physics A: Mathematical and General **25**, 5677–5691 (1992).

[140]H. M. Wiseman and G. J. Milburn, "Interpretation of quantum jump and diffusion processes illustrated on the bloch sphere", Phys. Rev. A **47**, 1652–1666 (1993).

[141]I. de Vega and D. Alonso, "Dynamics of non-markovian open quantum systems", Rev. Mod. Phys. **89**, 015001 (2017).

[142]L. Diósi, N. Gisin, and W. T. Strunz, "Non-markovian quantum state diffusion", Phys. Rev. A **58**, 1699–1712 (1998).

[143]I. Percival, *Quantum state diffusion* (Cambridge University Press, 1998).

[144]J. Bezanson, A. Edelman, S. Karpinski, and V. B. Shah, "Julia: a fresh approach to numerical computing", SIAM review **59**, 65–98 (2017).

[145]M. Born, "Zur quantenmechanik der stoßvorgänge", Zeitschrift für Physik **37**, 863–867 (1926).

[146]B. Misra and E. C. G. Sudarshan, "The Zeno's paradox in quantum theory", Journal of Mathematical Physics **18**, 756–763 (1977).

[147]H. Fröml, A. Chiocchetta, C. Kollath, and S. Diehl, "Fluctuation-induced quantum zeno effect", Phys. Rev. Lett. **122**, 040402 (2019).

[148]H. Fröml, C. Muckel, C. Kollath, A. Chiocchetta, and S. Diehl, "Ultracold quantum wires with localized losses: many-body quantum zeno effect", Phys. Rev. B **101**, 144301 (2020).

[149]T. Müller, M. Gievers, H. Fröml, S. Diehl, and A. Chiocchetta, "Shape effects of localized losses in quantum wires: dissipative resonances and nonequilibrium universality", Phys. Rev. B **104**, 155431 (2021).

[150]M. Gievers, T. Müller, H. Fröml, S. Diehl, and A. Chiocchetta, "Transport manifestations of fluctuation-induced effects in dissipative impurities", ArXiv:2312.12656 (2023).

[151]J. Dalibard, Y. Castin, and K. Mølmer, "Wave-function approach to dissipative processes in quantum optics", Phys. Rev. Lett. **68**, 580–583 (1992).

[152]C. M. Caves and G. J. Milburn, "Quantum-mechanical model for continuous position measurements", Phys. Rev. A **36**, 5543–5555 (1987).

[153]D. Yang, C. Laflamme, D. V. Vasilyev, M. A. Baranov, and P. Zoller, "Theory of a quantum scanning microscope for cold atoms", Phys. Rev. Lett. **120**, 133601 (2018).

[154]A. Kamenev, *Field theory of non-equilibrium systems* (Cambridge University Press, 2011).

[155]C. A. Brasil, F. F. Fanchini, and R. d. J. Napolitano, "A simple derivation of the lindblad equation", Revista Brasileira de Ensino de Física **35**, 01–09 (2013).

[156]U. Weiss, *Quantum dissipative systems* (World Scientific, 2008).

[157]D. Griffiths, *Introduction to quantum mechanics* (Prentice Hall International, 2004).

[158]I. Klich and L. Levitov, "Quantum noise as an entanglement meter", Phys. Rev. Lett. **102**, 100502 (2009).

[159]T. A. Sedrakyan and K. B. Efetov, "Supersymmetry method for interacting chaotic and disordered systems: the sachdev-ye-kitaev model", Physical Review B **102** (2020).

[160]K. Efetov, *Supersymmetry in disorder and chaos* (Cambridge University Press, 1996).

[161]J. Verbaarschot, H. Weidenmüller, and M. Zirnbauer, "Grassmann integration in stochastic quantum physics: the case of compound-nucleus scattering", Physics Reports **129**, 367–438 (1985).

[162]M. R. Zirnbauer, "The supersymmetry method of random matrix theory", ArXiv:math-ph/0404057 (2004).

[163]T. Prosen, "Third quantization: a general method to solve master equations for quadratic open fermi systems", New Journal of Physics **10**, 043026 (2008).

[164]T. Iadecola, S. Ganeshan, J. H. Pixley, and J. H. Wilson, "Dynamical entanglement transition in the probabilistic control of chaos", ArXiv:2207.12415 (2022).

[165]M. Coppola, E. Tirrito, D. Karevski, and M. Collura, "Growth of entanglement entropy under local projective measurements", Phys. Rev. B **105**, 094303 (2022).

[166]B. L. Altshuler, D. Khmel'nitzkii, A. I. Larkin, and P. A. Lee, "Magnetoresistance and hall effect in a disordered two-dimensional electron gas", Phys. Rev. B **22**, 5142–5153 (1980).

[167]J. Surace and L. Tagliacozzo, "Fermionic Gaussian states: an introduction to numerical approaches", SciPost Phys. Lect. Notes, 54 (2022).

[168]V. Alba and P. Calabrese, "Entanglement dynamics after quantum quenches in generic integrable systems", SciPost Phys. **4**, 17 (2018).

[169]P. Calabrese and J. Cardy, "Evolution of entanglement entropy in one-dimensional systems", Journal of Statistical Mechanics: Theory and Experiment **2005**, P04010 (2005).

[170]P. Calabrese and J. Cardy, "Entanglement entropy and quantum field theory", Journal of Statistical Mechanics: Theory and Experiment **2004**, P06002 (2004).

[171]P. Calabrese and J. Cardy, "Entanglement entropy and conformal field theory", Journal of Physics A: Mathematical and Theoretical **42**, 504005 (2009).

[172]Y. Bao, S. Choi, and E. Altman, "Symmetry enriched phases of quantum circuits", Annals of Physics **435**, Special issue on Philip W. Anderson, 168618 (2021).

[173]P. Hauke and L. Tagliacozzo, "Spread of correlations in long-range interacting quantum systems", Phys. Rev. Lett. **111**, 207202 (2013).

[174]J. Schachenmayer, B. P. Lanyon, C. F. Roos, and A. J. Daley, "Entanglement growth in quench dynamics with variable range interactions", Phys. Rev. X **3**, 031015 (2013).

[175]M. Ippoliti, T. Rakovszky, and V. Khemani, "Fractal, logarithmic, and volume-law entangled nonthermal steady states via spacetime duality", Physical Review X **12** (2022).

[176]Y. Bao, S. Choi, and E. Altman, "Theory of the phase transition in random unitary circuits with measurements", Phys. Rev. B **101**, 104301 (2020).

[177]D. A. Ivanov, T. Y. Ivanova, S. F. Caballero-Benitez, and I. B. Mekhov, "Feedback-induced quantum phase transitions using weak measurements", Phys. Rev. Lett. **124**, 010603 (2020).

[178]M. J. Gullans and D. A. Huse, "Dynamical purification phase transition induced by quantum measurements", Phys. Rev. X **10**, 041020 (2020).

[179]A. Zabalo, M. J. Gullans, J. H. Wilson, S. Gopalakrishnan, D. A. Huse, and J. H. Pixley, "Critical properties of the measurement-induced transition in random quantum circuits", Phys. Rev. B **101**, 060301 (2020).

[180]L. Zhang, J. A. Reyes, S. Kourtis, C. Chamon, E. R. Mucciolo, and A. E. Ruckenstein, "Nonuniversal entanglement level statistics in projection-driven quantum circuits", Phys. Rev. B **101**, 235104 (2020).

[181]Q. Tang and W. Zhu, "Measurement-induced phase transition: a case study in the nonintegrable model by density-matrix renormalization group calculations", Phys. Rev. Research **2**, 013022 (2020).

[182]X. Chen, Y. Li, M. P. A. Fisher, and A. Lucas, "Emergent conformal symmetry in nonunitary random dynamics of free fermions", Phys. Rev. Research **2**, 033017 (2020).

[183]A. Nahum and B. Skinner, "Entanglement and dynamics of diffusion-annihilation processes with majorana defects", Phys. Rev. Research **2**, 023288 (2020).

[184]P. Lecheminant, A. O. Gogolin, and A. A. Nersesyan, "Criticality in self-dual sine-Gordon models", Nuclear Physics B **639**, 502–523 (2002).

[185]A. Elben, B. Vermersch, M. Dalmonte, J. I. Cirac, and P. Zoller, "Rényi entropies from random quenches in atomic hubbard and spin models", Phys. Rev. Lett. **120**, 050406 (2018).

[186]S. Sang, Y. Li, T. Zhou, X. Chen, T. H. Hsieh, and M. P. Fisher, "Entanglement negativity at measurement-induced criticality", PRX Quantum **2** (2021).

[187]H. M. Wiseman, "Quantum theory of continuous feedback", Phys. Rev. A **49**, 2133–2150 (1994).

[188]S. Roy, J. T. Chalker, I. V. Gornyi, and Y. Gefen, "Measurement-induced steering of quantum systems", Physical Review Research **2**, 033347, 033347 (2020).

[189]R. A. Santos, F. Iemini, A. Kamenev, and Y. Gefen, "A possible route towards dissipation-protected qubits using a multidimensional dark space and its symmetries", Nature Communications **11** (2020).

[190]H. Hinrichsen, "Non-equilibrium critical phenomena and phase transitions into absorbing states", Advances in Physics **49**, 815–958 (2000).

[191]G. Ódor, "Universality classes in nonequilibrium lattice systems", Rev. Mod. Phys. **76**, 663–724 (2004).

[192]J. T. Young, A. V. Gorshkov, and I. B. Spielman, "Feedback-stabilized dynamical steady states in the bose-hubbard model", Physical Review Research **3** (2021).

[193]W. Wieczorek, S. G. Hofer, J. Hoelscher-Obermaier, R. Riedinger, K. Hammerer, and M. Aspelmeyer, "Optimal state estimation for cavity optomechanical systems", Phys. Rev. Lett. **114**, 223601 (2015).

[194]J. Marino and S. Diehl, "Driven markovian quantum criticality", Phys. Rev. Lett. **116**, 070407 (2016).

[195]G. Vidal, "Efficient simulation of one-dimensional quantum many-body systems", Phys. Rev. Lett. **93**, 040502 (2004).

[196]F. Verstraete, J. J. García-Ripoll, and J. I. Cirac, "Matrix product density operators: simulation of finite-temperature and dissipative systems", Phys. Rev. Lett. **93**, 207204 (2004).

[197]M. Fishman, S. R. White, and E. M. Stoudenmire, "The ITensor Software Library for Tensor Network Calculations", SciPost Phys. Codebases, 4 (2022).

[198]M. Fishman, S. R. White, and E. M. Stoudenmire, "Codebase release 0.3 for ITensor", SciPost Phys. Codebases, 4–r0.3 (2022).

[199]M. Mezard, G. Parisi, and M. Virasoro, *Spin glass theory and beyond* (World Scientific, 1986).

[200]G. Parisi, "The physical meaning of replica symmetry breaking", ArXiv:cond-mat/0205387 (2002).

[201]A. A. Ziolkowska and F. H. Essler, "Yang-Baxter integrable Lindblad equations", SciPost Phys. **8**, 44 (2020).

[202]F. H. L. Essler and L. Piroli, "Integrability of one-dimensional lindbladians from operator-space fragmentation", Phys. Rev. E **102**, 062210 (2020).

[203]O. Lunt and A. Pal, "Measurement-induced entanglement transitions in many-body localized systems", Phys. Rev. Research **2**, 043072 (2020).

[204]R. Gutiérrez, C. Simonelli, M. Archimi, F. Castellucci, E. Arimondo, D. Ciampini, M. Marcuzzi, I. Lesanovsky, and O. Morsch, "Experimental signatures of an absorbing-state phase transition in an open driven many-body quantum system", Physical Review A **96** (2017).

[205]S. Helmrich, A. Arias, and S. Whitlock, "Uncovering the nonequilibrium phase structure of an open quantum spin system", Phys. Rev. A **98**, 022109 (2018).

[206]L. Festa, N. Lorenz, L.-M. Steinert, Z. Chen, P. Osterholz, R. Eberhard, and C. Gross, "Blackbody-radiation-induced facilitated excitation of rydberg atoms in optical tweezers", Physical Review A **105** (2022).

[207]M. Howard, J. Wallman, V. Veitch, and J. Emerson, "Contextuality supplies the 'magic' for quantum computation", Nature **510**, 351–355 (2014).

[208]X. Wang, M. M. Wilde, and Y. Su, "Quantifying the magic of quantum channels", New Journal of Physics **21**, 103002 (2019).

[209]J. Haferkamp, P. Faist, N. B. T. Kothakonda, J. Eisert, and N. Yunger Halpern, "Linear growth of quantum circuit complexity", Nature Physics **18**, 528–532 (2022).

[210]D. Gottesman, "The heisenberg representation of quantum computers", ArXiv:quant-ph/9807006 (1998).

[211]T. Haug and M. Kim, "Scalable measures of magic resource for quantum computers", PRX Quantum **4** (2023).

[212]S. F. E. Oliviero, L. Leone, A. Hamma, and S. Lloyd, "Measuring magic on a quantum processor", npj Quantum Information **8** (2022).

[213]L. Leone, S. F. E. Oliviero, and A. Hamma, "Stabilizer rényi entropy", Phys. Rev. Lett. **128**, 050402 (2022).

[214]G. E. Fux, E. Tirrito, M. Dalmonte, and R. Fazio, "Entanglement-magic separation in hybrid quantum circuits", ArXiv:2312.02039 (2023).

[215]P. Niroula, C. D. White, Q. Wang, S. Johri, D. Zhu, C. Monroe, C. Noel, and M. J. Gullans, "Phase transition in magic with random quantum circuits", ArXiv:2304.10481 (2024).

[216]M. Frau, P. S. Tarabunga, M. Collura, M. Dalmonte, and E. Tirrito, "Non-stabilizerness versus entanglement in matrix product states", ArXiv:2404.18768 (2024).

[217]P. S. Tarabunga, E. Tirrito, T. Chanda, and M. Dalmonte, "Many-body magic via pauli-markov chains—from criticality to gauge theories", PRX Quantum **4**, 040317 (2023).

[218]P. S. Tarabunga, E. Tirrito, M. C. Bañuls, and M. Dalmonte, "Nonstabilizerness via matrix product states in the pauli basis", ArXiv:2401.16498 (2024).

[219]X. G. Wen, "Topological orders in rigid states", International Journal of Modern Physics B **04**, 239–271 (1990).

[220]A. Altland and M. R. Zirnbauer, "Nonstandard symmetry classes in mesoscopic normal-superconducting hybrid structures", Physical Review B **55**, 1142–1161 (1997).

[221]Z.-M. Huang and S. Diehl, "Mixed state topological order parameters for symmetry protected fermion matter", ArXiv:2401.10993 (2024).

[222]C.-E. Bardyn, M. A. Baranov, C. V. Kraus, E. Rico, A. İmamoğlu, P. Zoller, and S. Diehl, "Topology by dissipation", New Journal of Physics **15**, 085001 (2013).

[223]F. Tonielli, J. C. Budich, A. Altland, and S. Diehl, "Topological field theory far from equilibrium", Physical Review Letters **124** (2020).

[224]A. Y. Kitaev, "Unpaired majorana fermions in quantum wires", Physics-Uspekhi **44**, 131–136 (2001).